Glycerol and D-Glucose Valorization to Biorenewable Platform Chemicals by Waste Red Mud Derived Catalysts

A Thesis

Submitted in Partial Fulfilment of the Requirements for the Degree of

DOCTOR OF PHILOSOPHY

by

Bikashbindu Das

Department of Chemical Engineering

Indian Institute of Technology Guwahati

Guwahati - 781039, Assam (India)

August 2021

This thesis is dedicated to my beloved Grandfather who has always loved me and encouraged me to pursue higher goals in life.

DEPARTMENT OF CHEMICAL ENGINEERING

INDIAN INSTITUTE OF TECHNOLOGY GUWAHATI

STATEMENT

I do hereby declare that the content embodied in this thesis entitled *"**Glycerol and D-Glucose valorization to biorenewable platform chemicals by waste red mud derived catalysts**"* is the result of investigations carried out by me at the Department of Chemical Engineering, Indian Institute of Technology Guwahati, Guwahati, India, under the guidance of **Prof. Kaustubha Mohanty**.

In keeping with the general practice of reporting scientific observations, due acknowledgements have been made wherever the work described is based on the findings of other investigators.

Bikash bindu Das

May, 2021 **Bikashbindu Das**

DEPARTMENT OF CHEMICAL ENGINEERING

INDIAN INSTITUTE OF TECHNOLOGY GUWAHATI

CERTIFICATE

This is to certify that **Mr. Bikashbindu Das** has been working under my supervision since July 2015. I hereby forward his thesis entitled ***"Glycerol and D-Glucose valorization to biorenewable platform chemicals by waste red mud derived catalysts"*** to be submitted for the award of the degree of Doctor of Philosophy to IIT Guwahati. I certify that he has fulfilled all the requirements according to the rules of this institute and the investigations embodied in his thesis have not been submitted elsewhere for a degree or diploma.

Dr. Kaustubha Mohanty
Professor
Department of Chemical Engineering
Indian Institute of Technology Guwahati

Date: May 2021
IIT Guwahati

Acknowledgement

Foremost, I would like to extend my sincere gratitude to my thesis supervisor Prof. Kaustubha Mohanty for his continuous guidance and support for the successful implementation of the work. Throughout the duration of my Ph.D., his encouragement and valued advice have inspired me to pursue higher goals in life. I would like to express my deep sense of gratitude to my doctoral committee members Prof. G. Pugazhenthi, Dr. Partho S. G. Pattader, and Dr. Soumen Kumar Maiti, for their constructive suggestions towards improving the quality of the research. I am highly obliged to Prof. Mahuya De for sharing her knowledge and helping with the research at certain times during my Ph. D.

I am grateful to Prof. Anugrah Singh, Head Department of Chemical Engineering, for and Prof. Bishnupada Mandal, Head (Former) Department of Chemical Engineering, for their administrative assistance. I highly acknowledge the instrumental facility provided by the Central Instrument Facility (CIF) and Department of Chemical Engineering, IIT Guwahati, for the smooth conduct of the research.

I am very grateful for the support from the highly enthusiastic and co-operative research group, Dr. Himadri Sahu, Dr. Sanjukta Bhoi, Dr. Madhusmita Dash, Dr. Kulbhushan Samal, Dr. Ranjeet Kumar Mishra, Proloy Das, Sanjeev Mishra, Dr. Saran Sarangapany, Dr. Rahulkumar Maurya, Naveen, Aanisha, Ananya, Janaki, Ankit, Harsh, Om, Anindita, Madonna, Sounak, Deepesh, Barasa, Pranab, Sachankar, Santosh, Munmi, and Saptaswa. I am thankful to my research mates, Bitang, Dr. Ritesh, Rupam, Dr. Pyrimohan, Sidharth, and Saptarshi, for their constant support and motivation.

Last but not least, I highly express my gratitude for the selfless love, support, and patience of my family members towards the completion of my Ph.D. thesis. I extend my sincere thanks to all my dear friends and well-wishers who had consistently supported and encouraged me, without which this work would have never been completed.

Thank you all !!

Bikashbindu Das

ABSTRACT

The growing use of fossil fuels has adversely affected the climate and negatively impacted every aspect of life in the ecosystem. Hence, the energy and chemical industries have periodically pushed through several transitions in terms of technology and raw materials to eliminate the threat of fossil resources. Biodiesel, an important breakthrough in the synthesis of renewable fuel, involves a synthesis process that produces glycerol (GL) as a by-product. The sustainability of the biodiesel industries depends on the effective utilization of the surplus glycerol economically. Similarly, a highly demanded and important chemical is 5-Hydroxymethylfurfural (5-HMF), produced from lignocellulosic biomass, which has several important industrial applications as fuel and chemicals.

The cost and effectiveness of catalysts play a significant role in shaping the efficiency of the chemical and energy synthesis process. Hence, finding the potential low-cost materials and their effective utilization as catalysts for chemical processes always remains indispensable research for scientists. In context, various inexpensive and highly active catalysts derived from aluminum industry waste red mud (RM) for the GL transesterification to glycerol carbonate (GC) and D-Glucose conversion to 5-HMF are reported in this work. Calcined RM-based catalysts were developed by calcination of RM between 400 ^{o}C to 800 ^{o}C. The calcination temperature had a reasonable effect on the physicochemical properties of RM that, as a result, influenced the GL transesterification. RM sample calcined at 500 ^{o}C (RM-500) showed a maximum concentration of active $NaAlO_2$ and Ca_2SiO_4 sites, producing the highest GL conversion of 95.21% and GC yield of 92.02%. The highest GC yield could be achieved at mild reaction conditions of 75 ^{o}C, 90 min, and 1:3 molar ratio of GL to dimethyl carbonate (DMC). Calcination temperature above 500 ^{o}C, hematite (Fe_2O_3) became the dominant phase, and the concentration of $NaAlO_2$ and Ca_2SiO_4 decreased, decreasing the catalytic activity.

The promotional effect of potassium (K), strontium (Sr), and magnesium (Mg) on RM was studied to enhance its catalytic stability for GL transesterification.

From preliminary studies, K-doped RM catalysts were found to have better activity and stability than the Sr and Mg-doped RM catalysts. The RK-30%-800 catalyst prepared by 30% of K loading and calcination at 800 ^{o}C produced the highest activity (93.27% GC yield) and stability than other K-doped catalysts. The better activity of the RK-30% catalyst was attributed to the maximum surface concentration of active K_2O, as confirmed by the XRD analysis that contributed significantly to the increased basic properties of the catalyst. RM-500 and RK-30%-800 showed excellent catalytic activity for GL transesterification in the presence of impurities such as water and methanol.

Sn and sulfate (SO_4^{-2}) modified acid-treated red mud (ARM) catalysts were developed to transform glucose to 5-HMF. AS-W_s-H catalyst obtained by doping of Sn followed by functionalization of sulfate groups on ARM showed improved Lewis and Bronsted acid characteristics. The catalyst was predominantly composed of SO_4^{-2}/Fe_2O_3-SnO_2 and $Fe_2(SO_4)_3$ as the active components as suggested by the XRD and XPS analysis. The AS-13-H produced a 5-HMF yield of 26.22% at 180 ^{o}C and 5 min from D-Glucose with water as the solvent under microwave irradiation. In the presence of a solvent consisting of dimethyl sulfoxide (DMSO) and water in the weight ratio of 1:1, the 5-HMF yield improved to 53.8%. The synergistic interaction of Sn (13 wt%) with components of ARM improved the catalytic stability, due to which a satisfactory 5-HMF yield was found up to the 4th use.

Sulfonated carbon-based acidic catalysts that lack Lewis acid sites were used earlier for the successful fructose conversion to 5-HMF; however, they were significantly less active for the direct glucose transformation to 5-HMF. The AD-1:1/SO_3H catalyst produced by the acid (HCl) treatment, carbon coating, and SO_3H grafting on RM exhibited enhanced surface area, mesoporous characteristics, and suitable Lewis and Bronsted acid sites. Different active phases such as $Fe_2(SO_4)_3$, Fe_2O_3, and various carbon functionalities were observed in the AD-1:1/SO_3H catalyst from the XRD, XPS, and FTIR analysis. Under microwave heating at 180 ^{o}C, 30 min, and 90:10 DMSO/water weight percentage ratio, the catalyst produced a D-Glucose conversion and 5-HMF yield of 93.05% and 51.5%, respectively, with appreciable stability up to the 4th cycle.

CONTENTS

LIST OF TABLES

LIST OF FIGURES

NOMENCLATURE

2, 5-BHF	2, 5-Bis(hydroxymethyl)furan
2, 5- DFF	2, 5-Diformylfuran
2, 5-DMF	2, 5-Dimethylfuran
2 ,5-FDCA	2, 5-Furandicarboxylic acid
5-CMF	5- Chloromethylfurfural
5-HMF	5-Hydroxymethylfurfural
AA	Acetic acid
AARM	Acid-activated red mud
AAS	Atomic absorption spectroscopy
AD-Y:Z	Carbon coated acid-activated red mud
AD-Y:Z/SO_3H	Sulfonic acid functionalized carbon coated acid-activated red mud
AS-W_s	Sn impregnated acid-treated red mud
AS-W_sH	Sulfate functionalized Sn impregnated acid-treated red mud
ARM	Acid-treated red mud
CNT	Carbon nanotube
DBC	Dibenzyl carbonate
DEC	Diethyl carbonate
DHA	Dihydroxyacetone
DMC	Dimethyl Carbonate
DMF	N,N-dimethylformamide
DMSO	Dimethyl sulfoxide
EDX	Energy dispersive X-ray
FA	Formic acid
FCT	Fructose
FESEM	Field emission scanning electron microscope
FTIR	Fourier transform infrared spectroscopy
FU	Furfural

GC	Glycerol carbonate
GD	Glycidol
GL	Glycerol
HPLC	High-performance liquid chromatography
LA	Levulinic Acid
LCTA	Lactic acid
LDH	Layer double hydroxide
LGS	Levoglucosan
MET	Methanol
MIBK	Methyl isobutyl ketone
NALCO	National aluminum company
NHC	N-heterocyclic carbene
Py-ATR	Pyridine adsorbed attenuated total reflectance
RM	Red Mud
RM-X	Red Mud Calcined at X (temperature)
RW_k-X	Metals (K, Sr, Mg) impregnated Red Mud calcined at X (temperature)
THF	Tetrahydrofuran
TPD	Temperature programmed desorption
VPO	Vanadium phosphate
XPS	X-Ray photoelectron spectroscopy
XRD	X-ray diffraction
XRF	X-ray fluorescence
ZIF-8	Zeolitic imidazolate framework-8

SYMBOLS

C_{GL}	Glycerol concentration
C_{GL}	Initial glycerol concentration
C_{DMC}	Dimethyl carbonate concentration
C_{GC}	Glycerol carbonate concentration
C_{MET}	Methanol concentration

C_v	Vacant sites concentration on catalyst
C_o	Total active site concentration on catalyst surface
X_{GL}	Glycerol conversion
r	Rate of a reaction
t	Time
T	Temperature
k_s	Forward reaction rate constant
k'_s	Backward reaction rate constant
K_s	Overall rate constant
K_{GL}	Glycerol conversion rate constant
K_{DMC}	Dimethyl carbonate conversion rate constant
K_{GC}	Glycerol carbonate conversion rate constant
K_{MET}	Methanol conversion rate constant
w	Weight of catalyst
W_k	Different metals (K, Sr, and Mg) weight% on red mud
W_s	Weight% of Sn on acid-treated red mud
S	Catalyst surface
X	Calcination temperature
Y	Weight of acid-treated red mud
Z	weight of D-Glucose

Chapter 1

Introduction

1.1 Fossil Resources: Existential Concerns

More than six decades ago, a major transition in chemistry took place that introduced the concept of petrochemistry that mainly relied on olefin and aromatics [1]. The emergence of petrochemistry has been able to provide a major part of the energy and chemical demand of society since that time. However, the carbon feeds for the petroleum industries are derived from conventional fossil resources, which are on the verge of depletion. The energy and chemicals derived from fossil resources are associated with the emission of greenhouse gases, which has become a major reason for climate change. Moreover, the increasing demand for energy and chemicals with the growing industrialization and depleting fossil resources has thrown a major challenge for scientists to develop sustainable alternatives. In relation to this, the chemical and energy sectors worldwide have been driven by pushing factors such as the introduction of new resources and technologies to mitigate the future societal and industrial demands [2].

1.2 World Energy Consumption Forecast

It is estimated that worldwide energy consumption will be increased by 28% between 2015 and 2040 [3]. Coal, natural gas, and oil are the leading conventional sources for supplying the present energy demand. With the increasing world population and a significant increase in their living standards, the conventional energy resources are depleting very rapidly. In relation to this, there has been a fast-proceeding transition occurring in energy and chemical technologies through the introduction of renewable resources as alternative carbon feeds [2]. Among various renewable energy resources, biomass has been intensively studied as a promising

sustainable alternative for supplying carbon feeds for the chemical and energy industries [4].

1.3 Plant-Based Biomass as a Sustainable Alternative

Plant and plant-based biomass is mainly composed of lignocellulose. Lignocellulose is composed of three major components; cellulose, hemicellulose, and lignin (Figure1.1). The content of cellulose (25-55%), hemicellulose (24-50%), and lignin (10-35%) is found to be present in the lignocellulose of trees, grasses, and energy crops [5]. However, the percentage of these components varied with plant species, tissues, and maturity of cell walls [5]. Cellulose is a polysaccharide comprised of glucose units linearly connected with β-1,4 linkage. The glucose units from cellulose can be removed by acid hydrolysis or enzymatic hydrolysis [6]. The individual processes are associated with their own drawbacks, such as forming of side products through acid hydrolysis, while high cost and low turnover rates are linked to enzymatic processes [7,8]. The glucose units are further used as building blocks for different platform chemicals and fuel synthesis through various catalytic processes.

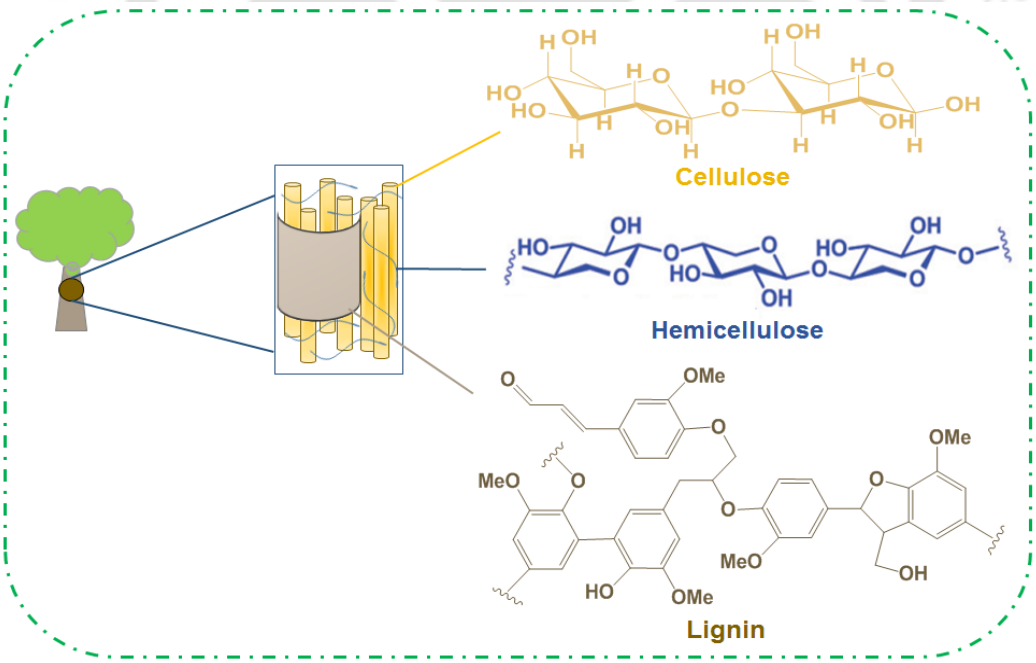

Figure 1.1. Structural compositions of lignocellulosic biomass.

Hemicellulose comprises a different group of carbohydrates such as pentose and hexose sugars [5]. Hemicellulose has a lower degree of polymerization, and the branched structure makes it non-crystalline in nature. Lignin is a polymer of C-O-C ether bonds, which are difficult to depolymerize into monomeric units [9]. There have been intensive studies performed worldwide for converting either whole lignocellulose or individual fractions such as cellulose, hemicellulose, and lignin to other high-value products through various processes [10,11].

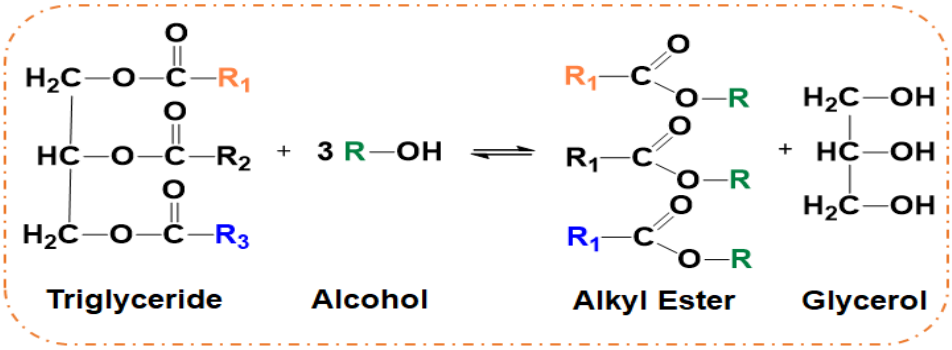

Figure 1.2. Transesterification route for biodiesel synthesis.

Due to its fossil fuel-like properties, biodiesel has been synthesized as an alternative to conventional diesel, and in the recent past, the production has increased to a significant extent [12]. With the increasing demand for alternative fuel, biodiesel production was expected to reach 12 billion gallons by 2020 [12,13]. The synthesis of biodiesel follows the convenient transesterification route, where a vegetable or animal oil is reacted with an alcohol (methanol or ethanol) [12,13] (Figure 1.2). The reaction takes place in the presence of a suitable acidic or alkaline catalyst. By this process of biodiesel synthesis, glycerol is produced as a by-product, the amount of which is approximately 10 wt% of the total biodiesel yield. It is clear that, with the increase in the production of biodiesel, the amount of the by-product glycerol is also increasing, and it was estimated that by 2020, the amount will overpass the actual demand at least by six times the actual demand [14]. The expansion of biodiesel industries and excess glycerol production has affected the glycerol market to a significant extent. For example, a sharp decrease in the market price of crude glycerol from USD 0.25/lb to USD 0.05/lb was seen in 2007 [15]. Similarly, a decrease in the

crude glycerol price by approximately four times was observed in mid-2014. Therefore, the sustainability of the biodiesel industry depends on how the excess glycerol is utilized in an economical way for some practical applications so that the net energy requirement of the biodiesel industry is reduced. For the efficient utilization of glycerol, many conversion routes have been studied in the last few decades [16]. Various conversion routes demand the use of different catalysts for maximizing the synthesis of the desired products in an efficient and economical way.

1.4 Catalysis: An Overview

In 1835 the term *"catalysis"* was coined by Swedish chemist Berzelius [17]. Many years later, in 1894, Ostwald proposed a suitable description of the phrase that *"catalysis is the acceleration of a small chemical process by the presence of a foreign material"* [17]. Today more than ten decades later, it is understood that the foreign material, which is called a "catalyst" accelerates a chemical process by decreasing the activation energy through interacting with the reactant species. With advances in technology, more detail on the adsorption and interaction between the catalyst and the molecules was revealed, and it was clear that mainly the defects at the edges and corners of the rough surface in a crystal are responsible for higher catalytic activity than single crystals [17].

Catalysis plays an important role in shaping the efficiency of a chemical process. The majority of the chemical compounds undergo at least one catalytic step during their synthesis [17]. Catalytic processes comprise directly or indirectly 20% to 30% of the world GDP [2]. With the continuous growing demand for energy and chemicals, the production of catalysts is also increasing, and in the catalyst market, it could reach US 34.3 billion by 2024 [2]. Scientists are focused upon developing novel heterogeneous catalysts for use in the energy and chemical sectors to overcome the challenge of reactor corrosion and the separation difficulties for homogeneous catalysts.

In the early 1800s, platinum was exploited as a heterogeneous catalyst for the facilitation of oxidation reactions initially by Faraday [18]. Since then, heterogeneous catalysts have gone through various modifications to accomplish the sustainability of

the energy and chemical sectors. Moreover, the environmental and economic concerns have motivated scientists to develop better catalysts that are more selective for the desired product and avoid other environmentally harmful by-products [2,18].

Precious metal particles are considered the active components for contributing to the conversion efficiency of a chemical process. However, in many cases it has been found that particle agglomeration could occur during their synthesis that makes it difficult for reactants to access some active sites [19]. In addition, these small metal particles could easily be lost with the reactant or products during the reaction that leads to difficulty in their reuse. Nonetheless, catalytic supports with a high surface area are preferred for better dispersion of the active metal particles to avoid the inaccessibility of reactants to agglomerated metal particles and to enhance conversion efficiency. Support materials are chosen cleverly, which can contribute to the overall efficiency of the catalytic process through directly participating in the reaction or indirectly by providing a high surface area for metal dispersion and enhancing the chemical and physical stability of the catalyst [19]. The cost of the support material has a direct impact on the final cost of the catalyst. Supports with desirable properties and low-cost are preferred for making the process economical. In this context, significant efforts were dedicated to find low-cost supports, particularly by utilizing various solid wastes for the preparation of support materials. Highly produced industrial wastes such as fly ash, red mud, slag, etc., have been utilized as catalysts or catalytic supports [20,21]. Other biological wastes such as mussel shells, turtle shells, animal bones, egg shells, etc., have also proven very suitable catalytic support [20,21].

1.5 Red Mud

1.5.1 Origin and Properties

Red mud (RM) is a waste residue generated from aluminum industries by the Bayer process of alumina production from bauxite (Figure 1.3). Due to its durability, flexibility, lightweight, corrosion-resistant, and high strength, the need for aluminum products all over the world is increasing. This has resulted in the formation of more RM, the disposal of which is a major issue for the entire aluminum community. For

every ton of alumina produced, the amount of RM generated is approximately 0.3 ton for high-grade ores, and it may reach up to 2.5 ton for low-grade ores [22]. The amount of RM produced from aluminum industries worldwide is more than 120 million tons annually. In India, the aluminum industries produce more than 6 million tons of RM in a year [22]. A summary of red mud and its composition originating from different aluminum industries across India is presented in Table 1.1 [23]. RM is highly alkaline (pH 11-13) and, in some cases, contains small quantities of radioactive elements such as yttrium, uranium, thorium, etc., due to which, it is considered a hazardous waste [24].

Table 1.1. Red mud compositions from different plant across India.

Plant	Major Constituent (wt%)					
	Fe_2O_3	Al_2O_3	SiO_2	TiO_2	Na_2O	CaO
HINDALCO Renukoot	28.1	21.9	7.5	15.6	4.5	10.2
INDAL Muri	24.5	24.3	6.2	18.0	5.3	-
BALCO Kobra	27.9	19.4	7.3	16.4	3.3	11.8
NALCO Damanjodi	54.8	14.8	6.4	3.7	4.8	2.5
INDAL Belgam	44.5	19.2	7.0	13.5	4.0	0.8
MALCO Mettur Dam	18.0	14.0	56.0	50.0	6.0-9.0	2.0-4.0

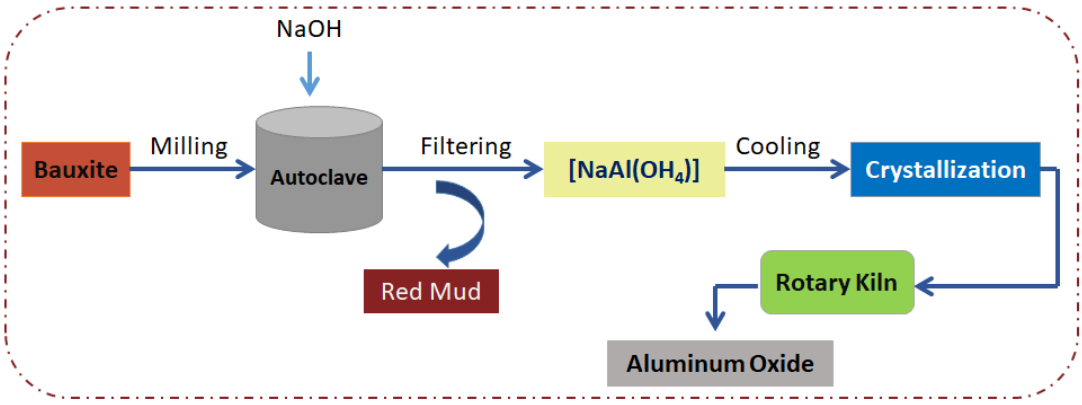

Figure 1.3. Bayer process for alumina production.

1.6 Glycerol: A Green Chemical Building Block

1.6.1 Structure and Properties

Glycerol, also known as glycerine or 1,2,3-propanetriol, is an organic compound with three hydroxyl (-OH) groups (Figure 1.4) [25]. As early as 2800 BC, glycerol was isolated from fats by heating it in the presence of ash [25]. The demand for glycerol slowly started to increase because of which its synthetic production started from propylene derived epichlorohydrin in the late 1940s [25]. In the present days, most of the glycerol production plants are closing as the growing biodiesel industries have produced a surplus amount of glycerol in the society [25].

In glycerol, three –OH groups are attached to three diferent carbon atoms because of which it is called a polyol. Glycerol is a colorless, non-toxic, and viscous liquid with a sweet taste. The presence of –OH groups makes glycerol water-soluble and hygroscopic. Glycerol has a density of 1.261 gm ml^{-1} with a boiling point of 290 ^{o}C [26].

1.6.2 Catalytic Conversion Routes

The presence of two primary and one secondary hydroxyl groups in GL creates the possibility of producing several derivatives of the material through more than the usual number of reactions. In addition, the production of H_2 and syngas from glycerol could be a suitable conversion pathway with a contribution to the clean and

renewable energy sources [16]. The different conversion route with the end-product of glycerol conversion is presented in Figure 1.4. As can be seen a number of chemicals can be produced from glycerol as a starting material, the efficient conversion largely depends on the nature and effectiveness of the catalysts. Tailoring of catalysts can be done by controlling their size, shape, surface composition, thermal-chemical stability, etc., to achieve maximum efficiency without compromising the rules of green chemistry [27].

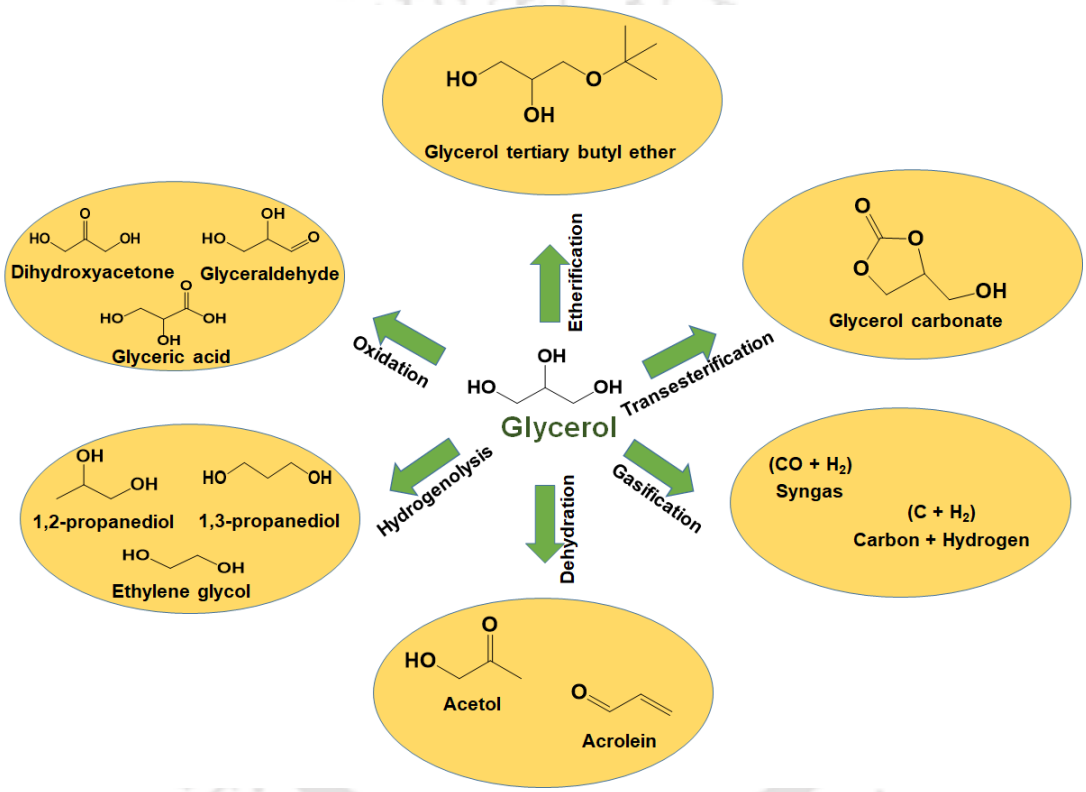

Figure 1.4. Various glycerol conversion routes.

Various glycerol oxygenate derivatives can be obtained by selective oxidation of glycerol. Glyceric acid and tartronic acid are produced by the oxidation of primary hydroxyl groups, whereas dihydroxyacetone (DHA) is obtained by the oxidation of the secondary hydroxyl group [25]. A highly functionalized compound ketomalonic (mesoxalic) acid could be synthesized by oxidation of all the three –OH groups of

glycerol [25]. Single noble metals such as Pt, Pd, and Au and carbon materials as catalytic support have been studied extensively for glycerol oxidation [27].

Glycerol as a direct fuel is not preferred as it can polymerize at high temperature and clog engines [25]. Etherification of glycerol with isobutylene produced glycerol tertiary butyl ether with improved octane properties, making it suitable as fuel additive [25]. The process can take place in the presence of acidic catalysts and two-phase reaction systems for getting an improved yield. Dehydration of glycerol in the presence of acidic catalysts such as H_3PO_4/C, ZSM-5, ZrO_2-FeO_x, etc, produce acrolein, which found application in the chemical industries for the production of polymers, acrylic acid esters, and detergents [25,28–30].

Glycerol can undergo hydrogenolysis selectively in the presence of a suitable catalyst and hydrogen to produce value-added molecules such as 1,2-propanediol, 1,3-propanediol, and ethylene glycol [16]. These products have important applications in the polymer, pharmaceutical, cosmetic, and paint industries. Different single metal catalysts such as Raney Ni, Cu, Ru, Rh, and Ir, [16] bimetallics such as, Cu-Pt, Cu-Ru, CuO-ZnO, and Pd-ZnO, [16,31] and supported catalysts such as Cu/C, Ru/C, Pd/C, and Pt/C [32,33] are used for this process.

Another potential application of glycerol is in producing synthesis gas from it via steam or aqueous phase reforming and gasification in supercritical water [16]. Steam reforming of glycerol takes place in the gas phase, usually at atmospheric pressure and temperatures above 400 ^oC that produce H_2/CO with a molar ratio of 1.33 [34]. Various catalysts used for the process include Ni, Pt, Ru, and Rh supported on Al_2O_3, ZrO_2, TiO_2, SiO_2, etc. [35–37]. The chemistry of aqueous phase reforming is similar to that of steam phase reforming. However, the reaction for the earlier one is performed in a liquid phase and at high pressure between 25 to 35 bar and at a lower temperature close to 125 ^oC [34]. Catalysts consist of metals such as Pt, Pd, Ni, Ni-Sn with alumina as a support material have been used for this process [38,39].

Glycerol carbonate is another important derivative of glycerol with major applications in polymer, cosmetic and pharmaceutical industries [16]. There are

numerous of ways in which glycerol can be converted into glycerol carbonate. A detailed description of all the processes with required catalysts is provided in the upcoming section.

1.7 Glycerol Carbonate

1.7.1 Structure, Properties and Important Applications

Glycerol carbonate (GC) (4-hydroxymethyl-1,3-dioxolan-2-one) is a five-membered ring carbonate compound (Figure 1.5). The compound can be synthesized from glycerol as raw material, and it is one of the recently commercialized bio-derived compounds [40]. Recently companies such as Ube Industries Limited and Huntsman have incorporated GC into their portfolio [41].

GC is a non-toxic, non-flammable (FP > 204 ^{o}C), bio-degradable and viscous liquid (85.4 mPa.s at 25 ^{o}C). GC is hydrophilic in nature and has a very low evaporation rate (bp 110 to 115 ^{o}C at 0.1 mmHg). It has high density (1.4 g mL^{-1} at 25 ^{o}C) and high dielectric constant (111.5) [40]. The renewable content (mass percent of molecules derived from renewable sources) range between 76% if it is synthesized from glycerol and another raw material except for CO_2. However, with CO_2 as the raw material along with glycerol, the renewable content is 100%.

The properties of GC, as mentioned, are very relevant for its use in various industrial purposes as a green chemical (Figure 1.5). The presence of the reactive sites such as the –OH group and the three carbon atoms of the dioxolan ring open various possibilities for the commercialization of GC in the production of chemical intermediates and polymers [41]. Other applications of GC includes its use in the production of adhesive, coating, lubricants, and foams [41].

1.7.2 Synthesis Techniques

Glycerol can be converted into glycerol carbonate (Figure 1.5) through a variety of reaction routes, with each route having its advantages and disadvantages. However, while selecting a route to synthesize GC, it is important to take note of the chemistry involves in that route, the nature and cost of the catalyst, nature of the solvent to be used, reaction parameters such as time, temperature, etc. and the

efficiency of the process. It is required to confirm that the norms of the green chemistry during the synthesis is not violated.

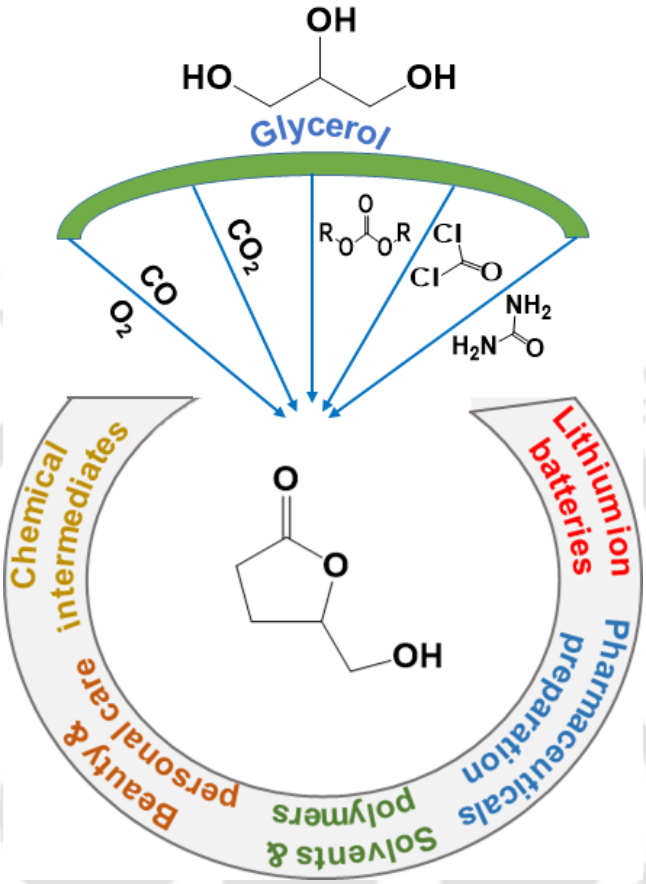

Figure 1.5. Synthesis routes and applications of glycerol carbonate.

1.7.2.1 Direct Reaction of GL and CO_2

One of the most desirable synthesis techniques is reacting GL with CO_2 as it involves reactants, which are green chemicals and are available at a low price. The reaction between GL and CO_2 produce GC, and water is the only by-product produced [40]. However, the direct synthesis route to produce GC is not industrially feasible because of the poor reactivity of CO_2. It led to the requirement of high energy input and high-cost active catalysts for the activation of CO_2 [42].

Catalysts such as CeO_2/Al_2O_3 and CeO_2/Nb_2O_5 were reported for the direct synthesis of GC from GL and CO_2 with a very low yield (up to 10%) [43,44]. A relatively higher yield of GC (32%) was reported by George and coworkers in the presence of $^nBu_2SnO$ catalyst and methanol as a solvent [45]. In another approach for the direct reaction of GL and CO_2 zeolite and basic ion exchange resins catalyst was used with ethylene carbonate (63 mol%) as a solvent that produced almost 32% GC yield [46]. However, the reaction in the absence of ethylene carbonate did not produce any GC, suggesting the reaction was more preceded by the transesterification route rather than direct carbonation. Carbon monoxide (CO) could be an alternative to eliminate the difficulty in activating CO_2. A remarkable GL conversion (> 92%) and GC selectivity (> 93%) could be obtained by the reaction of CO with GL in the presence of $CuCl_2$ and pyridine catalysts [47]. However, CO is poisonous and using it for the GC synthesis could lead to additional hazard for industrial applications. Viewing these results of GC synthesis by the direct reaction of CO_2 and GL, it is apparent that industrially feasible synthesis of GC is not preferred by the direct route and some indirect synthesis routes must be followed.

1.7.2.2 Indirect Synthesis: GL Carbonylation with Urea

The process is carried out by reacting GL with urea at an equimolar quantity in the presence of a suitable catalyst. The process is usually performed between 130 to 150 ^oC. However, a continuous vacuum is required to remove the ammonia formed during the reaction to drive the reaction towards the product formation [40,41]. Apart from using a continuous vacuum, the produced ammonia can also be displaced by continuous N_2 flow at ambient pressure. The GC produced could also react with urea by producing carbamate of glycerol carbonate, requiring careful selection of reaction conditions.

Zn based catalysts such as $ZnSO_4$ and ZnO are reported to produce GL conversion of as high as 83% with a 100% GC selectivity [48,49]. One major drawback of the process is that the catalyst are soluble in the reaction product making it difficult for its separation [49]. High selectivity of GC (77%) could be obtained by using a Au-Pd supported on MgO catalyst at 150 ^oC and with a GL to urea ratio of

1:1.5 [50]. A further increase in GC (93%) selectivity could be achieved by increasing the quantity of glycerol with respect to urea under the same reaction conditions [50]. Phu et al. reported 30.9% and 58.1% GC yield by using activated red mud and Zn/Al doped activated red mud catalyst that signifies the potential of the waste RM for this process [51]. Another technique is the phosgene-based synthesis of GC, where GL and phosgene ($COCl_2$) react to produce GC. However, the toxic nature of phosgene makes it very difficult to produce GC by this process [52].

1.7.2.3 Indirect Synthesis: GL Transesterification

To avoid the energy-intensive NH_3 recovery required during carbamoylation of urea with GL and the poisonous phosgene gas used for GC synthesis, researchers have shifted towards more safe and efficient methods for GC synthesis from GL. In this context, transesterification of GL with alkylene carbonate or dialkyl carbonate in the presence of a suitable catalyst was found as an suitable alternative to other processes [53]. Alkylene carbonate as a solvent and reactant for the GC synthesis via the transesterification with GL involves relatively high energy input, multi-step separation process, and high reaction time [54]. On the other hand, dialkyl carbonate such as dimethyl carbonate (DMC) is a suitable alternative to the alkylene carbonates because of the high efficiency of the process, mild reaction conditions, low toxicity and high yield [55,56]. The process produces one mole of GC along with two moles of methanol and is an equilibrium reversible reaction (Figure 1.6). Continuous removal of methanol or an excess DMC is thus required for achieving high GC yield [55–57]. The thermal stability and viscosity of glycerol demand high energy input for

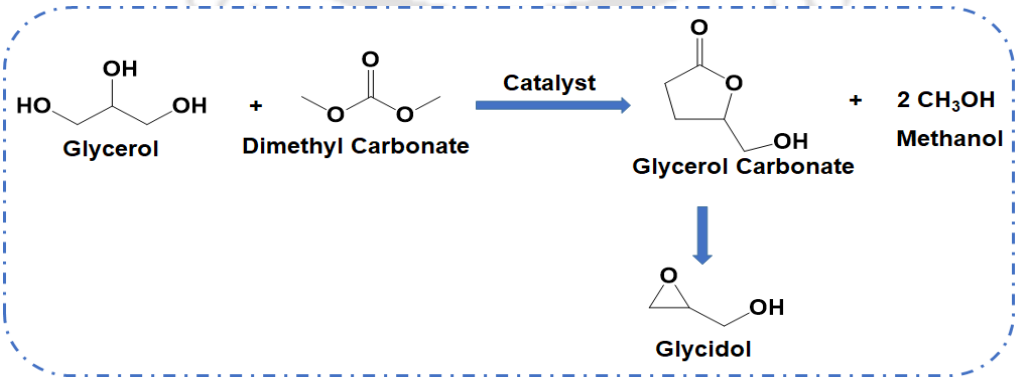

Figure 1.6. Glycerol transesterification route to glycerol carbonate.

bond cleavage, due to which various catalysts are used to carry out the process under milder conditions [55,56]. Homogeneous, heterogeneous, and enzymatic catalysts have been used for the process to enhance efficiency. However, heterogeneous catalysts are preferred over the other two because of their easy separation, which makes them reusable. Besides this, low-cost catalysts with suitable catalytic properties are often preferred for an economic synthesis of GC. In this context, exploiting RM as a low-cost catalyst or as catalytic support for other active metals could be a suitable option for making the GC synthesis industrially feasible.

1.8 Glucose: A Renewable Chemical Building Block

1.8.1 Properties and Important Conversion Routes

Glucose, more conventionally known as D- (+)-Glucose, has a chemical structure with a polyalcohol as well as an aldehyde (in linear structure), hence classified as an aldose also (Figure 1.7). It is a six-member carbon structure with a molecular weight of 180.16 g mol^{-1} and has four chiral carbons at C2, C3, C4, and C5. It has a melting point of 150 ^{o}C, and a density of 1.5620 g cm^{-3} [58]. It is also highly soluble in water and slightly soluble in ethanol. Besides alcohol and aldehyde groups, the ring structure of glucose also contains ester groups, making it a potential candidate as a substrate for chemical modifications [58]. Glucose is usually synthesized from polysaccharide sources from lignocellulogic biomass through the hydrolysis process [59].

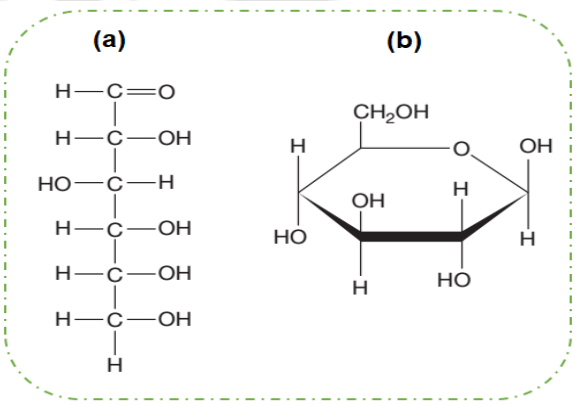

Figure 1.7. (a) Open chain and (b) ring structure of D-Glucose.

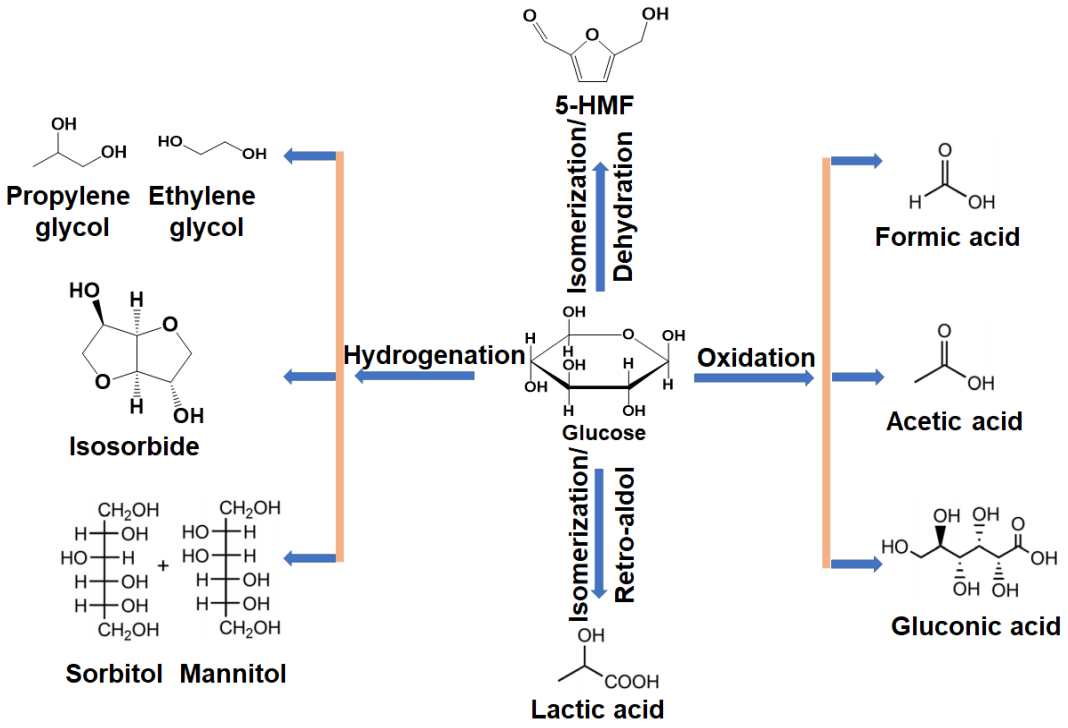

Figure 1.8. Various glucose conversion routes.

Different conversion routes of glucose to value-added products are shown in Figure 1.8. Every conversion process of glucose to important chemicals or fuels is performed efficiently by using various catalysts. For instance, the oxidation of glucose to formic acid and acetic acid, all having important industrial applications, is performed using various catalysts such as $H_5PV_2Mo_{10}O_{40}$ and $NaOH/H_2SO_4$, respectively [60,61]. Similarly, the synthesis of gluconic acid can be efficiently performed by using Au, Pt, Pd, Rh based catalysts [62–64]. Hydrogenation of glucose produces various important polyols in the presence of mono or bimetallic catalysts consisting of Ni, Pt, Pd, Ru, etc. [65–67]. Among various conversions, the dehydration of glucose to 5-Hydroxymethylfurfural (5-HMF) is considered one of the important chemical processes as well [68]. The physicochemical properties and importance of 5-HMF is discussed in details in the coming sections.

1.9 5-Hydroxymethylfurfural (5-HMF)

1.9.1 Structure and Properties

5-HMF is a multifunctional organic compound with a structure having an aromatic aldehyde, a furan ring, and aromatic alcohol. The presence of the furan ring makes 5-HMF belongs to the furan group of compounds. The ring lies on the center of furan moieties, while the formyl and hydroxyl-methyl groups are connected on the second and fifth positions [69].

The appearance of 5-HMF resembles a yellow solid substance [69]. It has a boiling point in the range of 114 to 116 ^{o}C (at 1 mm Hg), a melting point of 28 to 34 ^{o}C, and a density of 1.243 g mL^{-1} (at 25 ^{o}C). It is highly hygroscopic and is highly soluble in water.

One of the ideal routes of producing 5-HMF is from real biomass through a one-pot conversion technique. In the first step of 5-HMF synthesis from biomass, starch and cellulose in biomass undergo hydrolysis to glucose in the presence of a Bronsted acid catalyst. Next, glucose is isomerized into fructose by a Lewis acid catalyst followed by subsequent dehydration of fructose to 5-HMF by a Bronsted acid catalyst (Figure 1.9) [70]. Real biomass, whether edible or non-edible, and food wastes are sustainable substrates for upgradation to 5-HMF.

1.9.2 Important Applications

Because of the multifunctional characteristics of 5-HMF, it has exceptional chemical reactivity and is highly susceptible to many chemical reactions. These properties of 5-HMF make it a suitable platform molecule for a number of value-added product synthesis (Figure 1.9). The US Department of Energy (DOE) has listed 5-Hydroxymethylfurfural (5-HMF) as one of the promising platform compounds for the production of fuel and fine chemicals [11].

Selective oxidation of 5-HMF can produce important derivatives such as 2,5-diformylfuran (2,5-DFF), 2,5-furandicarboxylic acid (2,5 FDCA) etc. These derivatives found important applications in the synthesis of drugs, polymeric materials, and fungicides [71]. Hydrogenation of 5-HMF to 2,5-

bis(hydroxymethyl)furan (2,5-BHF) and 2,5-dimethylfuran (2,5-DMF) is considered an important up-gradation technique of 5-HMF. These valuable derivatives of 5-HMF are required for the production of polymeric materials and are used as biofuels [72,73]. During the reaction, hydrogenation of both the furan, hydroxyl as well as the –CHO group occurs, and the selectivity of 2,5-BHF requires careful control of the reaction [73].

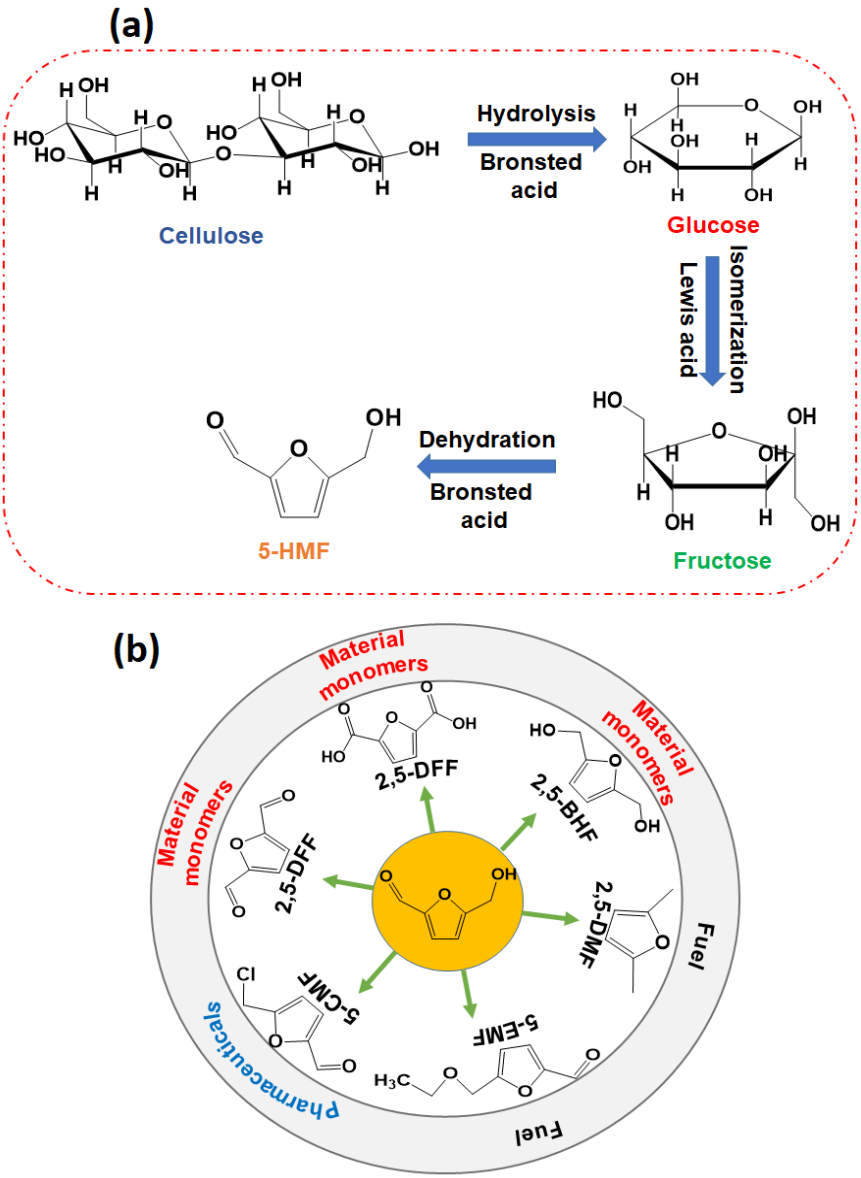

Figure 1.9. (a) Synthesis route of 5-HMF and (b) conversion routes and applications of 5-HMF derivatives.

Ether derivatives of 5-HMF can be obtained by the condensation reaction of 5-HMF with alcohols. Upon reaction with methanol, 5(methoxymethyl)furan-2-carbaldehyde, an important derivative of 5-HMF can be obtained [74]. The hydrolysis of the furan ring of 5-HMF producees a highly demanded industrial chemical called levulinic acid (LA). LA and its derivatives are known for their application for the synthesis of polymers, fuel, and fuel additives [75]. Other derivatives such as 5-chloromethylfurfural (5-CMF), maleic acid, maleic anhydride, etc. are used in various important industrial applications. It is clear that 5-HMF serves as an important building block for many value-added chemical and fuel synthesis. However, to unleash the potential of 5-HMF, sustainable large-scale synthesis of the compound is important. Developing efficient catalytic systems in compliance with the reaction chemistry of 5-HMF synthesis from different raw materials and coupling the system with the reactor configuration is a key challenge for its sustainable synthesis.

Chapter 2

Literature Review and Objectives

2.1 Glycerol Conversion to Glycerol Carbonate

Verities of catalytic systems including enzymes, homogeneous, and heterogeneous catalysts were developed and studied for the glycerol conversion to glycerol carbonate. Each catalytic system has its advantages and disadvantages that overall influenced the final efficiency of the process. All these catalytic systems are discussed in detail in the upcoming sections.

2.1.1 Catalytic Systems: Enzyme Catalysts

Enzymes have been widely used for glycerol transesterification with dimethyl carbonate (DMC) for GC synthesis (Table 2.1). Lipase as catalysts was among the various enzymes that have been particularly used for the GL transesterification and have produced considerable results. The state of enzymes for the transesterification are free or could be used by immobilizing on various supports.

Aspergillus niger in the free state was reported to produce a GL conversion of 74% and a GC yield of 59.3% when the transesterification reaction was performed at 60 ^{o}C for 4 h and with GL to DMC molar ratio of 1:10 [76]. However, when the enzyme was used in a cross-linked state with magnetic nanoparticles via glutaraldehyde, a slight decrease in GL conversion (61%) and GC yield (55%) was observed at the same reaction conditions [77].

Solvents also have a vital role in the transesterification of GL towards GC in the presence of enzymes. Previously reported experiments on the effect of various solvents had revealed a better reaction efficiency for DMC as compared to diethyl carbonate (DEC) and dibenzyl carbonate (DBC) [78]. In the presence of magnetic nanoparticles supported lipase, DMC produced approximately 45% GL conversion,

whereas only 3.4% and 0.1% conversion were obtained by DBC and DEC, respectively. Besides solvents, the impurities present in crude glycerol could also affect the activity of the enzyme. Methanol and water, which are impurities usually found in crude glycerol obtained from waste sunflower oil, produced 27% of GL conversion compared to 36% when commercial GL was used in the presence of *Aspergillus niger* [78].

Among other enzymes, *Candida antarctica lipase B* supported on Novozyme 435 was able to produce a high GC yield close to 97%, however, at a high reaction time of 48 h [79]. The same enzyme was also reported in the presence of an additional solvent tert-butanol where it was able to produce close to 100% GL conversion at GL/DMC molar ratio of 1:10 and reaction time of 12 h [79].

Besides the direct synthesis of GC from GL, various enzymes were used during the direct extraction-transesterification reaction involving microalgae *Botryococcus sp.* and microalgae *Chlorella sp.* KR-1 with DMC to produce a certain quantity of GC [80]. A GC yield of 1.9% was obtained from the direct transesterification of microalgae Botryococcus sp. and the yield slightly increased to 2.7% with ultrasound exposure [80].

These results of using enzymes as catalysts for the transesterification of GL to GC suggests that a reasonable GL conversion and GC yield could be obtained, however, at a high reaction time and a high molar ratio of DMC to GC. It is also clear that few additional solvents such as tert-butanol are necessary to improve the process efficiency. In many cases, the enzymes need to be immobilized on effective support for improving their activity for the GC synthesis process. These factors of using enzymes as catalysts for GL transesterification impede the industrial feasibility of the process and need significant attention for enhancing the activity of enzymes to make the process sustainable.

Table 2.1. Experimental conditions for the GL transesterification under various enzymes.

Catalyst	Solvent	Reaction conditions	GL conversion (%) /GC yield (%)	Ref.
Aspergillus niger	DMC	60 ^{o}C, 4 h	74.0/59.3	[76]
	DMC		61.0/55.0	
Magnetic nanoparticles attached lipase	DMC	60 ^{o}C, 6 h	45/-	[78]
Magnetic nanoparticles attached lipase	DMC	60 ^{o}C, 6 h	27%/-	[78]
Candida *antarctica lipase B* supported on Novozyme 435	DMC	70 ^{o}C, 48 h	-/97.0	[79]
Candida antarctica lipase B supported on Novozyme 435	DMC	70 ^{o}C, 12 h	100/-	[81]

2.1.2 Catalytic Systems: Homogeneous Catalysts

Although there exist numerous drawbacks such as high cost, reactor corrosion, and difficulty in separation of using homogeneous catalysts for a chemical process, they often produce a high selectivity of the desired product. There have been a few homogeneous, both acidic and basic catalysts reported for GC synthesis by transesterification of GL (Table 2.2) [82–84].

Basic homogeneous catalysts such as KOH, NaOH, and K_2CO_3 were successfully used for the GC synthesis through the transesterification route [84]. It was observed that GL conversion and GC yield, both as high as 100%, could be obtained by using the KOH and K_2CO_3 catalysts. For the NaOH catalyst, these values could reach as close to 99%. When compared with few acidic homogeneous catalysts such as H_2SO_4 and p-toluenesulfonic acid, considerably higher conversion and yield were obtained for the basic catalysts [84]. Under the same parametric conditions, the GL conversion and GC yield for H_2SO_4 was 10.6% and 3.5%, respectively. A slightly better GL conversion (19%) and GC yield (4.3%) was observed for the p-toluenesulfonic acid catalyst. Moreover, the reaction of GC synthesis under H_2SO_4 is kinetically controlled thus, demand a higher reaction time. It was also observed in the study reported by Ochoa-Gomez et al. [84], where an increased reaction time of 24 h produced a higher GL conversion of 94.5% as compared to only 10.6% at 1.5 h.

Homogeneous catalysts with facile separable characteristics and high selectivity are favorable for the sustainable GC synthesis. Triethylamine is a suitable candidate having such properties due to which it was explored for the GL transesterification to produce GC [83]. It was observed that high temperature and high trimethylamine/GL ratio enhanced the reaction rate, however, at the expense of the GC selectivity. A high trimethylamine/GL ratio could result in a further transesterification of GC to glycerol dicarbonate. It was also proposed that the formation of glycerol dicarbonate could be avoided by stopping the conversion of GL below 100%. However, this could further require additional steps, such as an extraction process for purifying the GL and GC mixture, which impacts the economy of the overall process. In addition, trimethylamine at a high temperature of the reaction could also produce another by-product glycidol. As suggested, a high

temperature (90^{o} C) favors the deprotonation of the hydroxyl moiety of GC by the trimethylamine and form a nucleophile 1,3-dioxolan-2-one-4-methoxide. The negatively charged oxygen in the formed nucleophile then attacks the carbon atom in the ring that produces 2,3-epoxy-1-prpanolate, another intermediate, which is finally converted to glycidol by reacting with the conjugated acid of triethylamine.

Table 2.2. Experimental conditions for the GL transesterification under various homogeneous catalysts.

Catalyst	Solvent	Reaction conditions	GL conversion (%) /GC yield (%)	Ref.
Triethylamine	DMC	88 ºC, 2.5 h	99.0/98.0	[83]
KOH	DMC	75 ºC, 1.5 h	100/100	[84]
NaOH	DMC	75 ºC, 1.5 h	98.9/98.5	[84]
K_2CO_3	DMC	75 ºC, 1.5 h	100/100	[84]
H_2SO_4	DMC	75 ºC, 1.5 h	10.6/3.5	[84]
p-tolunesulfonic acid	DMC	70 ºC, 48 h	19.0/4.3	[84]

2.1.3 Catalytic Systems: Heterogeneous Catalysts

2.1.3.1 Alkaline Earth Metal Oxides

Alkaline earth metal oxides are a group of heterogeneous catalysts with strong basic properties and appreciable catalytic stability. The strong basic sites on the surface of alkaline earth metal oxides create a suitable environment for activating GL molecules, which then further react with dialkyl carbonates to produce GC. The conversion of GL and selectivity of GC strongly depends on the characteristics of the basic sites on the metal oxides, which can be tuned by adopting appropriate synthesis procedures.

Calcium oxide (CaO) is an alkaline earth metal oxide that has been explored very widely for the transesterification of GL to synthesize GC (Table 2.3). The reaction rate of GL transesterification has been correlated with the basic strength of metal oxides, where oxides with higher basic strength were found more active for the process. In the uncalcined state, between CaO, MgO, and $CaCO_3$, the highest GL conversion of 74.4% was observed for CaO, followed by MgO (12% GL conversion) and $CaCO_3$ (>5% GL conversion) [84]. The decreased activity order was according to the decreased basic strength of these metal oxides. The mechanism of the GL transesterification is based on the deprotonation of the primary hydroxyl group of GL followed by subsequent nucleophilic reactions with the carbonyl carbon of dimethyl carbonate [84]. The basic strength of $CaCO_3$ is not so high to abstract a proton from the primary –OH group of GL, leading to a low reaction rate.

Calcination was also found to have a significant impact on the catalytic activity for the GL transesterification. The CaO catalyst in the calcined state (900 ^oC) tended to achieve higher GL conversion (94.1%) as compared to only 74.4% in the uncalcined state [84]. A similar enhancement in catalytic activity could be found for the calcined $CaCO_3$ (900 ^oC) where the GL conversion increased from >5% to 91.5% [84]. It is observed that these Ca-based catalysts are not very stable, due to which the activity decreased significantly during reuse. In an effort to reveal the deactivation reason, Li and coworkers studied the mechanism of calcium oxide, calcium methoxide, and calcium hydroxide catalyst for the GL transesterification [85].

Modification in the calcium-based catalysts composition to the basic calcium carbonate ($Ca_x(OH)_y(CO_3)_z$) upon interaction with GL and GC was the reason depicted for the low catalytic activity during reuse [85].

A more detailed investigation on the GL transesterification mechanism was performed by isolating the homogeneous Ca species from the reaction mixture [85]. The study revealed a different form of Ca species $Ca(C_3H_7O_3)(OCO_2CH_3)$, which was supposed to form due to the interaction of CaO with GL and DMC. The species was very active for the transesterification of GL and on further interaction (nucleophilic substitution) with the intermediate molecules produce GC.

Catalysts derived from wastes and other favorable natural resources have captured significant attention in concern to the deteriorating environment through the use of hazardous chemicals. CaO is found as a rich source in eggshells, cockle shells, and golden apple snail shells. Roscaht et al. [85] used these sources of calcium after a few pre-treatments of cleaning, drying, size reduction, and calcination (800 ^oC) for the GL transesterification process. GC yield of as high as 92% was observed for the cockle shells catalyst. It was observed that besides the basic strength, the catalyst surface area also had a linear impact on the GL transesterification activity.

Stable catalytic stability is a desired feature of using the heterogeneous catalyst for chemical processes. CaO as a heterogeneous catalyst has very low stability and tend to produce low activity during reuse for the GL transesterification. Efforts to enhance the catalytic stability of CaO include modifying its surface properties through incorporating other metals such as K and Li [86,87]. KNO_3 doped on CaO through a dry impregnation technique has significantly contributed to the catalytic stability of CaO with close to 95% of GL conversion obtained during the 5^{th} reuse condition [86]. Similar stability enhancing properties of LiCl on CaO was observed with close to 80% GC yield achieved at 5^{th} use as compared to only 43.1% for CaO [87]. Enhancement in basicity after K and Li loading and decreased leasing of active components was the reason for achieving higher stability of these catalysts during reuse.

Extruded CaO catalyst prepared using activated alumina binder and polyacrylamide pore-forming agent could result in a significant increase in stability of CaO [88]. The CaO/Al_2O_3 mass ratio of 3:1 calcined at 800 ^oC produced 90.5% GC yield under mild reaction conditions. The catalyst could produce a GC yield of 62.53% at the 5^{th} recycle, which was far greater than the CaO catalyst. The extruded catalyst had high mechanical strength, higher surface area, and larger pore volume that contributed significantly towards its activity and stability.

Apart from CaO, MgO has been extensively explored for the transesterification of GL. Various MgO based catalysts have been able to produce a low to moderate yield of GC [55,89]. However, in most cases, the catalytic activity of MgO based catalysts are low as compared to the CaO based catalysts, which could be mainly due to the low basic strength of MgO than CaO. The preparation techniques have a strong influence on the physical and chemical properties of MgO, including the basic characteristics and, thus, the catalytic activity [55,90].

MgO catalysts prepared with different procedures such as direct calcination of Mg precursor, precipitation technique, and surfactant-assisted preparation have been tested for the GL transesterification [89]. It was observed that MgO prepared with surfactant-assisted method possessed the highest basic strength as compared to other two and hence, produced the highest GC yield of 75.4%. The surfactant used enhanced the formation of low coordination O^{2-}, which increased the basicity and basic strength of MgO compared to others. However, the catalyst had low stability, due to which a continuous decrease in GC yield was found with number of uses.

Catalysts with a high surface area are desired for more favorable catalytic activities. MgO catalysts with different morphologies such as spherical, rod-like, flower-like, nest-like, and trapezoidal could be obtained by varying the reaction temperature and stirring time during precipitation [55]. These MgO catalysts possessed different surface areas and basicity, which ultimately affected their catalytic performance for the GL transesterification. Interestingly, MgO catalyst with trapezoidal morphology having low specific surface area and weaker basic sites exhibited superior catalytic activity for the GL transesterification than others. A

higher GC yield of more than 99% was observed for this particular MgO catalyst as a result of the bigger crystallite sizes and fewer Mg vacancies besides the low surface area and weaker basicity characteristics.

Zeolitic imidazolate framework-8 (ZIF-8) with favorable surface sites and microporous nature has been found as appropriate support for the deposition and growth of MgO nanoparticles [91]. A high atom efficiency of MgO nanoparticles could be obtained on the surface without much distorting the structure of the ZIF-8 support by following the wet impregnation technique. The immobilization of MgO nanoparticles introduced a higher number of basic sites onto the ZIF-8 support that led to higher catalytic activity for the GL transesterification than individual MgO and ZIF-8. An acid-base sites reaction mechanism with the ZIF-8 catalyst containing low coordinated Zn and NH groups as acidic sites for DMC adsorption and OH groups, N^- moieties along with incorporated MgO as basic sites for GL activation were proposed by Chang et al. [91].

Table 2.3. Experimental conditions for the GL transesterification under alkaline earth metal oxides.

Catalyst	Solvent	Reaction conditions	GL conversion (%) /GC yield (%)	Ref.
Trapezoidal MgO	DMC	90 ºC, 2 h	-/~100	[55]
KNO_3/CaO	DMC	70 ºC, 2 h	99.23/85.19	[86]
LiCl/CaO	DMC	65 ºC, 1 h	-/94.19	[87]
CaO/Al_2O_3	DMC	80 ºC, 2 h	95.39/90.57	[88]
Surfactant assisted synthesized MgO	DMC	90 ºC, 30 min	76.3/75.4	[89]
CaO	DMC	75 ºC, 1.5 h	94.1/91.1	[92]
MgO	DMC	75 ºC, 1.5 h	12.4/12.1	[92]
$CaCO_3$	DMC	75 ºC, 1.5 h	46.1/32.6	[92]
Na_2O	DMC	75 ºC, 30 min	95.5/92.6	[93]
ZnO	DMC	75 ºC, 30 min	0.5/0.5	[93]
CaO	DMC	75 ºC, 30 min	91.2/90.2	[93]
Cockle shells, and golden apple snail shells derived CaO	DMC	80 ºC, 2 h	-/92.1	[94]

2.1.3.2 Mixed Oxides

An undesirable property of using single metal oxide catalysts for GL transesterification is their low stability for the process. The active components of single metal oxides are easily leachable in the reaction products, which is a significant concern for its feasibility for commercialization. Mixed metal oxides with a stronger and higher density of basic sites have been prepared and utilized as a potential heterogeneous catalyst for the GL transesterification (Table 2.4). With careful tuning of the ratio of various metal compositions in the final catalyst during the preparation, desirable characteristics of the catalyst could be obtained with appreciable activity. Other factors such as precipitating agents, calcination temperature, etc., could also determine the final catalyst characteristics for the GL transesterification reaction.

The synergistic interactions between Ca and Mg mixed in a different metal proportion were evaluated, and the catalysts were used for the GL transesterification process [95]. The change in the morphology, including the textural and structural characteristics with the change in the mass ratio of metals and calcination temperature, was the key that decided the activity of the catalyst for the GL transesterification process. An enhanced basic property with high a surface area of catalyst was observed with an increase in Mg content, and an opposite was observed for increasing the Ca content. However, the basic amount of individual metal oxides was lower than the mixed oxides. Catalyst formulated with an optimum atomic composition $Mg_{1.2}Ca_{0.8}O_2$ produced the best catalytic activity with 100% GL conversion and GC yield. The catalyst was also stable, with no appreciable change in activity observed up to the 4^{th} recycle.

In an alternative to high-cost synthetic catalysts, natural dolomite after calcination at 800 ^oC was used for the GL transesterification [96]. The $MgCa(CO_3)_2$ content of dolomite was decomposed to produce CaO-MgO mixed oxides after calcination. Increased basicity and surface area obtained for the calcined dolomite was beneficial for the high conversion efficiency of the catalyst than the natural dolomite. Almost 97% GL conversion with 94% GC yield could be obtained with the calcined catalyst. Though not significant, a continuous decline in catalytic activity

was found for the calcined dolomite catalyst, which was due to the rehydration of the catalyst during reuse. However, by calcining the reused catalyst again, the initial activity was preserved.

Mixed oxide of Mg/Al/Zr with an optimized molar ratio of 3:1:1 was prepared and used for the GL transesterification with DMC [97]. The structural characteristics and basicity of the catalyst were directly influenced by the calcination temperature and molar composition of individual oxides that significantly affected the overall activity. Higher Mg content produced stronger basic sites in the catalyst with larger quantity and enhanced the conversion efficiency. A calcination temperature of 650 ^{o}C resulted in stronger basic sites, well-defined crystal particles of individual metal oxides, and the presence of active tetragonal zirconia phases that contributed to the enhanced catalytic activity. The catalyst could produce 94% of GC yield; however, no evidence of catalytic stability was presented. The promotional effect of Cu on Mg/Al mixed oxide catalyst was studied by Manikandan et al. [98]. It was mentioned that the synergistic effect of Cu^{+2} cations with the Mg/Al oxides increased the basic properties of the catalyst and produced 91.2% GC yield. The catalyst was also reasonably stable and produced almost 89% GC yield during the 5th use.

Mixed oxides of alkali and alkaline earth metals with other transition group metals have been used for the GL transesterification process [99–105]. Because of their strong basic characteristics, alkali metals are very important in imitating the GL transesterification reaction by abstracting the primary hydroxyl proton from the GL molecule. One major drawback of alkali metal oxides is their low stability, which scientists are continuously addressing through making synergistic interactions with other metals and their oxides.

Li doped ZnO catalysts prepared through wet impregnation successfully performed the GL transesterification with almost 97.4% GL conversion, and 95.8% GC yield [105]. The Li^{+} ions substituted the Zn^{+2} ions in the ZnO lattice, producing strong basic sites that improved the catalytic activity as well as the stability. Other weak and moderate basic sites were also formed through the interaction between Li^{+} and Zn^{+2} ions, but less responsible for the transesterification of GL. An almost

unchanged GL conversion was observed up to the 4th cycle of the catalyst; however, it then decreased significantly owing to the leaching of strong basic sites during the reaction. NaOH impregnated γ-Al_2O_3 possessed basic sites that were very suitable for the GC synthesis process [103]. The catalytic activity was sufficiently high that it could produce 98% GL conversion within 1 h. The decrease in catalytic activity during reuse was marginally low, suggesting appreciable catalytic stability. Other catalysts involved for the GC synthesis from GL, including KF/Al_2O_3 was also found highly active [100].

Similarly, the combination of alkaline earth metals with transition metals has been found advantageous in terms of both catalytic activity and stability for the GL transesterification process [99]. Highly dispersed MgO on ZrO_2 prepared through an evaporation induced self-assembly route was used for the GL transesterification [99]. The ordered mesoporous nature of the catalyst with stable and appropriate tetragonal Zr phases and highly dispersed MgO produced sufficient basic sites in the catalyst. High GL conversion of 96% with 88% GC yield could be obtained by this catalyst. A strong dependence of the molar ratio of Mg/Zr/Sr with its catalytic activity for GL transesterification was proposed by Parameswaram et al. [101]. An increase in Mg to Zr/Sr ratio produced increased basic sites that led to higher catalytic activity.

2.1.3.3 Mixed Oxides of Lanthanides

In a recent work by He et al., doping of Li on La_2O_3 catalyst was found to increase the basic sites in the catalyst through interaction between Li and La_2O_3 [104]. The catalyst could produce almost 95% of GL conversion with 92.1% GC selectivity. The catalyst showed considerable stability with a minor decrease in GL conversion found at the 4th cycle. Mg-La mixed oxides prepared through the co-precipitation method revealed a molar ratio of Mg/La [106], precipitating agent and calcination temperature dependence on the final catalytic activity. The catalytic activity increased with Mg content owing to the increased surface area and basic sites. After a proper optimization, the Mg3La1 calcined at 720 ^oC was found to have better catalytic activity for the GL transesterification that produced 81.3% GC yield. However, the low catalytic stability of the Mg3La1 catalyst was a major drawback of this work that needs to be addressed in the future. Similarly, Kumar and co-workers examined the

Ca/La mixed oxides for the GL transesterification, where an increase in the Ca ratio was found to have a positive effect on the basic site density as well as on the catalytic activity [107].

The catalyst preparation techniques for the lanthanide-based catalysts could also affect the activity of the catalyst for the GL transesterification. ZnO/La_2O_3 catalyst prepared by co-precipitation, combustion, and modified citrate technique suggested co-precipitation as a better technique than the other two in terms of its porosity and surface area [108]. Besides, a higher Zn molar ratio than La (Zn4La1 and Zn2La1) were found to be more suitable, with almost 98% GL conversion observed for the Zn4La1 catalyst. The decrease catalytic activity during the catalyst reuse could be eliminated by oxidizing the deposited hydrocarbons on the catalyst surface through re-calcining the used catalyst at 500 ^oC for 3 h.

Mixed oxides of Mg and Ce prepared by co-precipitation produced a better catalytic activity with the increase in Mg molar ration in the Mg/Ce oxides. Increased surface area and basic site density were the catalytic features observed with a higher Mg ratio that helped to improve the catalytic activity for the GL transesterification. The Mg3Ce1 catalyst prepared with a 3:1 molar ratio of Mg and Ce produced the best GC yield of 86% [109].

Table 2.4. Experimental conditions for the GL transesterification under various metal oxides.

Catalyst	Solvent	Reaction conditions	GL conversion (%) /GC yield (%)	Ref.
$Mg_{1+x}Ca_{1-x}O_2$	DMC	70 ^oC, 1.5 h	100/100	[95]
CaO-MgO	DMC	75 ^oC, 1.5 h	97.0/94.0	[96]
Mg/Al/Zr	DMC	75 ^oC, 1.5 h	-/94.0	[97]
MAC-0.6	DMC	90 ^oC, 1.5 h	96.4/91.2	[98]
MgO-ZrO_2	DMC	70 ^oC, 3 h	96.0/88.0	[99]
KF/ Al_2O_3	DMC	75 ^oC, 1 h	95.8/-	[100]
Mg/Zr/Sr	DMC	65 ^oC, 1 h	-/94.19	[101]
0.3KF/La-Zr	DMC	80 ^oC, 1 h	91.77/48.74	[102]
NaOH/γ-Al_2O_3	DMC	78 ^oC, 1 h	97.9/-	[103]
3.50Li/La_2O_3	DMC	85 ^oC, 3 h	94.4/92.1	[104]
Li/ZnO	DMC	95 ^oC, 4 h	97.4/95.84	[105]
Mg3La1	DMC	85 ^oC, 1 h	-/64.4	[106]
3CaLa	DMC	90 ^oC, 1.5 h	94.0/74.0	[107]
Mg3/Ce1	DMC	90 ^oC, 1.5 h	86.0/86.0	[109]
Zn4La1	DMC	150 ^oC, 80 min	97.3/-	[110]

2.1.3.4 Hydrotalcite/Layer double hydroxide (LDH) based catalysts

Hydrotalcites, also known as layered double hydroxides, are a type of anionic basic clay having basic formulas of $(M^{+2}_{1-x}\ M^{+3}_{x}(OH)_2)^{x+}(A_{x/n})^{n-}.yH_2O$. M^{+2} and M^{+3} are divalent and trivalent metals, respectively, and A^{n-} are layered n-valent anions. Upon calcination of the hydrotalcite, the corresponding mixed oxides, as well as hydroxides, could be obtained with the characteristics of both Lewis and Bronsted acids. These hydrotalcite based mixed oxides and hydroxides have wide applications in various industrial processes.

Hydrotalcite type LDH have been widely used for the GL transesterification to synthesize GC (Table 2.5) [100,111–119]. An Mg/Al mixed oxide with tuneable basicity obtained by the calcination of hydrotalcite-like LDH was used for the GL transesterification [115]. The catalytic activity strongly depended on the ratio of Mg/Al and the calcination temperature of the hydrotalcite. High basicity of the Mg/Al mixed oxides was observed with a Mg to Al molar ratio of 2:1 and calcination temperature of 600 ^{o}C. Uncalcined Mg/Al hydrotalcite prepared by the co-precipitation procedure was used for the GL transesterification [117]. The catalyst consisted of high surface area hydromagnesites, the basic site density of which could be enhanced with increasing Mg molar percentage. By using this catalyst, a GC yield as high as 98% was reported by Takagaki et al. [117].

Activation of hydrotalcite-like material by calcination and by subsequent calcination and ultrasound-assisted rehydration had different catalytic properties for the GL transesterification [119]. It was proposed that the total surface area and basic sites had no linear relationship with the activity of the hydrotalcite based catalyst. Instead, it strongly depended on the types of basic sites. The better catalytic activity of the calcined followed by ultrasound-assisted rehydrated Mg/Al catalyst was attributed to the presence of Bronsted basic sites having better proton abstracting capacity from alcohol. On the other hand, the non-rehydrated catalyst mainly consisted of Lewis basic sites with less catalytic activity.

Hydrotalcites with certain modifications such as doping on active catalytic supports or using as supports for other active agent doping have been done to enhance

their catalytic activity and stability for the GL transesterification [100,111–113,118,120,121]. Mg/Al hydrotalcite supported on carbon nanofibers produced 300 times superior activity than the bulk hydrotalcite catalyst for the GL transesterification with diethyl carbonate (DEC) [111]. However, the rehydration of hydotalcite in this study resulted in decreased catalytic activity because of the presence of large water content in the catalyst. Almost complete GL conversion could be obtained by the carbon nanofiber supported hydrotalcite with minimal decrease in catalytic activity up to the 3rd use. Mg/Al (2:1) supported on hexagonal mesoporous silica containing both acidic and basic catalytic sites could produce a GL conversion of 84.7% [113]. The hexagonal mesoporous silica used as support helped in increasing the catalytic thermal stability, surface area and provided sites for the adsorption of aromatic molecules during the reaction.

Transition metal cations doped hydrotalcites with tunable basic properties were developed for the GL transesterification to GC. The types of metal cations and the activation temperature had a significant effect on the overall catalytic activity. Among a series of metal cations Cr^{+3}, Mn^{+2}, Fe^{+3}, Co^{+2}, Ni^{+2}, Cu^{+2}, and calcined Zn^{+2}, Ni^{+2} impregnated hydrotalcites was more effective owing to its superior basic site density [120]. Although the catalyst produced considerable activity during reuse, the value of GC yield (55%) at the fresh use was significantly less than other alkali or alkaline earth metal-based catalysts. Other researches on the use of modified hydrotalcite such as fluorinated Mg/Al hydrotalcite and Ca doped hydrotalcite have been successfully prepared and used for the GC synthesis [122,123].

Table 2.5. Experimental conditions for the GL transesterification under hydrotalcite/LDH catalysts.

Catalyst	Solvent	Reaction conditions	GL conversion (%) /GC yield (%)	Ref.
CHT-F	DMC	110 ^{o}C, 3 h	100/95.3	[100]
HT-CNFrl	DEC	130 ^{o}C, 8 h	99.0/96.0	[111]
HTr2-Alpha	DEC	130^{o}C, 3 h	99.7/-	[112]
Al:Mg(1:2)	DMC	170 ^{o}C, 2.5 h	84.7/-	[113]
$LiNO_3/Mg_4AlO_{5.5}$	DMC	80 ^{o}C, 1.5 h	100/96.28	[114]
LDO2	DMC	100 ^{o}C, 2 h	-/66.0	[115]
Ca-HT	Propylene carbonate	80 ^{o}C, 5 h	67.0/66.0	[118]
HTr4	DMC	130 ^{o}C, 10 h	98.0/65.0	[119]

2.1.4 Miscellaneous Catalysts

Many other inorganic base catalysts and organocatalysts were developed for the GL transesterification process (Table 2.6) [122–130]. Sodium silicate catalyst with medium basicity was found very appropriate for the high GC yield [126]. The calcination temperature strongly influenced the basic characteristics of sodium silicate with a higher density of strong basic sites obtained at calcination temperature greater than 200 ^{o}C. The strong basic sites decreased the GC yield and enhanced the by-product formation. The effect of microwave irradiation on the catalytic activity of calcined sodium silicate was studied by Wang et al. [123]. A thorough experiment on the microwave-assisted GL transesterification revealed a power constant mode operation of microwave more effective than the constant temperature mode for the GC synthesis. Almost a similar GC yield (~94%) was observed under a relatively low reaction time and low catalyst requirement under constant mode than the constant temperature mode.

Small crystallites of $NaAlO_2$ microspheres with strong basic properties obtained by a one-pot spray drying route were found very active and stable for the GL transesterification process [129]. A GC yield as high as 94% could be obtained by using this catalyst. The low catalytic activity of Mg/Al mixed oxides was improved by promoting a small quantity of $NaAlO_2$ on it [128]. The $NaAlO_2$ promoted Mg/Al oxides showed an improved basic characteristic with an increased GL conversion of 94% and GC selectivity of 100%. The catalyst was truly heterogeneous with considerable stability for the GL transesterification process. Various zeolite-based catalysts such as fly ash derived K-zeolite and Li-oil palm ash zeolite has been found very effective for the GC synthesis [122,130]. Besides this, other inorganic base catalysts such as cinoptilolite, $BaCO_3$/C, $K_2Mg(SiO_4)$, Ni/METS-10, etc. were successfully used for the GC synthesis by the GL transesterification route.

A few organocatalysts based GL transesterification have been reported earlier [124,125,127,131]. Among them, amines as organic base catalysts both in homogeneous and heterogeneous forms were used for GC synthesis [124,127,131]. DABCO (1,4-diazabicyclo (2.2.2 octane)) as a homogeneous organocatalyst showed

though not very high, but a reasonable activity for the GC synthesis [131]. The drawback of catalyst recovery of homogeneous DABCO was eliminated by converting it into heterogeneous form by anchoring it with Merrifield resign, which was named as [p-DABCO]Cl [131]. A GC yield as high as 92.5% could be obtained by using the [p-DABCO]Cl catalyst with a minimum loss in catalytic activity up to the 5^{th} cycle. Besides this, DABCO embedded porous organic polymer has been used as a heterogeneous organocatalyst with appreciable GC yield up to the 13^{th} use of the catalyst [127]. The high surface area, basic sites, and amphiphilicity of the catalyst obtained through optimizing the divinylbenzene/DABCO monomer ratio were responsible for the high catalytic activity. Among other organocatalysts, N-heterocyclic carbene (NHC) was successfully reported for the GC synthesis process [125,132].

Table 2.6. Experimental conditions for the GL transesterification under miscellaneous catalysts.

Catalyst	Solvent	Reaction conditions	GL conversion (%) /GC yield (%)	Ref.
K-zeolite	DMC	75 ^{o}C, 1.5 h	100/96.0	[122]
Na_2SiO_3	DMC	95 ^{o}C, 15 min	96.7/94.3	[123]
DBU	DMC	40 ^{o}C, 1 h	90/-	[124]
N-heterocyclic carbenes	DMC	Room temperature, 20 min	-/95.7	[125]
Na_2SiO_3-200	DMC	75 ^{o}C, 2.5 h	97.8/95.5	[126]
10 SAHT	DMC	90 ^{o}C, 10 min	-/~58.0	[128]
$NaAlO_2$ microsphere	DMC	90 ^{o}C, 30 min	-/94.0	[129]
Li-OPAZ	DMC	70 ^{o}C, 1.5 h	100/98.1	[130]
[p-DABCO]Cl	DMC	80 ^{o}C, 1 h	69.8/68.5	[131]

2.2 5-HMF Synthesis

2.2.1 Catalytic Systems: Conventional Heating

A number of catalytic systems, including both the homogeneous and heterogeneous acidic catalysts, have been reported for the 5-HMF production from real biomass and biomass derived carbohydrate compounds. The multiple advantages of heterogeneous catalysts such as easy separation, recyclability, low corrosion, inexpensive nature, and high selectivity make them more suitable over homogeneous catalysts. Besides, the heterogeneous acidic catalysts, through the transfer of protons and electrons, could accelerate the chemical processes. Hence, the use of heterogeneous catalysts for the 5-HMF synthesis from various carbohydrates has been given importance in this research.

Besides various catalysts and raw materials, the solvents used for the 5-HMF synthesis have significant roles in the 5-HMF selectivity and yield. Aqueous, organic-aqueous mixture and ionic liquids as various solvents have been studied extensively for the 5-HMF synthesis in the past few decades. The organic solvent or an appropriate combination of aqueous-organic solvent are found to be responsible for high selectivity and yield of 5-HMF. The reason could be attributed to the continuous extraction of 5-HMF from the aqueous phase to the organic phase, hence, retarding its further degradation to undesired by-products [133]. On the contrary, a small percentage of water helps in the rapid dehydration of C6 carbohydrates to undesired products [133]. The various types of heterogeneous catalysts reported for the 5-HMF synthesis from carbohydrates are discussed thoroughly in the following sections.

2.2.1.1 Zeolite Based Catalysts

Zeolites are characterized as hydrated aluminosilicates of various cations with complex crystalline and large open-channel like structure. The composition of zeolites can be modified by replacing silicon atoms with various cations. The acidic characteristics of zeolites are attributed to the protons formed at the bridging –OH groups to achieve Si-OH-Al through the substation of Si^{4+} with Al^{3+} in the tetrahedra. The protons can also be exchanged with various alkali, alkaline, and transition metal cations to obtain modified zeolites with suitable efficiency for chemical processes.

Numerous zeolites based catalysts for the conversion of C6 carbohydrates to 5-HMF were reported previously (Table 2.7) [134–141]. H-ZSM-5 and Lewis acid incorporated ZSM-5 prepared by ion exchange technique was reported for the glucose dehydration to 5-HMF [135]. The incorporation of Fe and Cu enhanced the Lewis acid properties, with Cu-HSM-5 showing a slightly higher acid site. Inorganic salt, particularly NaCl, had a positive effect on the catalytic activity of H-ZSM-5. The H-ZSM-5 catalyst in the presence of NaCl at 195 ^{o}C and 30 min could achieve an enhanced yield of 42%. Under the aqueous condition, the activity of H-ZSM-5 in the absence of inorganic salt was significantly low compared to the Fe and Cu incorporated ZSM-5 owing to the absence of adequate Lewis acid sites for the 5-HMF synthesis. The salting-out effect of inorganic salts helped in modifying the partition coefficient, hence, improving the 5-HMF extraction from the aqueous phase to the organic phase. Dealuminated H-mordenite with different Si/Al ratios were tested for the 5-HMF synthesis from fructose [137]. The total acidity and structure of the catalyst were found to have a significant effect on the efficiency of the 5-HMF synthesis process. A Si/Al ratio of 11 and low mesoporous volume helped achieve higher fructose conversion and 5-HMF selectivity. The organic phase methyl isobutyl ketone (MIBK) enhanced the selectivity of 5-HMF approximately by 10% as compared to the aqueous phase. The catalyst at 165 ^{o}C and 90 min, under the water/MIBK volume ratio of 1:5, could produce a fructose conversion of 87% with a 5-HMF yield of 74%. In an effort to enhance the 5-HMF yield from fructose by continuous removal of water produced during the reaction, Shimizu et al. reported almost 97% 5-HMF yield at 120 ^{o}C and 2 h under dimethyl sulfoxide (DMSO) solvent [134]. The removal of water suppressed the undesired rehydration of fructose to levulinic acid (LA) and formic acid (FA), enhancing the overall 5-HMF yield.

Zeolites as catalysts with enhanced acidic characteristics, improved efficiency, and hydrothermal stability prepared by modifications such as incorporating active metals, sulfates, phosphates, etc., were reported for the 5-HMF synthesis. For instance, the Sn incorporated Beta zeolite (Sn-Beta zeolite) further treated with NH_4F (SN-Beta-F) was found as a hydrothermally stable catalyst for the 5-HMF synthesis from glucose and fructose [140]. Due to the lack of appropriate

Bronsted acid sites, the Sn-Beta-F was suitable mainly for the glucose isomerization to fructose. With HCl used with the SN-Beta-F catalyst, an enhanced 5-HMF yield of 53% was observed at 190 ^{o}C and 70 min under the tetrahydrofuran (THF)/water volume ratio of 3:1. Modified zeolite ([Sn, Al-Beta]) synthesized by partial dealumination of zeolite followed by Sn incorporation was observed to have enhanced Lewis acid characteristics than the dealuminate Beta zeolite [141]. The presence of Bronsted acid sites along with enhanced Lewis acid sites was beneficial for high catalytic efficiency for the glucose conversion to 5-HMF. The 5-HMF yield of 32% 5-HMF at 160 ^{o}C and 5 h, under the water/DMSO solvent, could be observed with appreciable stability by using the [Sn, Al-Beta] catalyst.

The effect of various organic solvents on the 5-HMF yield was tested by Ordomsky et al. over ZSM-5 catalyst [136]. The presence of organic solvent MIBK significantly improved the 5-HMF selectivity through rapid absorption of 5-HMF in the reaction product. Additionally, MIBK interacted with the acid sites of the zeolite catalyst, replacing the 5-HMF from the catalyst pores, hence, hindering the further conversion of 5-HMF to undesired by-product humin. Lima and coworkers applied an aluminum-containing mesoporous Al-TUD-1 catalyst (Si/Al = 21) for the conversion of various carbohydrate sugars such as glucose, fructose, xylose, etc., to 5-HMF [138]. The 5-HMF yield from the hexose sugars was in the range of 17-20%, suggesting very low catalytic activity of the catalyst for the hexose dehydration. Zeolite microspheres with uniform size and hierarchical pores developed by the polymerization-induced colloid aggregation technique were observed to be highly active for the fructose dehydration to 5-HMF [139]. The catalyst could produce almost 78% 5-HMF yield from fructose. It is clear that zeolites and modified zeolites with appreciable acidic characteristics, pore size, and structures were applied for the conversion of 5-HMF from various carbohydrates. However, the catalytic efficiencies of such zeolites, particularly with carbohydrates other than fructose such as glucose and cellulose, were still average and needs continuous improvement. The inadequacy of appropriate Bronsted acid sites also a major reason for the low catalytic activity of zeolites for the direct glucose or cellulose transformation to 5-HMF. Moreover, controlled synthesis of zeolites with suitable morphology and pore characteristics is

always necessary for achieving a reasonable catalytic efficiency for the 5-HMF synthesis.

Table 2.7. Experimental conditions for the 5-HMF synthesis under zeolite catalysts.

Catalyst	Process	Solvent	Reaction conditions	Conversion (%)/5-HMF yield (%)	Ref.
H-BEA zeolite	Fructose conversion	DMSO	120 ^{o}C, 2 h	100/97.0	[134]
H-ZSM-5	Glucose conversion	H_2O	195 ^{o}C, 30 min	57.0/1.6	[135]
H-ZSM-5	Glucose conversion	NaCl-H_2O/MIBK	195 ^{o}C, 30 min	80.0/42.0	[135]
H-MOR	Fructose conversion	MIBK/ H_2O	40 ^{o}C, 2.5 h	85.0/53.0	[136]
H-Mordenite	Fructose conversion	H_2O/MIBK	165 ^{o}C, 1.5 h	87.0/~74.0	[137]
Al-TUD-1	Sucrose conversion	Toluene/H_2O	170 ^{o}C, 6 h	100/17.0	[138]
Al-TUD-1	Cellobiose conversion	Toluene/H_2O	170 ^{o}C, 6 h	98/12.0	[138]
Beta-ZMS	Fructose conversion	DMSO	120 ^{o}C, 5 h	100/~78.0	[139]
SN-Beta-F/HCl	Glucose conversion	THF/ H_2O/NaCl	190 ^{o}C, 70 min	-/53.0	[140]
Sn/Al-Beta	Glucose conversion	DMSO/ H_2O	160 ^{o}C, 5 h	/32.0	[141]

2.2.1.2 Metal Oxides Based Catalysts

Metal oxides in their raw form or after certain modifications such as functionalization with sulfates, phosphates, etc., were successfully applied for the 5-HMF synthesis from various carbohydrates (Table 2.8) [8,9,142–159]. Characteristics such as acid strength and density, morphology and pore structures, etc., were observed as the important parameters of the metal oxides that influence the 5-HMF synthesis process. Among various metals, Ti, Nb, Al, Si, Sn and Zr have been extensively studied for the 5-HMF synthesis process. Mixed oxide of ceria and niobia prepared by the co-precipitation method was used for the fructose dehydration reaction [157]. The content of Nb and Ce in the mixed oxide had a reasonable effect on the acidic characteristics and surface area of the catalyst that directly influenced the final fructose conversion and 5-HMF selectivity. Particularly, the higher Nb content in the mixed oxides led to increased acidic strength and an enhanced 5-HMF selectivity. Oxides of Nb mixed with Ti, Zr, and Ce through the evaporation-induced self-assembly technique were observed to have different acidic characteristics for the 5-HMF synthesis process [156]. The CeO_2 presence led to a higher mesoporous volume whereas, TiO_2 was observed to impart the highest acid density in the mixed oxides. The higher acid density of NbO_2-TiO_2 produced the highest 5-HMF selectivity of 39% in 7 h reaction.

Sn-mont catalyst with combined Lewis and Bronsted acid sites and appreciable surface area was found to produce appreciable glucose conversion of 98% with a 5-HMF yield of 53.5% under the THF/DMSO solvent mixture [148]. The results could be obtained at a reaction temperature of 160 ^oC, and a reaction time of 3 h. The mechanism of glucose conversion was explained by a two-step process where the SnO_2 (Lewis acid) transformed the isomerization of glucose to fructose followed by the fructose dehydration to 5-HMF over the Sn-OH (Bronsted acid). The preparation condition could have a reasonable effect on the acidic properties and the final activity of the TiO_2-ZrO_2 catalyst. Chareonlimkun et al. explained that the TiO_2-ZrO_2 catalyst prepared by the co-precipitation technique had a better activity for the 5-HMF synthesis from corncob over the sol-gel synthesis [154]. However, due to the low catalytic activity, a 5-HMF yield of 8.6% was observed from corncob at 573 K.

A relative increase in 5-HMF yield close to 15% and 30% was observed when cellulose and glucose were used as the substrate. The variation in catalytic activity with surface acidity of the WO_3-ZrO_2 catalyst and its influence on the fructose conversion to 5-HMF was demonstrated by Kourieh et al. [150]. An enhanced glucose conversion with increased WO_3 percentage was observed owing to the enhanced acidity. However, the 5-HMF selectivity was significantly influenced by the ratio of basic to acidic sites, and only increased acidity was not helpful for the 5-HMF selectivity. The higher acidity obtained beyond a WO_3 loading of 9.8 wt% led to undesired 5-HMF conversion to different by-products.

Among the various modifications of the metal oxides, sulfated forms have been successfully applied for 5-HMF synthesis. For instance, encouraging results were observed for the sulfated zirconia tested for the 5-HMF production from carbohydrates. Qi et al. prepared sulfated zirconia (SO_4^{-2}/ZrO_2) by impregnating H_2SO_4 on zirconium hydroxide [151]. The catalyst showed a promising 5-HMF yield of 72.8% at 180 ^oC and 20 min under a solvent mixture of DMSO and acetone. However, the low 5-HMF yield of 33.2% indicated a low catalytic activity under an aqueous reaction condition. The same catalyst, when used under the ionic liquid (1-butyl-3-methyl imidazolium chloride) as a solvent, produced an enhanced 5-HMF yield of 88.4% [9]. The enhanced 5-HMF yield was attributed to the additional acidic characteristics of the ionic liquid apart from the catalyst that contributed to the reaction efficiency. In previous work by Osatiashtiani et al., sulfated zirconia with tuneable acid properties was tested for the glucose transformation to 5-HMF [8]. It was mentioned that the unsulfated zirconia mostly possessed a mixture of Lewis acid and base that accelerated the glucose isomerization to fructose only. The sulfate deposition produced the necessary Bronsted acid sites, driving the fructose conversion to 5-HMF. However, excess sulfate deposition was observed to diminish the Lewis acid characteristics and led to a decreased catalytic efficiency for the 5-HMF synthesis.

Niobium phosphate and H_3PO_4 treated niobic acid were reported for fructose dehydration [145,160]. A relatively strong acidity of the active sites in the niobic phosphate produced a better fructose conversion and 5-HMF selectivity than the

H_3PO_4 treated niobic acid. Among other modifications, niobium/carbon composite with ordered mesoporous structure tested for the fructose dehydration reaction produced 76.5% 5-HMF yield [158]. A strong enhancement in Lewis acid sites in the Nb/C composite due to the presence of Nb_2O_5 was observed by Li et al., which resulted in an efficient synthesis of 5-HMF directly from glucose [152]. The Lewis acid sites from Nb and Bronsted acids of various carbon functionalities such as –COOH and –OH groups contributed to the process of glucose isomerization to fructose and fructose dehydration to 5-HMF.

Mesoporous silica with several modifications such as functionalization with organic functional groups or heteroatoms were applied for the 5-HMF synthesis. SBA-15, a type of mesoporous silica functionalized with thioether and sulfonic acid groups, effectively conducted the fructose tautomerization to the furanose form followed by its dehydration to 5-HMF [146]. The catalyst could produce a reasonable fructose conversion of 66% with a 5-HMF selectivity of 74% at 180 ^oC and 30 min. Mesoporous silica nanoparticles functionalized with acid (3-(mercaptopropyl)trymethoxysilane) and base (3-aminopropyltrimethoxysilane) groups were applied for the 5-HMF synthesis from fructose, glucose, and cellulose [149]. The 5-HMF yield of 70%, 13%, and 19.2% could be achieved by using the catalyst from fructose, glucose, and cellulose, respectively. SO_3-H functionalized SBA-15 effectively produced 81% of 5-HMF yield from fructose at 120 ^oC and 1 h under an ionic liquid [BMIM]Cl medium [142].

Montmorillonite K-10 clay modified by exchanging cation (Cr) showed promising catalytic activity for the fructose conversion to 5-HMF [153]. The catalyst at 100 ^oC and 3 h under DMSO solvent produced a 5-HMF yield of 75.7%. In a similar study by Liu et al., the K-10 clay-Al catalyst was found highly active for fructose dehydration producing 93.2% of 5-HMF yield at 120 ^oC and 3 h [144]. The Zr-MCM-550 catalyst prepared by incorporating Zr on MCM-1 silica followed by thermal treatment at 550 ^oC had an appreciable surface area (635 m^2g^{-1}) and acidity (563 µmol g^{-1}) for the direct synthesis of 5-HMF from glucose [159]. The combined Lewis acid and Bronsted acid sites of the catalyst produced 23% 5-HMF yield at 175 ^oC under

an aqueous medium. The deposition of reaction intermediates and insoluble humins during the reaction resulted in a continuous decrease in catalytic activity during reuse.

Phosphate modification of metals such as Zr, Ti, Nb, Sn, etc., was successfully carried out for the application in the 5-HMF synthesis process. The metaphosphates were found to have excellent acidic strength for the acid-catalyzed reaction, such as 5-HMF synthesis from carbohydrates. The 20 wt% Sn-VPO (vanadium phosphate) catalyst possessing both Lewis and Bronsted acid characteristics was applied for the glucose conversion to 5-HMF [147]. The catalyst showed an excellent acid site density of 7.35 mmol g^{-1} that, as a result, produced a high 5-HMF yield of 73.79% 5-HMF yield at 100% glucose conversion under DMSO solvent. The catalytic activity for the direct glucose conversion to 5-HMF was very promising as compared to the other similar synthetic catalyst. The phosphate modification of Nb produced enhanced acidity in the $NbOPO_4$, due to which the catalyst produced almost 80% fructose conversion with 30% 5-HMF selectivity [155]. The results were reasonably better as compared to niobic acid catalyst; however, relatively low as compared to other similar synthetic catalyst. Zirconium phosphate under a subcritical water reaction medium at 240 ^oC was tested for the fructose dehydration process [143]. 80% fructose conversion with a 5-HMF selectivity to 61% could be obtained in 2 min reaction time.

Table 2.8. Experimental conditions for the 5-HMF synthesis under metal oxide catalysts.

Catalyst	Process	Solvent	Reaction conditions	Conversion (%)/ 5-HMF yield (%)	Ref.
SO_4/ZrO_2	Glucose conversion	H_2O	120 °C, 6 h	42.0/-	[8]
SO_4^{-2}/ZrO_2	Fructose conversion	[BMIM]Cl	100 °C, 30 min	95.8/88.4	[9]
SO_3-H/ SBA-15	Fructose conversion	[BMIM]Cl	120 °C, 1 h	-/81.0	[142]
ZrP	Fructose conversion	H_2O	240 °C, 2 min	80.9/50.2	[143]
K-10 Clay-Al	Fructose conversion	DMSO	120 °C, 3 h	-/93.2	[144]
Niobium phosphate	Fructose conversion	H_2O	100 °C, 2 h	65.5/-	[145]
Taa-SBA-15	Fructose conversion	H_2O/MIBK/2-butanol	180 °C, 30 min	66.0/-	[146]
Sn-VPO	Glucose conversion	DMSO	110 °C, 6 h	100/73.79	[147]
Sn-mont	Glucose conversion	THF/DMSO	160 °C, 3 h	98.0/53.5	[148]
LPMSN-NH_2	Glucose conversion	[EMIM]Cl	120 °C, 5 h	-/13.0	[149]
WO_3-ZrO_2	Fructose conversion	H_2O	130 °C, 4 h	~68.0/-	[150]
SO_4^{-2}/ZrO_2	Fructose conversion	DMSO/ acetone	180 °C, 20 min	93.6/72.8	[151]
NbC-50	Cellobiose conversion	THF/H_2O/NaCl	170 °C, 8 h	~100/53.3	[152]
K-10 Clay-Cr	Fructose conversion	DMSO	100 °C, 3 h	-/75.7	[153]
TiO_2-ZrO_2	Corncob conversion	H_2O	300 °C, 5 min	-/8.6	[154]

$NbOPO_4$	Fructose conversion	H_2O	110 ^oC	~80%/-	[155]
NbO_2-TiO_2	Fructose conversion	H_2O	130 ^oC, 7 h	~76.0/-	[156]
Nb_2O_5	Fructose conversion	H_2O	130 ^oC, 6 h	~82.0/~48.0	[157]
OMCN-5	Fructose conversion	DMSO	120 ^oC, 2 h	67.5/67.5	[158]
Zr-MCM-550	Glucose conversion	MIBK/ H_2O	175 ^oC, 2.5 h	82.0/23.0	[159]

2.2.1.3 Ion Exchange Resins

The basic composition of ionic acid resins are organic insoluble crosslinked polymers of small sizes (0.25 to 0.5 mm radius). Amberlyst and Dow type resins consisting of styrene-based sulfonic acid as the polymeric resins are among the most widely used ion exchange resins for the acidic catalysis reactions. These two resins have been widely used for the 5-HMF synthesis from fructose and, in some cases, from glucose as well (Table 2.9) [134,137,161–167]. For instance, 100% fructose conversion with 100% selectivity was reported using Amberlyst-15 under the DMSO reaction medium with a continuous water evacuation facility during the reaction [134]. Sampath et al. demonstrated the deactivation of Amberlyst-15 catalyst when used with N,N-dimethylformamide resulting due to the neutralization of its basic amino group with the acidic groups of Amberlyst-15 [161]. However, with DMSO as the solvent, the catalyst produced an excellent 83% 5-HMF yield with no significant loss in activity up to the 7^{th} cycle.

In similar studies for the 5-HMF synthesis, Qi et al. and Moreau et al. reported 83% and 87% of 5-HMF yield from fructose under [BMIM]Cl and DMSO-[BMIM]BF_4 solvent by using Amberlyst-15 and H-mordenite respectively [137,167]. The activity of Amberlyst in combination with other acidic catalysts for the 5-HMF synthesis was tested. The reaction medium of N,N-dimethylformamide (DMF) at 100 ^oC could produce almost a complete fructose conversion with76% selectivity to 5-HMF by using a combination of Hydrotalcide/Amberlyst-15 catalyst [166]. Relatively low activity of the catalyst was confirmed with a glucose conversion and 5-HMF selectivity of 73% and 58%, respectively. Similarly, Amberlyst-70, in combination with Sn-β as the catalyst, an excellent 5-HMF yield of 63% was reported under tetrahydrofuran reaction medium at 130 ^oC [165].

Among various Dow types of resin, Dowex AG 50W-X8 was reported to produce 77% 5-HMF yield from fructose at 80 ^oC under the DMSO solvent; however, at a long reaction time of 25.5 h [164]. Similarly, Lewatit SPC 108 has been tested up to some extent for the 5-HMF synthesis from fructose. An approximate 5-HMF yield between 42-44% could be achieved by using the catalyst at 80 ^oC, under a

water/MIBK reaction medium [163]. Diaion PK216 resin for the dehydration reaction revealed a complete inulin conversion and 92% fructose conversion [162].

Table 2.9. Experimental conditions for the 5-HMF synthesis under ion exchange resin catalysts.

Catalyst	Process	Solvent	Reaction conditions	Conversion (%)/ 5-HMF yield (%)	Ref.
Amberlyst-15	Fructose conversion	DMSO	120 ^{o}C, 2 h	100/100	[134]
H-Mordenite	Fructose conversion	DMSO-[BMIM]BF_4	165 ^{o}C, 2 h	93.0/73.0	[137]
Amberlyst-15	Fructose conversion	DMSO	120 ^{o}C, 1 h	-/83.0	[161]
Diaion PK216	Fructose conversion	H_2O/DCM/DMSO	120 ^{o}C, 5.5 h	92.0/-	[162]
Diaion PK216	Inulin conversion	H_2O/DCM/DMSO	120 ^{o}C, 5.5 h	100/-	[162]
Lewatit SPC 108	Fructose conversion	H_2O/MIBK	80 ^{o}C	-/42.0-44.0	[163]
Dowex AG 50W-X8	Fructose conversion	DMSO	80 ^{o}C, 25.5 h	-/77.0	[164]
Amberlyst-70/Sn-beta	Glucose conversion	THF/MTHF	130 ^{o}C, 40 min	-/63.0	[165]
Amberlyst-15/HT	Fructose conversion	DMF	100 ^{o}C, 3 h	100/-	[166]
Amberlyst-15	Fructose conversion	[BMIM]Cl	80 ^{o}C, 10 min	98.6/83.3	[167]

2.2.1.4 Functionalized Carbon Catalysts

Carbonaceous species functionalized with various functional groups, in particular, -SO_3H groups have been successfully used for acid-catalyzed reactions. The highlighting characteristics of the carbon-based catalysts are high stability, easy synthesis, low cost, and the presence of strong protonic acid sites. Notably, the SO_3H functionalized carbon materials are found to have acid density equivalent to concentrated H_2SO_4 [162]. Factors such as the nature of the substrate, temperature, and the preparation procedure could affect the final properties of the carbon catalyst. Usually, carbon particles formed by the incomplete carbonization of sugars produced rigid carbon materials of small polycyclic aromatic carbons, the sulfonation of which could produce a high density of sulfonated active sites [162]. The sulfonation of carbon catalysts could be done through an *in-situ* or post-grafting approach. The post-grafting approach, which is carried out by treating the pre-synthesized carbon support with sulfonating agents to create covalently bonded SO_3H, preserves the core carbon structure and is widely used [162]. It enables the synthesis of material with different surface chemistry and a degree of SO_3H grafting.

The use of sulfonated carbon-based catalysts for the 5-HMF production from fructose substrate is reasonable, however it is scarce for the glucose and other disaccharides as substrate (Table 2.10). For instance, an excellent fructose conversion of 99% with a 5-HMF yield of 98% was obtained by the sulfonated carbon catalyst at 160 ^oC and 60 min under THF/DMSO reaction medium [168]. The catalyst showed excellent stability up to the 5^{th} use with no loss in 5-HMF yield. Sulfonated carbon nanotubes and nanofibers were found to produce excellent catalytic activity with almost complete fructose conversion for both the catalyst and 5-HMF yield of 89% and 80%, respectively [169]. However, the yield reduced to 57% and 46%, respectively, when glucose was used as a substrate, suggesting the low efficiency of the sulfonated carbon.

Similarly, Kim et al. reported a 5-HMF yield of 72% from industrially supplied fructose syrup in the presence of sulfonated carbon catalyst with ethylene glycol as reaction medium [170]. The high 5-HMF yield was attributed to the stabilization of the reversible intermediates during the fructose dehydration by

ethylene glycol. Polyurethane derived carbon modified with sulfonic groups efficiently produced a complete fructose conversion with 70.1% 5-HMF yield under 1, 4-dioxane solvent [171]. However, the catalyst was significantly less active for the 5-HMF production from glucose, due to which only a 0.1% yield of 5-HMF was observed. Recently, sulfonated graphene quantum dots as a catalyst was tested by Li et al., where a 5-HMF yield of 51.7% was observed from fructose [172]. The 5-HMF yield (19.5%) from glucose by the catalyst was significantly low, again indicating the low activity of the catalyst for glucose substrate. It was mentioned that the glucose conversion to 5-HMF proceeded by its isomerization to fructose followed by fructose dehydration to 5-HMF. A combination of Lewis and Bronsted acid sites is required for a smooth operation of these two steps. However, as the sulfonated carbon catalysts mostly possess the Bronsted acid sites and a little or no Lewis acid sites, the efficiencies for the direct glucose transformation to 5-HMF are therefore low.

In effort to enhance the catalytic efficiency of sulfonated carbon catalysts, a few studies were performed by introducing Lewis acid sites in the sulfonated carbon catalysts for glucose transformation to 5-HMF. For instance, Zhang et al. applied Al and Ti modified sulfonated carbon catalyst, where an appreciable 5-HMF yield of 57.36% was observed at 130 ^{o}C and 5 h [173]. The enhanced Lewis acid sites in the sulfonated carbon due to the Ti and Al modification was the reason for the high 5-HMF yield. Similarly, niobia/carbon composite without any sulfonic groups produced 25.5% 5-HMF yield from glucose at 160 ^{o}C and 2 h [152]. Though the catalyst did not have the Bronsted acid characteristics of sulfonic groups, the functionalities of carbon such as –OH and –COOH was mentioned to act as Bronsted acid sites during the reaction. However, the low catalytic activity indicated the lack of appropriate Bronsted acid sites in the catalyst required for the 5-HMF synthesis from glucose. Under the ionic liquid ([BMIM]Cl) the sulfonated carbon catalyst derived from the corn stalk was found to produce a reasonable 5-HMF yield of 44.1% from corn stalk at 150 ^{o}C and 30 min [174].

Table 2.10. Experimental conditions for the 5-HMF synthesis under functionalized carbon catalysts.

Catalyst	Process	Solvent	Reaction conditions	Conversion (%)/ 5-HMF yield (%)	Ref.
Nb/C-50	Glucose conversion	NaCl/ H_2O/THF	160 ^oC, 2 h	43.9/25.5	[152]
GTS	Fructose conversion	THF/DMSO	160 ^oC, 1 h	99.0/98.0	[168]
CNT-PSSA	Fructose conversion	DMSO	120 ^oC, 30 min	>99.0/89.0	[169]
CNF-PSSA	Fructose conversion	DMSO	120 ^oC, 30 min	>99.0/80.0	[169]
AC-SO_3H	Fructose conversion	Ethylene glycol	120 ^oC, 4 h	-/72.0	[170]
Pu-cat	Fructose conversion	1, 4-dioxane	140 ^oC, 2 h	100/70.1	[171]
Pu-cat	Glucose conversion	1, 4-dioxane	140 ^oC, 2 h	100/0.1	[171]
SGQDs	Fructose conversion	DMSO/ H_2O	170 ^oC, 2 h	91.8/51.7	[172]
SGQDs	Glucose conversion	DMSO/ H_2O	170 ^oC, 2 h	45.1/19.5	[172]
Al-Ti@SCHOP	Glucose conversion	DMSO	130 ^oC, 5 h	-/57.36	[173]
HCSS	Corn stalk conversion	([BMIM]Cl)	150 ^oC, 30 min	-/44.1	[174]
TiO_2C_S	Fructose conversion	DMSO	120 ^oC, 1 h	-/95.0	[175]
S-TsC	Glucose conversion	GVL/ H_2O	180 ^oC, 30 min	~95.0/43.8	[176]

2.2.1.5 Heteropoly Acids

Heteropoly acids are a class of acidic catalysts composed of hydrogen, oxygen, metals, and non-metals with unique physico-chemical properties. Due to the excellent Bronsted acid characteristics of heteropoly acids, they have been used for the 5-HMF synthesis from various carbohydrates (Table 2.11). $H_3PW_{12}O_{40}$, one of the most common types of heteropoly acid, was reported to produce 95% of 5-HMF yield from fructose at 120 ^oC and 2 h under DMSO solvent [134]. The same catalyst produced 80% 5-HMF yield from fructose at a low reaction temperature of 80 ^oC and 1 h reaction time under ionic liquid [EMIM]Cl as the reaction medium [177]. However, with glucose as the substrate, the catalytic activity reduced to a significant extent, and only 8% of 5-HMF yield was obtained.

$H_3PW_{12}O_{40}$ modified with various metals such as Cs ($Cs_{2.5}H_{0.5}PW_{12}O_{40}$), and Fe ($FePW_{12}O_{40}$) was reported to produce an excellent 5-HMF yield of 91% and 97%, respectively from fructose [134]. The high 5-HMF yield was achieved with a continuous evacuation of water produced during the reaction. Among other modifications, the Ag exchanged silicotungstic acid ($Ag_4[Si(W_3O_{10})_4].nH_2O$) under superheated water reaction medium produced 86% of 5-HMF yield [178]. In a recent study, Song et al. modified the $H_3PW_{12}O_{40}$ with metals such as Cs, Ce, Zn, Cu, and Ni for the fructose dehydration reaction [179]. Among various metal modifications, $H_3PW_{12}O_{40}$ modified with Ce was reported to produce better catalytic activity with 98.15% 5-HMF yield at 158 ^oC and 2 h. For other metals, the 5-HMF yield remained in the range between 80-90%. Though an appreciable 5-HMF yield could be achieved with various heteropoly acids, the low stability of these catalysts due to the leaching of the active components is a serious issue for their sustainable large-scale application.

Table 2.11. Experimental conditions for the 5-HMF synthesis under heteropoly acid catalysts.

Catalyst	Process	Solvent	Reaction conditions	Conversion (%)/ 5-HMF yield (%)	Ref.
$H_3PW_{12}O_{40}$	Fructose conversion	DMSO	120 ^oC, 2 h	100/95.0	[134]
$Cs_{2.5}H_{0.5}PW_{12}O_{40}$	Fructose conversion	DMSO	120 ^oC, 2 h	100/91.0	[134]
$FePW_{12}O_{40}$	Fructose conversion	DMSO	120 ^oC, 2 h	100/97.0	[134]
$H_3PW_{12}O_{40}$	Fructose conversion	[EMIM]Cl	80 ^oC, 1 h	87.0/80.0	[177]
$H_3PW_{12}O_{40}$	Glucose conversion	[EMIM]Cl	80 ^oC, 1 h	63.0/8.0	[177]
$Ag_4[Si(W_3O_{10})_4].nH_2O$	Fructose conversion	H_2O	120 ^oC, 160 min	98.0/85.7	[178]
$CePW_{12}O_{40}$	Fructose conversion	*Sec*-Butanol	158 ^oC, 2 h	99.1/98.15	[179]

2.2.2 Catalytic Systems: Microwave Heating

Microwave heating in the application of various chemical reactions is growing at a rapid rate. The important advantages of microwave heating lie in the rapid and homogeneous heating of the reaction mixture due to the dielectric heating phenomenon of microwave [180]. The electromagnetic irradiation generated by the microwave causes rapid internal heating of the reactant molecules, hence, making the reactions faster than the conventional heating. Additional benefits of microwave heating over conventional heating are high product yield and high product purity [180]. A few studies were reported for the 5-HMF production from various carbohydrates by using microwave irradiation [167,181–190]. These processes were found to be very efficient in terms of low reaction time and high product yield than the conventional heating.

2.2.2.1 Homogeneous Catalysts

Various homogeneous Bronsted acid catalysts such as H_2SO_4, HCl, NH_2SO_3H, H_3PO_4, etc., and Lewis acid catalysts such as $SnCl_4$, $ZrCl_4$, $ScCl_3$, $AlCl_3$, and $CrCl_3$ were applied for 5-HMF synthesis from carbohydrates under microwave irradiation (Table 2.12) [181,182,186,187]. For instance, with HCl catalyst, a complete fructose conversion with a 5-HMF yield of 91% could be obtained in a short reaction time of 1 min at 160 ^oC under microwave heating [187]. However, the efficiency decreased for the glucose transformation to 5-HMF due to the lack of appropriate Lewis acid sites required for the isomerization step. Hence, a combination of HCl with $CrCl_3$ was used for enhancing the process efficiency of the glucose transformation to 5-HMF. Similarly, sulfamic acid (NH_2SO_3H) under reaction conditions of 180 ^oC, 40 min, and THF/H_2O reaction medium could achieve an appreciable 5-HMF yield of 53% from lignocellulosic compounds such as bamboo fibers [181].

Among various homogeneous Lewis acids, $ZrCl_4$ was reported to achieve 47.8% of 5-HMF yield from glucose under microwave heating at 400 W. The target yield was achieved at 3.5 min reaction time by using ionic liquid ([BMIM]Cl) as the reaction medium [182]. Similarly, $CrCl_3$ was found very efficient for the microwave

conversion of cellulose under the ionic liquid ([MMIm]Cl) reaction medium that produced a high 5-HMF yield of 62% within 1 min reaction time [186]. Though various homogeneous catalysts under microwave heating were found highly active for the 5-HMF synthesis, their corrosive properties, difficulty in separation and reusability, etc., are some disadvantages that discourage their sustainable commercial applications.

2.2.2.2 Heterogeneous Catalysts

The use of heterogeneous catalysts for the microwave-assisted synthesis of 5-HMF is very limited until now (Table 2.13). In a previous study, TiO_2 and ZrO_2 were used for the 5-HMF production from glucose and fructose under microwave heating [190]. Under aqueous (hot compresses water) medium, 38.1% and 30.5% of 5-HMF yield were achieved at 200 ^oC and 5 m by using TiO_2 and ZrO_2, respectively. ZrO_2 showed relatively less activity towards 5-HMF synthesis but a higher activity towards the glucose isomerization to fructose than TiO_2. Phosphates of metals such as Zr, Nb, and Sn were applied successfully for the microwave-assisted 5-HMF synthesis process [184]. For instance, Antonetti et al. reported ZrPO and NbPO for the aqueous phase fructose dehydration to 5-HMF and assessed the catalytic performance with respect to the acid characteristics [184]. As explained by the authors, NbPO was more active for the fructose conversion process though its acid density was lower compared to ZrPO. On the contrary, ZrPO had medium strength Bronsted acid sites and showed more selectivity towards 5-HMF. The strong Bronsted acid sites in NbPO enhanced the fructose conversion; however, it increased the formation of undesired heavy compounds, including humins.

SnPO was successfully used for the microwave-assisted glucose dehydration process under an ionic liquid ([EMIMBr]) reaction medium where an appreciable 5-HMF yield of 58.3% at 120 ^oC and 3 h was observed [183]. The Lewis acid sites in the Sn^{+4} were mentioned to catalyze the glucose isomerization to fructose whereas, the synergistic interaction between SnPO and the ionic liquid contributed to a high 5-HMF yield. Zr, W, and Mo Oxides and sulfates in a DMSO reaction medium were tested for the microwave fructose dehydration to 5-HMF [188]. Among various combinations, the SO_4^{-2}/WO_x-ZrO_2 produced the highest catalytic activity with

95.8% fructose conversion and 83.9% 5-HMF yield at 150 ^{o}C and 5 min. In the catalyst, the tetragonal phase of zirconia produced appropriate acidic sites responsible for the higher catalytic activity for the 5-HMF synthesis.

Ion exchange resin Amberlyst-70 used for the aqueous phase fructose dehydration process surprisingly produced a 5-HMF yield of 45.6% at 180 ^{o}C and 20 min [185]. The yield under water as the reaction medium was comparable to other highly active catalysts for 5-HMF synthesis from fructose. It was also observed that with the increase in reaction temperature, the 5-HMF yield as well as the other side products such as levulinic acid (LA) and formic acid (FA), along with other unidentified products, probably humins and other soluble polymers were increased. Dowex 50WX8 under [BMIM]Cl ionic liquid as the reaction medium produced ~95% fructose conversion with 82% 5-HMF yield at 80 ^{o}C and a low reaction time of 10 min [167].

Recently, carbon nanotubes (CNT) as catalyst support was used for preparing CNT-TiO_2 catalyst [189]. The catalyst was found to produce an appreciable 5-HMF yield of ~60% from fructose at 125 ^{o}C and 40 min. Under the same reaction conditions, pure TiO_2 produced only 18% of 5-HMF yield as compared to ~60 for the CNT-TiO_2, suggesting the positive effect of synergistic interaction between CNT and TiO_2 on the catalytic efficiency. It is clear that microwave-assisted 5-HMF synthesis processes are having advantages of low reaction time and high process efficiency than conventional heating. However, there lacks sufficient research on the use of active, efficient, and inexpensive catalysts for the 5-HMF production from glucose and other disaccharides.

Table 2.12. Experimental conditions for the 5-HMF synthesis by various homogeneous catalysts under microwave heating.

Catalyst	Process	Solvent	Reaction conditions	Conversion (%)/ 5-HMF yield (%)	Ref.
NH_2SO_3H	Bamboo fibres conversion	THF/H_2O	180 ^oC, 40 min	-/53.0	[181]
$ZrCl_4$	Glucose conversion	([BMIM]Cl	3.5 min	72.3/47.8	[182]
$CuCl_2$	Glucose conversion	([BMIM]Cl	3.5 min	69.4/30.3	[182]
$MnCl_2$	Glucose conversion	([BMIM]Cl	3.5 min	51.5/24.7	[182]
$CrCl_3.6H_2O$	Cellulose conversion	[C_4mim]Cl	400 W, 2.5 min	-/62.0	[186]
$CrCl_3.6H_2O$	Rice straw conversion	[C_4mim]Cl	400 W, 3 min	-/45.0	[186]
HCl	Fructose conversion	H_2O/MeCN/KBr	160 ^oC, 1 min	100/91.0	[187]
HCl/$CrCl_3.6H_2O$	Fructose conversion	H_2O/MeCN/KBr	160 ^oC, 1 min	98.0/71.0	[187]

Table 2.13. Experimental conditions for the 5-HMF synthesis by various heterogeneous catalysts under microwave heating.

Catalyst	Process	Solvent	Reaction conditions	Conversion (%)/ 5-HMF yield (%)	Ref.
Dowex 50WX8	Fructose conversion	[BMIM]Cl	80 °C, 10 min	~95.0/82.0	[167]
NbPO	Fructose conversion	H_2O	190 °C, 8 min	97.7/32.2	[184]
ZrPO	Fructose conversion	H_2O	190 °C, 8 min	96.3/39.4	[184]
SnPO	Glucose conversion	[EMIMBr]	120 °C, 3 h	94.1/58.3	[184]
Amberlyst-70	Fructose conversion	H_2O	180 °C, 20 min	80.1/45.6	[185]
WO_x-ZrO_2	Fructose conversion	DMSO	140 °C, 5 min	67.66/53.03	[188]
MoO_x-ZrO_2	Fructose conversion	DMSO	140 °C, 5 min	61.74/47.26	[188]
SO_4^{-2}/ WO_x-ZrO_2	Fructose conversion	DMSO	140 °C, 5 min	87.52/70.88	[188]
SO_4^{-2}/ MoO_x-ZrO_2	Fructose conversion	DMSO	140 °C, 5 min	86.05/67.11	[188]
CNT-TiO_2	Fructose conversion	H_2O	125 °C, 40 min	-/~60%	[189]
TiO_2	Fructose conversion	H_2O	200 °C, 5 min	83.6/38.2	[190]
TiO_2	Glucose conversion	H_2O	200 °C, 3 min	41.6/7.68	[190]
ZrO_2	Glucose conversion	H_2O	200 °C, 3 min	48.4/6.90	[190]

2.3 Red Mud Derived Catalysts

Despite the various drawbacks, the valuable components present in RM such as Fe, Al, Si, Na, Ca, and Ti in various phases generates great opportunities for researchers to utilize this waste as catalysts for different industrial processes. The application of red mud catalysts can be categorized into different fields such as environmental, energy, and chemical synthesis.

2.3.1 Red mud based catalysts for energy and chemical synthesis

Fe in RM and other different metals, which are commonly used as active and low-cost catalysts, make it very promising for energy production through coal liquefaction, pyrolysis, and bio-oil upgrading, hydrotreating/hydrodeoxygenation, H_2 production and transesterification.

Coal liquefaction to liquid fuels is performed to meet the fossil fuel needs in many countries. RM as a catalyst for the liquefaction could be a suitable option as it was able to achieve approximately 95 to 99% liquefaction in different studies [191,192]. In recent days, pyrolysis has evolved as a promising technology for converting biomass into liquid fuels under the absence of oxygen and at mild temperature conditions [193,194]. RM, with various modifications in its physical and chemical properties, has been able to produce excellent catalytic activity for the pyrolysis process [193,194].

Hydrodeoxygenation has proven as a promising method for removing O from bio-oil through reaction with H_2 in the presence of a suitable catalyst. RM has been successfully utilized as a catalyst or as a support material for the deposition of active metals such as Pd, Pt, Ru, and Ni for the hydrodeoxygenation process [195–197]. Ni-doped RM catalyst has been found very suitable for reducing the O content almost by 95% in the bio-oil [198]. Between Pt, Pd, and Ru, Pt-based RM catalyst showed more selectivity towards hydrocarbons with low coke yield. Hydrogen is often considered an attractive alternative to conventional fossil energy because of its clean synthesis. The high cost and limited availability associated with the use of noble catalysts for H_2 production is considered as a major drawback of this process. In efforts to synthesize low-cost catalysts, RM with various modifications such as acid (HCl)

digestion, reduction by NH_3, H_2S treatment, or active metals (Ni and Ru) deposition has been successfully used for H_2 production through ammonia and methane decomposition [199–203]. Acid digestion helped in the removal of alkali contents such as Na and Ca from RM and increase in Fe content on its surface [203]. The acid digestion also improved the surface area of RM, which in result provided better dispersion of active metals such as Ru leading to better activity [203]. The amount of iron content was found to play an important role in H_2 production through ammonia and methane decomposition, with a better activity observed with higher Fe content [204,205].

RM, apart from iron as a main component, also contains some amount of Na and Ca, which make this waste suitable for biodiesel production through the transesterification process. RM modified with thermal treatment or in combination with other alkali metal catalysts has been found very effective for the high yield of biodiesel (more than 90%) [206–208]. One major drawback of the RM based catalysts is their low stability for transesterification as the alkali metals in RM are easily leached during the reaction. Further efforts are required for enhancing the stability of RM catalysts for the transesterification process and extend its catalytic application for other energy and chemical synthesis processes.

2.4 Knowledge Gaps

Besides the activity of the catalyst having a substantial effect on the efficiency of a chemical process, the cost of the catalyst plays a vital role in shaping the economy of the overall process. Hence, catalysts with sufficient activity and low-cost as two important parameters for the sustainability of a catalytic process are highly desired. From the literature survey, it is clear that there exist many heterogeneous basic catalysts with appreciable catalytic activity for the GC synthesis from GL. Particularly, the mixed oxides catalyst were found to have significant activity as well as stability for the GC synthesis through the transesterification of GL. However, a significant percentage of the active catalysts reported used commercially available metals or non-metals, the cost of which could strongly affect the overall economy of the process. Hence, finding low-cost active catalyst always remains an indespensable

research area for scientists working on catalysis. In concern, RM, which contains various metal elements, particularly Na and Ca, which could act as basic active sites, could be an option for use as a catalyst for the economic and efficient GL transformation to GC.

Similarly, other elements in RM, such as Al, Ti, and Fe, could act as Lewis acid sites for converting glucose to 5-HMF, enabling its use as an acidic catalyst. Moreover, the carbonaceous catalysts reported for 5-HMF synthesis lack Lewis acid sites in the catalyst matrix and were mostly used to convert fructose to 5-HMF. However, due to the high-cost of fructose, it is not desired as a substrate for the 5-HMF synthesis. Hence, RM could be a suitable option for preparing low-cost, effective catalysts with characteristics of Lewis as well as Bronsted acid sites for the direct transformation of glucose to 5-HMF.

2.5 Objectives

From the literature survey and knowledge gaps, the following objectives are derived,

1. Preparation and characterization of various raw RM derived catalysts and their applications for the GL transesterification to GC.

2. Study the effect of various alkali and alkaline earth metals on the catalytic activity and stability of RM for the GL transesterification to GC.

3. Preparation and characterization of acidic metal impregnated RM-based catalysts for the direct D-Glucose transformation to 5-HMF.

4. Preparation and characterization of non-metal modified RM-based acidic catalysts for the direct D-Glucose transformation to 5-HMF.

Chapter 3

Materials and Methodology

3.1 Materials

Red mud sample was collected from National Aluminum Company (NALCO), Damonjodi, India. Different metal precursors used for doping into the surface of RM such as potassium nitrate (KNO_3), strontium nitrate ($SrNO_3$) and magnesium nitrate hexahydrate ($Mg(NO_3)_2$. $6H_2O$), tin chloride dihydrate ($SnCl_2.2H_2O$) were procured from Merck Millipore, India. Glycidol (GD), methanol and ethanol, were obtained from Sigma Aldrich, India. Glycerol (GL), dimethyl carbonate (DMC) and glycerol carbonate (GC) were obtained from Tokyo Chemical Industry Co. Ltd., India. D-Glucose, fructose, formic acid, HCl, lactic acid, acetic acid, and sulfuric acid (H_2SO_4) were procured from Merck Millipore, India. Levulinic acid, levoglucosan and 5-HMF were obtained from Alfa Aesar. All the chemicals were of high grade and used without any further modification.

3.2 Methodology

3.2.1 Pre-treatment of RM

The fresh RM collected was initially dried at 100 ^oC for 24 h in a hot air oven. The dried RM sample was ground and sieved through a 150-micron sieve to get a uniform particle size.

3.2.2 RM-Based Catalysts Preparation

3.2.2.1 Calcined RM Catalysts

The initially dried and ground RM sample was calcined in a muffle furnace in static air at different temperatures starting from 400 ^oC to 800 ^oC for 4 h. Different

catalysts obtained after calcination were identified as RM-X, where the symbol "X" denotes the temperature at which the catalyst was calcined.

3.2.2.2 K, Sr and Mg modified RM Catalysts

For the preparation of K, Sr, and Mg-doped RM catalyst, the conventional wetness impregnation technique was followed. A general procedure followed for preparing modified RM catalyst through wet impregnation is shown in Figure 3.1. RM after drying and size reduction to less than 150 µm was taken in a glass beaker with a certain amount of Millipore water and was mixed vigorously on a magnetic stirrer. A calculated amount of the metal precursor based on the wt% loading of the metal was then added slowly to that mixture and was kept under mixing for 2 h at room temperature. The temperature of the mixture solution was then increased at a rate of 10 ^{o}C min^{-1} to 70 ^{o}C, and water was allowed to evaporate from the mixture under stirring. After most of the water was evaporated and the mixture turned into a thick paste-like solution, it was removed from the stirrer and dried in a hot air oven at 100 ^{o}C for 15 h. The dried catalyst was ground and calcined at different temperatures of 500 ^{o}C to 800 ^{o}C for 4 h to get the final catalyst. Various catalysts produced after calcination were designated as RW_k-X, where the symbol R signifies RM, W_k signifies different metals (K, Sr, and Mg) weight% w.r.t. the weight of RM and X denotes the calcination temperature.

3.2.2.3 Sulfate and Sn Modified RM Catalysts

The preparation involves a three-step process. In the first step, to produce acid-treated red mud (ARM), 5 g of RM was dispersed in 25 mL of Millipore water. To that mixture, 50 mL of 3 M aqueous HCl solution was added, and it was then stirred for 1 h at 100 ^{o}C. After that, the aqueous ammonia solution was added slowly to it until a pH of 8 was reached. The precipitate formed was then centrifuged and washed several times with warm water to remove the excess ammonia. The sample was then dried at 100 ^{o}C for overnight to obtain ARM.

In the second step, the preparation of Sn doped ARM catalyst was undertaken by the simple wet-impregnation techniques. 5 g of ARM was dissolved in 150 mL of water, and the mixture was put under vigorous stirring. To that solution, an

appropriate amount of tin chloride dihydrate based on the weight percentage loading of Sn was added slowly. The mixture was then kept under stirring for 2 h, and after that, the temperature was increased to 70 ^{o}C. The excess water from the solution was allowed to evaporate until the time a thick paste-like solution was seen. The solution was then dried in a hot air oven at 120 ^{o}C for 15 h. The dried catalyst was then subjected to calcination at 450 ^{o}C for 4 h to obtain the Sn doped ARM (AS-W_s) catalyst where W_s represents the weight percentage of Sn loading.

In the third step, the preparation method as followed for the preparation of the AS-W_s catalyst was also followed for preparing the H_2SO_4 treated AS-W catalyst. 10, 30, and 50 mL of 1.5 M aqueous H_2SO_4 solution was added separately to 1 g of AS-W_s catalyst each and it was stirred in a magnetic stirrer for 2 h. After that, the mixture temperature was raised to 70 ^{o}C, and water was allowed to evaporate until it turned into a thick paste like solution. The solution was then dried for 15 h at 130 ^{o}C in an oven and calcined at 450 ^{o}C for 4 h to get the H_2SO_4 treated AS-W_s catalyst (AS-W_s-H).

3.2.2.4 Sulfonic acid and Carbon Modified RM Catalysts

The preparation involves a three-step process as mentioned below.

The acid-activated RM (AARM) was prepared by dispersing 10 g of RM in 50 mL of water and 100 mL of 6 molar HCl solution. The solution was kept on stirring at 100 ^{o}C for 1 h. Aqueous NH_3 solution was then slowly added to the mixture to bring the pH close to 8. It resulted in the formation of precipitates, which were separated from the liquid phase by centrifugation. Excess ammonia on the solid precipitates was removed by washing several times with warm water. The AARM was finally obtained by drying the washed sample at 100 ^{o}C overnight.

Unless otherwise stated, the carbon-coated AARM was prepared by a simple wet-impregnation followed by the thermal carbonization technique. AARM to D-Glucose (as carbon precursor) weight ratios of 1:0.5, 1:1, 1:1.5, and 1:2 were mixed in water and stirred at atmospheric temperature for 3 h. Following this, the temperature was increased to 75 ^{o}C to evaporate water from the mixture. The process

was continued until most of the water was evaporated, and the mixture turned into a gel-like substance. The sample was oven-dried at 100 ^{o}C for 15 h. The dried sample was carbonized under Ar atmosphere at 300 ^{o}C for 3 h to obtain the carbon-coated AARM catalyst. The catalysts prepared by impregnating different quantities of D-Glucose on AARM were named AD-Y:Z, where A, D, Y, and Z stands for AARM, D-Glucose, the weight of AARM, and weight of D-Glucose, respectively.

The preparation procedure of SO_3H functionalized AD-Y:Z catalysts was selected based on a thorough study on the previously reported work [209], which demonstrated the effect of temperature, time, and concentration of H_2SO_4 on the final characteristics of the catalyst. H_2SO_4 (98%) and AD-Y:Z in the weight ratio 12:1 was thoroughly mixed and kept in a 100 mL Teflon lined hydrothermal autoclave (4598: Parr, USA) at 150 ^{o}C for 12 h. The mixture was taken out of the autoclave once the temperature was reduced to atmospheric level and filtered to separate the remaining H_2SO_4 from the solid sample. Following this, the recovered solid part was washed thoroughly with warm water and filtered until the pH of the permeate water reached near neutral. The washed solid part was then dried at 80 ^{o}C under vacuum overnight to get the SO_3H functionalized AD-Y:Z catalyst (AD-Y:Z/SO_3H).

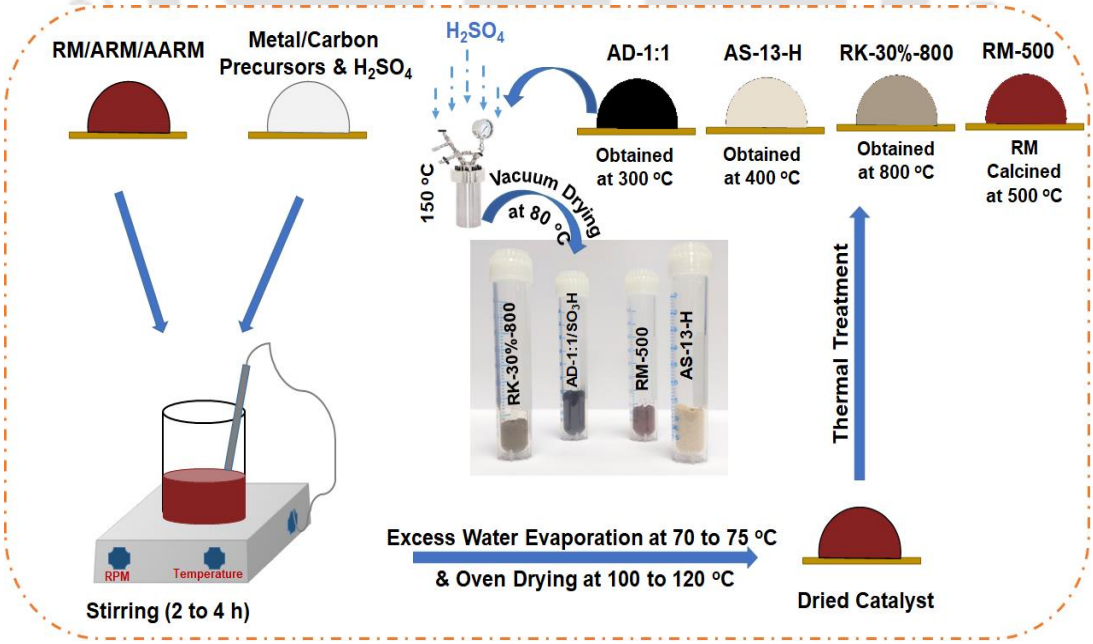

Figure 3.1. A general procedure for the modified RM catalysts preparation.

3.2.3 Catalyst Characterization

3.2.3.1 X-ray Fluorescence (XRF) Analysis

X-ray fluorescence spectroscopy was carried out by using a PANalytical AXIOS Sequential spectrometer to analyze the composition of the fresh RM. The analysis was performed with Rh Kα radiation of 0.0209 nm wavelength at 40 kV and 40 mA.

3.2.3.2 X-ray Diffraction (XRD) Analysis

X-ray diffraction (XRD) analysis of various catalysts were performed to identify different crystalline phases of catalysts. The analysis were performed by using a Rigaku SmartLab diffractometer with Cu Kα radiation of 0.154 nm wavelength at 45 kV and 112 mA. The analysis was carried out over a 2θ range of 10^o to 80^o with a step size of 0.2^o.

3.2.3.3 Fourier Transform Infrared Spectroscopy (FTIR) Analysis

Fourier transform infrared spectrometer (FTIR) analysis was carried out on a Shimadzu IRAffinity-1 spectrometer over a wavenumber range of 4000 cm^{-1} to 400 cm^{-1}. The FTIR analysis was performed for discovering different surface functional groups present on various catalysts.

3.2.3.4 N_2 adsorption-desorption analysis

N_2 adsorption-desorption analysis was performed on a Quantacrome, Autosorb-IQ MP surface area analyzer to examine the surface area, pore volume, and pore size distribution of different catalysts. The catalyst samples were degassed at 170 ^oC for 4 h under vacuum before the analysis was performed.

3.2.3.5 Morphology and Elemental Composition Analysis

Field Emission Scanning Electron Microscope (FESEM) and FESEM- Energy dispersive X-ray (EDX) analysis were carried out on a Zeiss Sigma-300 and Zeiss Sigma electron microscope, respectively, to study the morphology and elemental compositions of different catalysts. For both FESEM and FESEM-EDX analysis, all the catalyst samples were sputter-coated with a gold film to prevent charging during analysis.

3.2.3.6 CO_2/NH_3 – Temperature Programmed Desorption (TPD) Analysis

CO_2-Temperature programmed desorption (CO_2/NH_3-TPD) analysis was carried out on a Micromeritics USA, Chemisorb 2720 apparatus to study the basicity of different catalysts. The catalyst was pretreated under a He atmosphere at 150 ^oC for 1 h before analysis. Once the temperature was decreased to 50 ^oC, CO_2 at a flow rate of 30 mL min^{-1} was allowed to adsorb on the surface of the catalyst for 45 min. The sample was then heated at 100 ^oC for 1 h under 30 mL min^{-1} He gas to remove the physically adsorbed CO_2 from the catalyst surface. CO_2-TPD analysis was performed between 100 ^oC to 850 ^oC with a heating rate of 10 ^oC/min, and the CO_2 desorbed at different temperatures was monitored by a thermal conductivity detector (TCD) equipped with the instrument.

NH_3-TPD analysis was performed to study the acidity of catalysts. The procedure followed was similar as mentioned for the CO_2-TPD analysis. The NH_3 adsorption time of 40 min and the temperature range of NH_3 desorption analysis between 100 ^oC to 800 ^oC was different as compared to the CO_2-TPD analysis. Besides, the NH_3-TPD analysis of the sulfonic acid functionalized carbon-coated red mud catalyst was performed on a MicrotracBEL: BELCAT II-84 chemisorption instrument.

3.2.3.7 X-Ray Photoelectron Spectroscopy (XPS) Analysis

X-ray photoelectron spectroscopy (XPS) analysis was carried out on a Thermo Scientific (model: NEXSA surface analysis) spectrometer with a micro-focused (400 µm, 72 W, 12000 V) monochromatic Al-Kα radiation (1486.6 eV) and a multi-channel detector. The analysis was performed to study the electronic state of different elements in the catalysts.

3.2.3.8 Pyridine Adsorbed Attenuated Total Reflectance (Py-ATR) Analysis

Pyridine adsorbed attenuated total reflectance (PY-ATR) attached to a FTIR (Perkin Elmer, Spectrum two) was performed to study the nature of the acid (Lewis/Bronsted) sites in the catalysts. Before the analysis, the samples were dried at 300 ^oC for 2 h under vacuum to eliminate the physically adsorbed water. After cooling the temperature to the atmospheric level, the dried sample was exposed to neat

pyridine overnight under Ar atmosphere. After saturation with pyridine was achieved, the excess pyridine was removed under vacuum at 100 ^{o}C. The IR spectra were recorded in the range of 1400 to 1600 cm^{-1}.

3.2.3.9 Acid-Base Titration Analysis

The number of basic sites for different catalysts was determined by acid-base titration techniques. 100 mg of the catalyst was added to 10 mL of 0.5 mol L^{-1} aqueous HCl solution and kept under shaking for a period of 24 h. The mixture was then centrifuged to separate the solid catalyst from the liquid. The clear liquid containing the remaining HCl was titrated against NaOH aqueous solution (0.1 mL L^{-1}). Calculation of basic amount was done by following the equation as reported by Khayoon et. al. [95].

$$Basic\ amount\ (mmol\ g^{-1}) = \frac{(Initial\ moles\ of\ HCl - Final\ moles\ of\ HCl)}{amount\ of\ catalyst\ (g)} \qquad (1)$$

3.2.3.10 Base Site Strength Analysis

Different Hammett indicators such as phenolphthalein (H_ = 9.3), 2,4-dinitroaniline (H_ = 15.0), 4-nitroaniline (H_ = 18.4), and aniline (H_ = 27.0) were used to analyze the base site strength of different catalysts. A mixture of the catalyst (50 mg) and cyclohexane (10 mL) was prepared and sonicated for 1 h. After that, the indicator solution (0.75 wt% in benzene) was added dropwise to the mixture. Any change in color that occurred on the catalyst surface after adding the indicator solution was monitored visually. The relative base strength was presented as being stronger than the weakest indicator and weaker than the strongest indicator.

3.2.3.11 Atomic Absorption Spectroscopy (AAS) Analysis

Atomic absorption spectroscopy (AAS) was carried out on a Varian (model: Spectra AA 220 FS) AAS spectrometer to study the leaching of active metals in the product mixture separated from the catalyst after the reaction.

3.2.4 Catalytic Experiments for GC and 5-HMF Synthesis

3.2.4.1 Catalytic Experiments for GC Synthesis

Experimental analysis of GL transesterification with DMC was carried out in 100 mL three-neck round bottom glass vessel. GL and DMC in the ratio of 1:3 were taken in the vessel with an appropriate amount of the prepared catalyst and was stirred vigorously (600 rpm) using a magnetic stirrer. The temperature of the reaction mixture was measured by a thermocouple attached to the magnetic stirrer. A condenser was connected to the center neck of the three-neck flask, and chilled water was flown through the condenser to condense the vapor back into the reaction system. Different reactions were carried out by varying the parameters such as GL/DMC molar ratio, catalyst types, catalyst loading, temperature, and time of the reaction.

3.2.4.2 Study of the impurities effect on GL transesterification

It is well known that GL obtained from biodiesel industries contains several impurities in the form of water and methanol in it. Therefore, catalysts used for the transesterification of GL in the presence of such impurities must have the potential to produce similar activities, as it would be without the presence of these impurities. Different reactions were performed to examine the catalytic activity in the presence of water and methanol as impurities. The procedure followed for this experimental study is similar to that mentioned in section 3.2.3.1.

3.2.4.3 Catalytic Stability Study

The stability of the catalyst was checked by performing a reusability study by recovering the used catalyst by centrifugation after the completion of each reaction. Methanol was used to wash the recovered catalyst, and it was then dried at 120 ^{o}C for 8 h in a hot air oven. The dried catalyst was then used for the next run. For each reuse, the same procedure was followed as described above.

3.2.4.4 Reaction Product Analysis

After completion of the reaction, the reaction products were separated from the catalyst by centrifugation and were analyzed by high performance liquid chromatography (Shimadzu Prominence HPLC system, Singapore) equipped with a

Reprogel H^+ column and a RI detector. H_2SO_4 aqueous solution (9 mmol/L) was used as the mobile phase, and the flow rate was set at 1 mL min^{-1}. The conversion of GL, the selectivity of GC, and yield of GC were calculated by using the following equations.

$$Conversion\ of\ GL\ (\%) = \left(\frac{\text{Moles of } initial\ GL - Moles\ of\ \text{final } GL}{Moles\ of\ initial\ GL}\right) \times 100 \qquad (2)$$

$$Selectivity\ of\ GC\ (\%) = \left(\frac{No.of\ moles\ of\ GC\ produced}{No.of\ moles\ of\ total\ products\ produced}\right) \times 100 \qquad (3)$$

$$Yield\ of\ GC\ (\%) = \left(\frac{No.of\ moles\ of\ GC\ produced}{No.of\ initial\ moles\ of\ GL}\right) \times 100 \qquad (4)$$

3.2.4.5 Catalytic Experiments for 5-HMF Synthesis

The conversion of D-Glucose to 5-HMF was carried out using microwave irradiation (CEM: Model-Discover). The microwave was equipped with an automatic temperature controller and pressure sensor. 10 wt% of aqueous D-Glucose solution, a measured amount of catalyst, and a magnetic stir bar for stirring the mixture were taken in a 10 mL glass vial. The vial was closed with the help of a cap and was kept inside the microwave reactor. The glass vessel was designed to withstand the temperature of the reaction and the auto-generated pressure at the reaction temperature. Once the temperature was raised to the desired temperature, the sample was kept under stirring for the desired time. After the completion of the reaction, the sample was allowed to cool down to 60 ^oC inside the reactor and was centrifuged to separate the solid catalyst from the liquid product. A similar procedure was followed for carrying out reactions under the organic solvent (DMSO) by varying the weight% of organic to aqueous mixture.

3.2.4.6 Catalytic Stability Study

The reusability/stability test was performed by recovering the spent catalyst from the liquid products by centrifugation (Remi: R-24). It followed the washing of the recovered catalyst by ethanol and drying it at 110 ^oC for 10 h. The dried catalyst without any further modifications was applied for the successive batch of reaction.

3.2.4.7 Reaction Product Analysis

The liquid product separated from the solid catalyst was analyzed by using a high-performance liquid chromatography (HPLC) (Shimadzu Prominence HPLC System, Singapore). The HPLC system was equipped with a reprogel H^+ column, a RI detector and an autosampler. The eluent (9 mM H_2SO_4) was used with a flow rate of 1 mL min^{-1}. The conversion of D-Glucose and yield of different products were calculated by using the following formula.

$$\text{Conversion of D} - \text{Glucose (\%)} = \left(\frac{\text{No.of moles of D-Glucose fed} - \text{No.of moles of D-Glucose remained}}{\text{No.of moles of D-Glucose fed}}\right) \times 100 \quad (5)$$

$$\text{Yield of product (T) (\%)} = \left(\frac{\text{No.of moles of T produced}}{\text{No.of moles of D-Glucose fed}}\right) \times 100 \quad (6)$$

where T is reaction products such as fructose (FCT), 5-HMF, levulinic acid (LA), formic acid (FA), lactic acid (LCTA), levoglucosan (LGS), furfural (FU), and acetic acid (AA).

Figure 3.2. Reaction set-up for the transesterification of GL with DMC to GC.

Figure 3.3. Microwave reactor for the D-Glucose conversion to 5-HMF.

Chapter 4

Results and Discussion

This chapter reports the detailed interpretation and discussions of results obtained from the catalytic characterization and experimental study on the GC and 5-HMF synthesis process. The chapter is divided into the following major sections.

Section 4.1. Preparation and characterization of various raw RM derived catalysts and their applications for the GL transesterification to GC.

Section 4.2. Study of the effect of various alkali and alkaline earth metals on the catalytic activity and stability of RM for the GL transesterification to GC.

Section 4.3. Preparation and characterization of acidic metal impregnated RM-based catalysts for the direct D-Glucose transformation to 5-HMF.

Section 4.4. Preparation and characterization of non-metal modified RM-based acidic catalysts for the direct D-Glucose transformation to 5-HMF.

4.1 Preparation and characterization of various raw RM derived catalysts and their applications for the GL transesterification to GC

This section demonstrates the activity of calcined red mud catalysts for the GL transesterification to GC. The detail catalyst characterization and their activity results are presented in this section.

4.1.1 Catalysts characterization

4.1.1.1 XRF analysis

From the X-ray fluorescence spectroscopy (XRF) analysis carried out for the fresh RM sample, the composition obtained based on binary oxides is reported in

Table. 4.1. The XRF result revealed hematite (Fe_2O_3) as the major component present in the fresh RM (46.51%). Along with hematite, other components present were Na_2O, CaO, Al_2O_3, SiO_2, and TiO_2. In addition, a very small quantity of K_2O (0.33%) and MnO (0.15%) were also found to be present in the fresh RM sample.

Table 4.1. Chemical components of fresh red mud obtained from XRF analysis

Components	Amount (%)
Fe_2O_3	46.51
SiO_2	26.84
Al_2O_3	15.83
TiO_2	6.43
Na_2O	4.02
CaO	3.81
K_2O	0.33
MnO	0.15

4.1.1.2 XRD analysis

Figure 4.1 depicts the XRD patterns of RM calcined at 400 ^oC - 800 ^oC. For all the calcined RM samples, the characteristic peaks of Fe_2O_3 (hematite) were observed at 2θ values of 33.0^o, 35.68^o, 40.7^o, 49.23^o, 53.9^o, 62.2^o and 64.9^o with the corresponding Miller indices (014), (110), (113), (024), (116), (214) and (300) [210,211]. The highly crystalline phase of gibbsite ($Al(OH)_3$) was observed with the presence of high intensity peak at 2θ of 18.42 [211]. In the case of fresh RM, the intensity of hematite and gibbsite peaks were higher as compared to RM catalysts calcined at 400 ^oC and 500 ^oC. Calcination at 400 ^oC decreased the peak intensities for both gibbsite and hematite. With further increase in calcination temperature, the peak intensity of gibbsite decreased gradually, and the intensity of peaks related to hematite again started to increase. Thus, the results suggested the appearance of hematite as a dominant phase in the fresh RM sample and RM sample calcined at calcination temperatures above 500 ^oC. Calcite ($CaCO_3$) exhibited very low intensity peaks corresponding to 2θ of 27.1^o [211] and $Ca_2(SiO_4)$ at 44.2^o [212]. The diffraction

peaks at 2θ of 26.6° (110) and 37.6° (110) correspons to SiO_2 in the fresh RM sample [213] and peaks at 27.5° and 24.4° are assigned to TiO_2 (rutile). Sodium aluminate ($NaAlO_2$) was identified by the presence of diffraction peaks at 2θ of 20.7° (110) and 51.7° (040) [214] and a peak at 2θ of 14.08° (110) was due to the presence of $Na_8Al_6(SiO_4)_6Cl_2$ (sodalite) [211]. RM-500 showed the highest concentration of $NaAlO_2$, $Ca_2(SiO_4)$, and $Na_8Al_6(SiO_4)_6Cl_2$ phases amongst all the catalysts. With the increase in calcination temperature beyond 500 °C, the intensity of these peaks reduced, which can be attributed partly to the emergence of dominant hematite phases and partly to the occurrence of sintering and agglomeration of particles at higher calcination temperature.

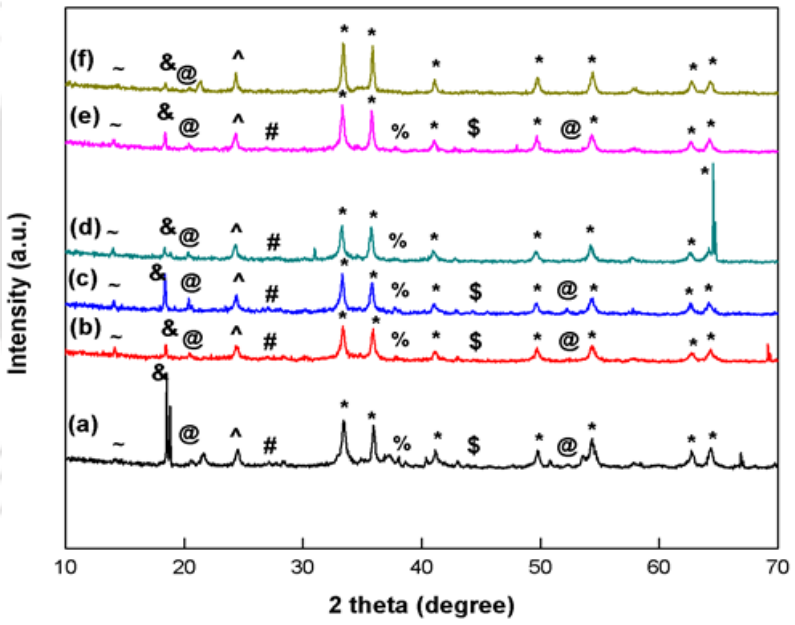

Figure 4.1. XRD patterns of (a) RM, (b) RM-400, (c) RM-500, (d) RM-600, (e) RM-700 and (f) RM-800 catalyst. * Fe_2O_3, & $Al(OH)_3$, @ $NaAlO_2$, # $CaCO_3$, % SiO_2, $ $Ca_2(SiO_4)$, ^ TiO_2 and ~ $Na_8Al_6(SiO_4)_6Cl_2$.

4.1.1.3 FTIR analysis

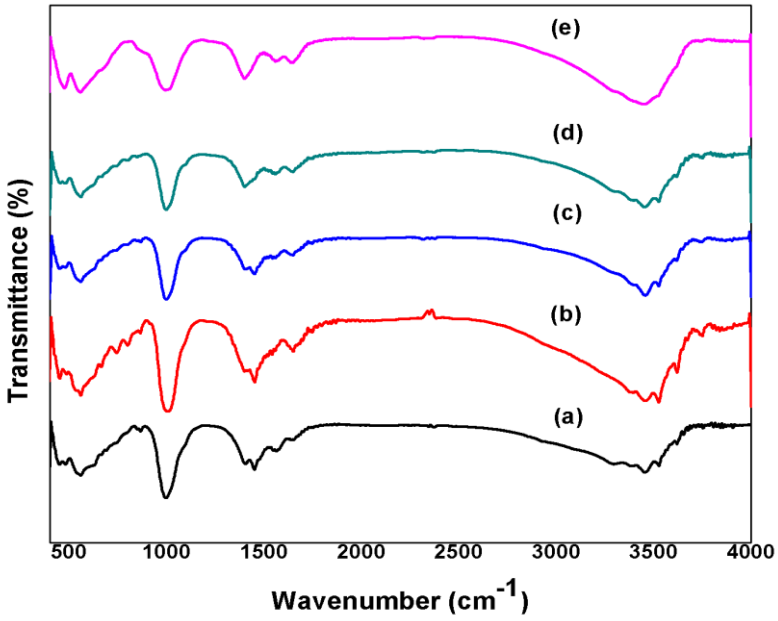

Figure 4.2. FTIR spectra of (a) RM-400, (b) RM-500, (c) RM-600, (d) RM-700 and (e) RM-800 catalyst.

An illustration of the FTIR profiles of RM calcined at different temperatures ranging from 400 ^{o}C - 800 ^{o}C is shown in Figure 4.2. The bands observed at 1400 cm^{-1} and 1440 cm^{-1} suggested the stretching vibration of the C=O group of CO_3^{-2} [215]. The intensity of this group at 1440 cm^{-1} decreased with the increase in calcination temperature, and it was absent for RM-800 catalyst, which could be due to the decomposition of carbonate groups at higher calcination temperature. For all the catalysts, the peak observed at 1001 cm^{-1} was related to the stretching vibration of Si-O-Si, and peaks at 460 cm^{-1} and 546 cm^{-1} were attributed to stretching vibrations of Fe-O, respectively [215]. Furthermore, stretching vibrations of –OH due to the presence of water molecules were observed at 3450 cm^{-1}, 3380 cm^{-1} and 1643 cm^{-1} for all the samples, which gradually got reduced with the increase in temperature and were almost lost when the temperature reached 800 ^{o}C [113,215]. In addition, the profile shows a very weak peak at approximately 3640 cm^{-1}, which could be due to the stretching vibration of –OH group associated with Na or Ca [216]. When the sample contains both Na and Ca, this peak is considered contentious because of the

close ionic radius of Ca and Na that leads to similar absorption bands between them [216,217]. Relatively weak spectra for the Al-O band at 680 cm^{-1}, and 748 cm^{-1} related to γ-Al_2O_3 were also identified for all the calcined RM samples [201,215]. Similarly, a weak spectrum for the Ca-O band at 880 cm^{-1} [218] that was seen for RM-500 started to get weaker with increasing temperature and almost got disappeared for the RM-800 catalyst. An increase in peak intensity for Fe-O bond and a decrease in intensity for Al-O and Si-O group was observed with the increase in calcination temperature as well, which confirmed the emergence of hematite as the dominant phase at higher temperatures. The results of FTIR were found to be in congruence with the results of XRD analysis.

4.1.1.4 FESEM Analysis

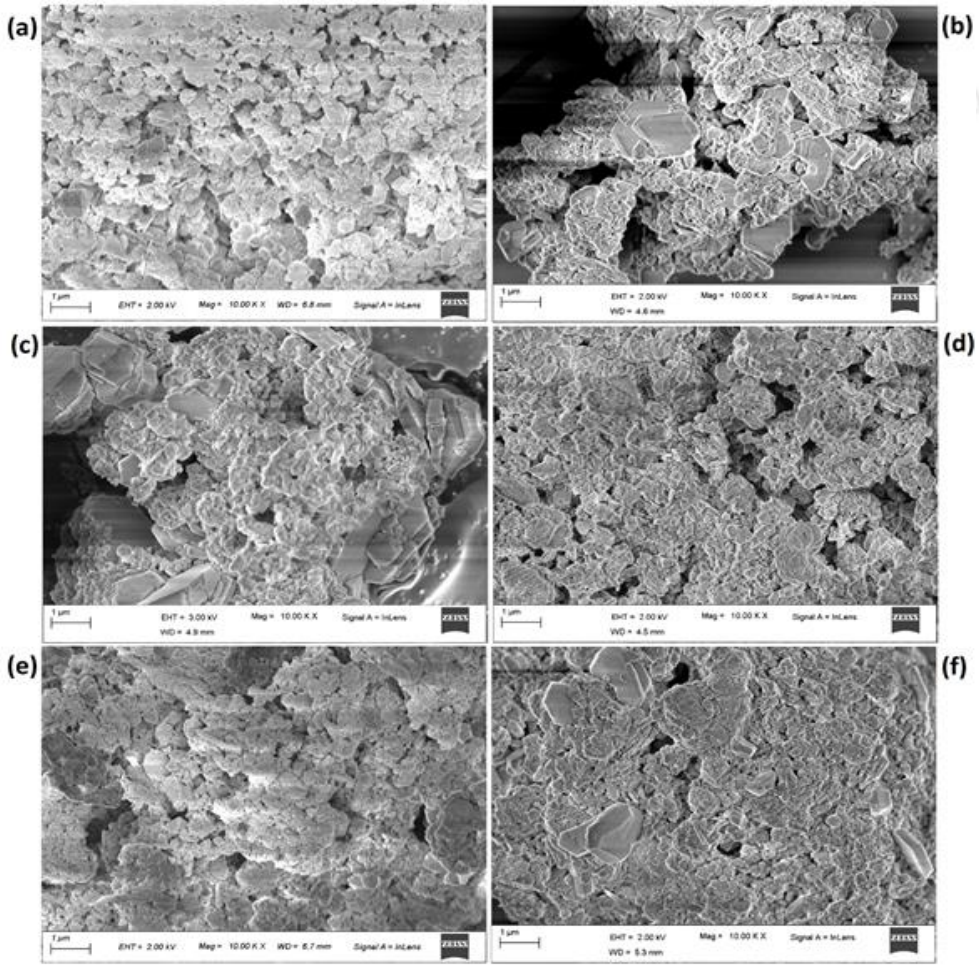

Figure 4.3. FESEM images of (a) RM, (b) RM-400, (c) RM-500, (d) RM-600, (e) RM-700 and (f) RM-800.

The FESEM analysis (Figure 4.3) revealed that particles in red mud were irregular in size with smoothed surfaces and nearly spherical in shape. For the RM-500 catalyst, the particles were bigger in size and possessed an increased number of pores as compared to the fresh RM. This could be attributed to the decompositions of some of the carbonate and hydroxyl groups bonded with different elements in fresh RM that produced higher porosity for RM-500 catalyst. Increasing the calcination temperature beyond 500 ^{o}C resulted in agglomeration of the particles, and particles of even larger size with fewer numbers of pores were observed.

4.1.1.5 FESEM-EDX analysis

EDX analysis (Table 4.2) revealed the presence of different elements in RM-500 and two times reused RM-500. Iron was found to be present in the highest amount in RM-500 along with other elements such as Na, Ca, Ti, Al, and Si. The presence of Na and Ca content (considered as active elements for the transesterification reaction) in the four times reused RM-500 was found to have decreased to a significant extent. This suggested the leaching of these active elements during the transesterification reaction of GL with DMC to produce GC.

Table 4.2. Elemental composition of RM-500 and 4th reused RM-500 catalyst obtained from FESEM-EDX analysis.

Elements	O	Fe	Al	Si	Ti	Na	Ca
RM-500	41.6	27.2	12.0	5.7	2.2	11.2	0.1
4th reused RM-500	45.4	29.7	14.7	3.6	2.9	3.6	0.1

4.1.1.6 N_2 adsorption-desorption analysis

The results of the BET surface area, pore volume, and average pore size analysis for different catalysts obtained from N_2 adsorption-desorption experiments are presented in Table. 4.3. The pore size distribution curves for different RM catalysts are provided in Figure 4.4. The fresh RM sample exhibited a lower surface area of 11.6 $m^2 g^{-1}$. The surface area of RM increased with the calcination temperature

of 400 °C (13.1 m^2 g^{-1}) to 500 °C (21.9 m^2 g^{-1}), and then it started to decrease with further increase in calcination temperature. RM calcined at 800 °C possessed the lowest surface area (5.3 m^2 g^{-1}) amongst all the catalysts. The decrease in surface area with the increase in calcination temperature can be attributed to the formation of agglomerated particles due to the sintering of fine crystals at higher temperatures. The total pore volume for fresh RM catalyst was 0.056 cm^3g^{-1}, and it increased to 0.078 cm^3g^{-1} for the RM-500 catalyst. Beyond 500 °C, the total pore volume started to reduce, which might be due to the partial blockage of pores occurred by the agglomerated particles formed at higher calcination temperature. The greater is the number of agglomerated particles formed; the more would be the partial occlusion of pores and hence, less would be the total pore volume and surface area.

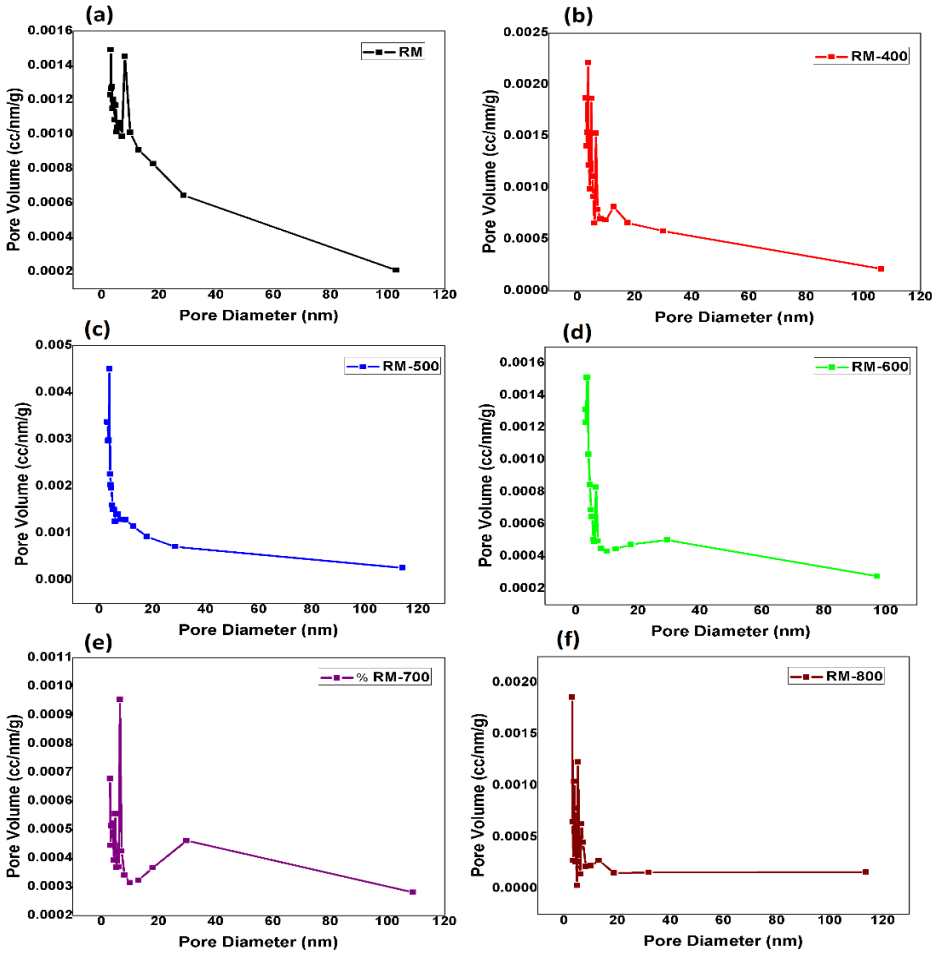

Figure 4.4. Pore size distribution of (a) RM, (b) RM-400, (c) RM-500, (d) RM-600, (e) RM-700, and (f) RM-800.

Table 4.3. Effect of calcination temperature on the catalyst surface area, basic properties and catalytic performance for transesterification of GL with DMC. Reaction conditions: molar ratio of GL to DMC = 1:3, 12.5 wt% catalyst, T = 75 ^{o}C, t = 90 min.

Catalyst	GL conversion (%)	GC yield (%)	GC selectivity (%)	S_{BET} (m^2 g^{-1})	Avg. pore size (nm)	Total pore volume (cm^3 g^{-1})	Basic strength	Base amount (mmol/g)
RM	67.6	65.6	97	11.6	19.26	0.056	9.3 < H_ < 15	19.2
RM-400	87.9	85.6	97.3	13.1	13.59	0.058	9.3 < H_ < 15	26.4
RM-500	95.2	92	96.6	21.9	14.29	0.078	9.3 < H_ < 15	32.1
RM-600	90.9	82.2	90.5	16.7	21.50	0.052	9.3 < H_ < 15	27.6
RM-700	89.4	86.5	96.7	8.9	32.16	0.055	9.3 < H_ < 15	27.8
RM-800	72.1	71.6	99.3	5.3	27.06	0.031	9.3 < H_ < 15	22.1

4.1.1.7 Basic strength analysis (Hammett indicator test)

Catalyst basicity and basic strength are reported to have significant effects on the transesterification reaction [92]. Catalysts with moderate basic strength and strong basic sites are very much desirable for the transesterification of GL to produce GC [216]. From the Hammett indicator test carried out to analyze the basic strength of different catalysts (Table. 4.3), it was observed that calcination temperature did not have significant effects on the basic strength of RM calcined at temperatures ranged between 400 ^{o}C - 800 ^{o}C and all the catalysts showed moderate basic strength (9.3 < H_ < 15) desirable for the transesterification reaction. Higher basic strength (H_ > 18.4) of catalysts usually leads to the decomposition of glycerol carbonate to undesirable glycidol, which was not observed for any of the catalysts prepared from RM. Many times it has been seen that single metal catalysts with high basic strength such as Na, Ca, and Sr lead to the formation of undesirable glycidol during the transesterification of GL [92,93,219]. However, the presence of some quantities of acidic sites such as alumina and silica in all the RM catalysts maintained a proper balance of basic strength of the catalyst and thereby contributed to the efficiency of the process by driving the reaction towards the desired direction.

4.1.1.8 TPD-CO_2 analysis

The TPD-CO_2 analysis (Figure 4.5) was carried out to investigate the basic site concentration of different RM catalysts. The nature of basic sites such as weak, moderate, and strong sites was defined according to the desorption peak at < 200 ^{o}C, 200 ^{o}C < 450 ^{o}C, and > 450 ^{o}C, respectively [107]. All the catalysts displayed a very similar small intensity peak at approximately 150 ^{o}C, which might be due to the CO_2 desorption from the weak basic sites of these catalysts. Furthermore, another CO_2 desorption peak was observed for all the catalysts at a higher temperature between 625 ^{o}C - 632 ^{o}C, which confirmed the presence of strong basic sites for all the catalysts. The strong basic site peak intensity increased slightly with the increase in calcination temperature from 400 ^{o}C to 500 ^{o}C, and it decreased thereafter from the temperature of 600 ^{o}C to 800 ^{o}C. The CO_2 desorption peak intensity was maximum for RM-500 and was lowest for RM-800 sample. This phenomenon can be attributed to the agglomeration of particles at higher calcination temperatures leading to the

formation of multilayer structures of particles that could restrict the access of CO_2 to some of the basic sites of the catalyst [107]. Furthermore, the occurrence of the dominant hematite phase at higher calcination temperatures as noticed from the XRD patterns of calcined RM (Figure 4.1), could also cover some of the active basic sites of the catalyst that decreased the basic strength of the catalyst. The results obtained from the acid-base titration techniques carried out to analyze the basic amount of different catalysts (Table. 4.3) supported the results of the TPD analysis. This leads to the conclusion that RM calcined at 500 ^{o}C contained the highest amount of active basic sites (32.10 mmol) as compared to other catalysts and therefore considered as the best suitable catalyst for the transesterification of GL.

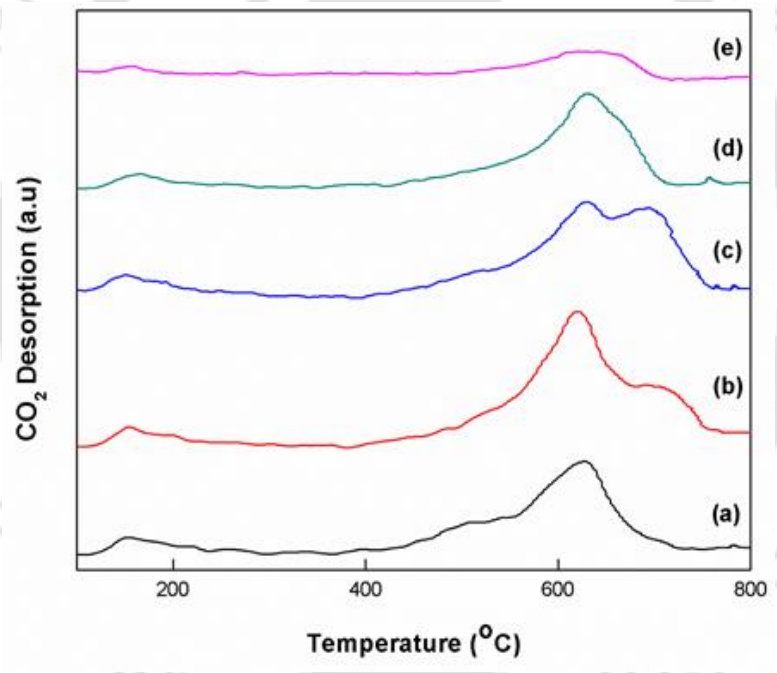

Figure 4.5. TPD-CO_2 profile of (a) RM-400, (b) RM-500, (c) RM-600, (d) RM-700, and (e) RM-800 catalyst.

4.1.2 Catalyst activity test

4.1.2.1 Catalyst screening for the GL transesterification

It has been reported that calcination temperature has a strong effect on the basic and acidic properties of the catalysts apart from their elemental compositions. The geometry and surface properties of mixed oxide catalysts vary with calcination temperature, affecting their activity towards the transesterification reaction [92,120,220]. In order to study the effect of different pretreatment temperatures on the catalytic activity of RM, it was calcined at different temperatures of 400 ^{o}C - 800 ^{o}C for 4 h, and the calcined sample was used for the transesterification of GL. The results are shown in Table 4.3. The catalytic activity increased with calcination temperature from 400 ^{o}C to 500 ^{o}C and then decreased with further increase in temperature. RM calcined at 500 ^{o}C produced the best catalytic activity with 95.2% GL conversion and 92% GC yield achieved at 90 min reaction time and 75 ^{o}C reaction temperature. The higher activity of RM-500 catalyst as compared to other catalysts could be ascribed to its larger amount of basic sites as observed from the TPD-CO_2 (Figure 4.5) and acid-base titration analysis (Table 4.3). In addition, the higher activity of RM-500 catalyst can be inferred from the XRD pattern (Figure 4.1), where the profile shows peaks related to active $NaAlO_2$, $Ca_2(SiO_4)$ and $Na_8Al_6(SiO_4)_6Cl_2$ phases in the RM-500 catalyst. The intensity of these peaks started to reduce with an increase in the calcination temperature, thus suggesting a relative decrease of these active sites in all other catalysts calcined at temperatures higher than 500 ^{o}C. This might have occurred due to the emergence of the dominant hematite phases at high calcination temperatures that could cover some of the active surfaces of the catalyst or due to the occurrence of sintering and agglomeration of particles on the active surfaces at higher temperatures. The results of the XRD analysis were in agreement with the results of FTIR (Figure 4.2), which also showed an increase in the peak intensity for the Fe-O bond at higher calcination temperature. Although the calcination temperature had different effects on the catalytic activity of catalysts calcined at different temperatures other than 500 ^{o}C, the effects were not observed to be that much significant, and all the other catalysts showed appreciable catalytic activities for the transesterification of GL. Fresh RM catalyst contains the lowest

amount of basic sites, which was also reflected in its poor catalytic activity for the transesterification reaction. With the increase in calcination temperature to 800 ^{o}C, the activity of the RM-800 catalyst decreased, and only 72.1% GL conversion with 71.6% GC yield was observed. This could be due to the lower exposure of active sites due to agglomeration of particles on active surfaces at higher temperatures that led to a decrease in the amount of basic sites in RM-800 catalyst (22.1 mmol) as compared to other catalysts calcined below 800 ^{o}C.

Catalyst surface area is also known to have a significant effect on the catalytic activity for the transesterification process. Catalysts of higher surface area and larger numbers of pores are found to exhibit higher activity for the transesterification reaction [216]. From the results obtained from surface area analysis (Table. 4.3), it was observed that the RM-500 catalyst possessed the highest surface area of 21.9 m^2 g^{-1}, which might be another reason for its higher activity for the transesterification of GL as compared to other catalysts. Further increase in calcination temperature resulted in a decrease of catalyst surface area, and hence, the catalytic activity also decreased. The decrease in surface area was attributed to the sintering of particles at higher temperatures, which was also supported by the results of FESEM analysis (Figure 4.3). FESEM analysis of RM calcined at different temperatures confirmed that catalyst calcined at higher temperatures exhibited more numbers of agglomerated particles with relatively larger particle size and less number of pores as compared to catalysts calcined at lower temperatures. As a result, some of the active components of the catalysts calcined above 500 ^{o}C might have lost access to the reactant particles, thereby resulted in decreased activity of these catalysts.

4.1.2.2 Reaction parametric study

The effect of reaction time on the catalytic activity of the RM-500 catalyst for the transesterification of GL with DMC was studied by performing different experiments at regular time intervals of 15 min up to 150 min. As shown in Figure (4.6 (a)), both the GL conversion and GC yield increased with reaction time. At a low reaction time of 30 min, the conversion of GL and yield of GC were only 53.2% and 50.8%, respectively. The reaction efficiency increased with the increase in reaction

time and reached 95.2% GL conversion and 92% GC yield at 90 min of reaction time for the RM-500 catalyst. By increasing the reaction time beyond 90 min, a very slight increase in the GL conversion and GC yield was observed. As shown in Figure (4.6 (a)), the GL conversion and GC yield obtained at 150 min of reaction time were 98.2% and 92.7%, respectively. Therefore, the reaction time of 90 min was considered as the optimum reaction time for all the transesterification reactions in this study.

The reaction temperature is considered as an important reaction parameter for the transesterification of GL as it can affect the reaction efficiency by affecting both the GL conversion and GC yield by having a direct impact on the heat sensitive carbonates and catalyst used [221]. Different reaction temperatures starting from 60 ^{o}C to 105 ^{o}C were chosen to observe the effect of reaction temperature on the catalytic activity of RM-500 for the transesterification of GL. As illustrated in Figure (4.6 (b)), the catalyst displayed very less activity at 60 ^{o}C reaction temperature, and only 36% of GL conversion with 32.9% of GC yield was obtained for the RM-500 catalyst. By increasing the temperature to 75 ^{o}C, a significant increase in catalytic activity was observed, and the GL conversion reached 95.2%. Further increase in temperature to 90 ^{o}C and 105 ^{o}C did not produce any significant change in the conversion and yield. The reaction at 105 ^{o}C produced only 1% increase in GL conversion as compared to the reaction carried out at 75 ^{o}C, and hence, 75 ^{o}C was considered as the optimum reaction temperature for this system. As reported by Parameswaram et al. (2013) [222], high reaction temperature could lead to the decomposition of GC to form glycidol. However, this only occurs when the basic strength of the catalyst is very high ($H_- > 18.4$). For RM-500 catalyst, the basic strength ($9.3 < H_- < 15$) was well below the GC decomposition zone, and therefore, no amount of glycidol was observed at any reaction temperature between 60 ^{o}C to 105 ^{o}C.

The effect of variation in GL to DMC molar ratio on the catalytic activity of transesterification of GL is shown in Figure (4.6 (c)). Reactions carried out at the 1:1 molar ratio of GL to DMC produced a very low conversion of GL (54.4%) with a very low yield of GC (41.3%) for the RM-500 catalyst. However, the GL conversion and GC yield increased significantly when 1:2 ratio of GL to DMC was used. The

value of GL conversion and GC yield reached 84.3% and 79.4%, respectively, at 75 ^{o}C of the reaction temperature and 90 min of the reaction time. Meanwhile, these values reached the maximum, i.e., 95.2% and 92%, with a 1:3 molar ratio of GL to DMC. The hydrophilic nature of glycerol and the hydrophobic nature of DMC makes the reaction system practically two-phase between the reactants. Thus, to prevent the two-phase system and to increase contacts between GL and DMC, excess DMC is required, which acts as a solvent as well as a reactant to promote the catalytic reaction [221]. In addition, to prevent the reversible reaction between methanol and GC and to drive the reaction in a positive direction of high GL conversion, an excess molar ratio of GL to DMC is required. For this study, the 1:3 molar ratio of GL to DMC produced the best GL conversion and GC yield, and therefore, this molar ratio was considered throughout this work.

The process of transesterification of GL strongly depends on the number of available active sites of the catalyst. In order to investigate the outcomes of the transesterification of GL with variation in catalyst loading, different experiments were carried out by varying the amount of RM-500 catalyst and by keeping all other parameters fixed. The results are shown in Figure (4.6 (d)). It was observed that both the GL conversion and GC yield increased steadily with the increase in catalyst amount from 5 wt% to 12.5 wt% w.r.t. weight of the GL taken for the reaction. The maximum value of GL conversion (95.2%) and GC yield (92%) was obtained when 12.5 wt% of the RM-500 catalyst was used. This can be attributed to the presence of a higher number of accessible active sites on the catalyst surface with the increase in catalyst loading, which positively shifted the reaction towards the desired direction by participating in the catalysis process. However, beyond a certain limit of catalyst loading, mass transfer resistance between the reactants and the active sites of the catalyst may exist. Moreover, chances of particle agglomeration can also occur at higher catalyst loading that actually hinders the GL conversion [120]. In this study, catalyst loading above 12.5 wt% did not produce any significant changes in the GL

conversion and GC yield, indicating the stability of the catalyst against abrasion normally occurred in slurry mixtures.

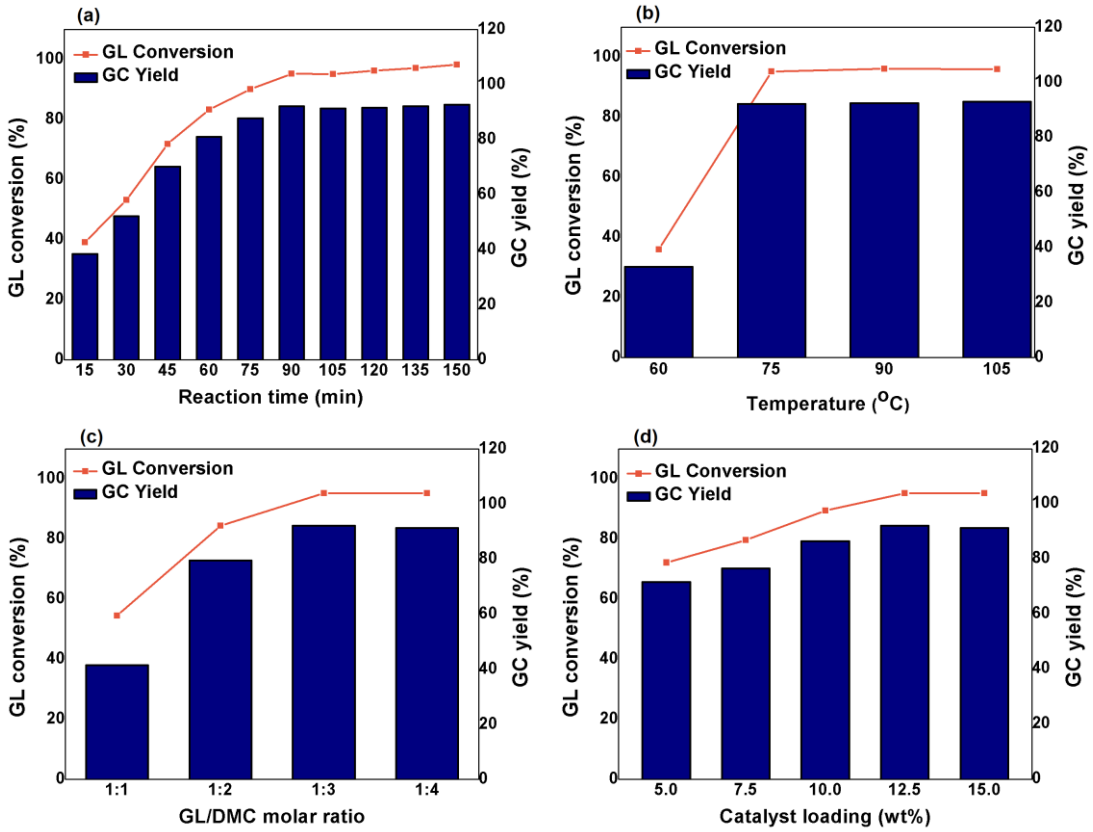

Figure 4.6. Effects of different reaction parameters on transesterification of GL with DMC using RM-500 catalyst: (a) effect of time at molar ratio of GL to DMC = 1:3, 12.5 wt% catalyst, T = 75 ^{o}C; (b) effect of temperature at molar ratio of GL to DMC = 1:3, 12.5 wt% catalyst, t = 90 min; (c) effect of GL to DMC molar ratio at T = 75 ^{o}C, 12.5 wt% catalyst, t = 90 min; (d) effect of catalyst loading at molar ratio of GL to DMC = 1:3, T = 75 ^{o}C , t = 90 min.

4.1.2.3 Impurities effect on the GL transesterification with DMC

Glycerol from biodiesel industries contains many impurities, including water and methanol. The amount of these impurities varies from one batch to another. Even in very small concentrations, they can influence the conversion of GL and the yield of GC by affecting catalyst stability. Considering this fact, different experiments were carried out to study the stability of RM-500 catalyst for the transesterification of GL

by taking water and methanol as impurities with the initial reactant mixture. 3 wt% (w.r.t. the initial GL wt) each of water and methanol individually and a mixture of both (3 wt% of each of methanol and water w.r.t. the initial GL wt) was taken with the initial reactant mixture. Interestingly, no significant decrease in GL conversion and GC yield was observed in either of the experiments performed by adding individual water and methanol or by adding the mixture of both impurities with the initial reactant mixture (Figure 4.7). With methanol and water present as individual impurities, only 1.5% and 1.7% decrease in GL conversion was observed, which suggested that the catalyst was very much stable for the transesterification of GL in the presence of these impurities. When a mixture of both water and methanol was taken as impurities, the conversion decreased only by 4.2%, and the yield of GC reduced by a value of 5% as compared to the reaction carried out under the same operating conditions without using these impurities. These results indicated the superior resistance of the RM-500 catalyst for such impurities as compared to other reported catalysts [216,220] and, thus, can be considered suitable for the transesterification of GL directly obtained from biodiesel industries.

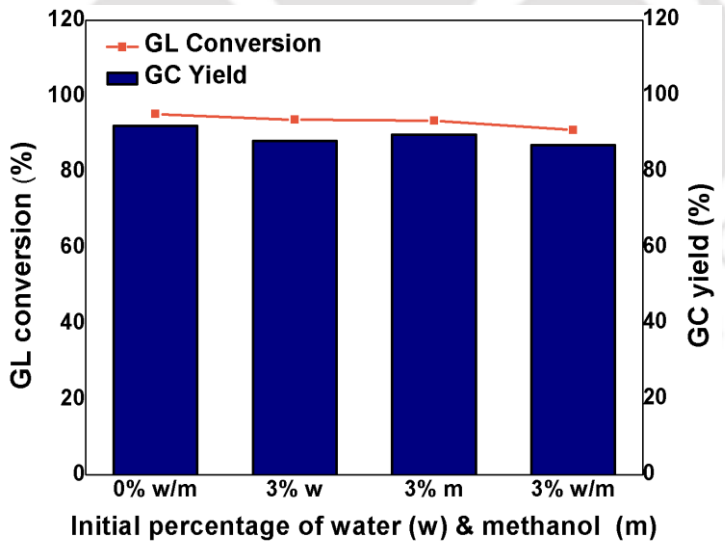

Figure 4.7. Effect of initial impurities on the performance of RM-500 catalyst for the transesterification of GL. Reaction conditions: molar ratio of GL to DMC: 1:3; reaction time: 90 min; catalyst: RM-500; 12.5 wt% catalyst; reaction temperature: 75 ^{o}C.

4.1.3 Proposed reaction mechanism and kinetic model development

The complex composition of RM-500 catalyst because of the presence of multiple metal oxides makes it challenging to determine the exact mechanism for the transesterification of GL and DMC to synthesize GC. However, by considering the fact that catalysts containing active basic sites are most effective for the transesterification of GL, the mechanism could be described in terms of Na and Ca as active components for GL transesterification. Different characterization results obtained for the reused catalyst, where a significant decrease in the catalytic activity occurred due to the decrease of Na and Ca, also support the above phenomenon. As shown in Figure 4.8, at the start of the reaction, glycerol is activated to glyceroxide ($C_3H_7O_3^-$) anion at the basic site of the catalyst. Following this, Lewis acid sites such as Al_2O_3, TiO_2, etc. present in RM-500 make the carbonyl carbon of DMC highly positive by coordinating with its carbonyl oxygen. Thereafter, a nucleophilic reaction takes place between the glyceroxide anion and the carbonyl carbon of DMC, due to which the intermediate called as methyl glyceryl carbonate along with a methoxide anion is produced. The methoxide anion combines with the H^+ ion abstracted by the base group to form methanol. Subsequently, the basic site of the catalyst extracts another H^+ ion from the secondary hydroxyl group of GL, hence leaving another oxygen anion group in GL. This anion oxygen of GL makes a second nucleophilic attack on the carbonyl carbon and finally undergoes a cyclization reaction to produce GC by removing another methanol group.

A kinetic model for the transesterification reaction between GL and DMC to produce GC was developed by using the reaction data collected from different experiments carried out at 75 ^oC. Langmuir-Hinshelwood model was used to develop the kinetic model by assuming that the external and internal mass transfer processes are very rapid as compared to the chemical rate processes. The overall reaction of GL transesterification with DMC to produce GC can be presented in the following steps.

Adsorption of GL on the catalyst surface:

$$GL + S \leftrightarrow GL.S \quad (7)$$

Adsorption of DMC on the catalyst surface:

$$DMC + S \leftrightarrow DMC.S \quad (8)$$

Surface reaction between GL and DMC:

$$GL.S + DMC.S \leftrightarrow GC.S + MET.S \quad (9)$$

Desorption of GC from the catalyst surface:

$$GC.S \leftrightarrow GC + S \quad (10)$$

Desorption of methanol from the catalyst surface:

$$MET.S \leftrightarrow MET + S \quad (11)$$

By assuming that, the rate is surface reaction controlling, the rate expression can be written as:

$$-r = -\frac{dC_{GL}}{dt} = k_S C_{GL.S} \,.\, C_{DMC.S} - k_S' C_{GC.S} \,.\, C_{MET.S} \quad (12)$$

Or, $$-r = -\frac{dC_{GL}}{dt} = k_S (C_{GL.S} \,.\, C_{DMC.S} - \frac{1}{K_S} C_{GC.S} \,.\, C_{MET.S}) \quad (13)$$

where $K_S = \frac{k_S}{k_S'}$

Since, all other steps are considered to be in equilibrium; hence, the concentration of different adsorbed species can be expressed as:

$$C_{GL.S} = K_{GL} C_{GL} C_v \quad (14)$$

$$C_{DMC.S} = K_{DMC} C_{DMC} C_v \quad (15)$$

$$C_{GC.S} = K_{GC} C_{GC.} C_v \quad (16)$$

$$C_{MET.S} = K_{MET} C_{MET.} C_v \quad (17)$$

where, C_v is the concentration of vacant sites on the catalyst.

By putting the above value for different concentrations of adsorbed species in Eq. (13), the rate expression can be described as:

$$-r = -\frac{dC_{GL}}{dt} = k_S (K_{GL} C_{GL} C_v \,.\, K_{DMC} C_{DMC} C_v - \frac{1}{K_S} K_{GC} C_{GC} C_v \,.\, K_{MET} C_{MET} C_v) \quad (18)$$

Or, $-\frac{dC_{GL}}{dt} = k_S \,.\, K_{GL} \,.\, K_{DMC} \left(C_{GL} \,.\, C_{DMC} - \frac{K_{GC} \,.\, K_{MET}}{K_S \,.K_{GL} \,.K_{DMC}} C_{GC} \,.\, C_{MET} \right) {C_v}^2$ (19)

The total active site concentration C_o on the catalyst surface is given by:

$$C_o = C_{GL.S} + C_{DMC.S} + C_{GC.S} + C_{MET.S} + C_v \quad (20)$$

By putting the value from Eqs. (14), (15), (16), and (17), on Eq. (20), C_v can be found as

$$C_v = \frac{C_o}{1 + K_{GL}C_{GL} + K_{DMC}C_{DMC.} + K_{GC}C_{GC} + K_{MET}C_{MET}} \quad (21)$$

By putting the value of C_v on Eq. (19), the rate equation will be in form as follows:

$$-\frac{dC_{GL}}{dt} = \frac{k_S \,.K_{GL} \,.K_{DMC} \left(C_{GL} \,.C_{DMC} - \frac{K_{GC} \,.\, K_{MET}}{K_S \,.K_{GL} \,.K_{DMC}} C_{GC} \,.C_{MET} \right) {C_o}^2}{(1 + K_{GL}C_{GL} + K_{DMC}C_{DMC.} + K_{GC}C_{GC} + K_{MET}C_{MET})^2} \quad (22)$$

By assuming the reverse reaction between methanol and GC to be very slow and therefore, the reaction is far away from equilibrium, the above reaction can be expressed as:

$$-\frac{dC_{GL}}{dt} = (k_S \,.K_{GL} \,.\, K_{DMC}\, {C_o}^2 .\, C_{GL} \,.C_{DMC}) \quad (23)$$

Since, excess amount of DMC was taken for the transesterification process, the concentration of DMC throughout the reaction can be considered same as the initial concentration. Therefore, Eq. (23) can be written as:

$$-\frac{dC_{GL}}{dt} = (KwC_{GL}) \quad (24)$$

where, $Kw = k_S K_{GL} K_{DMC} {C_o}^2$; w is the weight of the catalyst.

C_{GL} can be expressed in terms of fractional conversion as:

$$C_{GL} = C_{GL0}\,(1 - X_{GL}) \quad (25)$$

where, C_{GL0} is the initial GL concentration.

By putting the value of C_{GL} from Eq. (22) in Eq. (21) and after integrating, the final equation can be obtained in terms of conversion and time *(t)* as given below:

$$-\ln(1 - X_{GL}) = Kwt \quad (26)$$

The graph plotted between $-\ln(1-X_{GL})$ vs t produced an excellent fit to the experimental data (Figure 4.9) with a reaction constant K value of 0.1364 sec^{-1} at 75 ^{o}C, thereby suggested a pseudo-first order reaction for the transesterification of GL with DMC to obtain GC.

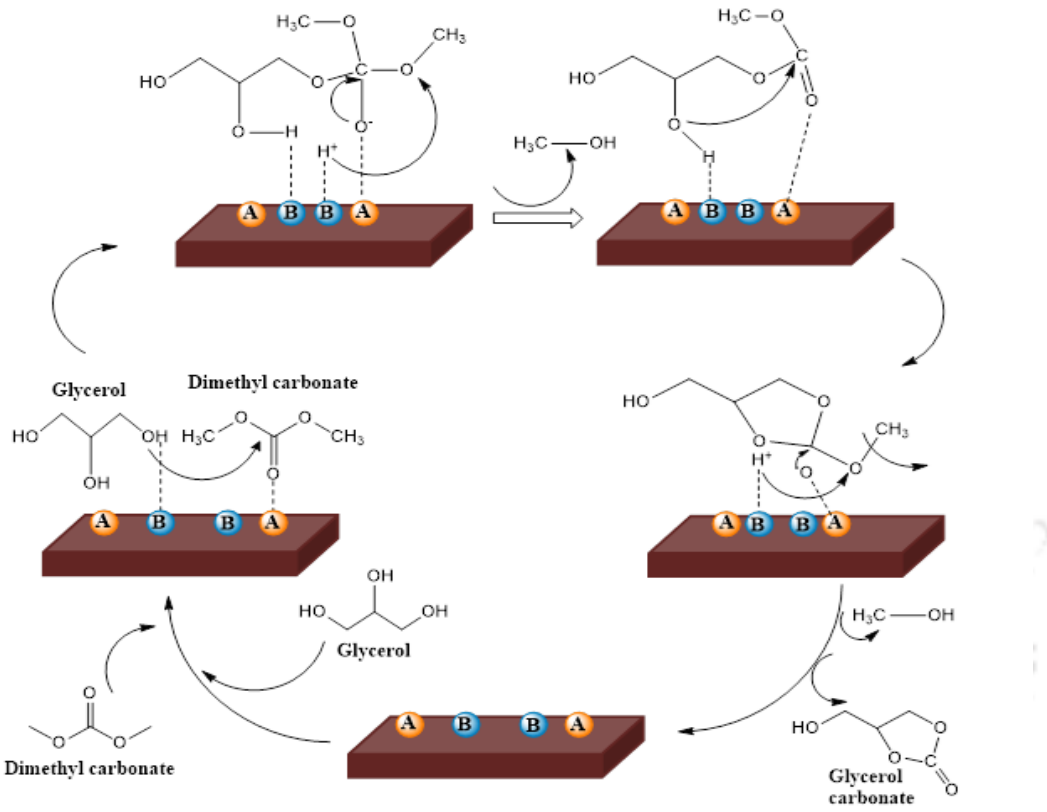

Figure 4.8. A plausible reaction mechanism for the transesterification of GL with DMC

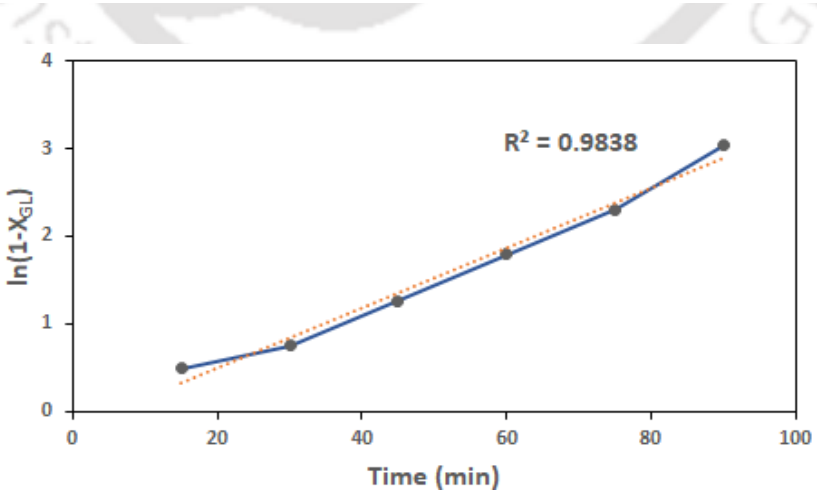

Figure 4.9. Plot of $\ln(1\text{-}X_{GL})$ against time.

4.1.4 Catalyst reusability study

A reusability study of the RM-500 catalyst was carried out by separating the catalyst from the product mixture through centrifugation after the completion of the reaction. The catalyst separated was washed with ethanol, dried at 120 ^{o}C for 6 h, and the dried catalyst was again used for the transesterification of GL. The same procedure was followed for each successive reuse of the catalyst. As shown in Figure 4.10, the activity of the RM-500 catalyst decreased when reused for the 1st time, where the GL conversion reduced from 95.2% for the fresh RM-500 to 63.2% for the 1st reused catalyst. The catalyst activity continued to decrease with the number of reuse and produced only 56.6% GL conversion with 18.6% GC yield at the 2nd reuse condition. Additional reusability study performed for the RM-500 catalyst revealed that the activity continued to decrease, and only 26.5% of GL conversion with 8.2% GC yield was observed at 4th reuse of the catalyst.

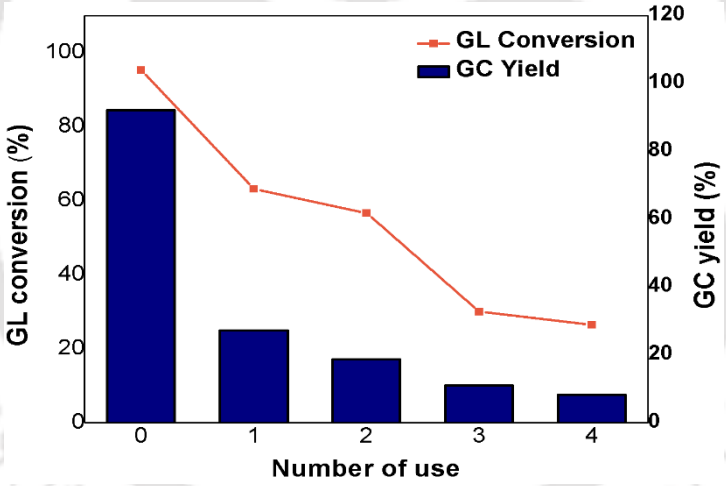

Figure 4.10. Reusability study of RM-500 for the transesterification of GL. Reaction conditions: molar ratio of GL to DMC: 1:3; reaction time: 90 min; catalyst: RM-500; 12.5 wt% catalyst; reaction temperature: 75 ^{o}C.

In order to study the deactivation mechanism, the RM-500 catalyst that was reused for the 4th time was recovered by the above-mentioned procedure and was analyzed by different techniques such as XRD, FTIR, and EDX. From the FTIR spectra of the 4th time reused RM-500 catalyst (Figure 4.11), an additional weak band

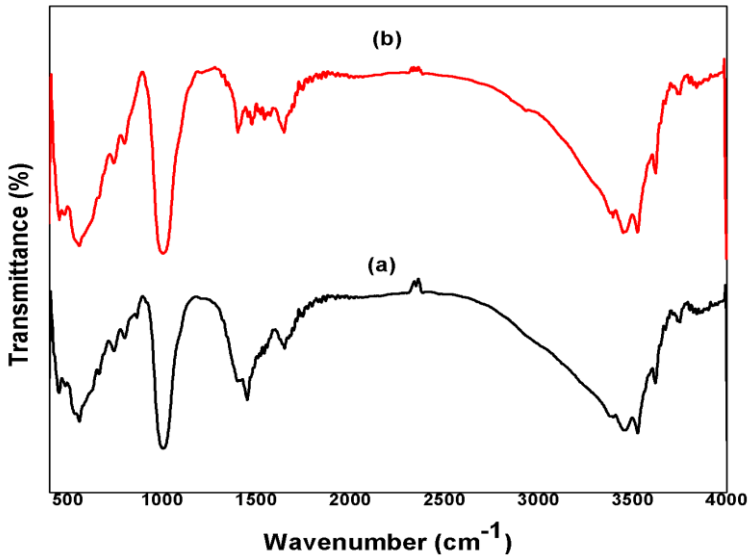

Figure 4.11. Comparison of FTIR spectra of (a) RM-500, (b) 4th reused RM-500.

observed at approximately 2940 cm^{-1} was attributed to the stretching bond of C-H groups that could have emerged due to the adsorption of different organic matters on the surface of RM-500 during the reaction [223]. In addition, the intensity of spectra related to the stretching vibration of –OH at 3450 cm^{-1}, 3380 cm^{-1}, and 1643 cm^{-1} due to the presence of H_2O molecules increased in the 4th reused RM-500 catalyst, suggesting a relative increase in the percentage of H_2O. The reduction in the intensity of the CaO group (880 cm^{-1}) and an increase in the intensity of carbonate groups (1400 cm^{-1}) was also noticed for the RM-500 catalyst reused for the 4th time. These observations from the FTIR technique confirmed the change in composition of active phases in the RM-500 catalyst to less active carbonate and hydroxyl groups after the 4th reuse. The XRD profile of the 4th reused RM-500 catalyst (Figure 4.12) suggested the reduction of active phases like $NaAlO_2$, $Na_8Al_6(SiO_4)_6Cl_2$, and $Ca_2(SiO_4)$ and an increase in carbonate groups as well. This evidence from FTIR and XRD analysis revealed that the leaching of active components such as Na and Ca was the reason for the decreased activity of the reused RM-500 catalyst. To analyze the leaching of active components during the reaction, the product mixture after separating from the catalyst was subjected to atomic absorption spectroscopy (AAS) analysis. Significant leaching of Na (approximately 1600 ppm) was observed in the product mixture

collected at the 2nd reuse condition, which confirmed the leaching of active components during the reaction.

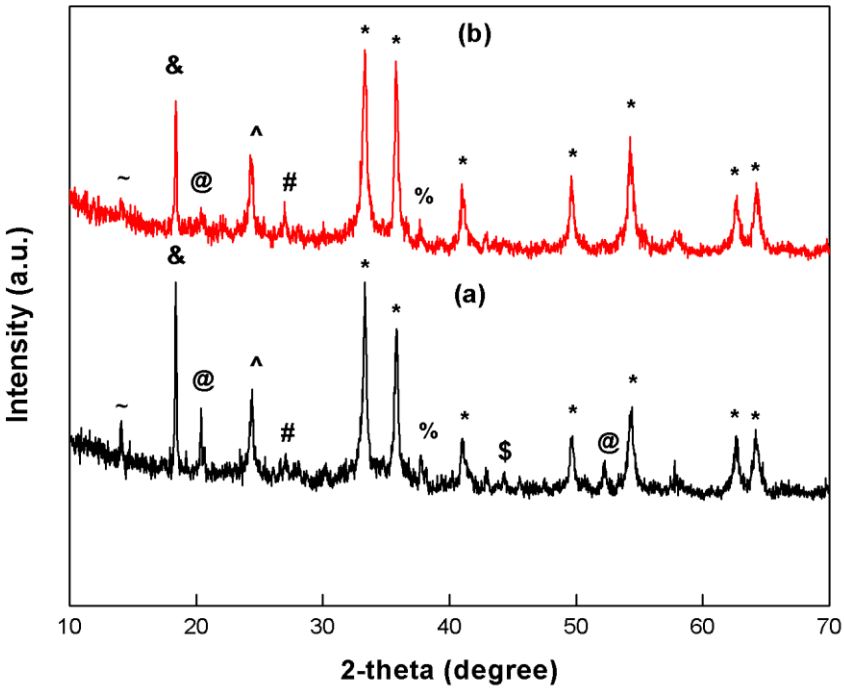

Figure 4.12. Comparison of XRD patterns of (a) RM-500, (b) 4th reused RM-500 catalyst. * Fe_2O_3, & $Al(OH)_3$, @ $NaAlO_2$, # $CaCO_3$, % SiO_2, $ $Ca_2(SiO_4)$, ^ TiO_2 and ~ $Na_8Al_6(SiO_4)_6Cl_2$.

4.1.5 Comparison of the catalytic activity of RM-500 with other reported catalysts

The outcomes of this study for the synthesis of GC by the transesterification reaction between GL and DMC were compared with other reported heterogeneous catalysts. As presented in Table 4.4, the activity of RM-500 is very much similar to other reported highly efficient catalysts, and in some cases, the value is even higher as compared to other reported catalysts. For example, the GL conversion and GC yield obtained by Parameswaram et al. (2013) [222] was 96% and 56%, respectively, at 90 ^oC reaction temperature. The activity of the catalyst, as reported by Parameswaram et al. (2013) [222], can be considered as low as compared to RM-500 catalyst, for which 95.2% GL conversion and 92% GC yield was obtained at 75 ^oC reaction temperature. Similarly, the activity of RM-500 catalyst was found to be far

superior as compared to the activity of Al/Mg loaded on hexagonal mesoporous silica reported by Yadav et al. [113], where they achieved 84.7% of GL conversion and 71.4% of GC yield at a very high temperature of 170 ^{o}C. In this study, the RM-500 catalyst was prepared from red mud, a waste generated from aluminum industries, without carrying out any further chemical treatments. Therefore, the cost for the preparation of the catalyst from RM as compared to other commercial catalysts reported for this process will be much less, which will make the process cost-effective. Moreover, the utilization of the largely produced industrial waste for the preparation of various catalysts would also avoid the risk of environmental contamination associated with its hazardous nature.

Table 4.4. Comparison of catalytic activity of RM-500 catalyst with other reported catalysts for the transesterification of GL.

Catalyst	Reaction time (min)	Reaction temperature (°C)	GL:DMC molar ratio	GL conversion (%)	GC yield (%)	Catalyst reusability	Ref
RM-500	90	75	1:3	95.2	92	GL conversion reduced to 26.5% at 4th reuse	Present work
CHT-HMS	150	170	1:3	84.7	71.4	GL conversion reduced to 75.6% at 5th reuse	[113]
HTC-Ni	120	100	1:3	55	55	GL conversion reduced to 45% at 5th reuse	[120]
10 wt% NaOH-LF	90	75	1:2	98.19	96.34	More than 90% GL conversion at 5th reuse	[216]
Mg/Zr/Sr (3:1:1)	90	90	1:5	96	56	Conversion data not given	[222]
Mg/Al/Zr	90	75	1:5	-	94	No reusability study done	[224]
LDO2	300	100	1:3	96	-	Conversion data not given	[225]

4.2 Study of the effect of various alkali and alkaline earth metals on the catalytic activity and stability of RM for the GL transesterification to GC

In the previous section, we observed the high catalytic activity of calcined RM catalysts for the GC synthesis by GL transesterification with DMC. However, the stability of the calcined RM catalyst was not appreciable. In this section, we demonstrate the contribution of various basic active elements such as K, Sr, and Mg on the catalytic activity and stability of RM catalyst for the transesterification of GL with DMC to synthesize GC.

4.2.1 Initial catalysts screening based on their activity and stability

Different RM based catalysts prepared by incorporating K, Sr, and Mg into the surface of RM were initially analyzed for their activity and stability for the GL transesterification process. The KNO_3 doped RM catalyst calcined at 800 °C produced the best activity as well as stability compared with other KNO_3 doped catalysts calcined at different temperatures. The details about the effect of calcination temperature are discussed in section 4.2.2. The results for different KNO_3 doped RM catalysts are shown in Figure 4.13. Incorporating KNO_3 into the surface of RM produced an excellent increase in the catalyst stability for the transesterification of GL. This phenomenon was mainly observed at higher KNO_3 loading. As shown in Figure 4.13, RK-30%-800 catalyst prepared by incorporating 30% K onto the RM surface produced 96.8% GL conversion with 93.2% GC yield from the fresh use of the catalyst. By using the same catalyst, 78% of GL conversion and 75.2% GC yield were achieved at the 4^{th} reuse. The stability of the catalyst was superior to the RM catalyst calcined at 800 °C, where only 17.4% GL conversion and 9.6% GC yield were observed under similar conditions. At lower KNO_3 loading of 5% to 15%, the activity and the stability were lower than those of the RK-30%-800 catalyst. For example, the RK-5%-800 catalyst produced only 75.8% and 73.2% GL conversion and GC yield from the fresh use, and the activity reduced to 21.7% GL conversion and 12.3% GC yield at the 4^{th} reuse. Beyond 800 ^{o}C, no significant changes in the catalytic activity and stability was observed. With the increase in the KNO_3 loading, both the activity and stability of the catalyst increased, which could be due to

improved basic properties in the catalyst. At 40% KNO_3 loading, the conversion of GL was very similar to other catalysts, but a slight decline in the yield of GC as compared to the RK-30%-800 catalyst was observed. Moreover, a slight formation of the byproduct GD was noticed in the case of the RK-40%-800 catalyst, which could be due to its higher basic strength ($18.4 < H_- < 27$) (Table 4.5). Similar activity was also reported by Hu et al. [220], where they used KNO_3/CaO catalyst for the transesterification of GL.

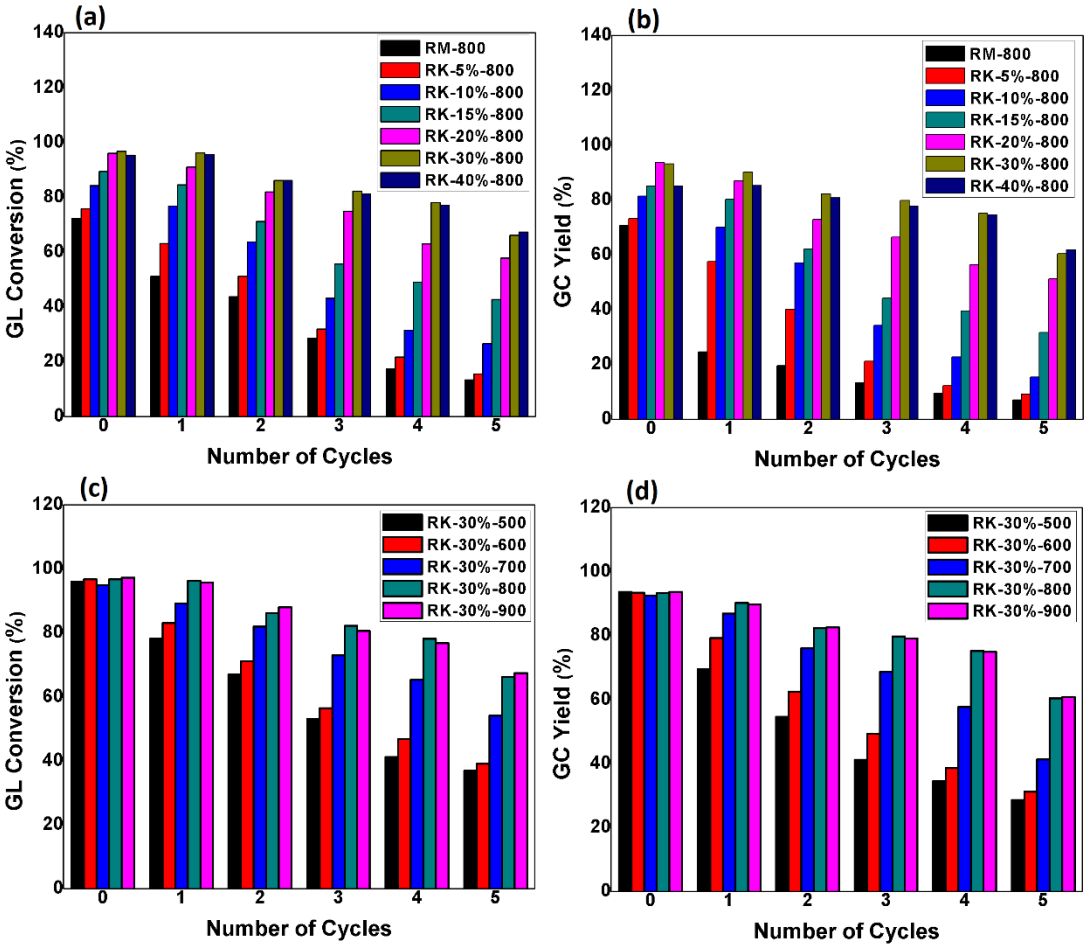

Figure 4.13. Effect of K doping on (a) GL conversion, (b) GC yield: Effect of calcination temperature on (c) GL conversion, (d) GC yield. Reaction conditions: GL/DMC molar ratio = 1:3, time = 90 min, T = 75 ^oC, catalyst loading = 10 wt%.

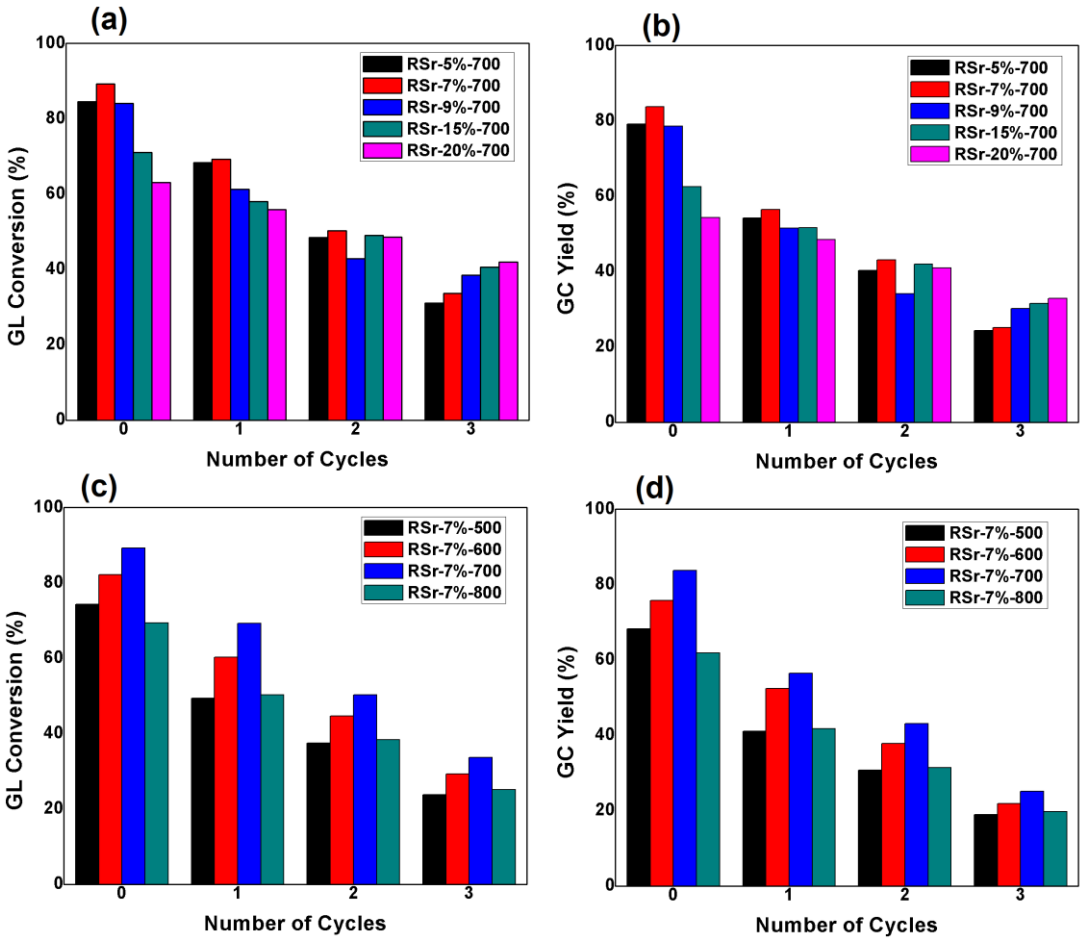

Figure 4.14. Effect of Sr doping on (a) GL conversion, (b) GC yield: Effect of calcination temperature on (c) GL conversion, (d) GC yield. Reaction conditions: GL/DMC molar ratio = 1:3, time = 90 min, T = 75 ^{o}C, catalyst loading = 10 wt%.

Catalysts prepared by doping $SrNO_3$ into the surface of RM were tested for the transesterifications of GL (Figure 4.14). Calcination at different temperatures between 500 ^{o}C and 800 °C revealed that the RSr catalyst calcined at 700 °C produced a better activity than catalysts calcined at other temperatures. As presented in Figure 4.14, the activity of RSr catalysts obtained by doping 5% of Sr and 7% of Sr produced a GL conversion of 84.5.% and 89.2%, respectively, from the 1st cycle of the catalyst. The stability of both catalysts decreased with the number of cycles, and only 31% and 33.6% conversion of GL was obtained at the 3rd cycle of RSr-5%-700 and RSr-7%-700, respectively. Above 7% Sr doping, the activity of the RSr catalyst started to

decrease because of which only 63.1% GL conversion and 54.3% GC yield was found for the fresh RSr-20%-700 catalyst. Interestingly, none of the RSr catalysts produced any comparable or better activity than the RK-30%-800 catalyst when recycled for the transesterification of GL. The best activity observed was for the RSr-20%-700 catalyst that produced 42% GL conversion with 32.9% yield at the 3rd cycle of the catalyst. These results were found to be inferior to the RK-30%-800 catalyst.

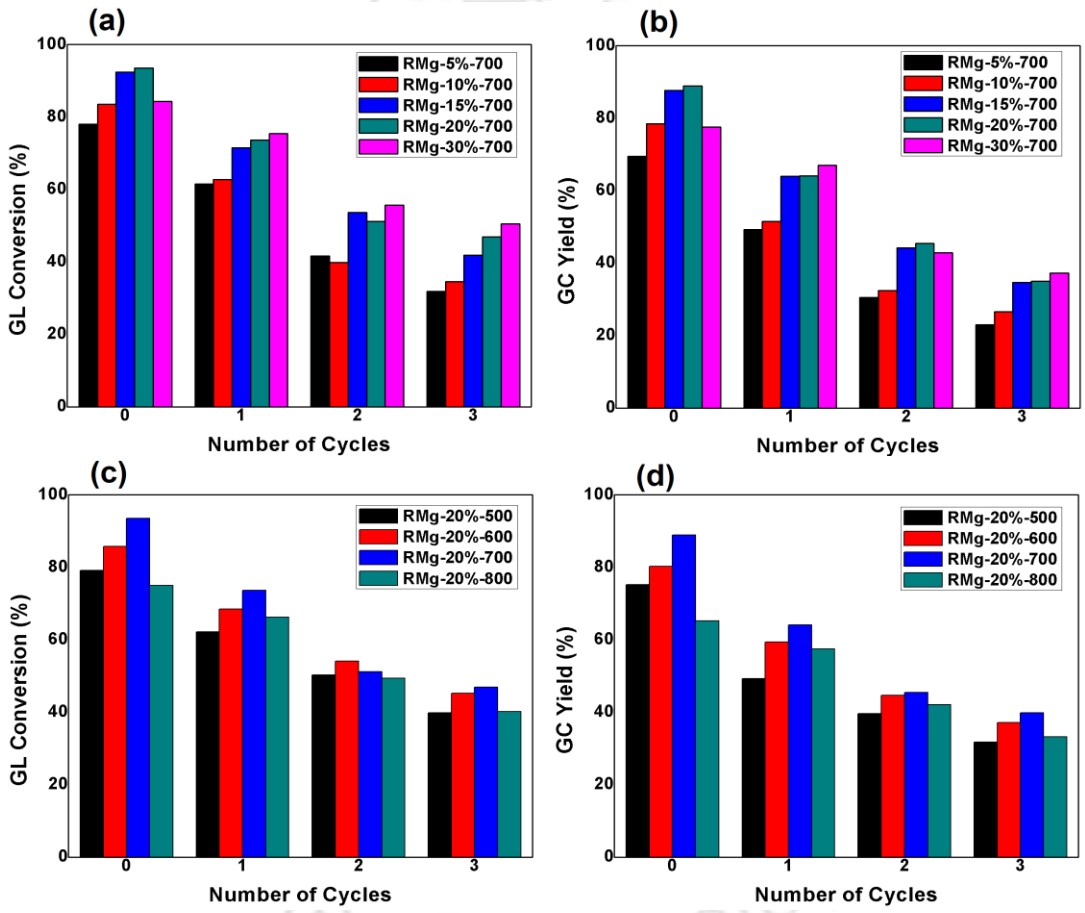

Figure 4.15. Effect of Mg doping on (a) GL conversion, (b) GC yield: Effect of calcination temperature on (c) GL conversion, (d) GC yield. Reaction conditions: GL/DMC molar ratio = 1:3, time = 90 min, T = 75 ^{o}C, catalyst loading = 10 wt%.

Similarly, results for the RMg catalysts prepared by doping $MgNO_3$ into RM surface are shown in Figure 4.15. The activity of RMg catalysts increased with Mg loading up to 20% and then started to decrease above this value of Mg loading. Fresh

RMg catalyst prepared by doping 20% Mg (RMg-20%-700) exhibited the best activity among all other RMg catalysts with 93.5% GL conversion and 88.9% GC yield. However, none of the RMg catalysts showed promising activity during the recycle conditions. The stability of different RMg catalysts was very similar to the RSr catalysts, which were lower than the RK-30%-800 catalyst. RMg-20%-700 catalyst produced only 46.9% GL conversion and 35% GC yield at the 3rd cycle of the catalyst. At higher Mg loading of 30%, the activity of the RMg catalyst started to decrease. However, it produced a slightly higher GL conversion (50.4%) and GC yield (37.2%) than the RMg-20%-700 catalyst at the 3rd reuse.

Based on the preliminary experiments carried out for examining the activity and stability of different RM based catalysts, it was found that RK-30%-800 produced the best catalytic activity and stability compared with other RM based catalysts. The better activity of KNO_3 doped catalyst as compared to $SrNO_3$ and $MgNO_3$ catalyst might be attributed to the better surface interaction of KNO_3 with other components of RM. It could also be due to the stronger bond interaction between the KNO_3 and other components of RM that decreased the leaching of active components such as Na and Ca from RM. These active sites usually are responsible for better activity during the production of GC from GL. Therefore, only catalysts that were produced by incorporating KNO_3 onto the RM surface were considered for further study of transesterification of GL with DMC to synthesize GC.

Table 4.5. Effect of K loading on the catalytic properties of RM for the GL transesterification process. Reaction conditions: GL/DMC molar ratio = 1:3, time = 90 min, T = 75 ^{o}C and catalyst loading = 10 wt%.

Catalyst	GL conversion (%)	GC yield (%)	GD yield (%)	Basic strength	Base amount (mmol g^{-1})
RM-800	72.3	70.8	-	9.3 < H_ < 15	22.1
RK-5%-800	75.8	73.2	-	9.3 < H_ < 15	24.9
RK-10%-800	84.3	81.4	-	9.3 < H_ < 15	26.5
RK-15%-800	89.5	85.1	-	9.3 < H_ < 15	28.6
RK-20%-800	96.1	93.7	-	15 < H_ < 18.4	32.4
RK-30%-800	96.8	93.2	-	15 < H_ < 18.4	33.1
RK-40%-800	95.4	85.1	5.3	18.4 < H_ < 27	33.9

4.2.2 Effect of calcination temperature on the activity of RK-30% catalysts

Preliminary studies carried out for examining the effect of wt% loading of K on the activity and stability of RM for the GL transesterification revealed that 30% K loading was more suitable than the others for the process of GC synthesis. Therefore, RK-30% catalyst was calcined at different temperatures of 500 to 800 °C to examine the physical and chemical changes occurring in the catalyst that could significantly affect the process of transesterification. The RK-30%-100 catalyst showed the lowest activity and was only able to convert 74.3% of GL during the transesterification process. The activity of the RK-30%-100 significantly reduced to 59.6% of GL conversion at the 1st reuse of the catalyst. As illustrated in Figure 4.13, the stability of the RK-30% increased with calcination from 500 ^{o}C to 800 °C. All the RK-30% catalysts calcined between 500 ^{o}C to 800 °C produced very similar activity for the production of GC at the fresh reuse condition, where a GC yield of close to 93% was achieved. However, the RK-30%-500 catalyst exhibited very low stability, and at the 1st reuse, the activity of the catalyst decreased to 78.2% GL conversion and 69.5% GC yield. With an increase in the number of reuses, the activity of the catalyst decreased, and it produced only 36.9% GL conversion with 28.6% GC yield at the 5th reuse. Calcination temperature above 500 °C produced a steady improvement in the stability of the RK-30% catalyst. The RK-30%-800 catalyst was able to achieve 78% GL conversion with 75.2% GC yield at the 4th reuse condition. RK-30%-900 did not produce any significant changes in catalytic activity than RK-30%-800. The improvement in the stability of RK-30%-800 as compared to RM800 catalyst was significant where the latter one was able to produce only 17.4% GL conversion and 9.6% GC yield at the 4th reuse. The activity of the RK-30% catalyst calcined at 600 ^{o}C and 700 °C was very similar to the RK-30%-800 catalyst at fresh use condition. However, the RK-30%-600 and RK-30%-700 catalyst did not show enough stability as the RK-30%-800 catalyst, which made the latter one more promising than the earlier two for the synthesis of GC.

4.2.2.1 ***Catalyst characterization***

4.2.2.2 CO_2-TPD analysis

Figure (4.16 (a)) represents the CO_2-TPD profile of the RM-800 catalyst and different RK-800 catalysts, revealing the occurrence of relatively weaker basic sites than those of the RM-800 catalyst. This could be due to the partial covering of Na and Ca present in RM by the layers of deposited KNO_3. The phenomenon inhibited the access of CO_2 to Na and Ca that are considered as relatively stronger bases than K. However, the acid-base titration indicated the presence of a higher amount of basic sites in the RK-5%-800 and the RK-15%-800 than the RM-800 catalyst (Table 4.5), producing a better GL conversion and GC yield than the RM-800 catalyst. During the acid-base titration, the used HCl could dissolve and react efficiently with all the basic elements in the catalyst and, therefore, produced a higher basic amount in the K-doped RM catalyst. It is also quite evident from Figure (4.16 (a)) that the basic strength of the catalyst continuously increased with the increase in K loading from 5% to 40%. The RK-800 catalysts prepared by doping 5% to 15% of K produced a very low-intensity CO_2 desorption peak, approximately at 150 °C, which could be assigned to the weak basic sites present in these catalysts. Besides this, all three catalysts possessed a second desorption peak approximately at 452, 465, and 545 °C that confirmed the presence of moderately strong basic sites. This was also confirmed from the Hammet indicator test, which showed a basic strength of $9.3 < H_- < 15$ for all these three catalysts (Table 4.5). The existence of weak basic sites was not identified in the case of catalysts prepared at higher K loading other than 15%. The catalyst RK-20%-800 possessed a CO_2 desorption peak at around 645 °C, RK-30%-800 had a peak at 605 °C with another shoulder peak at 679 °C, and RK-40%-800 showed three shoulder peaks at 635, 720, and 765 °C, respectively. The existence of these CO_2 desorption peaks indicated the presence of stronger basic sites in the RM-800 catalysts loaded with more than 15% K. The Hammett indicator test confirmed the higher basic strength of RK-20%-800 and RK-30%-800, which was $15 < H_- < 18.4$ for both of these catalysts. The number of basic sites found in the RK-20%-800 and RK-30%-800 was 32.4 and 33.1 mmol g^{-1}, respectively, which was higher than the 5% to 15% K-doped RM catalysts. Therefore, it was obvious that loading of KNO_3

into the surface of RM enhanced the basic properties of the catalyst to a significant extent, which could be considered a reason for its higher activity and stability than the RM-800 catalyst. For the RK-40%-800 catalyst, the basic sites were considered very strong as compared to others. This was also confirmed from the Hammett indicator test that produced a basic strength value of 18.4 < H_ < 27. This could be the reason for the slight formation of by-product GD (5.3%) in the case of this catalyst.

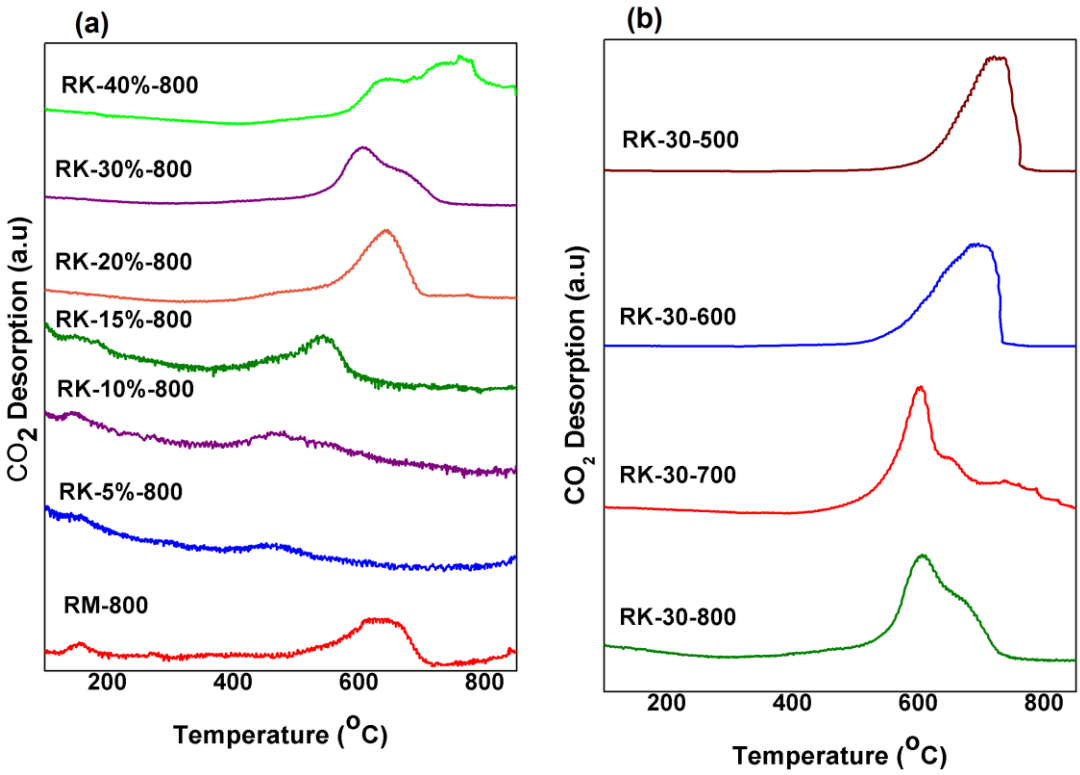

Figure 4.16. TPD-CO_2 profile of (a) RM-800 and RK-800 catalysts with K doping between 5% to 40%, (b) RK-30% catalyst calcined between 500 ºC to 800 ºC.

The CO_2-TPD profile of RK-30% catalyst calcined in the range of 500 ºC to 800 °C is shown in Figure (4.16 (b)). It was observed that all the RK-30% catalysts calcined in the temperature range of 500 ºC to 800 °C possessed a strong intensity CO_2 desorption peak at a temperature just above 450 °C. The peak indicated the presence of strong basic sites in all these catalysts. With the increase in calcination temperature, a decrease in CO_2 desorption temperature was observed, which also

indicated a relative decrease in the basic strength of the catalyst. However, Hammett indicator tests confirmed a basic strength of 15 < H_ < 18.4 for all the RK-30% catalysts calcined between 500 ºC and 800 °C (Table 4.6). No presence of any weak or medium basic sites in any of the RK-30% catalysts was obtained from the CO_2-TPD analysis. The RK-30%-500 and RK-30%-600 catalyst produced a CO_2 desorption peak approximately at 710 ºC and 695 °C, respectively. The RK-30%-700 and RK-30%-800 catalysts contained the CO_2-TPD desorption peak at 610 ºC and 604 °C with a shoulder peak for each at 650 ºC and 679 °C, respectively. The existence of strong and greater numbers of basic sites, as confirmed from the TPD-CO_2 and acid-base titration, suggested an improvement in the basic properties of all the RK-30% catalysts.

4.2.2.3 Acid-Base titration and Hammett indicator test

The acid-base titration experiments revealed an increase in the number of basic sites with the increase in calcination temperature for the RK-30% catalysts (Table 4.6). The uncalcined RK-30% catalyst contained only 23.2 mmol g^{-1} of basic sites. Calcination at 500 °C showed an enhancement in the concentration of basic sites to 26.8 mmol g^{-1}. The trend continued with the increase in calcination temperature, and an amount of 33.1 mmol g^{-1} of basic sites was obtained for the RK-30%-800 catalyst. The enhanced number of basic sites could be ascribed to the formation of highly active K_2O due to the decomposition of KNO_3 at a higher calcination temperature. The Hammett indicator test confirmed a basic strength of 15 < H_ < 18.4 for all the RK-30% catalysts calcined between 500 ºC and 800 °C. This value of basic strength has been proven to produce promising activity for the production of GC through GL transesterification [93,220]. A basic strength greater than 18.4 was found to be unsuitable for this process because it resulted in the decomposition of GC to GD as observed for the RK-40%-800 catalyst.

Table 4.6. Variation in catalytic properties of RK-30% catalysts with calcination temperatures and its effect on the transesterification of GL. Reaction conditions: GL/DMC molar ratio = 1:3, time = 90 min, T = 75 ^{o}C and catalyst loading = 10 wt%.

Catalyst	GL conversion (%)	GC yield (%)	GD yield (%)	Basic strength	Base amount
RK-30%-100	74.3	69.8	-	$9.3 < H_- < 15$	23.2
RK-30%-500	96.1	93.6	-	$15 < H_- < 18.4$	26.8
RK-30%-600	96.8	93.4	-	$15 < H_- < 18.4$	28.9
RK-30%-700	94.9	92.5	-	$15 < H_- < 18.4$	32.0
RK-30%-800	96.8	93.2	-	$15 < H_- < 18.4$	33.1

4.2.2.4 XRD analysis

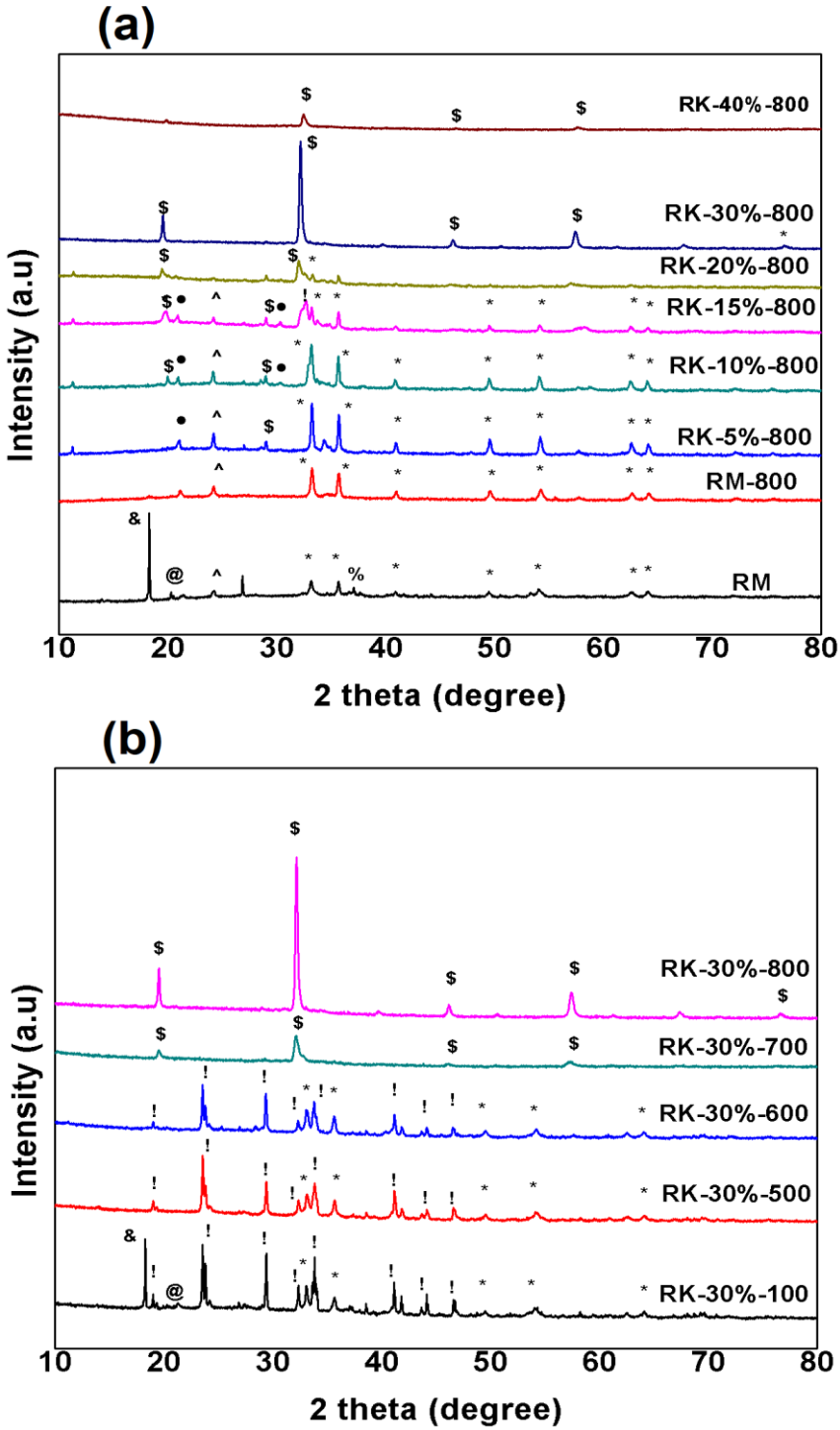

Figure 4.17. XRD profiles of (a) RM, RM-800 and RK-x%-800 catalysts with K loading of 5% to 40% and (b) RK-30% catalysts calcined in the temperature range of 500 ^{o}C to 800 ^{o}C. * Fe_2O_3, & $Al(OH)_3$, @ $NaAlO_2$, # $CaCO_3$, % SiO_2, $ $Ca_2(SiO_4)$, ^ TiO_2, ! KNO_3. $ K_2O.

The XRD profiles of the fresh RM, RM-800, and RK-800 catalysts with K doping of 5% to 40% are shown in Figure (4.17 (a)). Different crystalline phases found in the fresh RM sample were Fe_2O_3 (at 2θ of 33.0°, 35.68°, 40.7°, 49.23°, 53.9°, 62.2°, and 64.9°), $Al(OH)_3$ (2θ of 18.42°), SiO_2 (2θ of 37.6°), TiO_2 (2θ of 24.4°), and $NaAlO_2$ (2θ of 20.7°) [210,211,213,214]. As reported in section 4.1.1.2, calcination of RM at 800 °C resulted in a considerable increase in the surface concentration of Fe_2O_3 and a decrease in the concentration of active $NaAlO_2$. This resulted in a low activity of the catalyst. It can be seen from Figure (4.17 (a)) that KNO_3 remained in a well-dispersed phase on the surface of the RM at a lower percentage of K loading (5% to 15%), due to which there were no distinct XRD peaks of KNO_3 observed, and Fe_2O_3 remained as a dominant phase in the RK-800 catalysts loaded up to 15% K. This could be a reason for the low activity of the catalyst at low K loading. The low-intensity peaks observed at 2θ of 19.8° and 29.0° for the RK-5%-800, RK-10%-800, and RK-15%-800 catalysts could be due to the low concentration of surface K_2O formed in the catalyst [226]. A small concentration of $KAlSi_3O_8$ was also observed at 2θ of 20.9° and 30.5° in the 5% to 15% K doped catalyst [227]. Beyond 15% K loading, a significant decrease in the surface concentration of the Fe_2O_3 was observed, which was confirmed by the disappearance of most of the Fe_2O_3 peaks in the RK-20%-800 catalyst. At this percentage of K loading, the emergence of small intensity K_2O phases at 2θ of 19.8°, 32.3°, and 57.2° could be due to the decomposition of more KNO_3 phases at higher temperatures [226]. The surface concentration of K_2O significantly improved in the case of the RK-30%-800 catalyst, which was evident from the XRD profile that produced a highly crystalline phase of K_2O at 32.3°. The increase in the surface concentration of K_2O at high calcination temperatures might have contributed mostly toward the enhanced basic properties of the RK-30%-800. For the case of RK-40%-800 catalyst, a low-intensity peak related to the K_2O phase at 2θ of 32.3° was noticed, which suggested a relatively low surface concentration of K_2O in the catalyst. Surprisingly, there was also no evidence of KNO_3 phases found in the XRD profile of the RK-40%-800 catalyst. In general, the decomposition of KNO_3 to K_2O occurs through the formation of an intermediate KNO_2 phase, which then undergoes further decomposition to produce K_2O. The phenomenon of intermediate KNO_2 formation might have occurred in the case of RK-40%-800

catalyst, due to which it showed a low K_2O concentration on its surface. Although there was no sign of KNO_2 phases detected in the XRD profile of any of the RK-x%-800 catalysts, it was initially assumed that it might be present in very low concentration or in a very well dispersed condition. Thus, the XRD profile did not produce any distinct peak of KNO_2. This assumption was later validated through other characterization techniques, as discussed in the following sections. The results of the CO_2-TPD profile, acid-base titration, and Hammett indicator test validated the XRD results up to a reasonable extent that concluded the RK-30%-800 catalyst to be the most promising one for the transesterification of GL.

The XRD profiles of the RK-30%-100 and RK-30% catalysts calcined from 500 ^oC to 800 °C are shown in Figure (4.17 (b)). It was observed from the XRD profile that a majority of the hematite phases noticed in the raw RM (Figure 4.17 (a))disappeared, and only very low-intensity peaks of hematite at 33.0°, 35.68°, 49.23°, 53.9°, and 64.9° were noticed in the RK-30%-100 catalyst. This could be attributed to the surface masking occurring from the doped KNO_3 that decreased the concentration of hematite phases on the surface of the RK-30%-100 catalyst. Crystalline phases of KNO_3 were observed in the XRD profile of the RK-30%-100 catalyst at 2θ values of 19.02°, 23.62°, 29.4°, 32.65°, 33.9°, 41.2°, 44.3°, and 46.7° [220,228]. Very low-intensity peak related to the $NaAlO_2$ phases of fresh RM at 20.7° (Figure 4.17 (a)) was also found to be present in the RK-30%-100 catalyst. The RK-30%-100 catalyst was able to retain the strong intensity gibbsite ($Al(OH)_3$) phase of raw RM, which was observed at a 2θ of 18.42°. Calcination at 500 °C resulted in a reduced intensity of the KNO_3, $NaAlO_2$, and $Al(OH)_3$ crystalline phases, and reduction continued until the temperature reached 600 °C. With calcination at 700 °C, the intensity of KNO_3 phases decreased, and low-intensity peaks related to the crystalline phases of K_2O started to arise at 2θ values of 19.8°, 32.3°, 39.5°, 46.6°, 57.2°, and 76.7° [226]. This could be due to the decomposition of KNO_3 to K_2O on the surface of the catalyst at higher calcination temperatures. At 800 °C, a high-intensity peak of K_2O was detected at 32.3°, which indicated a significant increase in the concentration of the active K_2O phase on the surface of the catalyst. The dominant hematite phases, as observed in the case of RM-800 catalyst, disappeared in the RK-

30%-800 catalyst. The phenomenon of a decrease in KNO_3 phases and increase in K_2O phases suggested a phase transformation of KNO_3 to K_2O with increase in temperature. However, the absence of K_2O phases in the catalysts calcined at temperatures up to 700 °C also led to the presumption that there might also be an intermediate KNO_2 phase present in the calcined RK-30% catalysts. The low concentration of the KNO_2 phase could lead to it being well-dispersed, due to which no distinct peaks of the phase were noticed in the XRD profile. The enhanced basic properties of the catalyst occurring because of the higher surface concentration of K_2O at 800 °C could be a reason for the improved catalytic activity and stability of the catalyst for the transesterification of GL. It was also noticed visually that calcination at 800 °C resulted in a change in the color of the catalyst from dark red (color of RM) to pale yellow, which is a characteristic physical appearance of K_2O. Besides this, the physical structure of the catalyst was found to be a very hard and compact solid at 800 °C. This provided knowledge about the formation of a rigid layer of K_2O on the surface and the presence of a strong bond interaction between other elements present below the K_2O layer in the catalyst. It might have helped in decreased leaching of the active K, Na, and Ca from the catalyst, which could be another reason for the higher stability of the RK-30%-800.

4.2.2.5 FTIR analysis

The FTIR profiles of RK-30% catalysts calcined in the range of 500 °C to 800 °C are shown in Figure 4.18. At the wavenumbers of 825 cm^{-1} and 1385 cm^{-1}, the FTIR peaks were attributed to the $-NO_3$ group that confirmed the presence of KNO_3 in the catalyst [220]. It is also quite evident from the FTIR profile that the nitrate group at 825 cm^{-1} continued to decrease with the increase in calcination temperature and almost disappeared in the RK-30%-800 catalyst. This indicated the decomposition of KNO_3 to K_2O at higher temperatures, as observed in the XRD profile (Figure 4.17 (b)). Moreover, the sharp characteristic peaks of Fe−O at 460 cm^{-1} noticed in the RM-800 were not found in any of the RK-30% catalysts [215]. Further, the distinguished peak related to the stretching vibration of Si−O−Si groups at 1001 cm^{-1} of the RM-800 catalyst started to diminish with the increase in the temperature. The peaks observed at wavenumbers of approximately 3450 cm^{-1} and 1640 cm^{-1} were

due to the vibration of −OH groups of water molecules present in the catalyst. Moreover, the peak found at 1530 cm^{-1} of the RK-30%-800 catalyst could be due to the presence of the NO_2^- group of the KNO_2 formed due to the decomposition of KNO_3 species [220]. This validated the initial assumption about the formation of the intermediate KNO_2 phase during the decomposition of the KNO_3 component at high temperature.

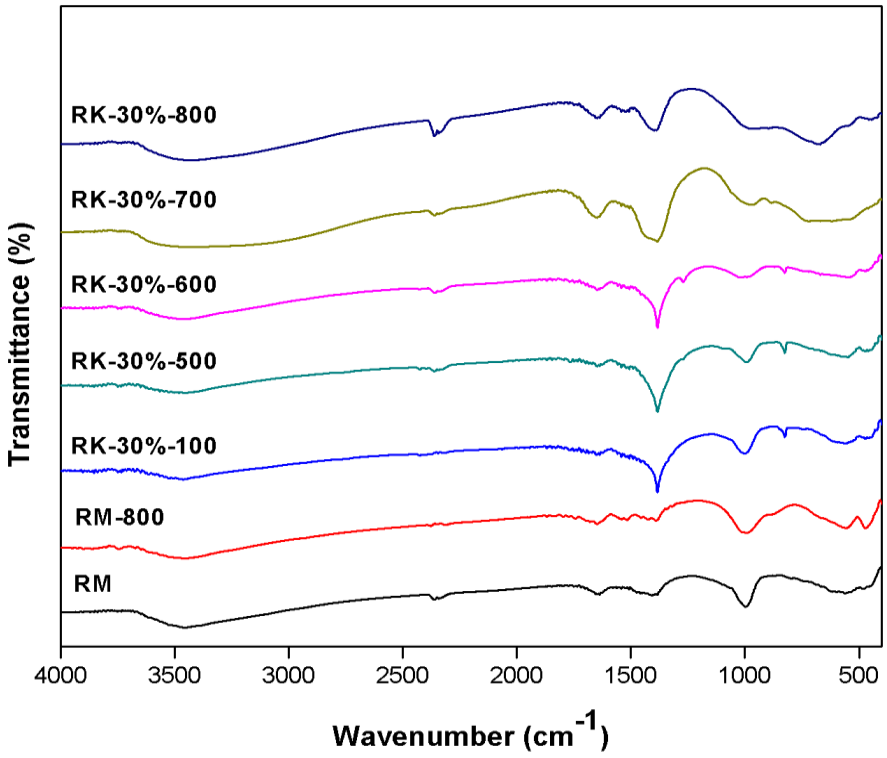

Figure 4.18. FTIR profile of different K-doped RM catalysts.

4.2.2.6 FESEM and FESEM-EDX analysis

Study on the effects of calcination temperature has proved that this factor could significantly affect the geometry, morphology, and basic properties of a catalyst and thus could alter the activity of the catalyst for the transesterification process. Effects of the calcination temperature on the RK-30% catalyst were also observed in the morphology of the RK-30% catalyst calcined between 500 °C and 800 °C (Figure 4.19). The RK-30%-100 catalyst was found to have relatively smaller particles than all other calcined RK-30% catalysts with irregular size and loosely bound to each other. Calcination at 500 °C and 600 °C resulted in the formation of bigger particles

with a relatively increased number of pores. The increased numbers of pores in the RK-30%-500 and RK-30%-600 could be attributed to the removal of chemically bound water, carbonate groups, and nitrate groups from the catalyst. However, a further increase in calcination temperature to 700 ^{o}C and 800 °C led to the formation of very compact and larger particles with a decreased number of pores. This could be due to the severe agglomeration of particles at higher calcination temperatures.

The FESEM-EDX analysis (Table 4.7) confirmed the presence of various elements such as Fe, Al, Ti, Na, Ca, and the doped K in the RK-30%-800 catalyst.

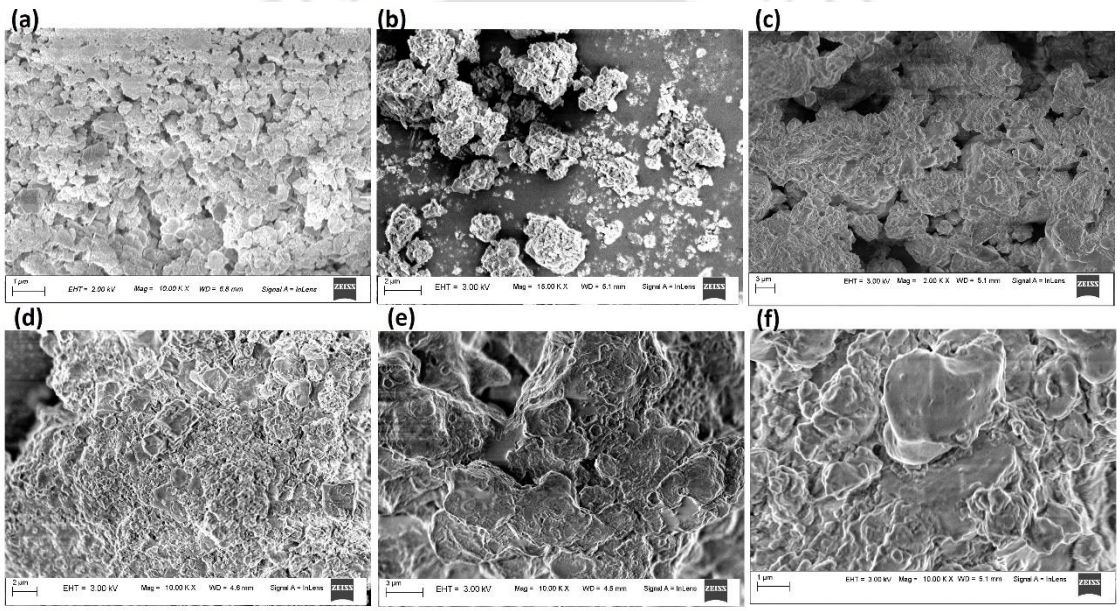

Figure 4.19. Surface morphology of (a) RM, (b) RK-30%-100, (c) RK-30%-500, (d) RK-30%-600, (e) RK-30%700, (f) RK-30%-800.

Table 4.7. FESEM-EDX analysis of fresh and the 5th reuse RK-30%-800 catalyst.

Elements	C	O	Fe	Al	Si	Ti	Na	Ca	K
RK-30%-800	10.4	39.9	15.8	4.9	2.0	3.1	3.6	0.2	20.1
5th reused RK-30%-800	13.0	46.5	14.1	4.9	6.2	2.3	2.1	0.2	10.7

4.2.2.7 N_2 Adsorption-Desorption analysis

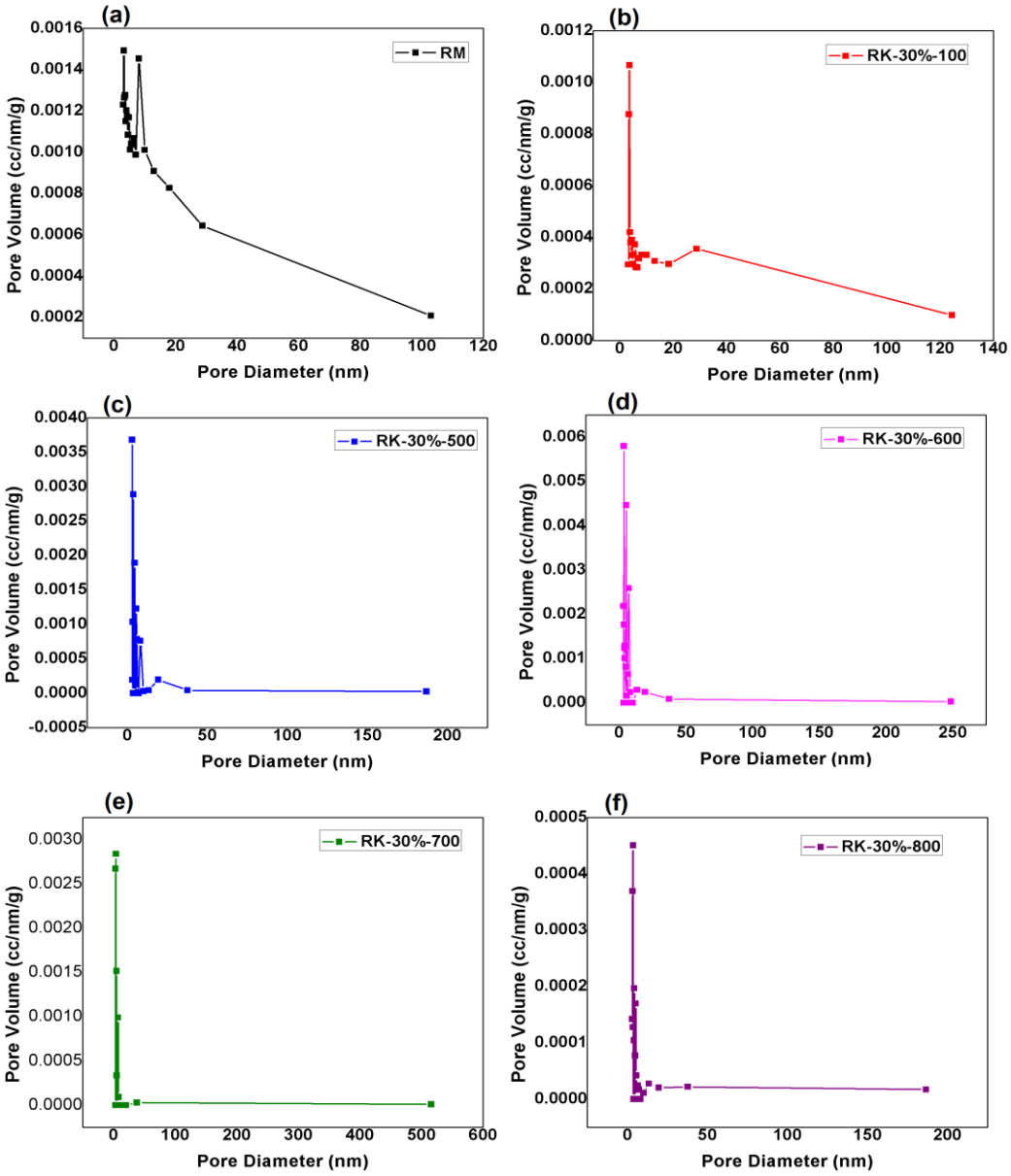

Figure 4.20. Pore size distribution curve of (a) RM, (b) RK-30%-100, (c) RK-30%-500, (d) RK-30%-600, (e) RK-30%-700, and (f) RK-30%-800.

The surface area and pore size analyses (Figure 4.20) carried out for all the K-30% catalysts were very consistent with the surface morphology results. As reported in Table 4.8, the RM catalyst possessed a BET surface area of 11.6 $m^2\ g^{-1}$ with an average pore size of 19.26 nm. At 30% K loading, the surface area was reduced to 4.4

$m^2 g^{-1}$, which could be due to the partial covering of pores by the deposited KNO_3 molecules. The surface area of the catalyst increased to a value of 5.0 and 6.5 $m^2 g^{-1}$ with calcination at 500 ºC and 600 °C, respectively. This might be due to the removal of some of the water and carbonate groups from the catalyst at these values of calcination temperatures. Above 600 °C, the catalyst showed a decrease in surface area to 1.3 m^2g^{-1} at 700 °C and to 1.3 m^2g^{-1} at 800 °C. The phenomenon could be attributed to the formation of agglomerated particles along with a very compact layer of K_2O on the surface of the catalyst at higher temperatures, as confirmed from the FESEM and XRD profile, respectively.

Table 4.8. Surface area and pore size analysis of different catalysts.

Catalyst	Surface area ($m^2 g^{-1}$)	Average pore size (nm)	Total pore volume ($cm^3 g^{-1}$)
RM	11.6	19.26	0.056
RK-30%-100	4.4	26.11	0.028
RK-30%-500	5.0	11.39	0.014
RK-30%-600	6.5	13.27	0.021
RK-30%-700	1.3	29.53	0.009
RK-30%-800	1.3	18.54	0.006

4.2.3 Activity test of RK-30%-800 for the GL transesterification

4.2.3.1 Reaction parametric study

Experimental results for the effect of reaction time on the transesterification of GL are shown in Figure (4.21 (a)). Experiments were carried out at different reaction times of 15 to 135 min. It was observed that with the increase in reaction time, the GL conversion and GC yield increased. The lowest value of GL conversion (51.9%) and GC yield (36.9%) was observed at 15 min of reaction time. With an increase in time, the efficiency of the reaction increased, and 96.8% GL conversion with 93.2% GC yield was obtained at 90 min of reaction time. During the initial period of the reaction (up to 15 min), the reaction was observed to be very rapid, and after

that, it slowed down. This could be due to the presence of a higher number of vacant active sites at the start of the reaction that allowed the reactant molecules to adsorb and react quickly. Moreover, during the initial phase of the reaction, more GL molecules were available for reaction with the DMC molecules, due to which the reaction proceeded at a faster rate. Beyond 90 min reaction time, there was a slight decrease in GL conversion, and GC yield was observed. At 105 min of reaction time, these values reduced to 93.9% and 88.5%, respectively. The GL conversion continued to decrease, and at 135 min of reaction time, it reached a value of 89.7%. The result suggested that at 90 min of reaction time, the reaction had reached equilibrium, and after that, the reverse reaction between GC and methanol started to occur. However, the reverse reaction between GC and methanol was very slow as compared to the forward reaction between GL and DMC; hence the decrease in GL conversion was not significant.

Reaction temperature has proven to have significant effects on the process of GC synthesis by GL transesterification. It could directly influence the heat-sensitive carbonate and active sites of the catalyst, which as a result, could affect the reaction efficiency significantly [221]. To analyze the effect of the reaction temperature on transesterification of GL, various experiments were performed between 45 ^{o}C and 105 °C with a temperature gap of 15 °C. As shown in Figure (4.21 (b)), at 45 ^{o}C and 60 °C, the efficiency of the reaction was relatively low, due to which only 47.5% and 73.5% of GL conversion were observed. A further increase in the temperature to 75 °C produced a significant increase in GL conversion (96.8%) and GC yield (93.2%). This could be attributed to the higher energy of reactant molecules at a higher temperature, which was required to overcome the energy barrier between the reactant and product molecules. Reaction temperature higher than 75 °C did not produce any significant improvement in the reaction efficiency. The GL conversion obtained at 90 ^{o}C and 105 °C was 97.1% and 97%, respectively. Hence, the reaction temperature of 90 °C was considered as the optimum temperature for the transesterification of GL using the RK-30%-800 catalyst.

Figure (4.21 (c)) shows the effect of GL to DMC molar ratio on the efficiency of the transesterification reaction. It was observed that 1:1 molar ratio of GL to DMC was not sufficient to convert all the GL molecules to GC, and only 58.4% of GL conversion was observed. Higher GL to DMC molar ratio favored the reaction in the desired direction, which was evident from the increased value of GL conversion to 77.6% at 1:2 GL to DMC ratio. The improvement in the efficiency of the transesterification process continued until a GL to DMC ratio of 1:3, where a maximum GL conversion of 96.8% and GC yield of 93.2% was achieved. A biphasic system is produced in the reaction system because of the hydrophilic and hydrophobic nature of the GL and DMC, respectively [221]. Higher DMC amount than equimolar ratio has proven to promote the transesterification of GL by partially preventing the biphasic system between GL and DMC through increasing contacts between them. Moreover, by using an excess of DMC, the process could favor the forward reaction between GL and DMC, which could reduce the possibility as well as the speed of the reverse reaction between GC and methanol. For this system, GL to DMC molar ratio beyond 1:3 did not show any significant increment in the reaction efficiency; hence a molar ratio of 1:3 was considered as optimum.

Effects of catalyst loading on the transesterification of GL were analyzed at a different catalyst loading of 5 wt% to 20 wt% with respect to the weight of GL (Figure 4.21 (d)). RK-30%-800 catalyst with a loading of 5 wt% produced 80.6% GL conversion and 75.6% GC yield. Increasing the catalyst loading to 7.5% and 10% increased the process efficiency significantly. The corresponding value of GL conversion obtained at 7.5 wt% and 10 wt% loading of the catalyst was 88.6% and 96.8%, and the GC yield was found to be 82.7% and 93.2%, respectively. The better efficiency of the GL transesterification observed at a higher catalyst loading could be because of the presence of higher numbers of active catalytic sites at a given time that favorably participated in the catalytic reaction. Nevertheless, catalyst loading higher than a certain limit could also result in particle agglomeration. Consequently, the mass transfer limitations between the reactant molecules and the active sites of the catalyst could occur, which could result in a decrease in the overall efficiency of the process. For this system, no such activity was observed at a higher catalyst loading other than

10 wt%, and no significant improvement in GL conversion or GC yield was noticed as well. Therefore, 10 wt% of RK-30%-800 catalyst was considered suitable for the GL transesterification process.

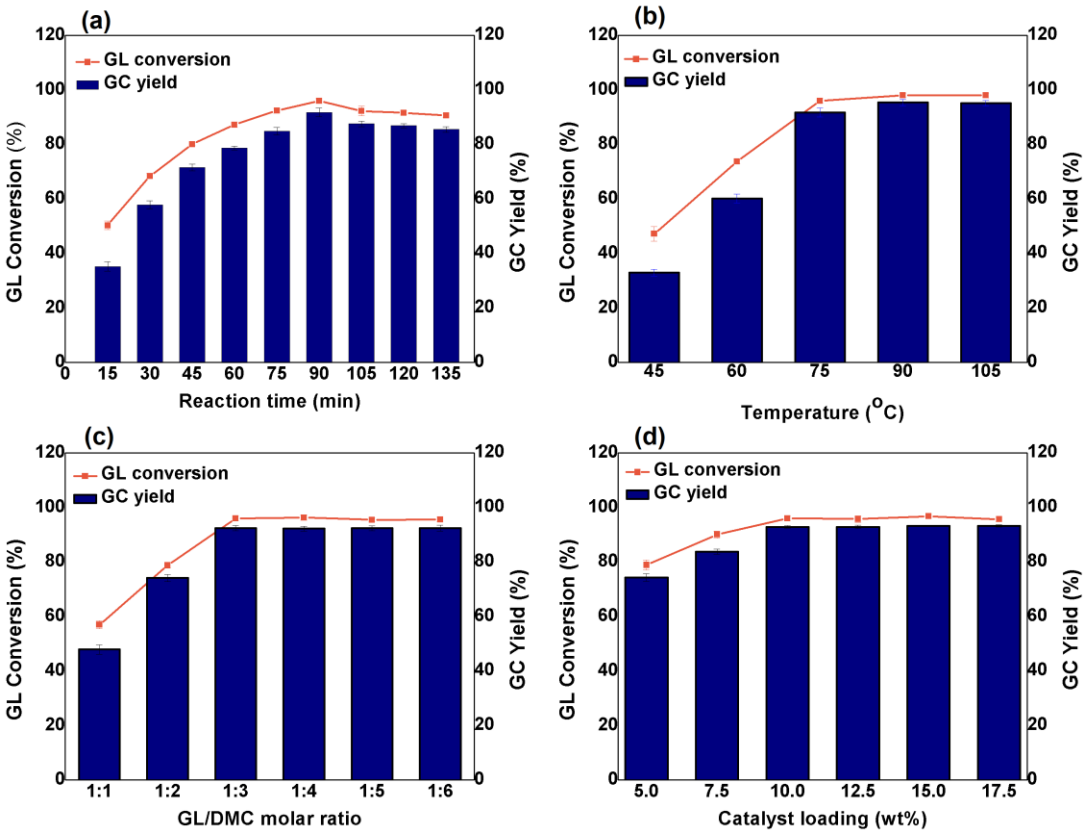

Figure 4.21. Effects of reaction influencing parameters on the GL transesterification by using RK-30%-800 catalyst: (a) effect of reaction time: GL/ DMC molar ratio = 1:3, T = 75 ^{o}C, catalyst loading = 10 wt%; (b) effect of temperature: GL/ DMC molar ratio = 1:3, t = 90 min, catalyst loading = 10 wt%; (c) effect of GL/ DMC molar ratio: T = 75 ^{o}C, t = 90 min, catalyst loading = 10 wt%; (d) effect of catalyst loading: GL/DMC molar ratio = 1:3, T = 75 ^{o}C , time = 90 min.

4.2.3.2 Effect of impurities on the catalytic activity of RK-30%-800

It has been found that GL directly obtained from biodiesel industries contains impurities such as water and methanol. These impurities could adversely affect the activity of the catalyst when used for the transesterification of crude GL from biodiesel industries. Thus, a catalyst that can resist these impurities and can produce

similar activity as for pure GL is desired for the sustainability of the process. The activity of the RK-30%-800 catalyst was tested in the presence of water or methanol (individual amount of 6 wt% with respect to GL weight) and a mixture of both the impurities (6 wt% each with respect to GL weight). The activity of the RK-30%-800 catalyst in the presence of such impurities was observed to be excellent (Figure 4.22). GL conversion of 93.9% and GC yield of 89.3% were achieved in the presence of water as an impurity. These values are only 2.9% and 3.9% less than the GL conversion and GC yield that was obtained in the absence of water as an impurity. Similarly, the presence of only methanol reduced the GL conversion and GC yield by only 1.9% and 3.5%, respectively. In the presence of both water and methanol as impurities, the RK-30%-800 catalyst was still able to produce 92.3% GL conversion and 87.6% GC yield. These results obtained in the presence of different impurities demonstrated that the RK-30%-800 catalyst was quite efficient for the production of GC in the presence of such impurities. Moreover, these results obtained for the RK-30%-800 catalyst were better than other reported catalysts [216,220], which make this catalyst considered as a strong candidate for GC synthesis.

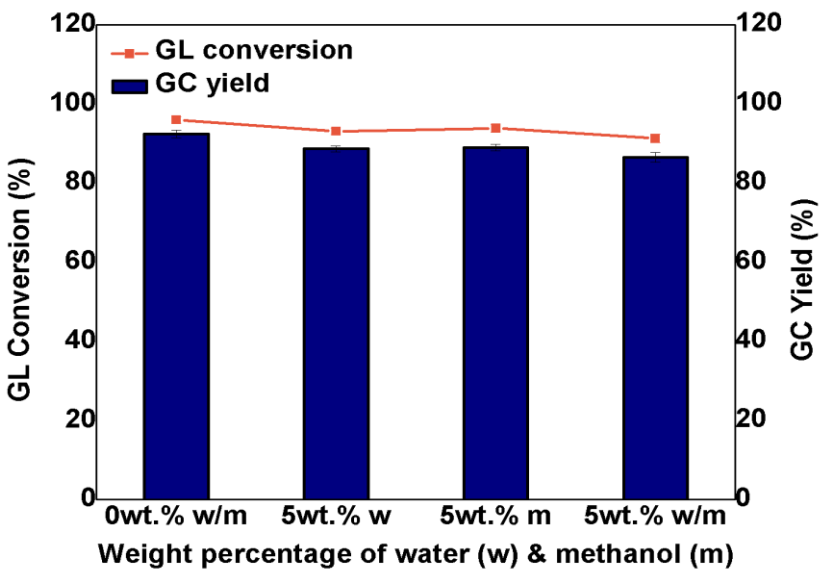

Figure 4.22. Activity of the RK-30%-800 catalyst in the presence of water (wat) and methanol (met) as impurities. Reaction conditions: GL/DMC molar ratio = 1:3, time = 90 min, T = 75 ^{o}C and catalyst loading = 10 wt%.

4.2.4 Plausible reaction mechanism and development of kinetic model

A probable reaction pathway for the production of GC by the reaction of GL with DMC can be presented by the concept of conventional transesterification process where both the basic and acidic sites of the catalyst take part in the reaction (Figure 4.23). Besides the presence of K, Na, and Ca in the RK-30%-800 catalyst, it also contains some amounts of Al and Si in their oxide forms, which act as acidic sites in the reaction. Different reaction steps that might occur during the transesterification of GL are as follows: GL and DMC were adsorbed on the surface of the catalyst where GL was activated to glyceroxide anion (by donating a H^+ ion) on the basic sites. DMC was activated on the acidic sites, which produced a highly positive carbonyl carbon in it. Subsequently, a nucleophilic reaction occurred between the two active molecules that resulted in the formation of methyl glyceryl carbonate along with one mole of methoxide anion as intermediates. Afterward, a repeat of the initial step occurred where another −OH group of GL was activated, and another nucleophilic reaction with the carbonyl carbon of DMC happened. At last, the intermediate encountered a cyclic rearrangement to produce a GC molecule.

The Langmuir-Hinshelwood model was used for the kinetic study of the GL transesterification with DMC to obtain GC by using RK-30%-800 catalyst.

The variation of reaction rate beyond a stirring speed of 600 rpm was observed to be insignificant, which confirmed the absence of external mass transfer limitations. The approximate particle size of the catalyst taken for the reaction was less than 15 µm, for which the Weisz-Prater parameter remains less than 1; thus, the internal mass transfer limitations could be neglected.

Following are the necessary assumptions considered for the development of the kinetic model

(i) The rate was surface reaction controlling, and all other steps except the surface reactions were considered to be in equilibrium.

(ii) Although the existence of reversible reaction between GC and methanol was observed at a longer reaction period (after 90 min), the rate of reverse reaction was not significant and, therefore, was neglected for developing the kinetic model.

iii) The concentration of DMC throughout the reaction was considered as same, since, it was taken in excess.

Different reaction steps for production of GC by the transesterification of GL with DMC are provided below.

GL adsorption on the surface of the catalyst:

$$GL + S \leftrightarrow GL.S \quad (27)$$

DMC adsorption on the surface of the catalyst:

$$DMC + S \leftrightarrow DMC.S \quad (28)$$

Reaction between the adsorbed GL and DMC on the surface of the catalyst:

$$GL.S + DMC.S \leftrightarrow GC.S + MET.S \quad (29)$$

Desorption of GC and methanol from the surface of the catalyst:

$$GC.S \leftrightarrow GC + S \quad (30)$$

$$MET.S \leftrightarrow MET + S \quad (31)$$

By considering the assumption (ii), the rate of the reaction can be expressed as:

$$-r = -\frac{dC_{GL}}{dt} = k_S C_{GL.S} \cdot C_{DMC.S} - k'_S C_{GC.S} \cdot C_{MET.S} \quad (32)$$

$$\text{Or, } -\frac{dC_{GL}}{dt} = k_S (C_{GL.S} \cdot C_{DMC.S} - \frac{1}{K_S} C_{GC.S} \cdot C_{MET.S}) \quad (33)$$

where, K_S can be defined as, $K_S = \frac{k_S}{k'_S}$

The concentration of different adsorbed species are as expressed below.

$$C_{GL.S} = K_{GL} C_{GL} C_v \quad (34)$$

$$C_{DMC.S} = K_{DMC} C_{DMC} C_v \quad (35)$$

$$C_{GC.S} = K_{GC} C_{GC.} C_v \quad (36)$$

$$C_{MET.S} = K_{MET} C_{MET.} C_v \quad (37)$$

C_v is the concentration of vacant site on the catalyst.

By putting the value of Eq. 34 to 37 on Eq. 33, the rate expression becomes:

$$-\frac{dC_{GL}}{dt} = k_S \,.K_{GL}\,.K_{DMC}\left(C_{GL}\,.C_{DMC} - \frac{K_{GC}\,.K_{MET}}{K_S\,.K_{GL}\,.K_{DMC}} C_{GC}\,.C_{MET}\right) {C_v}^2 \quad (38)$$

Vacant site concentration C_v can be presented as:

$$C_v = \frac{C_o}{1+ K_{GL}C_{GL}+K_{DMC}C_{DMC.}+K_{GC}C_{GC}+K_{MET}C_{MET}} \quad (39)$$

where, C_o is the total concentration of active sites on the catalyst.

Eq. 38, after putting the value of Eq. 39 becomes,

$$-\frac{dC_{GL}}{dt} = \frac{k_S\,.K_{GL}\,.K_{DMC}\left(C_{GL}\,.C_{DMC} - \frac{K_{GC}\,.K_{MET}}{K_S\,.K_{GL}\,.K_{DMC}} C_{GC}\,.C_{MET}\right){C_o}^2}{(1+ K_{GL}C_{GL}+K_{DMC}C_{DMC.}+K_{GC}C_{GC}+K_{MET}C_{MET})^2} \quad (40)$$

By neglecting the reverse reaction as per the assumption (iii) and considering the DMC concentration constant as per the assumption (iv), the rate expression reduced to,

$$-\frac{dC_{GL}}{dt} = (KwC_{GL}) \quad (41)$$

where, $Kw = k_S K_{GL} K_{DMC} {C_o}^2$; w is the weight of the catalyst.

The final rate expression in terms of conversion after integration of Eq. (41) can be expressed as:

$$-\ln(1 - X_{GL}) = Kwt \quad (42)$$

The plot of $-\ln(1 - X_{GL})$ vs t at 75 ^{o}C produced an excellent fit of the experimental data (Figure 4.24) with a rate constant K of 0.1775.

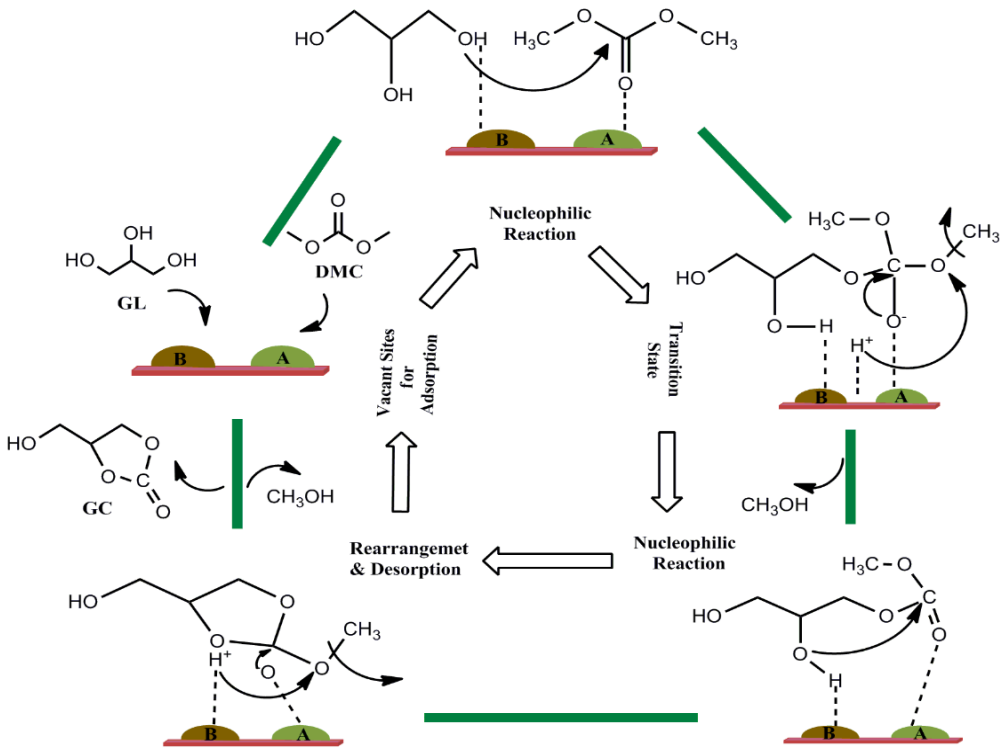

Figure 4.23. A probable reaction pathway for the GL transesterification with DMC to produce GC.

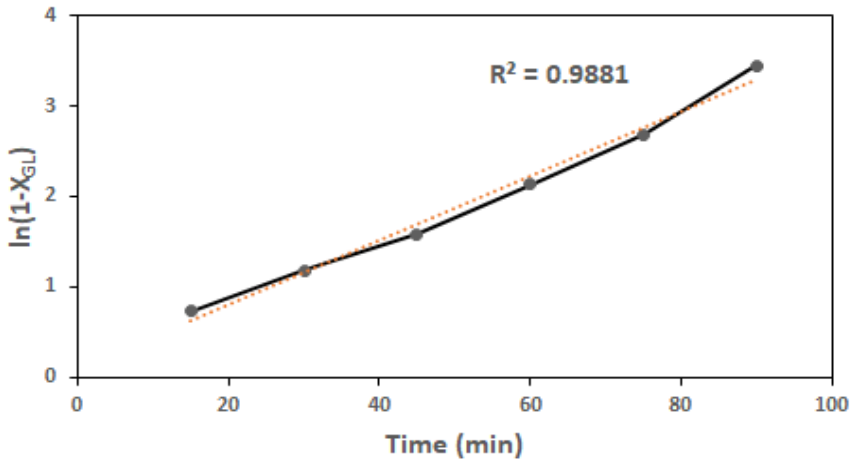

Fig. 4.24. Plot of ln (1-X_{GL}) vs time (t).

4.2.5 Catalyst reusability and deactivation mechanism

As discussed in sections 4.2.1 and 4.2.2, it was clear that RK-30%-800 catalyst resulted in better stability than other prepared catalysts. As shown in Figure 4.13, the RK-30%-800 catalyst was able to produce 82.2% and 78% GL conversion at the 3rd and 4th reuse of the catalyst, which was considerably higher than the RM-800 catalyst produced. At the 5th reuse, the RK-30%-800 catalyst showed a consistent decrease in activity to 68.2% GL conversion. Therefore, to reveal the mechanism behind the decreased activity of the 5th reuse RK-30%-800 catalyst, it was recovered and characterized by the XRD, FTIR, and EDX techniques.

The XRD results (Figure 4.25 (a)) suggested a change in crystallinity of the catalyst to an amorphous state after the 5th reuse. The basic strength was also found to be reduced from 15 < H_ < 18.4 for the fresh catalyst to 9.3 < H_ < 15 for the 5th reuse catalyst, which suggested a decrease in basic properties of the RK-30%-800 catalyst. FTIR analysis (Figure 4.25 (b)) revealed a relative decrease in the intensity of NO_3 groups at 825 cm^{-1} and 1385 cm^{-1} in the reused catalyst. Moreover, the appearance of a relatively high-intensity peak at 1453 cm^{-1} (Figure 4.25 (b)) suggested the increase in carbonate groups in the 5th reuse RK-30%-800 catalyst. Hu et al. [220] reported similar behavior in the KNO_3/CaO catalyst that they used for the transesterification of GL. According to them, the carbonate species formed in the reused species are relatively weaker basic sites than the oxide sites, which could be a reason for the decrease in activity at 5th reuse. Further, an increase in the NO_2^- group at 1530 cm^{-1} suggested a relative increase in KNO_2 species in the 5th reuse RK-30%-800 catalyst. The EDX analysis of the 5th reuse RK-30%-800 catalyst confirmed a relative decrease in the content of K from 20.1% to 10.7% (Table 4.7), which could be due to the leaching of elements during the reaction. From the AAS analysis, 1980 ppm, 1067 ppm, and 324 ppm of K were found in the reaction product collected from the fresh use, 1st reuse, and 3rd reuse conditions, respectively. In addition, 365 ppm, 225 ppm, and 115 ppm of Na were also found in the reaction product collected at the same conditions as described above. However, the leaching of Na was very much less, as compared to that in the calcined RM catalyst (RM-500), as reported in our earlier study where approximately 1500 ppm of Na was found in the product mixture.

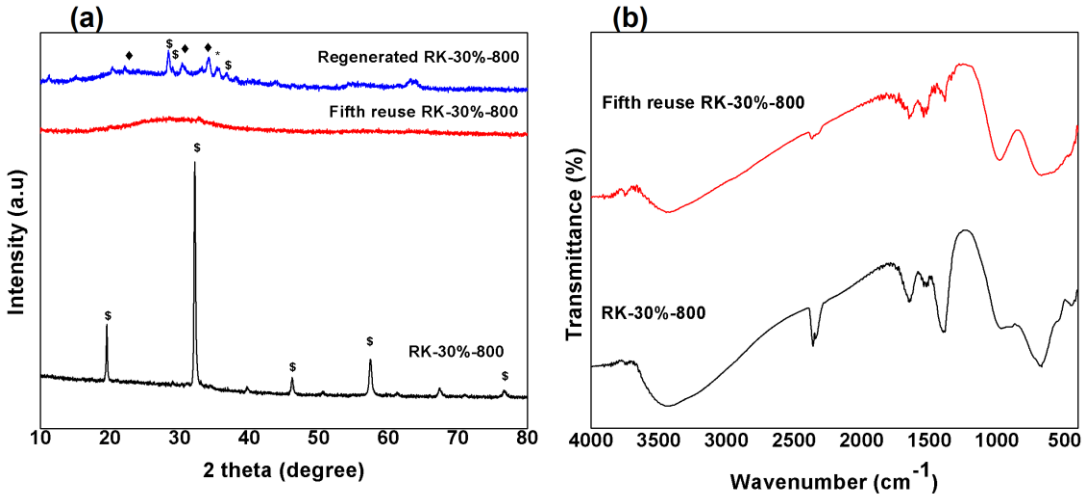

Figure 4.25. (a) Comparison of XRD profile and (b) FTIR profile of fresh and 5th reuse RK-30%-800 catalyst. $ K_2O, ♦ $KAlSi_3O_8$ and * Fe_2O_3.

The decreased concentration of K as observed from the FTIR and EDX results might be considered as another reason for the lower activity of the catalyst at the 5th reuse. However, at the 4th reuse condition, the catalyst was still able to produce 80% of GL conversion, thus suggesting that there was still a significant amount of active sites (Na and K) present at the 4th reuse of the catalyst, which was also confirmed from the EDX analysis. The RK-30%-800 catalyst was regenerated by calcining at 800 °C for 2 h and was again used for the transesterification of GL. The GL conversion and GC yield obtained with the regenerated catalyst were 82.3% and 76.1%, respectively. The XRD analysis of the regenerated RK-30%-800 catalyst (Figure 4.25 (a)) revealed that a major change in phases occurred in the regenerated catalyst. Different peaks related to the $KAlSi_3O_8$ compound at 2θ of 22.3°, 30.5°, and 34.2° were observed in the regenerated catalyst [227]. The high-intensity peaks of K_2O in the fresh RK-30%-800 catalyst were not observed in the regenerated catalyst, and relatively low-intensity peaks approximately at 28.9°, 36.7°, and 28.8° were found for the K_2O phase [226]. This suggested that the remaining K in the regenerated catalyst was well-dispersed, and some of it formed new compounds by interacting with other elements of RM. These new phases formed might have lower basic

properties than the K_2O phase, due to which a reasonable decrease in activity was observed at the 5th reuse of the catalyst.

4.2.6 RK-30%-800 catalytic activity comparison with other reported catalysts

The catalytic activity of the RK-30%-800 for the transesterification of GL was compared with other reported catalysts (Table 4.9). Kumar et al. [107] reported the 3LaCa catalyst for the transesterification of GL, where they achieved 94% GL conversion and 74% GC yield at 90 °C. In comparison to the RK-30%-800 catalyst reported in this article, the activity is considered relatively low in terms of the GC yield, temperature, and GL to DMC molar ratio used. The stability of the RK-30%-800 catalyst as compared to the 3CaLa catalyst was also better when compared at the 4th reuse condition. Similarly, the catalyst HTC-Ni reported by Liu et al. [120] required a very high temperature (120 °C) as compared to the RK-30%-800 catalyst (90 °C) for the GL transesterification, and that too produced relatively low GL conversion (55%). These comparison data suggested that the RK-30%-800 catalyst possessed very similar or superior activity (in some cases) in comparison to other reported catalysts. Hence, the catalyst can be used for the efficient synthesis of GC from GL through the transesterification route.

Table 4.9. Comparison of efficiency of the RK-30%-800 catalyst with other similar catalysts.

Catalyst	Reaction time (min)	Reaction Temperature (°C)	GL-DMC molar ratio	GL conversion (%)	GC yield (%)	Catalyst stability	Ref.
RK-30%-800	90	75	1:3	96.8	93.2	GL conversion 80% at 4th reuse	Present work
0.01 Li/ZnO-500	240	95	1:3	97.59	-	GL conversion 60.57% at 3rd reuse	[105]
3CaLa	90	90	1:5	94	74	GC yield 67% at 4th run	[107]
Zn4La1	80	150	1:4	97.3	-	GL conversion 63.96% at 4th reuse	[110]
HTC-Ni	120	100	1:3	55	55	GL conversion 45% at 5th reuse	[120]
Mg/Zr/Sr	90	90	1:5	96	56	Data not provided	[222]

4.3 Preparation and characterization of acidic metal impregnated RM-based catalysts for the direct D-Glucose transformation to 5-HMF

This section presents the preparation, characterization, and application of RM derived acidic catalysts for the 5-HMF production from D-Glucose. The direct synthesis of 5-HMF from D-Glucose by RM-based catalysts having both the Lewis and Bronsted acid sites was performed under microwave irradiation.

4.3.1 Catalysts screening based on the 5-HMF yield

Different catalysts prepared were initially screened based on the 5-HMF yield from D-Glucose under microwave irradiation (Figure 4.26). As presented in Figure 4.26 (a), the catalytic activity of RM for the conversion of D-Glucose to 5-HMF was very low, and only 40.1% D-Glucose conversion with 1.5% 5-HMF yield was obtained. The ARM catalyst produced by HCl treatment of RM did not contribute much towards the efficiency of the process and produced only 1.2% 5-HMF yield. A slight higher production of 5-HMF in case of RM could be due to the presence of different salts of Na in RM that helped in a better separation of 5-HMF from the aqueous phase and prevent its further degradation to byproducts such as LA, FA, and humins as suggested by Saravanan et al. [229]. However, Na in RM easily leached out in the reaction solution under microwave heating, as confirmed from the FESEM-EDX analysis of the recovered RM catalyst (Table 4.10). Therefore, to avoid the additional contamination of the product with these leachable elements, ARM based catalysts were prepared and tested for the 5-HMF synthesis. The AS-13 catalyst prepared by introducing 13% of Sn on ARM surface and calcining at 450 ^{o}C produced a slight increase in 5-HMF yield to 3.6% as compared to 1.2% for the ARM catalyst. The conversion of D-Glucose to 5-HMF occurred via the isomerization followed by the dehydration pathway. It can be confirmed from the Py-ATR-FTIR results (Figure 4.33) that the catalyst ARM and AS-13 mostly possessed the Lewis acidic sites coming specifically from Al, Fe, Si, or Sn present in the catalyst that normally performed the isomerization of D-Glucose to fructose and then further polymerization to humins [230]. The absence of sufficient Bronsted acid sites in these catalysts required for the dehydration of fructose to 5-HMF could be considered the reason for

the lower 5-HMF yield, as observed by Antonetti and coworkers [184]. It is important to note that the amount of fructose obtained from RM, ARM, and AS-13 catalysts was very low in the range of 2-4% yield. As mentioned above, the fructose formed during the reaction was due to the D-Glucose isomerization mechanism catalyzed by the Lewis acids. However, such a low fructose yield signifies the rapid conversion/decomposition of the formed fructose to other by-products such as humins under high temperature and in the presence of microwave irradiation. Upon functionalization of sulfate groups on ARM by the treatment with H_2SO_4 (1.5 M, 30 mL/1 g catalyst) followed by calcination at 450 ^oC, the resulted ARM-H catalyst produced a significant increase in the yield of 5-HMF (25.7%), which clearly indicated the catalytic effect of Bronsted acid sites formed due to the H_2SO_4 deposition on ARM. Similarly, the AS-13-H catalyst produced D-Glucose conversion of 80.7% with a 5-HMF yield of 26.2%. The treatment with H_2SO_4 produced sulfated Fe and Sn oxides as observed in the XRD analysis (Figure 4.27) that delivered a combination of Lewis and Bronsted acidic sites in the catalytic system and increased the 5-HMF yield. The presence of significant Bronsted acid sites could be observed in the Py-ATR-FTIR spectra of AS-13-H catalyst (Figure 4.33) with a high-intensity IR peak at 1542 cm^{-1}, which was very less intense in the case of the ARM and AS-13 catalyst. A similar observation was also reported by Lopes and coworkers, who carried out the 5-HMF synthesis from D-Glucose in the presence of sulfated tin oxide catalyst.[230] Besides the increased yield of 5-HMF after the sulfate functionalization, a further decrease in the fructose yield to less than 1% was observed. This could be partly also attributed to the introduction of Bronsted acid sites in the catalysts that further enhanced the fructose conversion to 5-HMF in addition to the rapid decomposition at high temperature under microwave irradiation.

The effect of the quantity of sulfate functionalization on the AS-13 catalyst by varying the H_2SO_4 quantity is presented in Figure 4.26 (b). A relatively low D-Glucose conversion and 5-HMF yield were observed when the quantity of 1.5 M H_2SO_4 was only 10 mL/1 g catalyst compared to 30 mL/1 g catalyst. The D-Glucose conversion and 5-HMF yield increased with the increase in the H_2SO_4 quantity to 30 mL/1 g catalyst and reached 80.7% and 26.2%, respectively. It signifies the

enhancement in the number of Bronsted acid sites in the catalyst with the increase in the H_2SO_4 quantity that had a positive effect on the conversion and yield. However, further increase in the H_2SO_4 quantity did not produce any enhancement in the 5-HMF yield. In fact, a slight decrease was observed, which could be due to the further conversion of 5-HMF to other by-products under a high acid density. It can be noted that at the fresh use condition, the performance of ARM-H and AS-13-H (Figure 4.26 (a)) was very similar, mainly in terms of 5-HMF yield. However, from the catalyst reusability experiments performed to study the stability of the catalysts, it was observed that the AS-13-H showed better stability than the ARM-H catalyst. The detailed reusability study is discussed later under section 4.3.5. Thus, the better stability of the AS-13-H catalyst was an important reason for choosing the catalyst as the most appropriate one for the 5-HMF synthesis in this study.

The effect of Sn wt% loading on the catalytic activity of AS-x-H catalyst is presented in Figure (4.26 (c)). It is quite clear from Figure (4.26 (c)) that with the increase in Sn wt% up to 9%, the D-Glucose conversion increased gradually and reached 83.2%. Beyond that, a slight decrease (approx. 2.4%) in D-Glucose conversion was observed for the AS-13-H catalyst. Further increase in Sn loading resulted in more decrease in D-Glucose conversion, and it reached 70.7% at 21 wt% of Sn loading (AS-21-H). The 5-HMF yield also followed a decreasing trend with the increase in Sn loading. However, the decrease up to 17% of Sn loading was minimal, and beyond that, a comparatively prominent decrease in 5-HMF yield was observed. With more quantity of Sn available, the concentration of the Lewis acidic sites in the catalyst could increase, and 5-HMF could undergo further rehydration on the Sn surface to produce more LA and FA in the reaction product. Behera and coworkers also reported a decrease in 5-HMF selectivity when they used more than 20 wt% of Sn loading on vanadium phosphate catalyst [147]. It can also be noted that at the Sn loading of 13 wt%, the decrease in D-Glucose conversion as well as the 5-HMF yield than the 9 wt% Sn loading could be considered negligible. Moreover, from the initial study carried out for catalytic stability test (discussed in section 4.3.5), 13 wt% of Sn loading was found to produce the best catalytic activity during the reuse condition, and beyond that, no significant improvement in catalytic stability was observed.

Considering all these factors, it was therefore decided that AS-13-H catalyst was more suitable for the 5-HMF synthesis and was used to further study the reaction parameters.

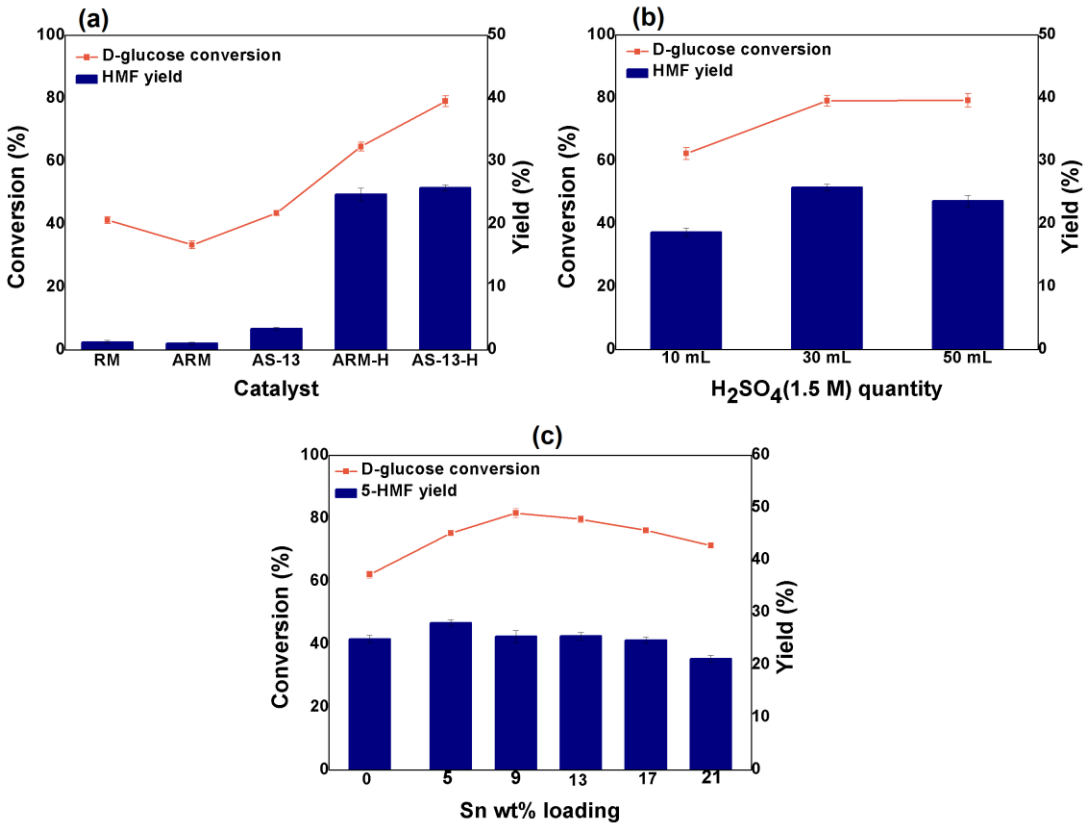

Figure 4.26. (a) Catalytic activity comparison of different catalysts for the microwave D-Glucose conversion to 5-HMF: (b) Effect of H_2SO_4 (1.5M) quantity on the AS-13 catalyst (c) Effect of Sn wt% doping on the D-Glucose conversion and 5-HMF yield. Temperature = 180 ^oC, Time = 5 min, Catalyst/D-Glucose weight ratio = 0.5.

4.3.2 Catalyst characterization

4.3.2.1 XRD analysis

The XRD patterns of different prepared catalysts are shown in Figure 4.27. RM, is mainly composed of crystalline phases of Fe_2O_3 that were observed at 2θ of 33.1^o, 35.6^o, 40.9^o, 49.7^o, 54.1^o and 62.8^o with lattice planes (1 0 4), (1 1 0), (1 1 3), (0 2 4), (1 1 6), and (2 1 4), respectively [210,211]. Besides this, the crystalline phases

of $Al(OH)_3$ at a 2θ of 18.42° (0 1 0) were also observed in the raw RM [211]. After acid (HCl) treatment, the crystallinity of the sample was lost to a significant extent due to which a relatively decreased peak intensities of Fe_2O_3 were observed at all the respective 2θ positions except at 49.7° as observed in RM. The incorporation of Sn and calcination at 450 °C produced a very small intensity XRD peak of SnO_2 at 27° in the AS-13 as well all the AS-H catalysts [231]. It suggested that Sn remained in well-dispersed form with small crystal particles on the surface of ARM. The Sn incorporation did not alter the crystal lattice of Fe_2O_3, and all the Fe_2O_3 phases which were observed in the ARM catalyst remained intact in the AS-13 catalyst. After the sulfuric acid deposition, a significant loss in Fe_2O_3 peaks occurred in the catalyst, due to which this phase only appeared at 33.1°, 35.6° and 54.1°. On the other hand, the H_2SO_4 deposition produced new XRD peaks with high intensity at 2θ of 14.8° (0 1 2), 20.8° (0 2 0), 25.16° (1 0 2), 30.1° (2 2 -2), and 33.8° (1 3 0) and other small intensity peaks at 21.6° (1 1 0), 24.6° (1 2 0), 37.6° (3 0 0) and 59.4° (1 4 0) were related to the $Fe_2(SO_4)_3$ phases [232]. Fe_2O_3 in ARM could also react and form $Fe_2(SO_4)_3$ during the treatment with H_2SO_4, because of which these peaks were observed. The higher peak intensity of all the Fe-related phases at higher Sn loaded catalysts could be due to the increasing content of crystalline particles. This could be partially also explained on the basis of the X-ray absorption factor between Sn and Fe, as reported by Zhai et al. [233]. Sn has a lower X-ray absorption factor than Fe. Thus, the more the concentration of Sn on the surface, higher will be the intensity of crystalline phases. So the higher intensity of Fe-related phases at high Sn loading indicates the presence of more Sn on the Fe surface in a homogeneously distributed form. The XRD profile suggested that the catalyst after H_2SO_4 deposition was able to retain its core structure up to some extent, which is evident from the existence of a few Fe_2O_3 and the SnO_2 phases of the non-sulfated catalysts. The sulfates from H_2SO_4 could be present as SO_4^{-2}/SnO_2-Fe_2O_3 form without distorting the crystal structure of tin (IV) and iron (III) oxide [233]. However, the existence of $Fe_2(SO_4)_3$ signifies that H_2SO_4 also reacted with iron particles to some extent during the impregnation process forming $Fe_2(SO_4)_3$ besides its deposition as sulfate (SO_4^{-2}) form on Fe_2O_3 and the SnO_2 surfaces. A similar observation was noticed for the H_2SO_4 deposited ZrO_2-TiO_2 catalyst reported by Reddy and coworkers [234], where apart from the oxide phases,

sulfates of Zr and Ti were also observed. More detail on the surface properties of the catalyst supporting the XRD data could be found from the XPS analysis in the upcoming paragraphs in this article.

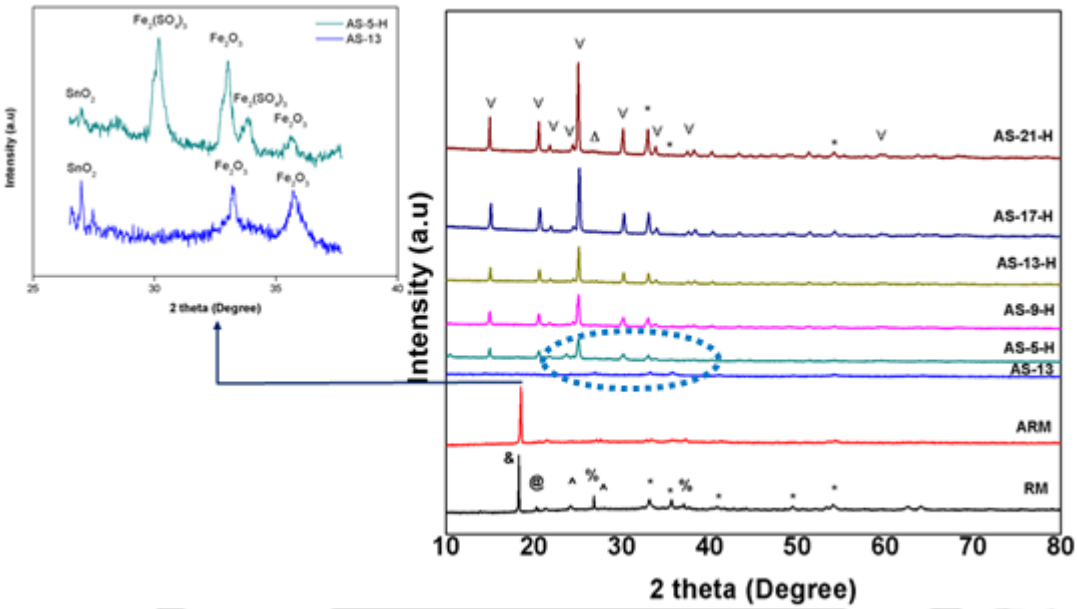

Figure 4.27. XRD analysis of various prepared catalysts. * Fe_2O_3, & $Al(OH)_3$, @ $NaAlO_2$, % SiO_2, ^ TiO_2, ∀ $Fe_2(SO_4)_3$.

4.3.2.2 FESEM and FESEM-EDX analysis

The surface of RM is comprised of small irregular size particles with small voids present between them (Figure 4.28). After HCl treatment, the crystallinity of the sample was lost to a major extent, which can be seen in Figure 4.28 (b). Due to the presence of multiple metal elements in RM, it is difficult to identify the Sn particles in the morphology of AS-13 catalyst. After the functionalization of sulfate groups, particles of nearly cubical shape with a highly crystalline nature was observed (Figure 4.28 (d, e, f)). These particles could be due to the formation of the SO_4^{-2}/ Sn(IV)- Fe (III) oxides and $Fe_2(SO_4)_3$ after H_2SO_4 treatment. The deposition of sulfate groups could be confirmed from the appearance of a thick layer-like structure around and in between the particles in the morphology of AS-13-H catalyst (Figure 4.28 (d, e, f)). The sulfate groups occupied most of the surface area on the catalyst, due to which the number of pores also decreased in the AS-13-H catalyst. The morphology

analysis was in agreement with the results of the XRD analysis where highly crystalline phases related to the SO_4^{-2}/SnO_2-Fe_2O_3 along with $Fe_2(SO_4)_3$ were observed after the H_2SO_4 deposition.

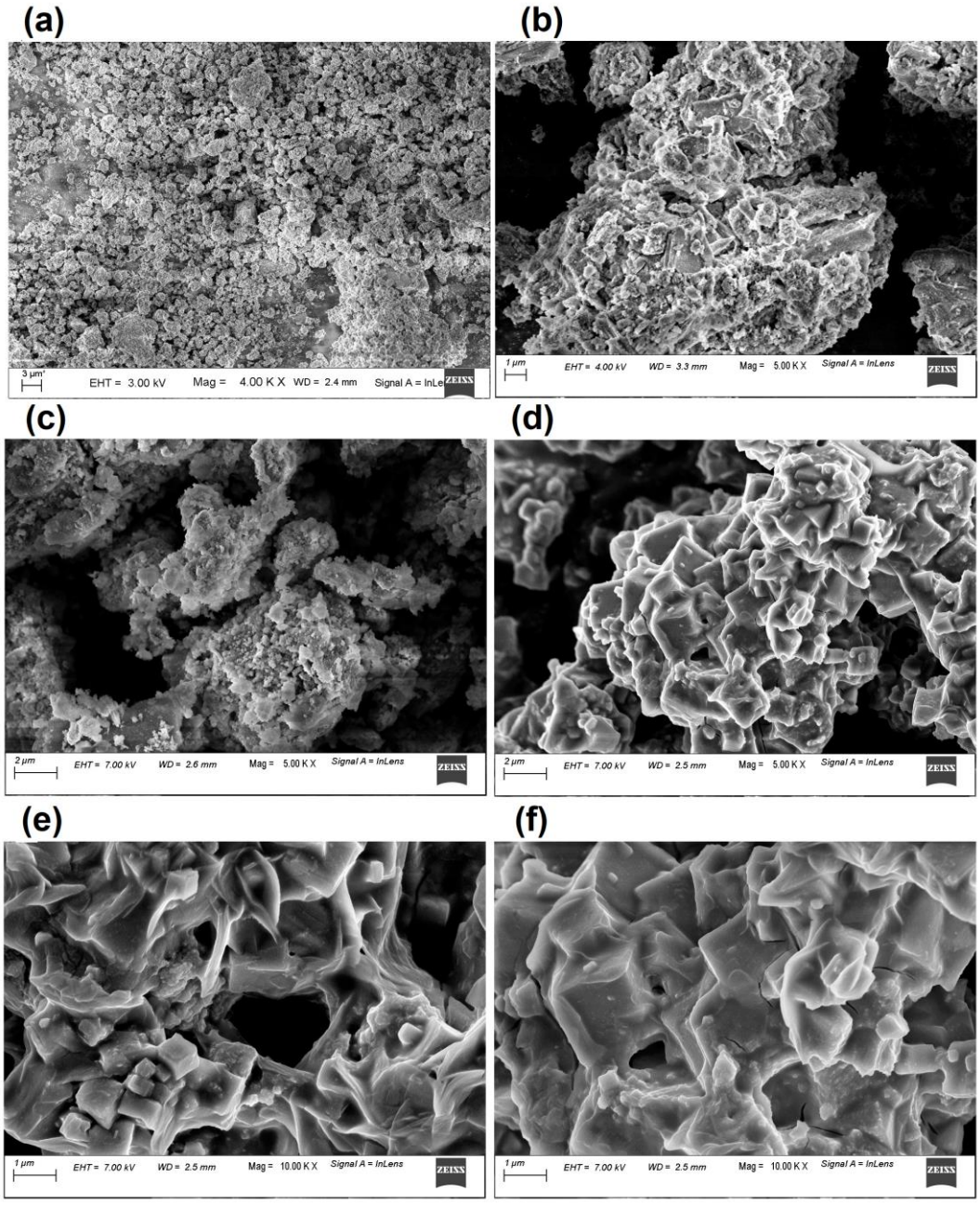

Figure 4.28. Surface morphology study (a) RM, (b) ARM, (c) AS-13, and (d, e, f) AS-13-H.

Table 4.10. Elemental composition of RM, ARM and RM after 1st use.

Elements	O	Fe	Si	Al	Ti	Na	Ca
RM	47.0	28.8	5.3	9.8	1.6	7.0	0.6
ARM	46.6	37.1	3.5	11.1	1.6	0.0	0.0
RM after 1st use	45.2	33.1	3.3	13.7	1.7	0.1	2.9

4.3.2.3 N_2 Adsorption-Desorption analysis

The N_2-sorption isotherm (Figure 4.29) for all the RM based catalysts produced a type IV isotherm. The adsorption and desorption isotherms did not coincide with each other, and a H3 type of hysteresis was observed for the RM, ARM, and AS-13 catalyst, which is typical for mesoporous materials. The AS-13-H catalyst showed a H4 type of hysteresis. The BET surface area, average pore size, and pore volume data are provided in Table 4.11. The pore volume of AS-13-H catalyst was the lowest owing to the deposition of sulfate groups on SnO_2 and Fe_2O_3 surfaces along with the formation of $Fe_2(SO_4)_3$ that blocked the pore mouth and impeded the access of N_2 to the pores. The BET analysis revealed a significant increase in the surface area of RM from 11.6 m^2 g^{-1} to 97.8 m^2 g^{-1} after acid (HCl) activation. It could be due to the removal of Na and Ca from the RM sample by acid digestion that resulted in a higher surface area. The AS-13 catalyst possessed a slightly higher surface area of 114.6 m^2 g^{-1} than 97.8 m^2 g^{-1} for ARM. The relatively higher surface area of AS-13 compared to the ARM catalyst reiterates the fact that Sn remained in a very well dispersed condition in the form of SnO_2 particles and contributed to a relatively larger surface area. In addition, the thermal treatment at 450 ^oC could also contribute to a relatively higher porosity of the AS-13 catalyst that resulted in an increased surface area. Upon functionalization of sulfate groups in the AS-13 catalyst, the surface area of AS-13-H significantly reduced to 3.2 m^2 g^{-1}. The average pore size of AS-13-H increased relative to that of ARM, and AS-13 and the pore volume was decreased. The sulfuric acid treatment on the AS-13 catalyst could result in the formation of both physically and chemically bound sulfate radicals on the surface of SnO_2 and Fe_2O_3 that occupied most of the vacant pores and decreased the surface area. This was also confirmed

from the surface morphology of the AS-13-H catalyst (Figure 4.28 (d, e, f)), where a thick layer of sulfate group was found to be formed on the surface of the catalyst.

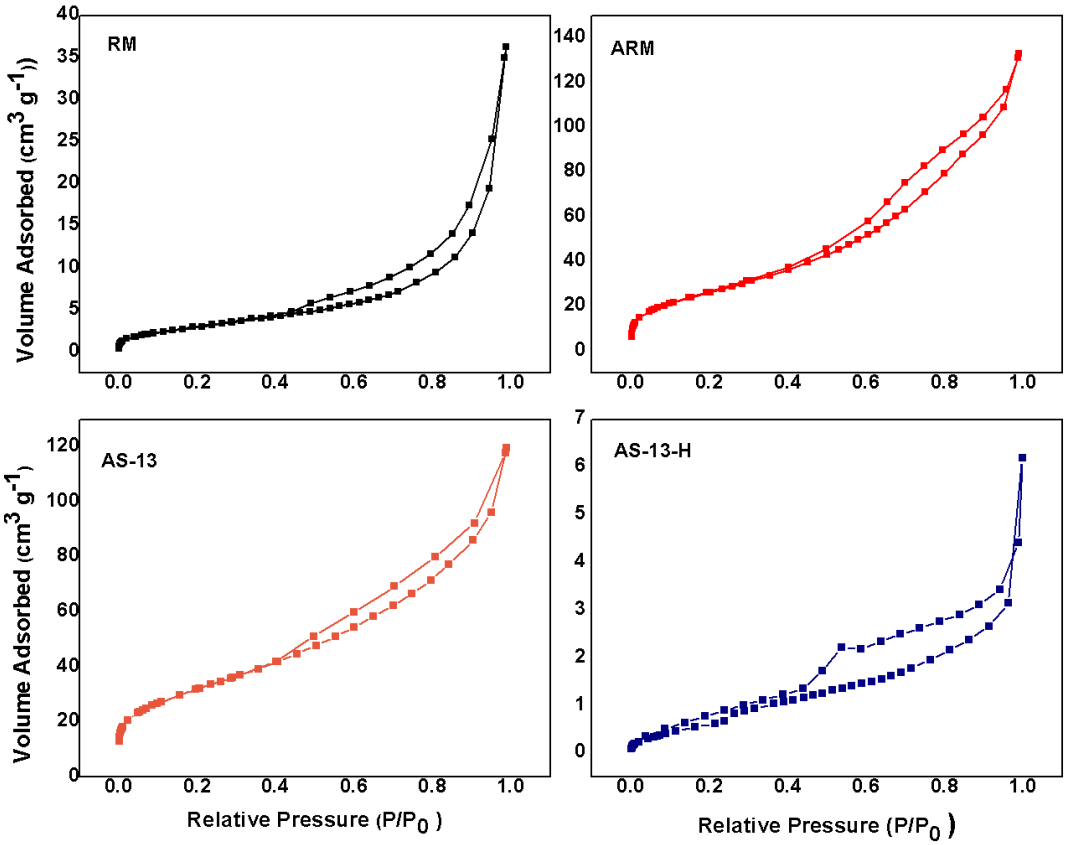

Figure 4.29. N_2 adsorption-desorption isotherms of (a) RM, (b) ARM, (c) AS-13, and (d) AS-13-H.

Table 4.11. BET analysis of various catalysts.

Catalyst	BET Surface area (m^2 g^{-1})	Average pore size (nm)	Total pore volume (cm^3 g^{-1})
RM	11.6	19.26	0.056
ARM	97.8	8.42	0.206
AS-13	114.6	6.48	0.185
AS-13-H	3.2	11.9	0.009

4.3.2.4 FTIR analysis

Figure 4.30 represents the IR spectra of various RM based catalysts. All the catalysts exhibited the characteristics stretching vibration of –OH groups in the wavelength range of 3380 cm^{-1} to 3450 cm^{-1}[235]. Besides this, all the catalysts also showed an IR peak close to the wavenumber of 1644 cm^{-1} that could be due to the bending vibration of the adsorbed molecular water [236]. The presence of bidentate sulfate ion coordinated to the Sn^{+4} or Fe^{+3} can be observed from the IR peaks in the region of 995 cm^{-1}, 1112 cm^{-1}, and 1185 cm^{-1} in the sulfated AS catalysts [236]. The IR peak at 667 cm^{-1} could be assigned to the Sn-O-Sn vibration [235]. The intensity of the peak was found to be increased with the increase in Sn loading. In RM, additional peaks related to the Fe-O and Si-O-Si vibration were found at 460 cm^{-1} and 1001 cm^{-1}, respectively.

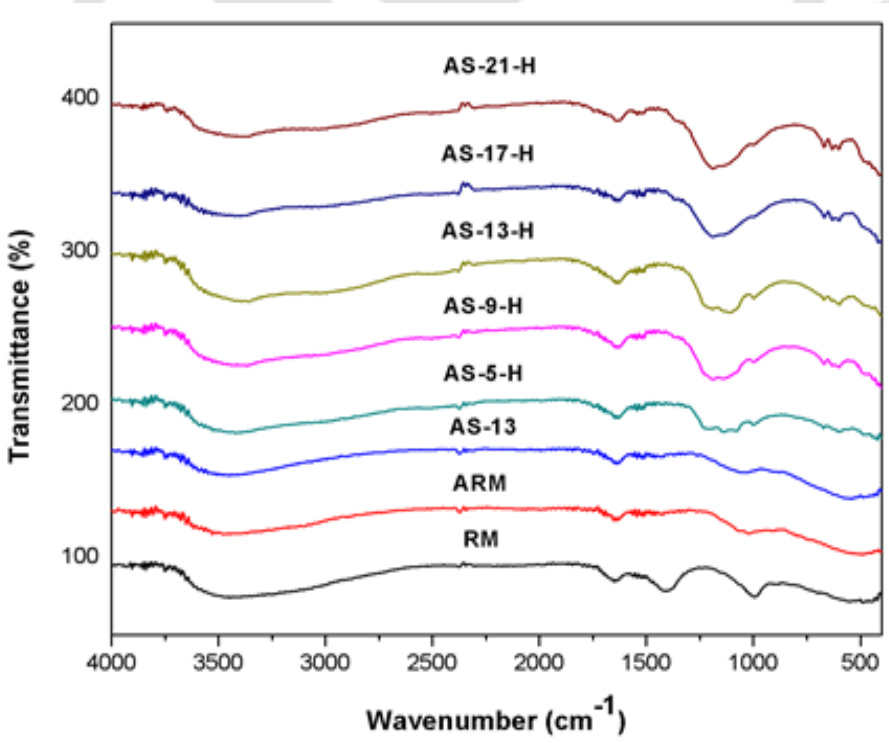

Figure 4.30. FTIR analysis of various prepared catalysts.

4.3.2.5 XPS analysis

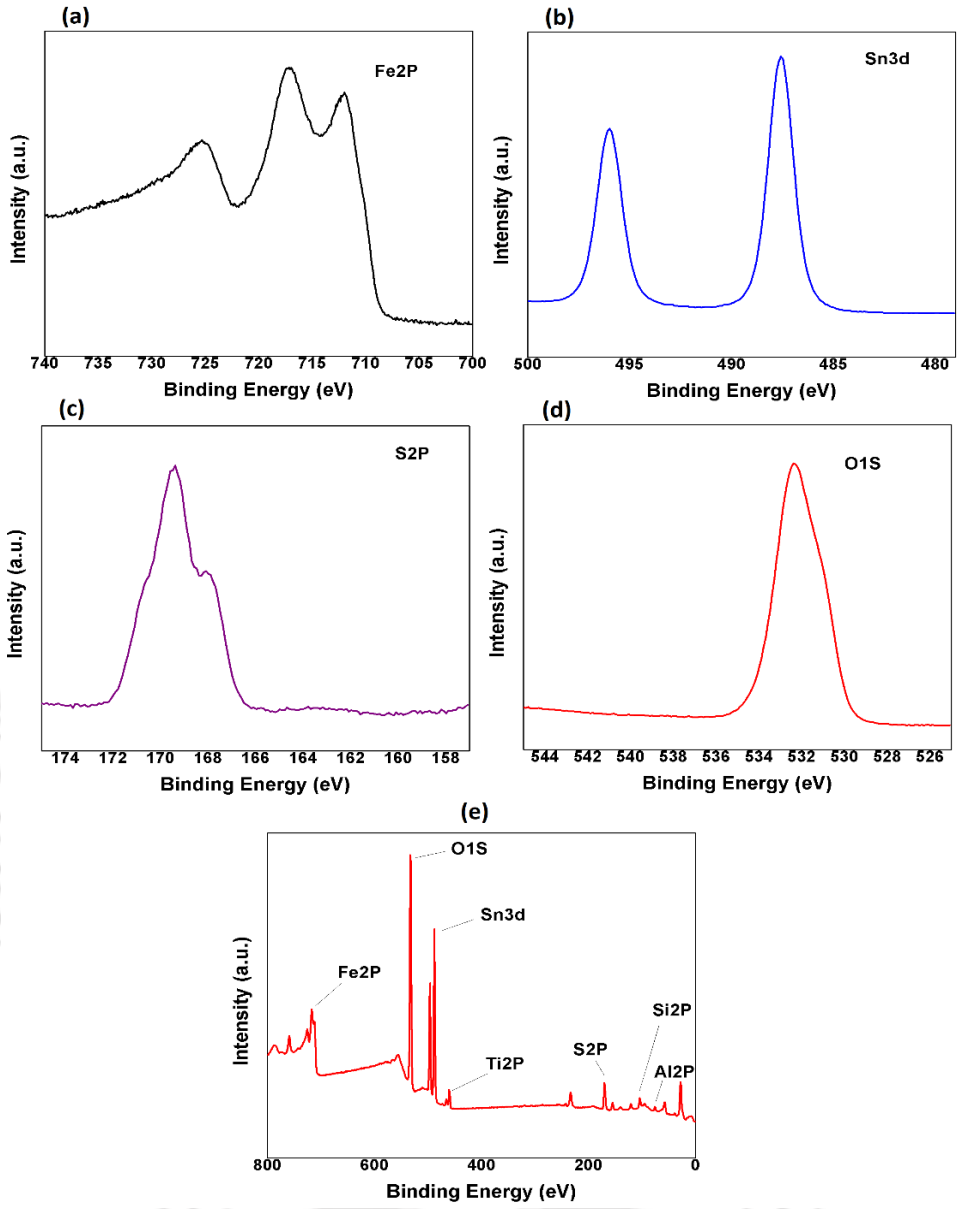

Figure 4.31. XPS spectra (a) Fe2p, (b) Sn3d, (c) S2p (d) O1s and (e) XPS survey of AS-13-H catalyst.

The surface properties of the AS-13-H catalyst was investigated by XPS analysis (Figure 4.31). The XPS survey revealed the presence of elements such as Fe, Sn, Al, Si, Ti, and S in the AS-13-H catalyst. The XPS spectrum of Sn produced peaks at 488.03 eV and 496 eV that were symmetric and corresponded to the $Sn3d_{5/2}$ and

$Sn3d_{3/2}$ of Sn^{4+} [230,237]. The Fe2P XPS spectra of AS-13-H catalyst were observed at the binding energy of 711.6 eV and 724.9 eV, which were ascribed to the Fe^{+3} particles on the catalyst surface [238,239]. An overlapped XPS spectrum of $Sn3p_{3/2}$ with the XPS spectra of Fe was also observed at a binding energy of 717.1 eV. The presence of surface S species was confirmed from the XPS spectrum of the SO_4 peak at 169 eV with another shoulder peak at 167.6 eV, which corresponded to the S^{+6} charge [230]. The peak at 169 eV is also evidence of the presence of $Fe_2(SO_4)_3$ on the catalyst surface, as observed by Wu et al. [240]. The spectrum observed at a binding energy of 532.34 eV was attributed to the O1S peak of SO_4^{-2}/SnO_2-Fe_2O_3 formed after H_2SO_4 deposition on the catalyst [241]. The XPS spectrum in agreement with the XRD peaks of different species confirmed the formation of sulfated iron and tin oxides as well as the $Fe_2(SO_4)_3$ in the AS 13-H catalyst that contributed towards enhanced acidity of the catalyst.

4.3.2.6 NH_3-TPD analysis

The surface acidities of ARM, AS-13, and AS-13-H were analyzed by NH_3-TPD (Figure 4.32). The relative position of the peak in the NH_3-TPD profile signifies the amount of energy required for the NH_3 desorption, which is proportional to the acidic strength of the catalyst [242]. In ARM, a small intensity peak at 170 ^oC was observed, which could be assigned to the presence of weak acidic sites in the catalyst. Additional small intensity peaks at approximately 455 ^oC and 770 ^oC could be due to the ammonia desorption from the moderate and strong basic sites in the catalyst, respectively. The AS-13 catalyst produced a very similar NH_3-TPD profile as of ARM catalyst but with slightly higher intensity peaks that indicated a relatively higher concentration of acidic sites. Moreover, another small hump of NH_3 desorption was observed at a temperature of 825 ^oC in the AS-13 catalyst, which specified the presence of another strong acidic region in the catalyst. Upon functionalization of sulfate groups, a high-intensity NH_3 desorption peak close to 720 ^oC was observed in the AS-13-H catalyst, which is evidence of a strong and high concentration of acidic sites in the catalyst. Besides this, the NH_3-TPD profile also produced another small and wide peak at 498 ^oC for the AS-13-H catalyst that suggested the presence of another strong acidic site. Although the TPD analysis does not identify the types

(Lewis or Bronsted) of acidic sites in the catalyst, based on the demonstration of few previously published studies, it can be suggested that the incorporation of sulfate groups could increase the concentration of Bronsted acid sites [243]. The high-intensity NH_3 desorption peak as observed in the NH_3-TPD profile of AS-13-H catalyst could be considered as evidence of the high concentration of Bronsted acid sites in the catalyst.

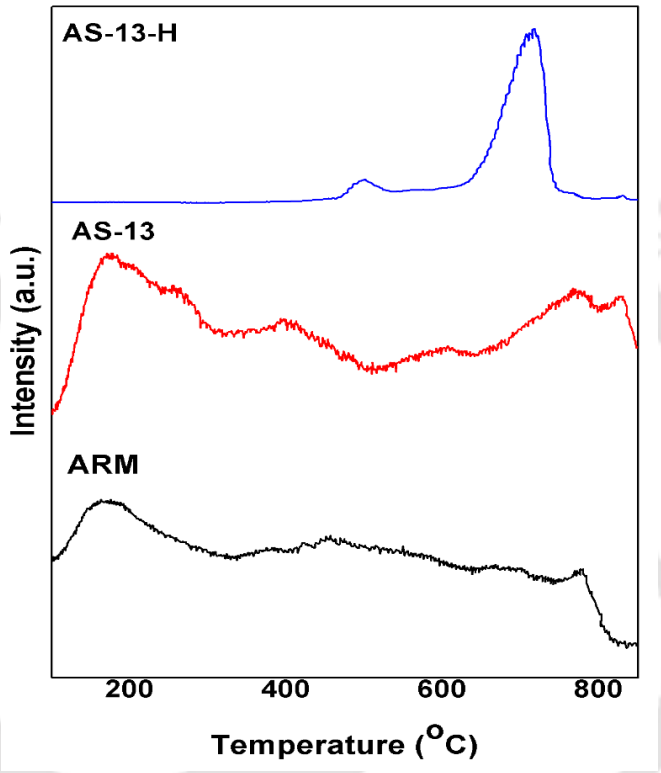

Figure 4.32. NH_3-TPD analysis of various catalysts.

4.3.2.7 Py-ATR-FTIR analysis

The IR spectra of pyridine adsorbed ARM, AS-13, and AS-13-H in the range between 1400 cm^{-1} to 1600 cm^{-1} are shown in Figure 4.33. Both ARM and AS-13 produced a well-defined IR spectrum at 1442 cm^{-1} corresponded to the Lewis acid sites [7]. Another strong intensity IR spectrum at 1592 cm^{-1} also confirmed the presence of strong Lewis acid sites in the ARM and AS-13 catalysts. In the AS-13-H catalyst, the presence of Lewis acid sites was confirmed from the IR spectrum at 1453 cm^{-1}, 1464 cm^{-1}, and 1512 cm^{-1}, however, with a relatively lower intensity than ARM

and AS-13 [8,244]. A strong IR spectrum attributed to the pyridinium ion coordinated to the Bronsted acid sites at 1542 cm^{-1} was observed in the AS-13-H catalyst [8]. The intensity of the spectrum at 1542 cm^{-1} was stronger for AS-13-H than ARM and AS-13, suggesting an enhancement in Bronsted acid sites in the catalyst after sulfate functionalization. The Bronsted to Lewis sites ratio in the catalysts was calculated by integrating the IR peaks, and results are provided in Table 4.12. The IR peak at 1488 cm^{-1} was observed for all the three catalysts that could be ascribed to the presence of both Bronsted as well as Lewis acid sites [7].

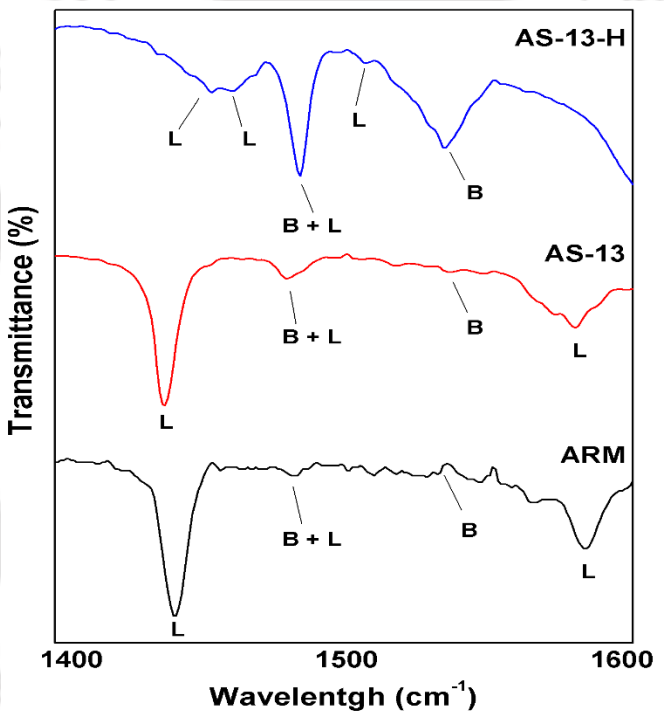

Figure 4.33. Py-ATR-FTIR spectra of various catalysts.

Table 4.12. Bronsted to Lewis acid ratio of various catalysts.

Catalyst	Ratio of Bronsted to Lewis sites (B/L)
ARM	0.088
AS-13	0.112
AS-13-H	1.472

4.3.3 Effect of reaction parameters on 5-HMF synthesis

The effect reaction parameters such as the effect of temperature, time and catalyst to substrate ratio on the reaction output are discussed below (Figure 4.34).

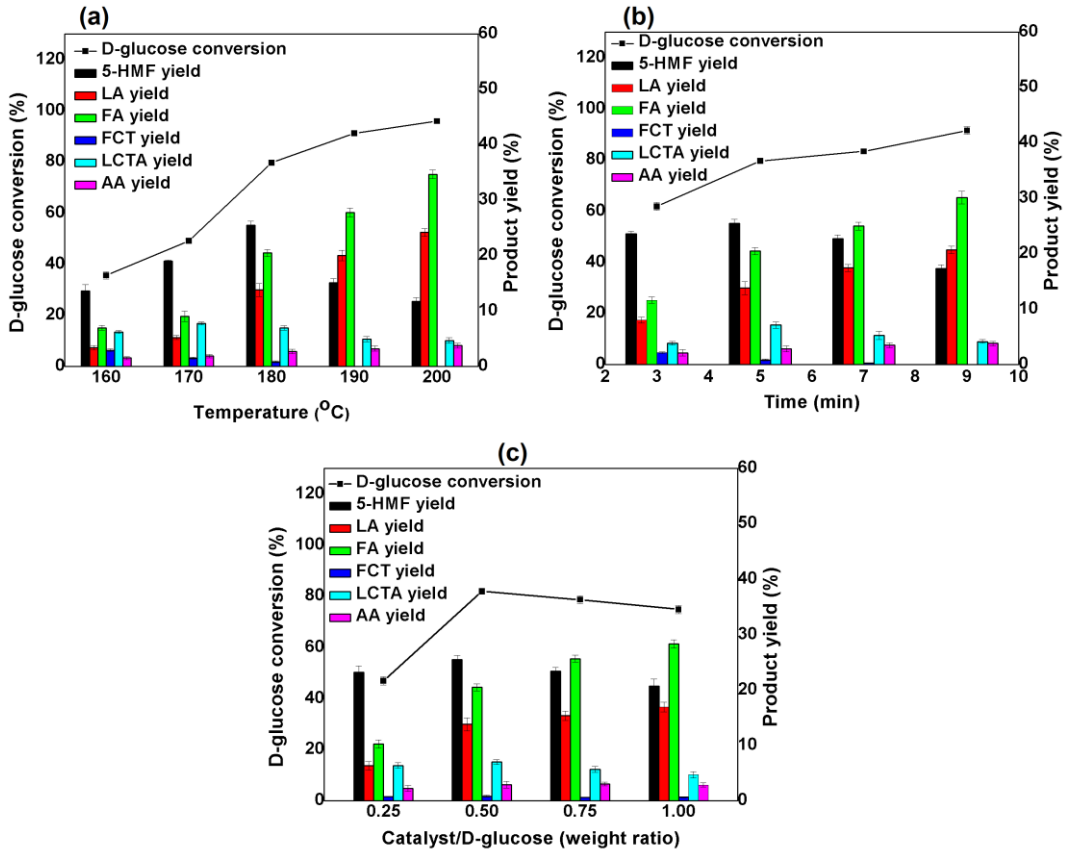

Figure 4.34. Effect of various reaction parameters on microwave D-Glucose conversion to 5-HMF: (a) effect of reaction temperature (Catalyst = AS-13-H, Time = 5 min, Catalyst/D-Glucose weight ratio = 0.5): (b) effect of reaction time (Catalyst = AS-13-H, Temperature = 180 ^{o}C, Catalyst/D-Glucose weight ratio = 0.5,): (c) effect of catalyst/D-Glucose weight ratio (Catalyst = AS-13-H, Temperature = 180 ^{o}C, Time = 5 min).

The effect of microwave temperature was studied in the range between 160 ^{o}C to 200 ^{o}C (Figure 4.34 (a)). In the presence of the AS-13-H catalyst, the D-Glucose conversion continuously increased with the increase in temperature from 160 ^{o}C to 200 ^{o}C. At 160 ^{o}C, the D-Glucose conversion was 36.9%. The low D-Glucose

conversion at this low temperature could be due to the non-availability of sufficient activation energy that is required for the isomerization of D-Glucose to fructose followed by dehydration of fructose to 5-HMF. The highest D-Glucose conversion of 95.1% was achieved at 200 ^{o}C. However, the 5-HMF yield was found to increase only up to a temperature of 180 ^{o}C. Therefore, the temperature of 180 ^{o}C was chosen as the optimal temperature for the microwave 5-HMF synthesis in this study. With an increase in the temperature from 160 ^{o}C to 200 ^{o}C, the FCT yield decreased from 3.2% to 0%, and an increased formation of byproducts such as LA, FA, AA, and humin was observed. It suggested that higher temperatures beyond 180 ^{o}C favored the conversion of D-Glucose, FCT, and 5-HMF to various byproducts, thus, decreasing the desired 5-HMF yield in the product mixture. A similar observation was also reported by Antonetti and co-workers [184]. Moreover, another byproduct LCTA was also observed; however, the product yield did not follow a particular trend and varied inconsistently with the variation in the temperature.

As presented in Figure (4.34 (b)), the D-Glucose conversion linearly increased with the increase in the reaction time from 3 min to 10 min. The D-Glucose conversion reached 90.1% with a corresponding 5-HMF yield of 16.7% at 10 min, and at 180 ^{o}C. The maximum 5-HMF yield of 26.2% was obtained at 5 min and at a prolonged reaction time greater than 5 min, it started to decrease. A decrease in the FCT yield was also found with an increase in reaction time. On the contrary, a monotonic increase in the yield of LA, FA, and AA was found with the increase in reaction time, which suggested the emergence of side reactions (rehydration of 5-HMF) on the catalyst surface at an increased reaction time. At higher reaction time, the polymerization of 5-HMF was also more prominent, due to which a higher amount of humins were also found in the reaction product. The optimum reaction time of 5 min with the highest 5-HMF yield of 26.2% was found at a temperature of 180 ^{o}C in this study.

The effect of catalyst to the D-Glucose weight ratio in the microwave-assisted 5-HMF synthesis process was analyzed (Figure 4.34 (c)). It was found that with the increase in the catalyst to substrate weight ratio from 0.25 to 0.75, a continuous

increase in D-Glucose conversion was observed. This suggested the rapid acceleration of the reaction due to the availability of more number of active catalytic sites at a higher catalyst to D-Glucose weight ratio. The 5-HMF yield was found to increase up to a catalyst to D-Glucose weight ratio of 0.5, at which a maximum 5-HMF yield of 26.2% was obtained. At a catalyst to D-Glucose weight ratio higher than 0.5, a decrease in 5-HMF yield was observed. As suggested by Marianou and coworkers, at a higher catalyst loading, the undesirable side reactions such as rehydration of 5-HMF to LA and FA or polymerization of 5-HMF to humins could result in a decrease in the final 5-HMF yield in the reaction product [133]. In this study, the formation of LA, FA, and AA became more prominent with the increase in catalyst to D-Glucose ratio (Figure 4.34 (c)). Therefore, a catalyst to D-Glucose weight ratio of 0.5 was found as optimum for the 5-HMF synthesis process.

4.3.4 5-HMF synthesis in an organic and aqueous-organic solvent system

The use of an organic solvent such as DMSO along with water for the 5-HMF synthesis has been found to produce a better 5-HMF yield, as reported in previous studies [133,245]. However, the process is not encouraged due to the drawbacks of high cost and difficulty in separation of the organic solvent that could affect the overall economy of the process. Only to compare the yield of 5-HMF by using our prepared catalyst (AS-13-H) with other reported works where an aqueous-organic system has been used, we performed the microwave 5-HMF synthesis by taking DMSO as the co-solvent with water (Figure 4.35). It was found that the presence of DMSO along with water in the weight ratio of 1:1 improved the 5-HMF yield to 53.8% as compared to 26.2% when only water was used as a solvent. The improved 5-HMF yield with water and DMSO as solvent could be explained by the decrease in the side reactions such as 5-HMF rehydration to LA and FA and polymerization of 5-HMF and fructose to humins. However, with only DMSO as a solvent, the 5-HMF yield was not so significant, and only 33.4% of 5-HMF yield was obtained compared to the 5-HMF yield of 53.8% when water and DMSO (mass ratio of 1:1) was taken as solvent. As reported in previous studies [133], the presence of water up to a certain extent always helps to prevent the dehydration of D-Glucose to levoglucosan or other by-products by facilitating the bridging of the dehydration process with a primary

hydrolysis step in the aqueous medium. Thus, the presence of water along with DMSO was more suitable for the 5-HMF synthesis in the presence of the AS-13-H catalyst rather than using only DMSO.

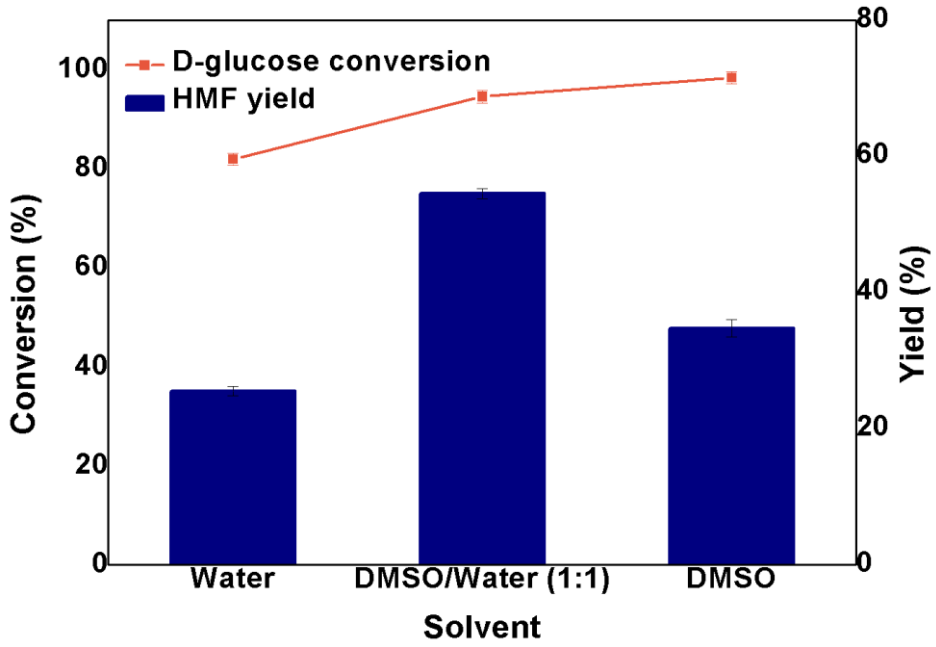

Figure 4.35. Effect of various solvents on the microwave D-Glucose conversion to 5-HMF (Catalyst = AS-13-H, Temperature = 180 ^{o}C, Time = 5 min, Catalyst/D-Glucose weight ratio = 0.5).

4.3.5 Stability study of the AS-x-H catalysts

The catalyst stability test was carried out by reusing the recovered catalyst for the next batch of 5-HMF synthesis. As shown in Figure 4.36, the ARM-H catalyst produced an appriciablet 5-HMF yield of 25.7% at the fresh use. However, the activity of the catalyst continued to decrease with the number of reuse, due to which it produced only 8.3% 5-HMF yield at the 4th use. On the other hand, the incorporation of Sn was found to improve the stability of the catalyst to a significant extent. With 5 wt% Sn doping, the AS-5-H was able to produce 14.8% of 5-HMF yield at the 4th use condition. With increase in Sn loading up to 13%, a positive effect on the catalytic stability was observed, and a maximum 5-HMF yield of 22.1% was obtained by using the AS-13-H catalyst at the 4th use. Beyond 13% of Sn loading, the 5-HMF yield

started to decrease compared to the value at the fresh use, which could be because of the prominent side reactions at such high Sn loading as discussed in section 4.3.1.

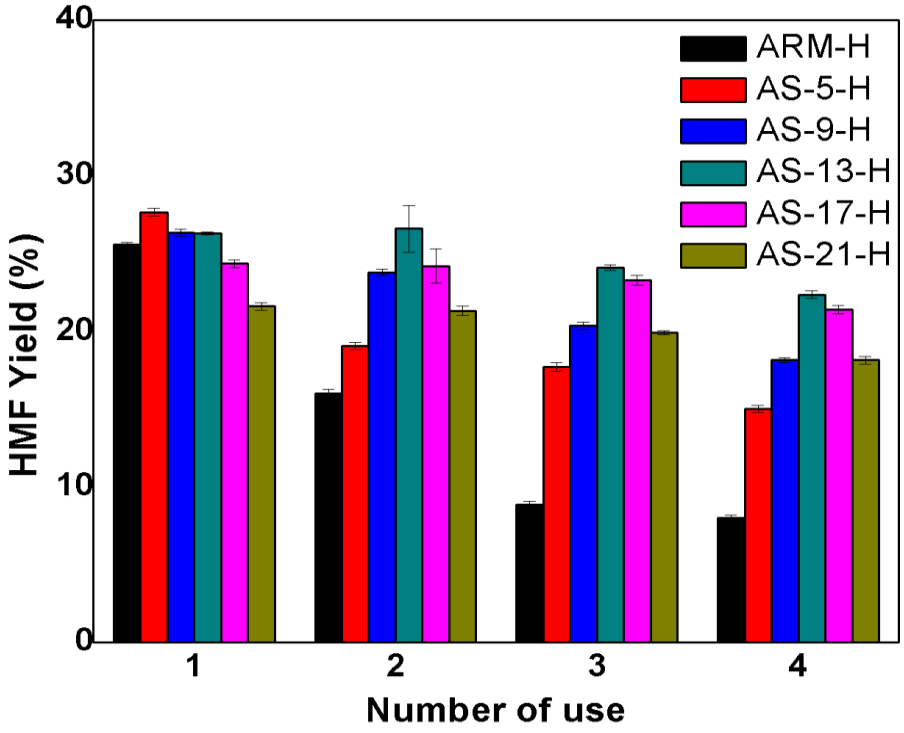

Figure 4.36. Stability study of various catalysts for the microwave 5-HMF synthesis from D-Glucose. (Temperature = 180 ^{o}C, Time = 5 min, Catalyst/D-Glucose weight ratio = 0.5).

The mechanism behind the decrease in the catalytic activity of the AS-13-H catalyst with the increasing number of use was analyzed by FESEM-EDX and FTIR analysis of the catalyst. From the FESEM-EDX analysis, a significant decrease in sulfur content in the 4th used catalyst was observed, as presented in Table 4.13. The decrease in S content could be due to the leaching of weakly bound sulfate groups from the catalyst during the process of 5-HMF synthesis from D-Glucose under microwave irradiation. As discussed earlier in this article, the deposition of sulfuric acid on the surface of AS-13 catalyst significantly improved the D-Glucose conversion as well as the 5-HMF yield. The improved activity of the catalyst was attributed to the presence of a sufficient amount of Bronsted acid sites in the catalyst

after sulfuric acid deposition that helped the dehydration of fructose to 5-HMF. With the number of reuse, the decrease in sulfur groups as observed from the FESEM-EDX analysis led to the decrease in Bronsted acid sites in the catalyst, which decreased the catalytic activity for the 5-HMF synthesis.

Table 4.13. Elemental composition of AS-13-H and 4th used AS-13-H.

Elements	O	S	Fe	Sn	Si	Al	Ti	Na	Ca	C
AS-13-H	56.0	19.2	7.4	4.8	1.3	4.6	3.6	0.1	0.1	2.9
AS-13-H after 4th use	39.9	4.2	11.1	28.0	4.2	1.6	7.7	0.1	0.4	3.1

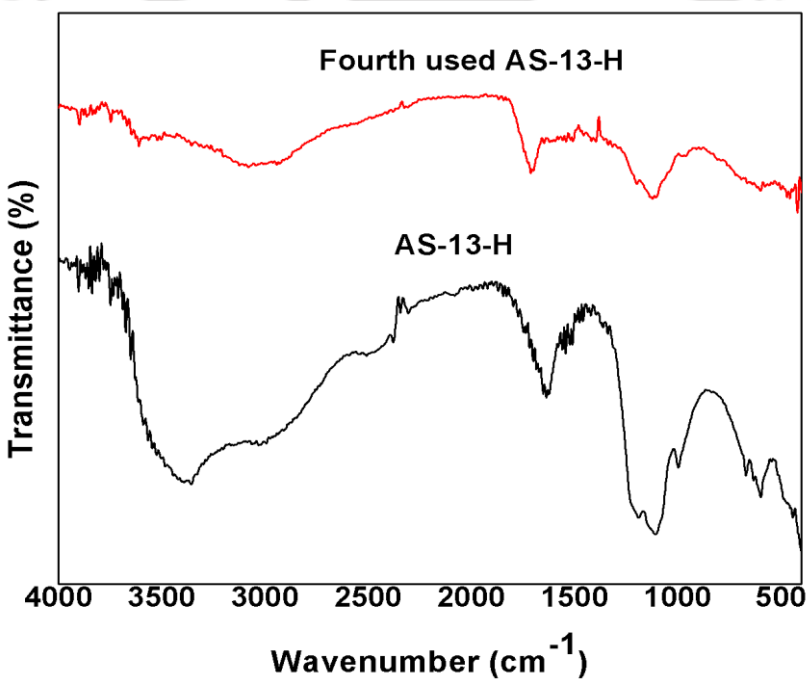

Figure 4.37. Comparison of FTIR spectrum of AS-13-H and 4th used AS-13-H catalyst.

The FTIR analysis (Figure 4.37) of the 4th used AS-13-H catalyst produced IR peaks at a wavenumber close to 1704 cm^{-1} which could be due to the stretching bond of C=O group of organic substances such as humins formed due to the polymerization of 5-HMF during the reaction [184]. The organic deposit could also affect the

catalytic activity by occupying most of the active surface area, thus prohibiting the access of reactant molecules to these active sites in the catalyst. Besides this, much lower intensity IR peaks related to the sulfate groups at 995 cm^{-1}, 1112 cm^{-1}, and 1185 cm^{-1} as compared to the fresh catalyst were also observed. It suggested a decrease in sulfate groups in the 4^{th} used catalyst that resulted in a decrease in the quantity of Bronsted acid sites and hence the 5-HMF yield.

4.3.6 Activity comparison of AS-13-H with other reported catalyst

The catalytic activity of the AS-13-H for the microwave-assisted synthesis of 5-HMF from D-Glucose was compared with other reported synthetic catalysts (Table 4.14). De and coworkers reported a 5-HMF yield of 52.4% from D-Glucose by $AlCl_3$ catalyst under microwave irradiation and in a 100% DMSO solvent [246]. The reaction temperature and time were 140 ^oC and 5 min, respectively. The process required a relatively low temperature compared to our reported process. However, a relatively higher 5-HMF yield (53.8%) was observed in our reported process in a mixture of aqueous and organic phases that excludes the extra cost when only an organic phase is used. Similarly, Lu and coworkers performed the D-Glucose conversion under microwave irradiation and observed ~20% of 5-HMF yield at 150 ^oC and 90 min of reaction time in the presence of phosphate buffer catalyst [247]. The reaction time was quite high, and the yield of 5-HMF was relatively low as compared to the 5-HMF yield obtained by AS-13-H catalyst. In another study, Liu and coworkers reported a 5-HMF yield of 41.4% from D-Glucose in the presence of Al_5B_5 catalyst under the conventional heating system [244]. The yield of 5-HMF was relatively high; however, the process was carried out by taking DMSO as a solvent, which could increase the overall cost of the process. In addition, the extra cost required for the product separation from the solvent is also another drawback of using such organic solvents for the 5-HMF synthesis. The catalyst we reported is prepared from an industrial waste material, which is inexpensive. Using the catalyst, a comparable or even higher amount of 5-HMF yield was obtained, compared to other reported synthetic catalyst. Hence, the RM based catalyst could be considered as a suitable one for the sustainable production of 5-HMF from D-Glucose in the future.

Table 4.14. Activity and stability comparison of AS-13-H with other reported catalysts.

Catalyst	Reaction	Temperature (°C)	Time (min)	Solvent	5-HMF yield (%)	Catalyst stability	Ref.
Sn20/γ-Al_2O_3	Glucose conversion to 5-HMF	150	60	DMSO:H_2O (80:20)	27.5	5-HMF yield of 23.3% obtained after regeneration of catalyst at 200 °C.	[133]
Al_5B_5	Glucose conversion to 5-HMF	140	120	DMSO	41.4	5-HMF yield of 32.2% obtained at 5th run	[244]
Anhydrous $AlCl_3$	Microwave conversion of glucose	140	5	DMSO	52.4	No stability study reported for glucose as substrate	[246]
Phosphate buffer system	Microwave conversion of glucose	150	90	Two phase system	~ 20	No stability study reported	[247]
AS-13-H	Microwave conversion of D-Glucose	180	5	Water & water/DMSO (1:1)	26.2 & 53.8	5-HMF yield of 22.1% obtained at 5th run	Present study

4.4 Preparation and characterization of non-metal modified RM-based acidic catalysts for the direct D-Glucose transformation to 5-HMF

In this section, a sulfonic acid grafted carbon-coated red mud-based catalyst is reported for the microwave conversion of D-Glucose to 5-HMF. The carbonaceous catalyst reported here contains both Lewis and Bronsted acid sites, making it different from other reported less efficient carbonaceous catalysts for D-Glucose conversion to 5-HMF synthesis with only Bronsted acid sites.

4.4.1 Activity comparison of different catalysts based on 5-HMF yield

The catalysts prepared from RM were applied for the conversion of D-Glucose under microwave heating, and based on the yield of the desired product 5-HMF, the catalyst that showed the best performance was figured out and used for the successive reactions. From the initial assessment, the raw RM catalyst was found to be less effective for the 5-HMF production from D-Glucose (Figure 4.38 (a)). Though a reasonable D-Glucose conversion (53%) could be achieved by RM catalyst, particularly because of the metal elements such as Al, Ti, Si, and Fe present in it, the 5-HMF yield was very low (3.2%). It strongly suggested that these metal elements, which could act as Lewis acids during the D-Glucose transformation to 5-HMF without appropriate Bronsted acid sites, were not capable of producing a reasonable 5-HMF yield. The acid activation of RM exclusively performed to remove the leachable Na and Ca from RM led to a significant increase in surface area as well (Table 4.16). It avoided the further contamination of the reaction product and produced catalytic support with an enhanced surface area (219.6 m^2g^{-1}, Table 4.16) for the impregnation of D-Glucose. The catalytic activity of AARM was very similar to that of RM, which indicated that the catalyst with higher surface area and Lewis acid sites without Bronsted acid sites was still inefficient for the production of 5-HMF. The AD-1:1 catalyst developed by impregnating D-Glucose on AARM with an equal weight ratio followed by thermal treatment at 300 ^oC produced a reasonably higher D-Glucose conversion (78.2%) and 5-HMF yield (15.7%) than RM and AARM. It has been observed that the incomplete carbonization of carbon precursors,

including D-Glucose, could retain few oxygen functional groups such as phenolic –OH, and –COOH, which have Bronsted acid characteristics [248]. The enhanced catalytic activity of the AD-1:1 catalyst could be ascribed to the enhanced Bronsted sites because of the –COOH and phenolic –OH groups in this case as well. The presence of these functional groups was confirmed from FTIR analysis (Figure 4.40) presented in the upcoming sections. A notable increase in D-Glucose conversion to 93% and 5-HMF yield to 51.5% was observed after functionalization of the SO_3H groups on the AD-1:1 catalyst. The AD-1:1/SO_3H catalyst exhibited appropriate Lewis acid sites in the form of Fe, Si, Al, and Ti and Bronsted acid sites from SO_3H, OH, and COOH groups, which enhanced the efficiency of the 5-HMF production process. The detailed catalyst characterization identifying the Bronsted and Lewis acid sites and the total acid site density is discussed in the following sections. Previously, several authors also reported the enhanced catalytic activity of the carbonaceous catalyst after SO_3H functionalization, ascribed to the increased Bronsted acid density [171,248].

The SO_3H functionalized AD:X:Y catalysts (AD-X:Y/SO_3H) prepared, as mentioned in section 3.2.2.4, were applied for the 5-HMF production process. It can be observed that a higher D-Glucose conversion and 5-HMF yield were obtained when the D-Glucose (carbon precursor) amount increased from 50% to 100% with respect to the weight of the AARM (Figure (4.38(b)). At the AARM/D-Glucose weight ratio of 1:0.5 (AD-1:0.5/SO_3H), the conversion reached 87.5%, and the 5-HMF yield was 40.7%. The conversion and yield increased to 93% and 51.5%, with an increase in the D-Glucose quantity on AARM to 100% (AD-1:1/ SO_3H). It indicated that there could be more carbon species and the acidic –COOH and phenolic -OH sites present on the catalyst at higher D-Glucose loading, leading to a higher catalytic activity. As discussed previously, in addition to the -SO_3H acid sites, the –COOH and polycyclic aromatic –OH groups in the sulfonated carbon catalysts formed after incomplete carbonization could also contribute to the activity of the catalyst for the production of 5-HMF [248]. However, there was no significant variation in catalytic activity found with the further increase in D-Glucose quantity beyond 100%. This suggested that the AD-1:1/ SO_3H catalyst prepared with a D-Glucose to AARM

weight ratio of 1:1 followed by carbonization and SO_3H functionalization was best suitable for the D-Glucose transformation to 5-HMF.

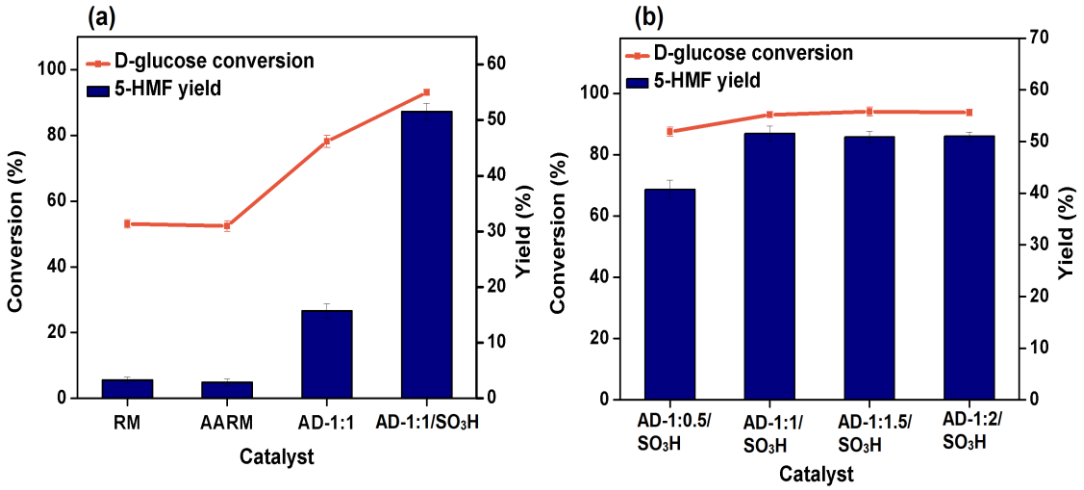

Figure 4.38. Activity of different catalyst for the microwave-assisted 5-HMF production from D-Glucose. Time = 5 min, temperature = 180 ^oC, catalyst/D-Glucose weight ratio = 0.6, DMSO/water = 90:10 (weight% ratio).

4.4.2 Characterization study

4.4.2.1 XRD analysis

The XRD analysis of RM and AARM indicated peaks at 2θ of 33^o, 35.5^o, 40.8^o, 49.6^o, 54^o and 62.75^o, which were attributed to (104), (110), (113), (024), (116), and (214) planes of hematite (Fe_2O_3) (Figure 4.27). It suggested a dominant surface composition of Fe_2O_3 in RM and AARM. A relative loss in crystallinity of the Fe_2O_3 phases could be seen in the AARM catalyst, which was due to the acid activation with HCl. Besides Fe_2O_3, $Al(OH)_3$, SiO_2, and TiO_2 were observed with the peak at 2θ of 18.5^o (010), 26.6^o (101), and 27.5^o (110), respectively [249,250]. After D-Glucose impregnation followed by carbonization at 300 ^oC, the AD-X:Y based catalysts produced a new XRD pattern in the 2θ range of 15^o to 30^o ascribed to the amorphous structure of carbon (Figure (4.39 (a)). All the other phases found in RM and AARM, such as Fe_2O_3, SiO_2, and TiO_2, remained intact at their respective 2θ positions. The AD-X:Y/SO_3H catalysts produced after SO_3H functionalization showed additional XRD peaks of $Fe_2(SO_4)_3$ at 20.2^o (104), 21.4^o (110), 39.7^o (033),

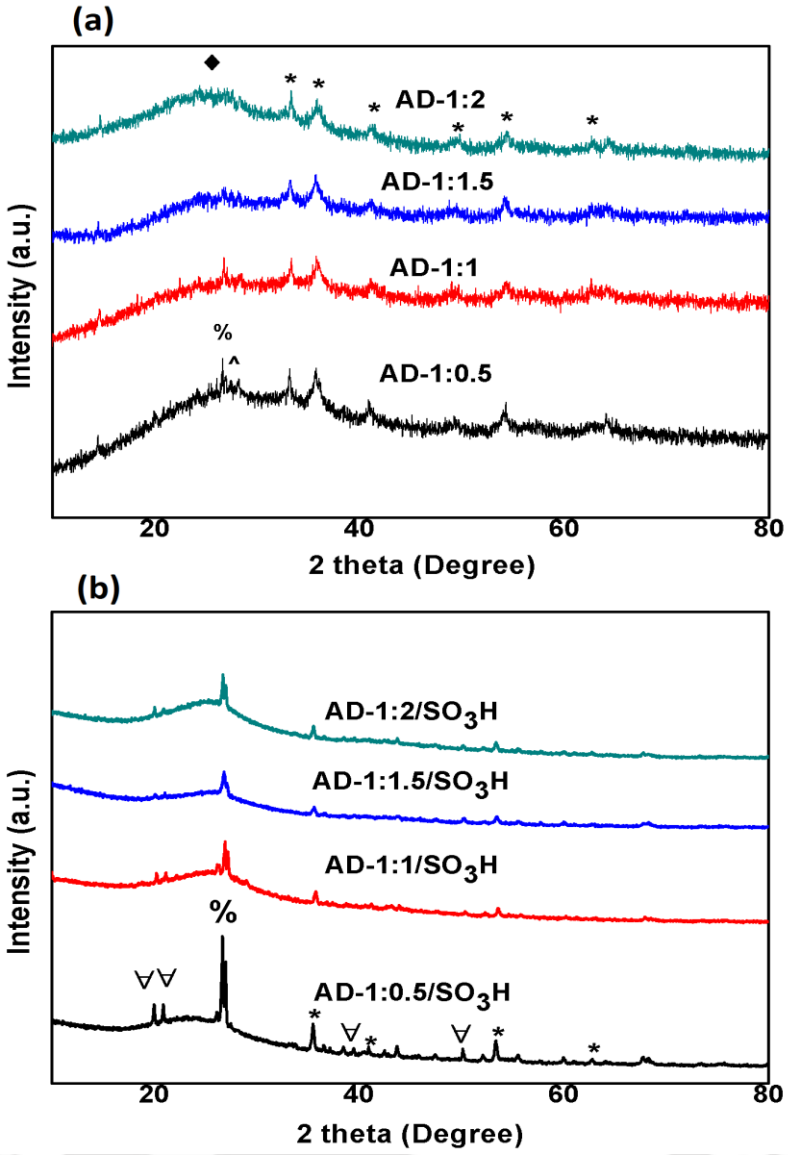

Figure 4.39. XRD analysis of (a) AD-X:Y and (b) AD-X:Y/SO_3H catalysts. * Fe_2O_3, % SiO_2, ^ TiO_2, ∀$Fe_2(SO_4)_3$.

and 50.6^o (226) [251] (Figure (4.39 (b)). It is possible that during the treatment of AD-X:Y catalysts with concentrated H_2SO_4, few Fe could get convert to their sulfates, due to which the $Fe_2(SO_4)_3$ peaks were observed. The Fe_2O_3 peaks were observed in the AD- X:Y/SO_3H based catalysts at 35.5^o, 40.8^o, 53.6^o, and 62.7^o, however, with relatively low intensity. It could be ascribed to the carbon species formation on the catalyst surface after the carbonization of D-Glucose and conversion of a few amount of Fe_2O_3 to $Fe_2(SO_4)_3$ that decreased the relative concentration of Fe_2O_3. The XPS

study discussed in the impending sections also confirmed the $Fe_2(SO_4)_3$ species in the catalyst after sulfonation. An identical phenomenon was also reported previously by Daizo et al., where the formation of $Fe_2(SO_4)_3$ was observed after sulfonation of carbon-based Fe_2O_3 catalyst [252]. The slightly soluble nature of the $Fe_2(SO_4)_3$ in water is expected to leach some of the compounds from the catalyst matrix during the washing of the catalyst. However, following the sulfonation, the catalyst was washed thoroughly with warm water until the pH reached near neutral. Therefore, further leaching of $Fe_2(SO_4)_3$ during the 5-HMF synthesis reaction was very unlikely to occur. This was also confirmed from the XRD, FTIR, and FESEM-EDX study of the catalyst discussed in the upcoming paragraphs that suggested very similar characteristics between the fresh and the reused catalyst.

4.4.2.2 FTIR analysis

The surface functional groups in the prepared catalysts were identified by FTIR analysis (Figure 4.40). The stretching vibration of Fe-O was observed in the FTIR spectra of RM at 460 cm^{-1} and 540 cm^{-1} (Figure 4.40 (a)). Other functional groups in RM such as Si-O-Si and Al-O were identified at 1002 cm^{-1} and 670 cm^{-1}, respectively. The spectrum close to 1400 cm^{-1} in RM was due to the C=O stretching vibration in CO_3^{-2}. A broad IR peak in the range of 3300 cm^{-1} to 3550 cm^{-1} was attributed to the –OH groups stretching vibration in RM. The IR peaks in AARM remained almost similar to RM. In AD-X:Y catalysts, additional IR peaks related to the carbon and its functional groups were observed (Figure 4.40 (a)). At 760 cm^{-1} and 1715 cm^{-1}, the two shoulder IR spectrum could be ascribed to the C-H bending vibration and the C=O groups of COOH, respectively [173]. Further, IR peaks at 1607 cm^{-1} and 2930 cm^{-1} corresponded to the skeletal vibration of phenyl groups and vibration in the $–CH_3$, respectively [173]. The H_2SO_4 treated AD-X:Y catalysts (AD-X:Y/SO_3H) exhibited all the functional groups of carbon, as observed in the AD-X:Y catalysts. Additional IR peaks produced in the AD-X:Y/SO_3H catalysts related to the functional groups of sulfur in SO_3H at 1040 cm^{-1} [248] (Figure 4.40 (b)). Moreover, the IR spectrum at 1195 cm^{-1} and a shoulder spectrum at 980 cm^{-1} corresponded to

the bidentate sulfate ions coordinated with Fe [253]. It confirmed the presence of both SO_3H and SO_4^{-2} groups in the catalyst matrix.

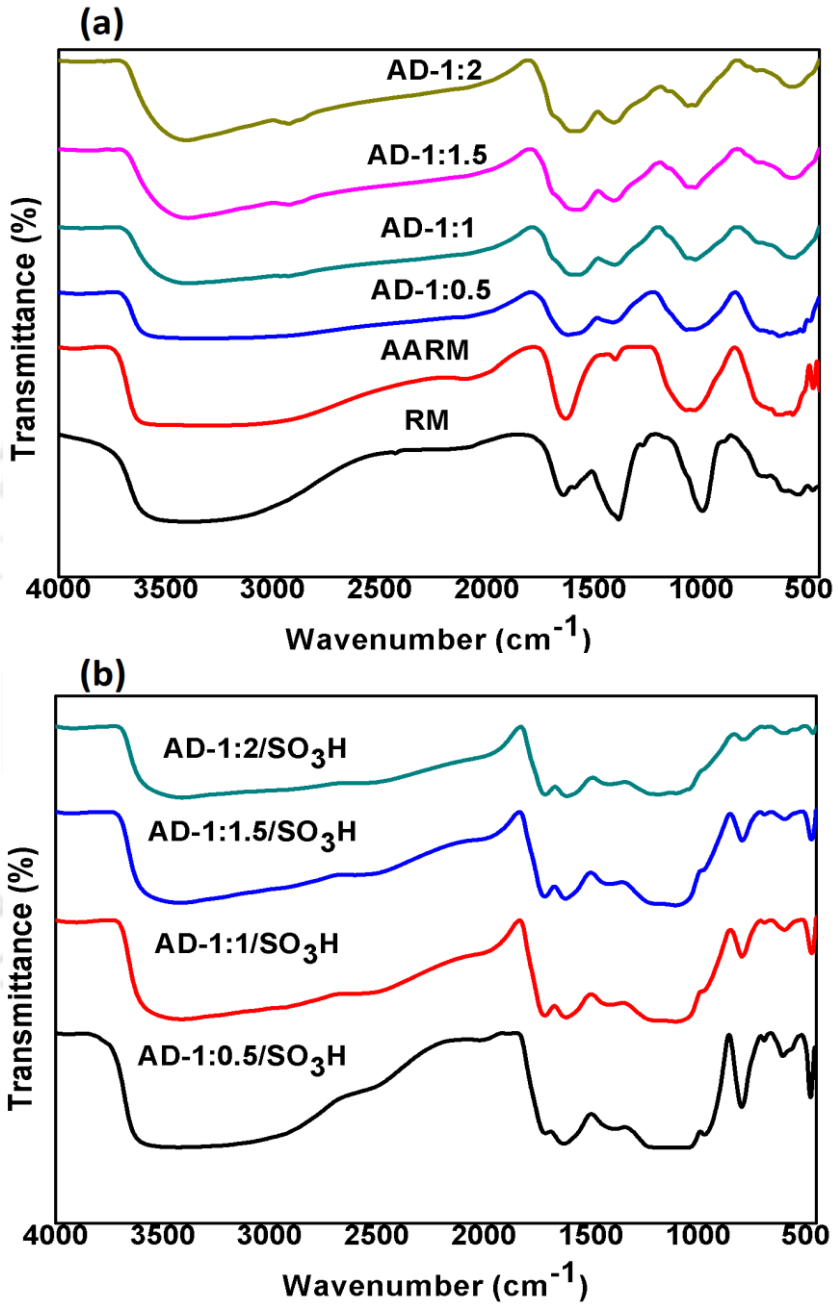

Figure 4.40. FTIR spectra of (a) RM, AARM and AD-X:Y and (b) AD-X:Y/SO_3H catalysts.

4.4.2.3 XPS analysis

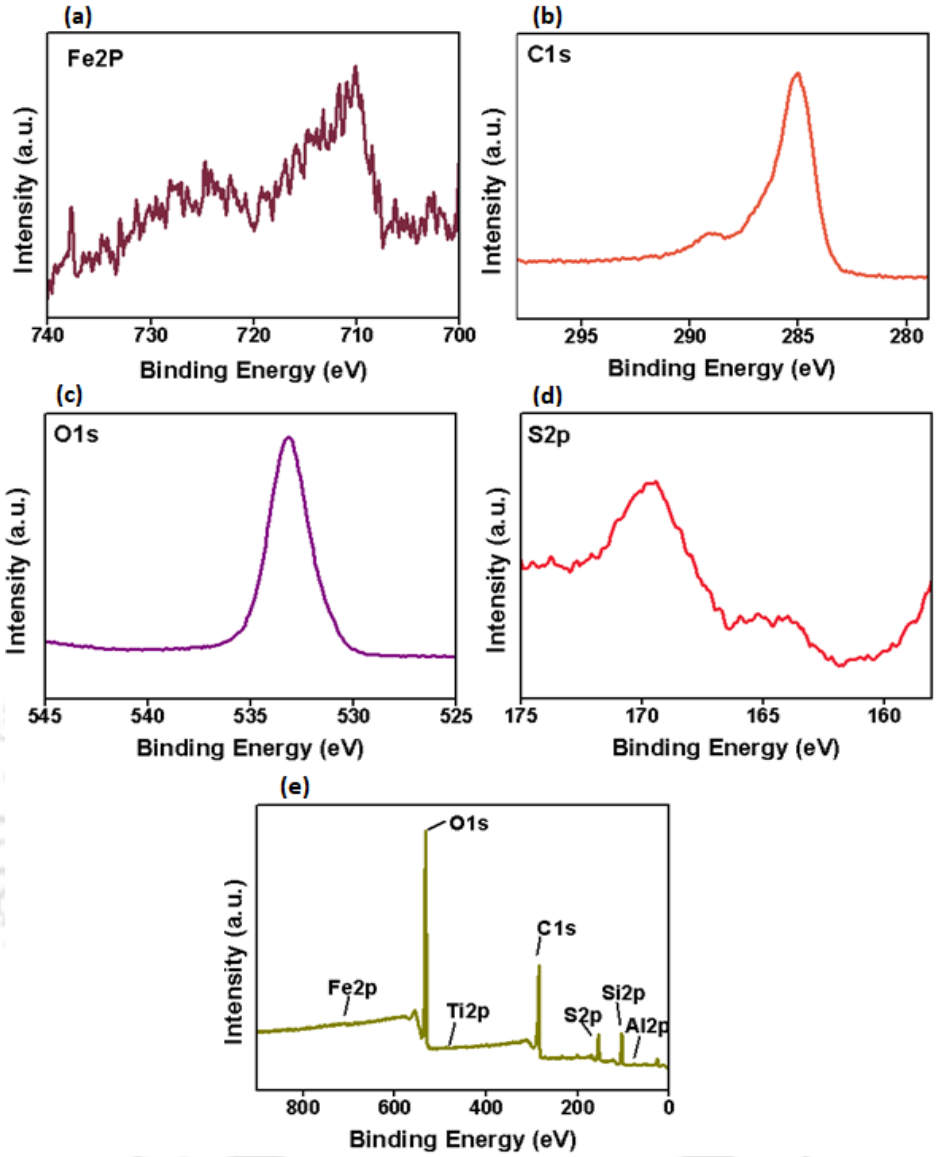

Figure 4.41. Deconvoluted XPS spectra (a) Fe2P, (b) C1s, (c) O1s (d) S2p, and (e) XPS survey of the AD-1:1/SO_3H catalyst.

The XPS analysis of the AD-1:1/SO_3H catalyst confirmed Fe, Al, Ti, Si, O, C, and S in the catalyst matrix (Figure 4.41). The Fe2p XPS spectrum at 711.4 eV and 724.9 eV indicated the presence of Fe^{+3} particles in the catalyst [254]. The C1s XPS spectra of AD-1:1/SO_3H consisted of peaks at the 284.6 eV and 289 eV assigned to the sp^2 (C=C)/sp^3 (C-C) carbon and COOH, respectively [255]. The well-

recognized XPS spectra of sulfur groups with peaks at 164 eV and 169 eV of binding energy corresponded to the sulfur in SH/-C-S-C- and SO_3H/SO_4^{-2} groups. The intensity of the latter was higher, suggesting a larger percentage of sulfur in the SO_3H/SO_4^{-2} groups [171,255]. It confirmed the presence of both sulfonic and sulfate groups in the catalyst matrix as well. The O1s spectrum at 532.6 eV in the catalyst was assigned to the oxygen atom in SO_3H/SO_4^{-2} [171]. Moreover, the XPS analysis confirmed the presence of Al2p, Si2p, and Ti2p, spectrum at 75 eV, 104 eV, and 458.7 eV, respectively as well.

4.4.2.4 FESEM and FESEM-EDX analysis

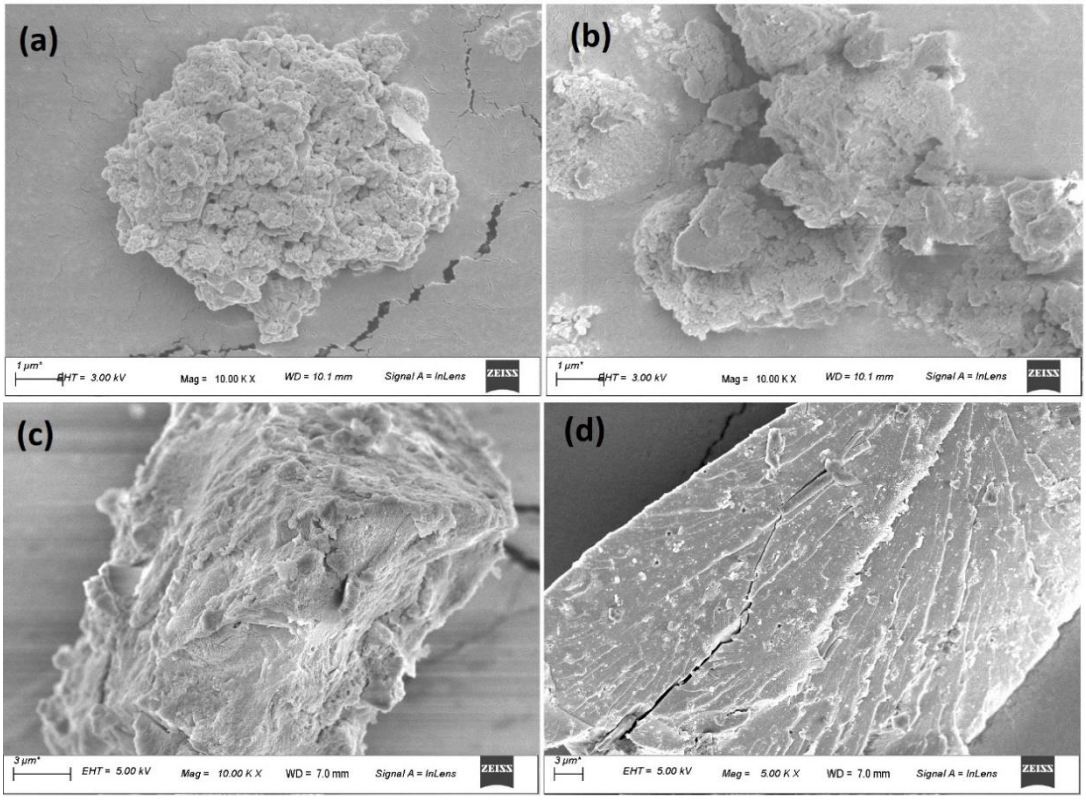

Figure 4.42. FESEM images of (a) RM, (b) AARM, (c and d) AD-1:1/SO_3H catalyst.

The morphology of RM is based on small and aggregated particles with varying sizes and structures. The catalyst exhibited well-defined pores between the particles (Figure 4.42 (a)). The acid (HCl) activation of RM led to particles with relatively smaller sizes with amorphous nature (Figure 4.42 (b)). The morphology of

the AD-1:1/SO_3H catalyst produced after sulfonation of AD-1:1 showed a rigid composite-like appearance (Figure 4.42 (c and d)). The carbon coating and SO_3H functionalization reduced the relative numbers of pores in the AD-1:1/SO_3H than the AARM. The elemental composition of AD-1:1/SO_3H catalyst obtained from the FESEM-EDX analysis is presented in Table 4.15. The study confirmed the presence of C, O, S, Si, Fe, Ti, and Al in the AD-1:1/SO_3H catalyst.

Table 4.15. FESEM-EDX analysis of catalysts.

Elements	C	O	Fe	Si	S	Al	Ti
AD-1:1/SO_3H	46.5	31.7	7.6	6.0	5.2	1.6	1.4
AD-1:1/SO_3H after 4^{th} use	57.0	31.5	3.8	1.9	4.7	0.7	0.4

4.4.2.5 N_2 adsorption-desorption isotherm analysis

The N_2 adsorption-desorption isotherm (Figure 4.43) of RM, AARM, and AD-1:1/SO_3H indicated a type IV isotherm with a distinct hysteresis loop. The occurrence of the hysteresis loop was due to the capillary condensation at a P/P_0 of 0.6 to 0.85, typical for a mesoporous material. Enhanced N_2 adsorption in this pressure range signified the increased pore size as well. RM had a low surface area of 10.2 $m^2 g^{-1}$ (Table 4.16). The average pore size and total pore volume of RM were 16.19 nm and 0.041, respectively. The acid treatment of RM produced a surface area of 219.6 $m^2 g^{-1}$, which was almost 21.5 times higher than the RM. It was ascribed to the Na and Ca removal from the RM surface that increased the number of pores and pore volume to a reasonable extent. The AD-1:1/SO_3H catalyst showed an appreciable surface area of 69.2 $m^2 g^{-1}$ with an average pore size of 6.84 that remained in the mesoporous range. The carbon deposition followed by SO_3H functionalization could occupy some of the vacant pores, due to which a relative decrease in the surface area of AD-1:1/SO_3H as compared to AARM was observed.

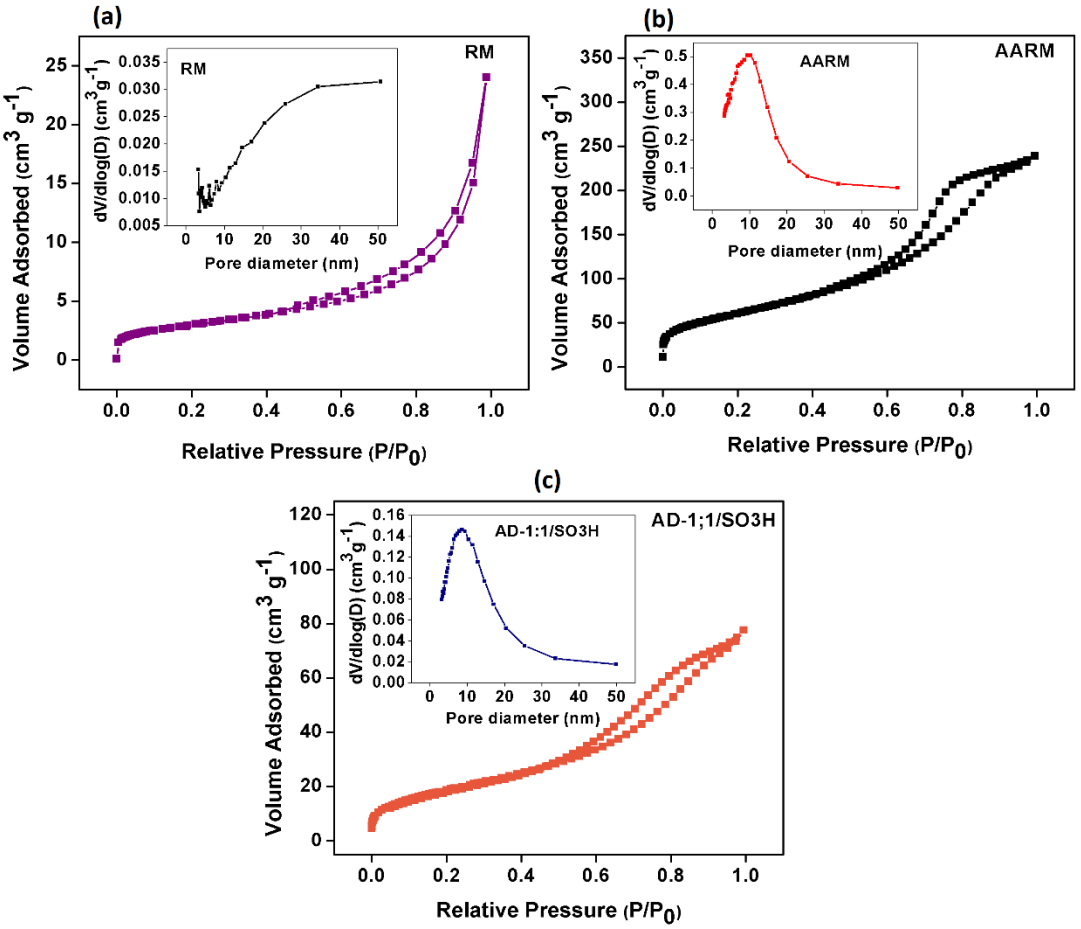

Figure 4.43. N_2 adsorption-desorption isotherm of (a) RM, (b), AARM, and (c) AD-1:1/SO_3H.

Table 4.16. BET analysis of catalysts.

Catalyst	Surface area (m^2 g^{-1})	Average pore size (nm)	Total pore volume (cm^3 g^{-1})
RM	10.2	16.19	0.041
AARM	219.6	6.68	0.366
AD-1:1/SO_3H	69.2	6.84	0.118

4.4.2.6 Py-ATR-FTIR analysis

The Bronsted and Lewis acid sites in the AD-1:1 and AD-1:1/SO_3H catalysts were identified by the Py-ATR-FTIR techniques (Figure 4.44 (a)). The Py-ATR-FTIR peak at 1452 cm^{-1} was attributed to the Lewis acids in both AD-1:1 and AD-1:1/SO_3H catalyst [173]. In the AD-1:1 catalyst, the Bronsted acids coordinated pyridinium ion was observed at 1552 cm^{-1} [173]. The Bronsted acids could be assigned to the polycyclic aromatic -OH and –COOH groups in the AD-1:1 catalyst formed after the incomplete carbonization of D-Glucose [152]. The peak corresponded to the Bronsted acid sites with higher intensity than AD-1:1 was detected in the AD-1:1/SO_3H catalyst at a higher frequency of 1580 cm^{-1} [256]. It suggested a relative improvement in the Bronsted acids in the AD-1:1/SO_3H catalyst produced after sulfonation of AD-1:1 catalyst. Besides this, a shoulder IR spectrum at 1488 cm^{-1} detected in the AD-1:1/SO_3H catalyst was the characteristic of pyridine adsorbed on both Lewis and Bronsted acids [256]. The ratio between Bronsted to Lewis acid density was calculated by integrating the corresponding IR peaks (Table 4.17).

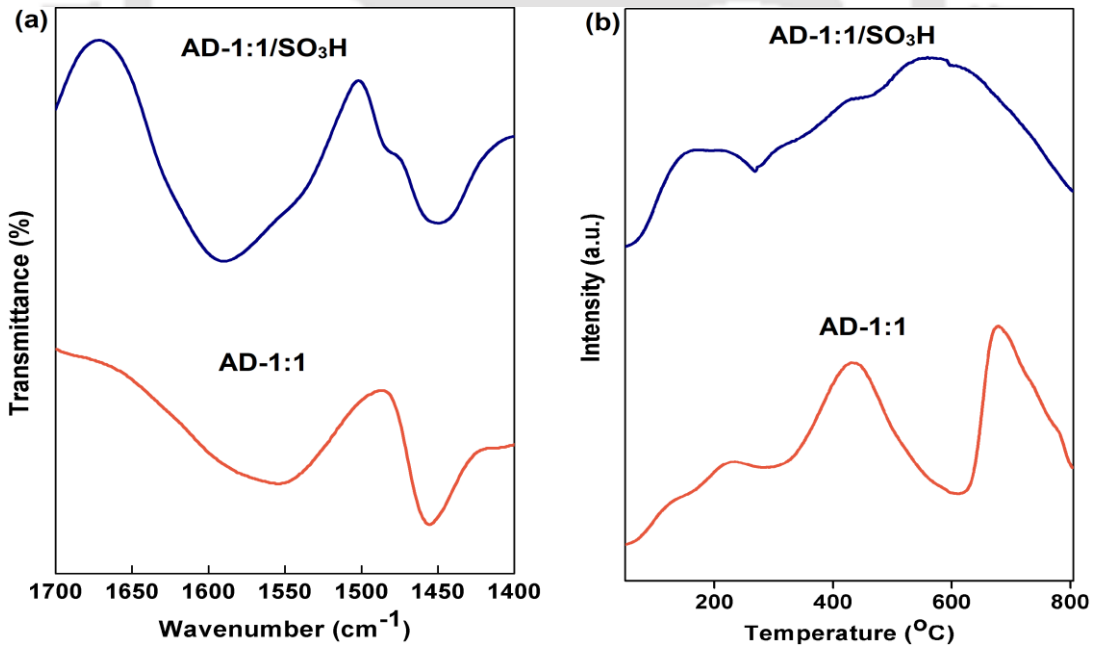

Figure 4.44. (a) Py-ATR-FTIR spectra and (b) NH_3-TPD profile of AD-1:1 and AD-1:1/SO_3H catalysts.

4.4.2.7 NH_3-TPD analysis

The acid site density and strength of AD-1:1 and AD-1:1/SO_3H catalyst were analyzed by the NH_3-TPD analysis (Figure 4.44 (b)). The NH_3-TPD profile indicated broad and small intensity peaks in the region between 90 ^oC to 280 ^oC assigned to the NH_3 desorption from weak acid sites in both AD-1:1 and AD-1:1/SO_3H catalysts. Additional sharp NH_3 desorption peaks at 425 ^oC and 670 ^oC in the AD-1:1 catalyst suggested medium and strong acid sites. In the AD-1:1/SO_3H catalyst, the medium and strong acid sites can be observed from the relatively broader and intense NH_3 desorption peaks in the range between 290 ^oC to 800 ^oC. The total acid site density calculated from the NH_3-TPD analysis was 5.1 mmol g^{-1} and 6.8 mmol g^{-1} for the AD-1:1 and AD-1/SO_3H catalyst (Table 4.17), respectively. It confirmed a higher number of acid sites in the AD-1:1/SO_3H catalyst owing to the presence of SO_3H groups after sulfonation.

Table 4.17. Acid sites analysis of catalysts.

Catalyst	Total acid density mmol g^{-1} (From NH_3-TPD)	Bronsted /Lewis acid ratio (B/L)
AD-1:1	5.1	1.23
AD-1:1/SO_3H	6.8	2.25

4.4.3 Reaction parametric study

The effectiveness of the AD-1:1/SO_3H catalyst for the microwave production of 5-HMF from D-Glucose at different reaction parametric conditions was studied. The solvent types could affect the efficiency of the 5-HMF synthesis process to a reasonable extent [133]. In this study, the reactions were performed in different weight percentage ratios of DMSO and water. It can be seen in Figure (4.45 (a)) that under pure DMSO solvent, D-Glucose conversion of 97.1% and 5-HMF yield of 41% could be achieved at 180 ^oC and 30 min. DMSO/water percentage weight ratio of 90:10 enhanced the 5-HMF yield to 51.5%. However, a further increment in the water amount was unable to produce any positive effect on the 5-HMF yield. DMSO itself

helps disrupt the intermolecular hydrogen bonding in glucose and stabilizes its furanic form, acting as an excellent dehydration medium [133]. However, the strong dehydrating nature of DMSO could drive the undesired and rapid dehydration of D-Glucose towards levoglucosan. Hence, water up to a certain percentage along with DMSO inhibits the rapid D-Glucose dehydration to levoglucosan. Nevertheless, higher water quantity could also accelerate the rehydration of 5-HMF to LA and decrease the overall 5-HMF yield. In our system, a levoglucosan yield of 12.8% was observed under pure DMSO solvent. Water with a DMSO to water weight percent ratio of 90:10 decreased the levoglucosan to 8.3%, and the trend continued with the increased water percentage. Though DMSO/water at 90:10 produced an enhanced 5-HMF yield, higher water quantity beyond that did not contribute positively towards more 5-HMF production. An increased amount of LA was observed at higher water content, suggesting more rehydration reactions of 5-HMF. Besides this, a continuous increase in FCT yield and an inconsistent variation in LCTA and FU yield was observed with increased water quantity. Previously, few authors also reported similar observations on 5-HMF synthesis under DMSO and water solvent mixture [133,245,257]. The study suggested a DMSO/water weight ratio of 90:10 most appropriate for the 5-HMF yield.

The temperature had a remarkable influence on the 5-HMF production process (Figure 4.45 (b)). At 160 ^{o}C, 53.4% conversion of D-Glucose and 27.3% yield of 5-HMF were observed. The D-Glucose conversion increased continuously up to 190 ^{o}C and reached close to 100%. The improved catalytic efficiency at higher temperatures was attributed to an adequate activation energy availability for 5-HMF production from D-Glucose through the isomerization and dehydration pathway. However, the positive effect of temperature on the 5-HMF yield was seen up to 180 ^{o}C only, at which it reached 51.5%, and beyond that, a decreasing trend was observed. A decrease in the FCT yield from 4.3% at 160 ^{o}C to 0% at 190 ^{o}C was observed as well. With the increased temperature, the formation of LGS, LCTA, and FU increased. It indicated an upsurge in the unwanted reactions such as rapid dehydration and retro-aldol processes that transformed D-Glucose, FCT, and 5-HMF towards these undesired products at higher temperatures (Figure 4.46). Moreover, at a temperature above 180

^{o}C, higher production of solid humins was observed, suggesting the occurrence of undesired dehydration and polymerization process. Therefore, the temperature of 180 ^{o}C that produced the highest 5-HMF yield was considered the optimum temperature here.

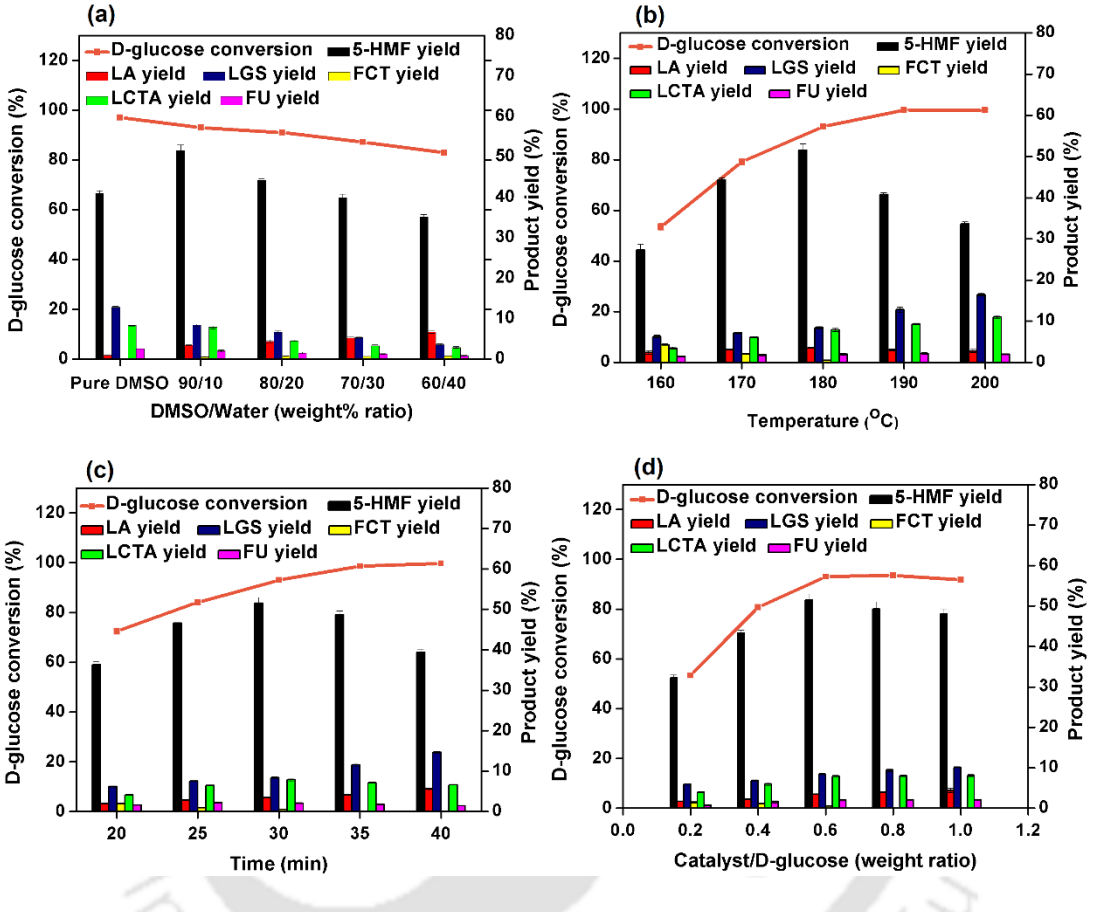

Figure 4.45. Reaction parametric study on microwave D-Glucose conversion to 5-HMF (a) effect of solvent (time = 30 min, temperature = 180 ^{o}C, catalyst/D-Glucose weight ratio = 0.6): (b) effect of reaction temperature (time = 30 min, catalyst/D-Glucose weight ratio = 0.6, DMSO/water weight% ratio = 90:10): (c) effect of reaction time (temperature = 180 ^{o}C, catalyst/D-Glucose weight ratio = 0.6, DMSO/water weight% ratio = 90:10): (d) effect of catalyst dosage (time = 30 min, temperature = 180 ^{o}C, DMSO/water weight% ratio = 90:10).

The reaction time was beneficial for the D-Glucose conversion, due to which a continuous increment in conversion was observed up to 40 min (Figure 4.45 (c)).

At the reaction time of 20 min, the AD-1:1/SO_3H catalyst showed 72.5% of D-Glucose conversion. The corresponding 5-HMF yield was 36.4% only. The D-Glucose conversion continuously increased and at 40 min, it reached almost 100%. On the contrary, an increment in the yield of 5-HMF was seen up to 30 min only, and beyond that, it started to decrease. At prolonged reaction time, the undesired polymerization/dehydration of fructose, D-Glucose, and 5-HMF to humins, 5-HMF rehydration to LA, and D-Glucose retro-aldol reaction to LCTA could be significant (Figure 4.46). As shown in Figure 4.45 (c), with the increment in the reaction time, the higher production of undesired LGS, LA, FU, and LCTA, and decrement in 5-HMF and FCT yield confirmed the above phenomenon. Hence, 30 min of reaction time was more suitable for the production of 5-HMF.

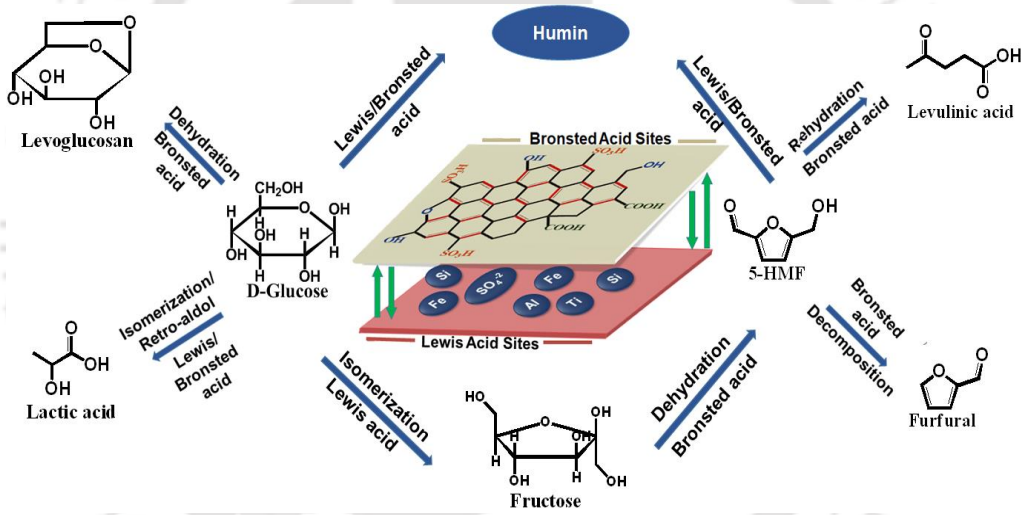

Figure 4.46. Plausible pathway for the D-Glucose transformation to 5-HMF and other products.

The effect of the AD-1:1/SO_3H loading on the efficiency of the 5-HMF synthesis process is presented in Figure 4.45 (d). An increment in the weight ratio of AD-1:1/SO_3H to D-Glucose from 0.2 to 0.6 positively drove the D-Glucose conversion from 53.4% to 93% and 5-HMF yield from 32.2% to 51.5%. A higher catalyst loading could produce a larger active site quantity for the adsorption of reactant molecules and facilitate the interaction between them for shifting the reaction

towards the product formation. However, no significant variation in the conversion of D-Glucose was seen at the AD-1:1/SO_3H to D-Glucose weight ratio beyond 0.6. On the contrary, a minimal decrease in 5-HMF yield to 48% occurred at the AD-1:1/SO_3H to D-Glucose weight ratio of 1. A notable increase in the LA, LCTA, LGS, FU and solid humins yield was observed, owing to the presence of higher active sites enabling an acceleration in the rate of undesired reactions at higher catalytic loading.

4.4.4 Reusability of AD-1:1/SO_3H catalyst

The AD-1:1/SO_3H was successively reused for the 5-HMF production to reveal its catalytic stability. From Figure 4.47, it can be seen that no significant decrease in the D-Glucose conversion and 5-HMF production was seen up to the 4th cycle. The loss in 5-HMF yield from 51.5% in the 1st cycle to 48.3% at the 4th cycle was insignificant. It indicated the appreciable stability of the AD-1:1/SO_3H catalyst for the 5-HMF production from D-Glucose under microwave heating.

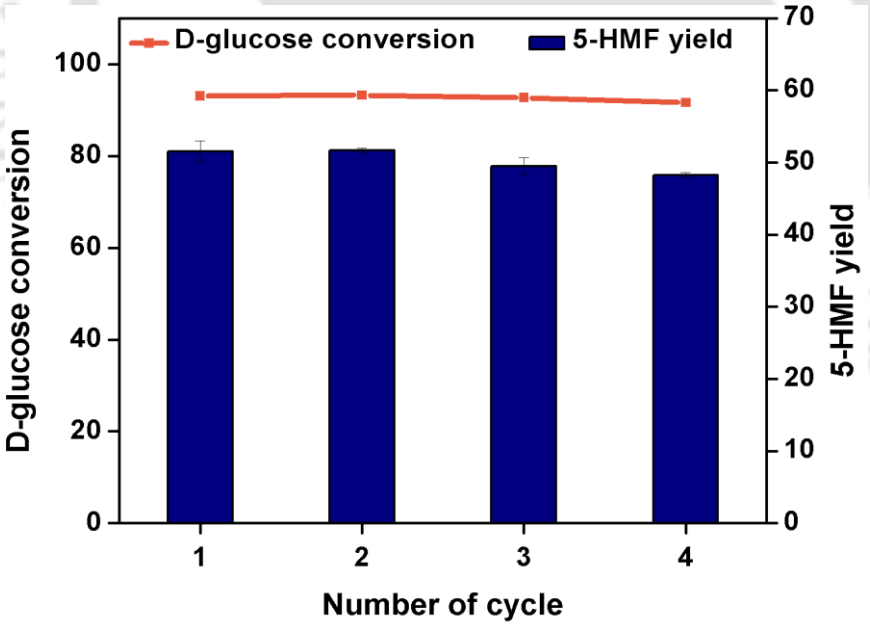

Figure 4.47. Reusability of AD-1:1/SO_3H catalyst (temperature = 180 ^oC, time = 30 min, catalyst/D-Glucose weight ratio = 0.6, DMSO/water weight% ratio = 90:10).

The fresh and spent catalyst was characterized by XRD, FTIR, and FESEM-EDX techniques to analyze any change in their properties. The XRD analysis of the fresh was found very similar to the spent catalyst (Figure 4.48 (a)). All the active phases of the fresh AD-1:1/SO_3H catalyst remained intact in the 4th used AD-1:1/SO_3H catalyst. The FTIR analysis of the spent catalyst confirmed all the functional groups as detected in the fresh catalyst (Figure 4.48 (b)). Particularly, no changes in the bidentate sulfate (SO_4^{-2}) functional groups at 980 cm^{-1} and 1195 cm^{-1} were seen, indicating no leaching of $Fe_2(SO_4)_3$ during the reaction. The elemental composition analysis performed by the FESEM-EDX technique showed a relative increase in carbon content in the spent catalyst during the reaction (Table 4.15). It could be ascribed to the deposition of carbonaceous compounds such as solid humins on the catalyst surface during the 5-HMF synthesis process. The increased carbon content led to a relative decrease in the percentages of other elements in the FESEM-EDX analysis. The minor loss in catalytic activity observed during the catalyst reuse could be due to loss in certain active sites due to the carbon deposition on the surface of the catalyst.

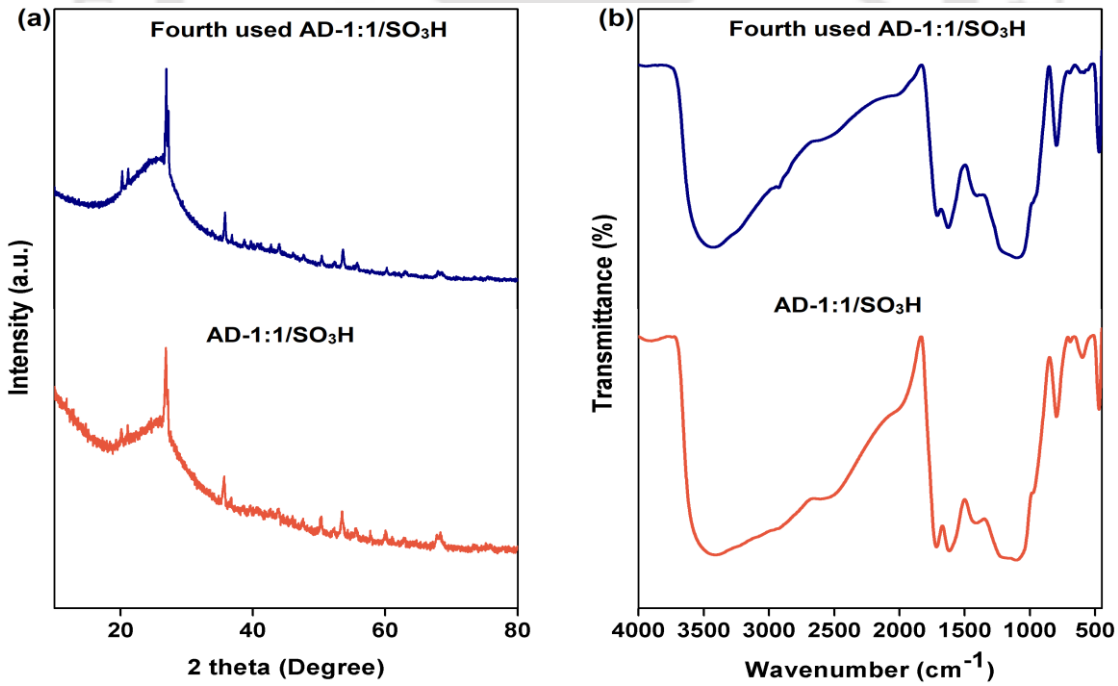

Figure 4.48. Comparison of (a) XRD and (b) FTIR analysis of fresh AD-1:1/SO_3H and 4th used AD-1:1/SO_3H catalyst.

4.4.5 Comparison of the AD-1:1/SO_3H efficiency with previously reported catalysts

The catalytic activity of the AD-1:1/SO_3H for the production of 5-HMF was compared with other synthetic sulfonated carbon and metal-based catalysts (Table 4.18). Waste polyurethane (PU) derived sulfonated carbon catalyst was used for the production of 5-HMF by Li and coworkers [171]. A high 5-HMF yield of 70.1% from fructose was reported by the PU based catalyst under the ethanol/1,4-dioxane solvent at 140 ^oC, and 2 h. However, the catalyst showed less activity for transforming Glucose to 5-HMF, due to which only 0.1% yield of 5-HMF was seen. Yuan et al. developed sulfonated carbon modified with Al_2O_3-TiO_2 catalyst with Lewis and Bronsted acid characteristics for the 5-HMF production from glucose [173]. The authors reported an appreciable 5-HMF yield of 40.3% at 130 ^oC, and 3 h under DMSO solvent. At an extended reaction time of 5 h, 57.36% of 5-HMF yield was achieved. The catalyst stability test performed at 3 h reaction time produced a 6.2% loss in the 5-HMF yield during the 5^{th} cycle as compared to the 1^{st} cycle. Sulfonated graphene quantum dots prepared from carbon black were used for the conversion of carbohydrate to 5-HMF [172]. Glucose conversion of 45.1% and 5-HMF yield of 19.5% was seen at 170 ^oC, and 2 h. Comparing the catalytic activity of our prepared AD-1:1/SO_3H catalyst with other similar synthetic catalysts, it is clear that AD-1:1/SO_3H has comparable or even higher efficiency than others. It suggests the suitability of the AD-1:1/SO_3H catalyst for economical and efficient 5-HMF production from D-Glucose.

Table 4.18. A comparison of AD-1:1/SO_3H catalytic efficiency for the 5-HMF production with other reported catalysts.

Catalyst	process	Temperature (^oC)	Time (min)	Solvent	5-HMF yield (%)	Catalyst stability	Ref.
Nb/C-50	Glucose conversion	160	120	NaCl saturated water/THF	25.5	Glucose substrate was not used for stability test	[152]
PU-Cat	Glucose conversion	140	240	Ethanol/1,4-dioxane (V/V = 70/30)	0.1	Glucose substrate was not used for stability test	[171]
Sulfonated graphene quantum dots	Glucose conversion	170	120	DMSO/Water (V/V = 70/30)	19.5%	Glucose substrate was not used for stability test	[172]
Al_2O_3-TiO_2 modified sulfonated carbon	Glucose conversion	130	180	DMSO	40.3	6.2% decrease in 5-HMF yield at 5^{th} cycle.	[173]
Sulfonated tobacco stem carbon	Glucose conversion	180	30	GVL/water (V/V = 4.7:0.3)	43.8	5-HMF yield decreased to 36.3% at the 5^{th} cycle	[176]
AD-1:1/SO_3H	Microwave D-Glucose conversion	180	30	DMSO:Water (W/W = 90:10)	51.5	Minor loss in 5-HMF yield to 48.3% at the 4^{th} cycle	Present work

Chapter 5

Conclusion and Future Scope

5.1 Conclusion

The current research comprehensively demonstrated the catalytic utilization of aluminum industry waste red mud for the application of industrially important chemical synthesis. The inherent composition of RM such as Na and Ca greatly contributed as basic catalytic sites and Fe, Al, Ti, and Si as acidic catalytic sites for the synthesis of two important chemicals, glycerol carbonate and 5-hydroxymethylfurfural. Only thermal treatment of red mud at 500 ^{o}C produced excellent activity for the transesterification of GL with 95.2% GL conversion and 92% GC yield achieved at 75 ^{o}C reaction temperature and 90 min of reaction time. Leaching of some active components during the reaction reduced the stability of the RM-500 catalyst during reuse. To enhance the stability of RM for the GL transesterification, various alkaline earth metals such as K, Sr, and Mg were doped on the RM surface, and their promotional effect on RM catalytic stability was studied. Out of different catalysts prepared by doping K, Sr, and Mg on the surface of RM, K-doped RM catalysts produced a better activity than others. The RK-30%-800 catalyst resulted in a GL conversion of 96.8% and GC yield of 93.2% and showed a significant increase in stability, due to which 78% GL conversion was obtained at the 4th reuse of the catalyst. The high surface concentration of K_2O contributed largely towards the enhanced basic properties, resulting in appreciable catalytic stability.

The acidic catalysts derived from red mud were successfully applied for the D-Glucose conversion to 5-HMF under microwave irradiation. The Sn doping enhanced the Lewis acidic properties and contributed to the greater stability of the AS-13-H catalyst. The H_2SO_4 deposition on the AS-13 catalyst improved the

Bronsted acidic sites that helped in the 5-HMF synthesis by the dehydration of fructose. An appreciable 5-HMF yield of 26.2% was obtained by the AS-13-H catalyst at an optimized reaction condition of 180 ^{o}C, 5 min. The leaching of sulfur groups during the reaction led to a decrease in catalytic stability; however, the catalyst was still able to retain almost 84.2% of the initial 5-HMF yield during the 4th use condition. The catalyst AD-1:1/SO_3H prepared by modifying RM with HCl followed by carbon coating, and sulfonic group functionalization produced an excellent catalytic activity with 93% D-Glucose conversion and 51.5% 5-HMF yield at 180 ^{o}C and 30 min, and DMSO/water weight percentage ratio of 90:10. The catalyst could maintain almost 98.5% of initial D-Glucose conversion and 93.8% of initial 5-HMF yield at the 4th recycle, suggesting its excellent catalytic stability.

The RM-500, RK-30%-800, AS-13-H, and AD-1:1/SO_3H catalysts being developed from an inexpensive and abundant industrial by-product have economic advantages over the other synthetic metal-based catalysts and have equal or higher catalytic efficiency (in some cases) than the other reported synthetic catalysts for the production of GC and 5-HMF. It suggested the potential of these RM-based catalysts for future application in the large-scale synthesis of GC and 5-HMF. The utilization of such a hugely generated waste decreases its adverse environmental effect and helps enable the circular economy.

5.2 Future Scope

The research carried out explored an economical and efficient utilization of waste red mud as catalysts. The research can be further extended in the following mentioned areas.

- Leaching of active components is still an issue for the reported RM-based catalysts, which need further attention to reduce or eliminate them. It would help in enhancing the stability of the catalysts further.

- RM was explored for the GC and 5-HMF synthesis for the first time in this work. Hence, there exists a good opportunity to explore other various active

metal and non-metal elements for doping on the RM surface for the GC and 5-HMF synthesis.

- The developed catalysts could be used for direct conversion of crude glycerol from biodiesel industry and lignocellulosic biomass into glycerol carbonate and 5-hydroxymethylfurfural, respectively.

- A cost-economic analysis will provide an insight into the economic advantages that could be precisely achieved with the RM-based catalysts compared to other synthetic catalysts when considered for a pilot-scale study.

References

[1] J. Áejka, P. Nachtigall, G. Centi, Chem. Soc. Rev. 47 (2018) 8066–8071.

[2] S. Perathoner, S. Gross, E.J.M. Hensen, H. Wessel, H. Chraye, G. Centi, ChemCatChem 9 (2017) 904–909.

[3] International energy outlook 2017. US Energy Information Administration (EIA), (2017).

[4] N. Brun, P. Hesemann, D. Esposito, Chem. Sci. 8 (2017) 4724–4738.

[5] Y. Liao, B.O. de Beeck, K. Thielemans, T. Ennaert, J. Snelders, M. Dusselier, C.M. Courtin, B.F. Sels, Mol. Catal. 487 (2020) 110883.

[6] H. Kobayashi, A. Fukuoka, Green Chem. 15 (2013) 1740–1763.

[7] M.T. Reche, A. Osatiashtiani, L.J. Durndell, M.A. Isaacs, Â. Silva, A.F. Lee, K. Wilson, Catal. Sci. Technol. 6 (2016) 7334–7341.

[8] A. Osatiashtiani, A.F. Lee, D.R. Brown, J.A. Melero, G. Morales, K. Wilson, Catal. Sci. Technol. 4 (2014) 333–342.

[9] X. Qi, H. Guo, L. Li, Ind. Eng. Chem. Res. 50 (2011) 7985–7989.

[10] J.N. Putro, F.E. Soetaredjo, S.Y. Lin, Y.H. Ju, S. Ismadji, RSC Adv. 6 (2016) 46834–46852.

[11] S.G. Wettstein, D. Martin Alonso, E.I. Gürbüz, J.A. Dumesic, Curr. Opin. Chem. Eng. 1 (2012) 218–224.

[12] S. Rezania, B. Oryani, J. Park, B. Hashemi, K.K. Yadav, E.E. Kwon, J. Hur, J. Cho, Energy Convers. Manag. 201 (2019) 112155.

[13] I. Ambat, V. Srivastava, M. Sillanpää, Renew. Sustain. Energy Rev. 90 (2018) 356–369.

[14] W.K. Teng, G.C. Ngoh, R. Yusoff, M.K. Aroua, Energy Convers. Manag. 88 (2014) 484–497.

[15] F. Yang, M.A. Hanna, R. Sun, Biotechnol. Biofuels 5 (2012) 1–10.

[16] C.H. Zhou, J.N. Beltramini, Y.X. Fan, G.Q. Lu, Chem. Soc. Rev. 37 (2008) 527–549.

[17] E. Roduner, Chem. Soc. Rev. 43 (2014) 8226–8239.

[18] S.M. George, Chem. Rev. 95 (1995) 475–476.

[19] J. Liu, ACS Catal. 7 (2017) 34–59.

[20] J.A. Bennett, K. Wilson, A.F. Lee, J. Mater. Chem. A 4 (2016) 3617–3637.

[21] J.S.J. Hargreaves, Catalysis 30 (2018) 1–20.

[22] S. Sushil, V.S. Batra, Appl. Catal. B 81 (2008) 64–77.

[23] S. Samal, A.K. Ray, A. Bandopadhyay, Int. J. Miner. Process. 118 (2013) 43–55.

[24] Z. Liu, H. Li, Hydrometallurgy 155 (2015) 29–43.

[25] M. Pagliaro, R. Ciriminna, H. Kimura, M. Rossi, C. Della Pina, Angew. Chemie - Int. Ed. 46 (2007) 4434–4440.

[26] H.W. Tan, A.R. Abdul Aziz, M.K. Aroua, Renew. Sustain. Energy Rev. 27 (2013) 118–127.

[27] S. Bagheri, N.M. Julkapli, W.A. Yehye, Renew. Sustain. Energy Rev. 41 (2015) 113–127.

[28] E. Tsukuda, S. Sato, R. Takahashi, T. Sodesawa, Catal. Commun. 8 (2007) 1349–1353.

[29] V. Montes, M. Checa, A. Marinas, M. Boutonnet, J.M. Marinas, F.J. Urbano, S. Järas, C. Pinel, Catal. Today 223 (2014) 129–137.

[30] M.H. Haider, C. D'Agostino, N.F. Dummer, M.D. Mantle, L.F. Gladden, D.W. Knight, D.J. Willock, D.J. Morgan, S.H. Taylor, G.J. Hutchings, Chem. - A Eur. J. 20 (2014) 1743–1752.

[31] C. Montassier, J.C. Ménézo, L.C. Hoang, C. Renaud, J. Barbier, J. Mol. Catal. 70 (1991) 99–110.

[32] C. Montassier, J.M. Dumas, P. Granger, J. Barbier, Top. Catal. 121 (1995) 231–244.

[33] M.A. Dasari, P.P. Kiatsimkul, W.R. Sutterlin, G.J. Suppes, Appl. Catal. A Gen. 281 (2005) 225–231.

[34] N.H. Tran, G.S.K. Kannangara, Chem. Soc. Rev. 42 (2013) 9454–9479.

[35] I. Rossetti, A. Gallo, V. DalSanto, C.L. Bianchi, V. Nichele, M. Signoretto, E. Finocchio, G. Ramis, A. Di Michele, ChemCatChem 5 (2013) 294–306.

[36] M. Slinn, K. Kendall, C. Mallon, J. Andrews, Bioresour. Technol. 99 (2008) 5851–5858.

[37] F. Pompeo, G. Santori, N.N. Nichio, Int. J. Hydrogen Energy 35 (2010) 8912–8920.

[38] G.W. Huber, J.W. Shabaker, S.T. Evans, J.A. Dumesic, Appl. Catal. B Environ. 62 (2006) 226–235.

[39] S.A. Tupy, A.M. Karim, C. Bagia, W. Deng, Y. Huang, D.G. Vlachos, J.G. Chen, ACS Catal. 2 (2012) 2290–2296.

[40] S. Christy, A. Noschese, M. Lomelí-Rodriguez, N. Greeves, J.A. Lopez-Sanchez, Curr. Opin. Green Sustain. Chem. 14 (2018) 99–107.

[41] J.R. Ochoa-Gómez, O. Gómez-Jiménez-Aberasturi, C. Ramírez-López, M. Belsué, Org. Process Res. Dev. 16 (2012) 389–399.

[42] A. Dibenedetto, A. Angelini, M. Aresta, J. Ethiraj, C. Fragale, F. Nocito, Tetrahedron 67 (2011) 1308–1313.

[43] M. Aresta, A. Dibenedetto, C. Pastore, A. Angelini, B. Aresta, I. Pápai, J. Catal. 269 (2010) 44–52.

[44] M. Aresta, A. Dibenedetto, C. Pastore, C. Cuocci, B. Aresta, S. Cometa, E. De Giglio, Catal. Today 137 (2008) 125–131.

[45] J. George, Y. Patel, S.M. Pillai, P. Munshi, J. Mol. Catal. A Chem. 304 (2009) 1–7.

[46] C. Vieville, J.W. Yoo, S. Pelet, Z. Mouloungui, Catal. Letters 56 (1998) 245–247.

[47] M. Casiello, A. Monopoli, P. Cotugno, A. Milella, M.M. Dell'Anna, F. Ciminale, A. Nacci, J. Mol. Catal. A Chem. 381 (2014) 99–106.

[48] S. Claude, Z. Mouloungui, J.-W. Yoo, A. Gaset, Method for Preparing Glycerol Carbonate, 2000.

[49] T. Kitsuki, Process for the Preparation of Glycerol Carbonate, 2002.

[50] L. Wang, Y. Ma, Y. Wang, S. Liu, Y. Deng, Catal. Commun. 12 (2011) 1458–1462.

[51] H. Nguyen-Phu, C. yi Park, W.S. Eun, Catal. Commun. 85 (2016) 52–56.

[52] J. Li, T. Wang, Chem. Eng. Process. Process Intensif. 49 (2010) 530–535.

[53] P.U. Okoye, B.H. Hameed, Renew. Sustain. Energy Rev. 53 (2016) 558–574.

[54] C.H. Zhou, J.N. Beltramini, G.Q. Lu, Chem. Soc. Rev. 37 (2008) 527–549.

[55] Z. Bai, Y. Zheng, W. Han, Y. Ji, T. Yan, Y. Tang, G. Chen, Z. Zhang, CrystEngComm 20 (2018) 4090–4098.

[56] Y. Syamsuddin, M.N. Murat, B.H. Hameed, Energy Convers. Manag. 106 (2015) 1356–1361.

[57] P.U. Okoye, A. Longoria, P.J. Sebastian, S. Wang, S. Li, B.H. Hameed, Sci. Total Environ. 719 (2020) 134595.

[58] A.M. Shendurse, C.D. Khedkar, Glucose: Properties and Analysis, 1st ed., Elsevier Ltd., 2015.

[59] Y. Jing, Y. Guo, Q. Xia, X. Liu, Y. Wang, Chem 5 (2019) 2520–2546.

[60] R. Wölfel, N. Taccardi, A. Bösmann, P. Wasserscheid, Green Chem. 13 (2011) 2759–2763.

[61] L. Calvo, D. Vallejo, Ind. Eng. Chem. Res. 41 (2002) 6503–6509.

[62] H. Zhang, N. Toshima, J. Colloid Interface Sci. 394 (2013) 166–176.

[63] A. Mirescu, H. Berndt, A. Martin, U. Prüße, Appl. Catal. A Gen. 317 (2007) 204–209.

[64] E. Sulman, V. Doluda, S. Dzwigaj, E. Marceau, L. Kustov, O. Tkachenko, A. Bykov, V. Matveeva, M. Sulman, N. Lakina, J. Mol. Catal. A Chem. 278 (2007) 112–119.

[65] A. Fukuoka, P.L. Dhepe, Angew. Chemie - Int. Ed. 45 (2006) 5161–5163.

[66] P. Gallezot, P.J. Cerino, B. Blanc, G. Flèche, P. Fuertes, J. Catal. 146 (1994) 93–102.

[67] J. Pang, A. Wang, M. Zheng, Y. Zhang, Y. Huang, X. Chen, T. Zhang, Green Chem. 14 (2012) 614–617.

[68] J. Song, H. Fan, J. Ma, B. Han, Green Chem. 15 (2013) 2619–2635.

[69] U.M. Shapla, N. Alam, I. Khalil, S.H. Gan, Chem. Cent. J. (2018) 1–18.

[70] F. Menegazzo, E. Ghedini, M. Signoretto, Molecules 23 (2018) 1–18.

[71] O.C. Navarro, A.C. Canós, S.I. Chornet, Top. Catal. 52 (2009) 304–314.

[72] J.N. Chheda, G.W. Huber, J.A. Dumesic, Angew. Chemie - Int. Ed. 46 (2007) 7164–7183.

[73] K. Kohli, R. Prajapati, B.K. Sharma, Energies 12 (2019).

[74] A.A. Rosatella, S.P. Simeonov, R.F.M. Frade, C.A.M. Afonso, Green Chem. 13 (2011) 754–793.

[75] D.M. Alonso, J.Q. Bond, J.A. Dumesic, Green Chem. 12 (2010) 1493–1513.

[76] M. Tudorache, L. Protesescu, S. Coman, V.I. Parvulescu, Green Chem. 14 (2012) 478–482.

[77] M. Tudorache, A. Nae, S. Coman, V.I. Parvulescu, RSC Adv. 3 (2013) 4052–4058.

[78] M. Tudorache, A. Negoi, L. Protesescu, V.I. Parvulescu, Appl. Catal. B Environ. 145 (2014) 120–125.

[79] H. Jung, Y. Lee, D. Kim, S.O. Han, S.W. Kim, J. Lee, Y.H. Kim, C. Park, Enzyme Microb. Technol. 51 (2012) 143–147.

[80] R. Sivaramakrishnan, A. Incharoensakdi, Fuel 191 (2017) 363–370.

[81] K.A. Cushing, S.W. Peretti, RSC Adv. 3 (2013) 18596–18604.

[82] Z. Wang, R. Gérardy, G. Gauron, C. Damblon, J.C.M. Monbaliu, React. Chem. Eng. 4 (2019) 17–26.

[83] J.R. Ochoa-Gómez, O. Gómez-Jiménez-Aberasturi, C. Ramírez-López, B. Maestro-Madurga, Green Chem. 14 (2012) 3368–3376.

[84] J.R. Ochoa-Gómez, O. Gómez-Jiménez-Aberasturi, B. Maestro-Madurga, A. Pesquera-Rodríguez, C. Ramírez-López, L. Lorenzo-Ibarreta, J. Torrecilla-Soria, M.C. Villarán-Velasco, Appl. Catal. A Gen. 366 (2009) 315–324.

[85] J. Li, T. Wang, React. Kinet. Mech. Catal. 102 (2011) 113–126.

[86] K. Hu, H. Wang, Y. Liu, C. Yang, J. Ind. Eng. Chem. 28 (2015) 334–343.

[87] Y. Tang, Y.Y. Xue, Z. Li, T. Yan, R. Zhou, Z. Zhang, J. Saudi Chem. Soc. 23 (2019) 494–502.

[88] P. Lu, H. Wang, K. Hu, Chem. Eng. J. 228 (2013) 147–154.

[89] F.S.H. Simanjuntak, S.R. Lim, B.S. Ahn, H.S. Kim, H. Lee, Appl. Catal. A Gen. 484 (2014) 33–38.

[90] Y. Ding, G. Zhang, H. Wu, B. Hai, L. Wang, Y. Qian, Chem. Mater. 13 (2001) 435–440.

[91] C.W. Chang, Z.J. Gong, N.C. Huang, C.Y. Wang, W.Y. Yu, Catal. Today 351 (2020) 21–29.

[92] J.R. Ochoa-Gómez, O. Gómez-Jiménez-Aberasturi, B. Maestro-Madurga, A. Pesquera-Rodríguez, C. Ramírez-López, L. Lorenzo-Ibarreta, J. Torrecilla-Soria, M.C. Villarán-Velasco, Appl. Catal. A Gen. 366 (2009) 315–324.

[93] F.S.H. Simanjuntak, T.K. Kim, S.D. Lee, B.S. Ahn, H.S. Kim, H. Lee, Appl. Catal. A Gen. 401 (2011) 220–225.

[94] W. Roschat, S. Phewphong, T. Kaewpuang, V. Promarak, Mater. Today Proc. 5 (2018) 13909–13915.

[95] M.S. Khayoon, B.H. Hameed, Appl. Catal. A Gen. 466 (2013) 272–281.

[96] Y.T. Algoufi, G. Kabir, B.H. Hameed, J. Taiwan Inst. Chem. Eng. 70 (2017) 179–187.

[97] M. Malyaadri, K. Jagadeeswaraiah, P.S. Sai Prasad, N. Lingaiah, Appl. Catal. A Gen. 401 (2011) 153–157.

[98] M. Marimuthu, P. Marimuthu, A.K. Ashok, S. Palanivelu, V. Rajagopalan, Mol. Catal. 460 (2018) 53–62.

[99] M. Varkolu, D.R. Burri, S.R.R. Kamaraju, S.B. Jonnalagadda, W.E. Van Zyl, J. Porous Mater. 23 (2016) 185–193.

[100] S. Sandesh, G. V. Shanbhag, A.B. Halgeri, Catal. Letters 143 (2013) 1226–1234.

[101] G. Parameswaram, M. Srinivas, B. Hari Babu, P.S. Sai Prasad, N. Lingaiah, Catal. Sci. Technol. 3 (2013) 3242–3249.

[102] X. Song, D. Pan, Y. Wu, P. Cheng, R. Wei, L. Gao, J. Zhang, G. Xiao, J. Alloys Compd. 750 (2018) 828–837.

[103] R. Bai, Y. Wang, S. Wang, F. Mei, T. Li, G. Li, Fuel Process. Technol. 106 (2013) 209–214.

[104] Y. Li, J. Liu, D. He, Appl. Catal. A Gen. 564 (2018) 234–242.

[105] X. Song, Y. Wu, F. Cai, D. Pan, G. Xiao, Appl. Catal. A Gen. 532 (2017) 77–85.

[106] F.S.H. Simanjuntak, V.T. Widyaya, C.S. Kim, B.S. Ahn, Y.J. Kim, H. Lee, Chem. Eng. Sci. 94 (2013) 265–270.

[107] P. Kumar, P. With, V.C. Srivastava, R. Gläser, I.M. Mishra, Ind. Eng. Chem. Res. 54 (2015) 12543–12552.

[108] D. Singh, B. Reddy, A. Ganesh, S. Mahajani, Ind. Eng. Chem. Res. 53 (2014) 18786–18795.

[109] G. Parameswaram, P.S.N. Rao, A. Srivani, G.N. Rao, N. Lingaiah, Mol. Catal. 451 (2018) 135–142.

[110] D. Singh, B. Reddy, A. Ganesh, S. Mahajani, Ind. Eng. Chem. Res. 53 (2014) 18786–18795.

[111] M.G. Álvarez, A.M. Frey, J.H. Bitter, A.M. Segarra, K.P. de Jong, F. Medina, Appl. Catal. B Environ. 134–135 (2013) 231–237.

[112] M.G. Álvarez, M. Plíšková, A.M. Segarra, F. Medina, F. Figueras, Appl. Catal. B Environ. 113–114 (2012) 212–220.

[113] G.D. Yadav, P.A. Chandan, Catal. Today 237 (2014) 47–53.

[114] Z. Liu, J. Wang, M. Kang, N. Yin, X. Wang, Y. Tan, Y. Zhu, J. Ind. Eng. Chem. 21 (2015) 394–399.

[115] P. Liu, M. Derchi, E.J.M. Hensen, Appl. Catal. A Gen. 467 (2013) 124–131.

[116] X. Zhang, D. Wang, J. Ma, W. Wei, Catal. Letters 147 (2017) 1181–1196.

[117] A. Takagaki, K. Iwatani, S. Nishimura, K. Ebitani, Green Chem. 12 (2010) 578–58.

[118] S. Kondawar, C. Rode, Energy and Fuels 31 (2017) 4361–4371.

[119] M.G. Alvarez, A.M. Segarra, S. Contreras, J.E. Sueiras, F. Medina, F. Figueras, Chem. Eng. J. 161 (2010) 340–345.

[120] P. Liu, M. Derchi, E.J.M. Hensen, Appl. Catal. B Environ. 144 (2014) 135–143.

[121] M. Hong, L. Gao, G. Xiao, J. Chem. Res. 38 (2014) 679–681.

[122] Y.T. Algoufi, B.H. Hameed, Fuel Process. Technol. 126 (2014) 5–11.

[123] S. Wang, L. Xu, P.U. Okoye, S. Li, C. Tian, Energy Convers. Manag. 164 (2018) 543–551.

[124] Y. Qing, H. Lu, Y. Liu, C. Liu, B. Liang, W. Jiang, Chinese J. Chem. Eng. 26 (2018) 1912–1919.

[125] B. Hervert, P.D. McCarthy, H. Palencia, Tetrahedron Lett. 55 (2014) 133–136.

[126] S. Wang, P. Hao, S. Li, A. Zhang, Y. Guan, L. Zhang, Appl. Catal. A Gen. 542 (2017) 174–181.

[127] Y. Wan, Y. Lei, G. Lan, D. Liu, G. Li, R. Bai, Appl. Catal. A Gen. 562 (2018) 267–275.

[128] S. Ramesh, F. Devred, L. van den Biggelaar, D.P. Debecker, ChemCatChem 10 (2018) 1398–1405.

[129] S. Ramesh, D.P. Debecker, Catal. Commun. 97 (2017) 102–105.

[130] W.A. Khanday, P.U. Okoye, B.H. Hameed, Energy Convers. Manag. 151 (2017) 472–480.

[131] F.S.H. Simanjuntak, J.S. Choi, G. Lee, H.J. Lee, S.D. Lee, M. Cheong, H.S. Kim, H. Lee, Appl. Catal. B Environ. 165 (2015) 642–650.

[132] P.U. Naik, L. Petitjean, K. Refes, M. Picquet, L. Plasseraud, Adv. Synth. Catal. 351 (2009) 1753–1756.

[133] A.A. Marianou, C.M. Michailof, A. Pineda, E.F. Iliopoulou, K.S. Triantafyllidis, A.A. Lappas, Appl. Catal. A Gen. 555 (2018) 75–87.

[134] K. ichi Shimizu, R. Uozumi, A. Satsuma, Catal. Commun. 10 (2009) 1849–1853.

[135] M. Moreno-Recio, J. Santamaría-González, P. Maireles-Torres, Chem. Eng. J. 303 (2016) 22–30.

[136] V. V. Ordomsky, J. Van Der Schaaf, J.C. Schouten, T.A. Nijhuis, J. Catal. 287 (2012) 68–75.

[137] C. Moreau, R. Durand, S. Razigade, J. Duhamet, P. Faugeras, P. Rivalier, R. Pierre, G. Avignon, Appl. Catal. A Gen. 145 (1996) 211–224.

[138] S. Lima, M.M. Antunes, A. Fernandes, M. Pillinger, M.F. Ribeiro, A.A. Valente, Molecules 15 (2010) 3863–3877.

[139] Y. Shi, X. Li, J. Hu, J. Lu, Y. Ma, Y. Zhang, Y. Tang, J. Mater. Chem. 21 (2011) 16223–16230.

[140] G. Yang, C. Wang, G. Lyu, L.A. Lucia, J. Chen, BioResources 10 (2015) 5863–5875.

[141] L. Li, J. Ding, J.G. Jiang, Z. Zhu, P. Wu, Cuihua Xuebao/Chinese J. Catal. 36 (2015) 820–828.

[142] X. Guo, Q. Cao, Y. Jiang, J. Guan, X. Wang, X. Mu, Carbohydr. Res. 351 (2012) 35–41.

[143] F.S. Asghari, H. Yoshida, Carbohydr. Res. 341 (2006) 2379–2387.

[144] B. Liu, Z. Gou, A. Liu, Z. Zhang, J. Ind. Eng. Chem. 21 (2015) 338–339.

[145] C. Carlini, M. Giuttari, A.M.R. Galletti, G. Sbrana, T. Armaroli, G. Busca, Appl. Catal. A Gen. 183 (1999) 295–302.

[146] A.J. Crisci, M.H. Tucker, J.A. Dumesic, S.L. Scott, Top. Catal. 53 (2010) 1185–1192.

[147] G.C. Behera, K.M. Parida, Catal. Sci. Technol. 3 (2013) 3278–3285.

[148] J. Wang, J. Ren, X. Liu, J. Xi, Q. Xia, Y. Zu, G. Lu, Y. Wang, Green Chem. 14 (2012) 2506–2512.

[149] K.C.W. Wu, RSC Green Chem. 2015-Janua (2015) 1–27.

[150] R. Kourieh, V. Rakic, S. Bennici, A. Auroux, Catal. Commun. 30 (2013) 5–13.

[151] X. Qi, M. Watanabe, T.M. Aida, R.L. Smith, Catal. Commun. 10 (2009) 1771–1775.

[152] X. Li, K. Peng, Q. Xia, X. Liu, Y. Wang, Chem. Eng. J. 332 (2018) 528–536.

[153] Z. Fang, B. Liu, J. Luo, Y. Ren, Z. Zhang, Biomass and Bioenergy 60 (2014) 171–177.

[154] A. Chareonlimkun, V. Champreda, A. Shotipruk, N. Laosiripojana, Bioresour. Technol. 101 (2010) 4179–4186.

[155] P. Carniti, A. Gervasini, S. Biella, A. Auroux, Catal. Today 118 (2006) 373–378.

[156] D. Stošić, S. Bennici, V. Pavlović, V. Rakić, A. Auroux, Mater. Chem. Phys. 146 (2014) 337–345.

[157] D. Stošić, S. Bennici, V. Rakić, A. Auroux, Catal. Today 192 (2012) 160–168.

[158] J.L. Gao, S. Gao, C.L. Liu, Z.T. Liu, W.S. Dong, Mater. Res. Bull. 59 (2014) 131–136.

[159] I. Jiménez-Morales, J. Santamaría-González, A. Jiménez-López, P. Maireles-Torres, Fuel 118 (2014) 265–271.

[160] T. Armaroli, G. Busca, C. Carlini, M. Giuttari, A.M. Raspolli Galletti, G. Sbrana, J. Mol. Catal. A Chem. 151 (2000) 233–243.

[161] G. Sampath, S. Kannan, Catal. Commun. 37 (2013) 41–44.

[162] J.N. Chheda, J.A. Dumesic, Catal. Today 123 (2007) 59–70.

[163] L. Rigal, J.P. Gorrichon, A. Gaset, J.C. Heughebaert, Biomass 7 (1985) 27–45.

[164] G.A. Halliday, R.J. Young, V. V. Grushin, Org. Lett. 5 (2003) 2003–2005.

[165] J.M.R. Gallo, D.M. Alonso, M.A. Mellmer, J.A. Dumesic, Green Chem. 15 (2013) 85–90.

[166] A. Takagaki, M. Ohara, S. Nishimura, K. Ebitani, Chem. Commun. (2009) 6276–6278.

[167] X. Qi, M. Watanabe, T.M. Aida, R.L. Smith, Green Chem. 11 (2009) 1327–1331.

[168] Z. Qiao, Z. Wang, C. Zhang, S. Yuan, Y. Zhu, J. Wang, AIChE J. 59 (2012) 215–228.

[169] R. Liu, J. Chen, X. Huang, L. Chen, L. Ma, X. Li, Green Chem. 15 (2013) 2895–2903.

[170] B. Kim, C.A. Antonyraj, Y.J. Kim, B. Kim, S. Shin, S. Kim, K.Y. Lee, J.K. Cho, Ind. Eng. Chem. Res. 53 (2014) 4633–4641.

[171] J. Li, Y. Wang, B. Lu, Y. Wang, T. Deng, X. Hou, Appl. Catal. A Gen. 566 (2018) 140–145.

[172] K. Li, J. Chen, Y. Yan, Y. Min, H. Li, F. Xi, J. Liu, P. Chen, Carbon N. Y. 136 (2018) 224–233.

[173] Y. Zhang, J. Wang, J. Wang, Y. Wang, M. Wang, H. Cui, F. Song, X. Sun, Y. Xie, W. Yi, ChemistrySelect 4 (2019) 5724–5731.

[174] L. Yan, N. Liu, Y. Wang, H. Machida, X. Qi, Bioresour. Technol. 173 (2014) 462–466.

[175] L. Jiao, S. Sun, X. Meng, P. Ji, Catalysts 9 (2019).

[176] F. Huang, W. Li, Q. Liu, T. Zhang, S. An, D. Li, X. Zhu, Fuel Process. Technol. 181 (2018) 294–303.

[177] Y. Zhang, V. Degirmenci, C. Li, E.J.M. Hensen, ChemSusChem 4 (2011) 59–64.

[178] A.H. Jadhav, H. Kim, I.T. Hwang, Bioresour. Technol. 132 (2013) 342–350.

[179] Y. Song, X. Wang, Y. Qu, C. Huang, Y. Li, B. Chen, Catalysts 6 (2016).

[180] J.D. Moseley, C.O. Kappe, Green Chem. 13 (2011) 794–806.

[181] J. Sun, X. Yuan, Y. Shen, Y. Yi, B. Wang, F. Xu, R. Sun, Ind. Crops Prod. 70 (2015) 266–271.

[182] B. Liu, Z. Zhang, Z.K. Zhao, Chem. Eng. J. 215–216 (2013) 517–521.

[183] Q. Hou, M. Zhen, L. Liu, Y. Chen, F. Huang, S. Zhang, W. Li, M. Ju, Appl. Catal. B Environ. 224 (2018) 183–193.

[184] C. Antonetti, M. Melloni, D. Licursi, S. Fulignati, E. Ribechini, S. Rivas, J.C.

Parajó, F. Cavani, A.M. Raspolli Galletti, Appl. Catal. B Environ. 206 (2017) 364–377.

[185] C. Antonetti, A.M. Raspolli Galletti, S. Fulignati, D. Licursi, Catal. Commun. 97 (2017) 146–150.

[186] Z. Zhang, Z.K. Zhao, Bioresour. Technol. 101 (2010) 1111–1114.

[187] P. Wrigstedt, J. Keskiväli, T. Repo, RSC Adv. 6 (2016) 18973–18979.

[188] J. Wang, T. Qu, M. Liang, Z. Zhao, RSC Adv. 5 (2015) 106053–106060.

[189] T. Ji, R. Tu, L. Mu, X. Lu, J. Zhu, ACS Sustain. Chem. Eng. 5 (2017) 4352–4358.

[190] X. Qi, M. Watanabe, T.M. Aida, R.L. Smith, Catal. Commun. 9 (2008) 2244–2249.

[191] B. Klopries, W. Hodek, F. Bandermann, Fuel 69 (1990) 448–455.

[192] J.R. Mitra, P.B. Chowdhury, D.K. Mukherjee, Fuel Process. Technol. 8 (1984) 283–291.

[193] B.K. Yathavan, F.A. Agblevor, Energy and Fuels 27 (2013) 6858–6865.

[194] A. López, I. de Marco, B.M. Caballero, M.F. Laresgoiti, A. Adrados, A. Aranzabal, Appl. Catal. B Environ. 104 (2011) 211–219.

[195] A. Castille, C. Bessette, F. Thomas, M. Etemad, Catal. Commun. 121 (2019) 5–10.

[196] H. Jahromi, F.A. Agblevor, Ind. Eng. Chem. Res. 57 (2018) 13257–13268.

[197] J. Weber, A. Thompson, J. Wilmoth, R.J. Gulotty, J.R. Kastner, Energy and Fuels 31 (2017) 9529–9541.

[198] H. Jahromi, F.A. Agblevor, Appl. Catal. B Environ. 236 (2018) 1–12.

[199] S.F. Kurtoğlu, S. Soyer-Uzun, A. Uzun, Int. J. Hydrogen Energy 43 (2018) 20525–20537.

[200] S. Uemiya, M. Uchida, H. Moritomi, Mater. Trans. 46 (2005) 2709–2712.

[201] J.L. Cao, Z.L. Yan, Q.F. Deng, Y. Wang, Z.Y. Yuan, G. Sun, T.K. Jia, X.D. Wang, H. Bala, Z.Y. Zhang, Int. J. Hydrogen Energy 39 (2014) 5747–5755.

[202] S.F. Kurtoglu, A. Uzun, Sci. Rep. 6 (2016) 1–8.

[203] F.N. Pei, L. Li, S. Wang, Z. Zhu, G. Lu, Z. Yan, Environ. Sci. Technol. 41 (2007) 3758–3762.

[204] X. Fang, Q. Liu, P. Li, H. Li, F. Li, G. Huang, J. Nanomater. 2016 (2016).

[205] M. Balakrishnan, V.S. Batra, J.S.J. Hargreaves, A. Monaghan, I.D. Pulford, J.L. Rico, S. Sushil, Green Chem. 11 (2009) 42–47.

[206] Q. Liu, R. Xin, C. Li, C. Xu, J. Yang, J. Environ. Sci. (China) 25 (2013) 823–829.

[207] L.Y. Zhang, Y.Z. Wang, G.T. Wei, Z.Y. Li, H.N. Huang, Energy Sources, Part A Recover. Util. Environ. Eff. 38 (2016) 1713–1720.

[208] A. Wahyudi, W. Kurniawan, H. Hinode, J. Chem. Eng. Japan 50 (2017) 561–567.

[209] L.J. Konwar, P. Mäki-Arvela, J.P. Mikkola, Chem. Rev. 119 (2019) 11576–11630.

[210] M.K. Sahu, R.K. Patel, J. Ind. Eng. Chem. 40 (2016) 72–82.

[211] S.S. Prajapati, P.A.M. Najar, V.M. Tangde, Adv. Phys. Chem. 2016 (2016).

[212] R.S. K. H. Jost, B. Ziemer, Acta Crystallogr. 33 (1977) 1696–1700.

[213] J. Glinnemann, H.E. King Jr., H. Schulz, T. Hahn, S.J. La Placa, F. Dacol, Z. Krist. 198 (1992) 177–212.

[214] L.M. Foster, G. V. Chandrashekhar, J.E. Scardefield, R.B. Bradford, J. Am. Ceram. Soc. 63 (1980) 509–512.

[215] Z.P. Hu, Z.M. Gao, X. Liu, Z.Y. Yuan, Adsorpt. Sci. Technol. 36 (2018) 62–79.

[216] P.U. Okoye, A.Z. Abdullah, B.H. Hameed, Energy Convers. Manag. 133 (2017) 477–485.

[217] J. Duchesne, E.J. Reardon, Cem. Concr. Res. 25 (1995) 1043–1053.

[218] M.S. Khayoon, B.H. Hameed, Appl. Catal. A Gen. 466 (2013) 272–281.

[219] J. Hua Zhu, Y. Chun, Y. Qin, Q.H. Xu, Microporous Mesoporous Mater. 24 (1998) 19–28.

[220] K. Hu, H. Wang, Y. Liu, C. Yang, J. Ind. Eng. Chem. 28 (2015) 334–343.

[221] W.K. Teng, G.C. Ngoh, R. Yusoff, M.K. Aroua, Energy Convers. Manag. 88 (2014) 484–497.

[222] G. Parameswaram, M. Srinivas, B. Hari Babu, P.S. Sai Prasad, N. Lingaiah, Catal. Sci. Technol. 3 (2013) 3242.

[223] G. Chen, B. Zhang, J. Zhao, Materials (Basel). 8 (2015) 2346–2360.

[224] M. Malyaadri, K. Jagadeeswaraiah, P.S. Sai Prasad, N. Lingaiah, Appl. Catal. A Gen. 401 (2011) 153–157.

[225] P. Liu, M. Derchi, E.J.M. Hensen, Appl. Catal. A Gen. 467 (2013) 124–131.

[226] P. Touzain, F. Brisse, M. Caillet, Can. J. Chem. 48 (1970) 3358–3361.

[227] T. Ito, R. Sadanaga, Acta Crystallogr. 5 (1952) 441–449.

[228] J.K. Nimmo, B.W. Lucas, Acta Crystallogr. Sect. B Struct. Crystallogr. Cryst. Chem. 32 (1976) 1968–1971.

[229] P. Körner, S. Beil, A. Kruse, React. Chem. Eng. 4 (2019) 747–762.

[230] M. Lopes, K. Dussan, J.J. Leahy, V.T. da Silva, Catal. Today 279 (2017) 233–243.

[231] Y. Du, S. Liu, Y. Zhang, C. Yin, Y. Di, F.S. Xiao, Catal. Letters 108 (2006) 155–158.

[232] P.C. Christidis, P.J. Rentzeperis, Zeitschrift Fur Krist. - New Cryst. Struct. 144 (1976) 341–352.

[233] D. Zhai, Y. Nie, Y. Yue, H. He, W. Hua, Z. Gao, Catal. Commun. 12 (2011) 593–596.

[234] B.M. Reddy, P.M. Sreekanth, Y. Yamada, Q. Xu, T. Kobayashi, Appl. Catal. A Gen. 228 (2002) 269–278.

[235] F. Davar, M. Salavati-Niasari, Z. Fereshteh, J. Alloys Compd. 496 (2010) 638–643.

[236] X. Cui, H. Ma, B. Wang, H. Chen, J. Hazard. Mater. 147 (2007) 800–805.

[237] H. Ma, K. Teng, Y. Fu, Y. Song, Y. Wang, X. Dong, Energy Environ. Sci. 4 (2011) 3067–3073.

[238] M. Descostes, F. Mercier, N. Thromat, C. Beaucaire, M. Gautier-Soyer, Appl. Surf. Sci. 165 (2000) 288–302.

[239] C. Li, H. Zeng, P. Liu, J. Yu, F. Guo, G. Xu, Z.G. Zhang, RSC Adv. 7 (2017) 53622–53630.

[240] B. Wu, Y. Xiong, Y. Ge, Chem. Eng. J. 331 (2018) 343–354.

[241] L. Ma, J. Li, R. Ke, L. Fu, J. Phys. Chem. C 115 (2011) 7603–7612.

[242] E. Díaz, S. Ordóñez, A. Vega, J. Coca, Microporous Mesoporous Mater. 83 (2005) 292–300.

[243] B. Mallesham, P. Sudarsanam, B.M. Reddy, Catal. Sci. Technol. 4 (2014) 803–813.

[244] J. Liu, H. Li, Y.C. Liu, Y.M. Lu, J. He, X.F. Liu, Z.B. Wu, S. Yang, Catal. Commun. 62 (2015) 19–23.

[245] S. Jia, Z. Xu, Z.C. Zhang, Chem. Eng. J. 254 (2014) 333–339.

[246] S. De, S. Dutta, B. Saha, Green Chem. 13 (2011) 2859–2868.

[247] J. Lu, Y. Yan, Y. Zhang, Y. Tang, RSC Adv. 2 (2012) 7652–7655.

[248] J. Zhao, C. Zhou, C. He, Y. Dai, X. Jia, Y. Yang, Catal. Today 264 (2016) 123–130.

[249] K.K. Dae-Weon Kim, Naoya Enomoto, Zenbe-e Nakagawa, J. Am. Ceram. Soc. 79 (1996) 1095–1099.

[250] F.D. J. Glinnemann, H. E. King Jr, H. Schulz, Th. Hahn, S. J. La Placa, Zeitschrift Für Krist. - Cryst. Mater. 198 (1992) 177–212.

[251] P.J. Rentzeperis, P.C. Christidis, Zeitschrift Für Krist. - Cryst. Mater. 144 (1976) 341–352.

[252] D. Yamaguchi, K. Watanabe, S. Fukumi, Sci. Rep. 6 (2016) 1–7.

[253] S. Ganesan, S. Nadarajah, M. Khairuddean, G.B. Teh, Renew. Energy 140 (2019) 9–16.

[254] D.R. Milburn, R.A. Keogh, D.E. Sparks, B.H. Davis, Appl. Surf. Sci. 126 (1998) 11–15.

[255] P.P. Upare, J.W. Yoon, M.Y. Kim, H.Y. Kang, D.W. Hwang, Y.K. Hwang, H.H. Kung, J.S. Chang, Green Chem. 15 (2013) 2935–2943.

[256] X. Wang, T. Lv, M. Wu, J. Sui, Q. Liu, H. Liu, J. Huang, L. Jia, Appl. Catal. A Gen. 574 (2019) 87–96.

[257] R.J.J. Ganado, D.E.C. Yu, F.C. Franco, Ind. Eng. Chem. Res. 58 (2019) 14621–14631.

List of Publications

Peer Reviewed Journals

- **B. Das**, K. Mohanty, A green and facile production of catalysts from waste red mud for the one-pot synthesis of glycerol carbonate from glycerol, **J. Environ. Chem. Eng**. 7, **2019**, 102888.
- **B. Das**, K. Mohanty, Exploring the Promotional Effects of K, Sr, and Mg on the Catalytic Stability of Red Mud for the Synthesis of Glycerol Carbonate from Renewable Glycerol, **Ind. Eng. Chem. Res**., 58, **2019**, 15803-15817.
- **B Das**, K Mohanty, A review on advances in sustainable energy production through various catalytic processes by using catalysts derived from waste red mud, **Renewable Energy** 143, **2019**, 1791-1811.
- **B. Das**, K. Mohanty, Microwave induced one-pot conversion of D-glucose to 5-hydroxymethylfurfural by a novel sulfate-functionalized Sn-red mud catalyst, **Sustainable Energy & Fuels**, 4, **2020**, 6030-6044.
  (**2020 Hot Article under themed collection**, https://pubs.rsc.org/en/journals/articlecollectionlanding?sercode=se&themeid=41ef7639-feef-4960-957e-0c985811fb9e)
- **B. Das**, K. Mohanty, Sulfonic acid-functionalized carbon coated red mud as an efficient catalyst for the direct production of 5-HMF from D-glucose under microwave irradiation. **Applied Catalysis A: General**, 622, **2021**, 118237**.**

Book Chapters

- **B Das**, K Mohanty, Progress on red mud-based catalysts for the removal of environmental pollutants through oxidation and advanced oxidation process, **Sustainable Green Chemical Processes and their Allied Applications**, (Eds: Inamuddin and A. Asiri) 2020, Page: 461-480, Springer.

International Conferences

- **B. Das**, K. Mohanty, Modified Red Mud as an Efficient Catalyst for the Synthesis of Glycerol Carbonate by the Transesterification of Glycerol, **UK Catalysis Conference 2020 (UKCC 2020**), **January 7-9, 2020,** Holywell Park, Loughborough, UK.

National Conferences

- **B. Das**, K. Mohanty, Microwave assisted efficient conversion of glucose to 5-HMF in a low-cost catalytic system, **International Conference on Advances in Chemical Engineering-2020 (AdChE-2020), February 5-7, 2020,** UPES, Dehradun, India.

Journal of Environmental Chemical Engineering 7 (2019) 102888

Contents lists available at ScienceDirect

Journal of Environmental Chemical Engineering

journal homepage: www.elsevier.com/locate/jece

A green and facile production of catalysts from waste red mud for the one-pot synthesis of glycerol carbonate from glycerol

Bikashbindu Das, Kaustubha Mohanty*

Department of Chemical Engineering, Indian Institute of Technology Guwahati, Guwahati, 781039, India

ARTICLE INFO

Keywords:
Glycerol
Glycerol carbonate
Cost-efficient catalyst
Transesterification
Reaction kinetics

ABSTRACT

In this study, waste red mud (RM) from aluminum industry was calcined at different temperatures between 400 °C–800 °C and was applied as catalysts for the efficient production of glycerol carbonate (GC) through transesterification of glycerol (GL) with dimethyl carbonate (DMC). No chemical pretreatments or incorporation of any other foreign active components into the surface of RM was performed before its application as a catalyst. XRD and FTIR analysis revealed that RM calcined at 500 °C (RM-500) possessed the maximum concentration of active $NaAlO_2$ and Ca_2SiO_4 sites, thus produced the highest catalytic activity (92.02% GC yield). At calcination temperature above 500 °C, hematite became the dominant phase and the concentration of $NaAlO_2$ and Ca_2SiO_4 decreased, which also decreased the catalytic activity. The RM-500 catalyst showed excellent resistant for the transesterification of GL in the presence of initial impurities like water and methanol. Based on the results of different characterization techniques, a plausible reaction mechanism and the deactivation mechanism was proposed. Further, the kinetic analysis and reusability study was also studied in details.

1. Introduction

Dwindling supply of fossil fuels and increasing concern about environmental pollution associated with the use of fossil fuels has generated interest among researchers to look for renewable energy sources. Renewable energy sources such as solar, wind, hydroelectric, geothermal and biomass can act as alternative sources of fuel to the conventional petroleum-based fuels. The production of biodiesel from different kinds of biomass through the transesterification route generates glycerol as a by-product, which is about 10 wt% of the total transesterification product yield [1]. With the increasing demand for biodiesel production, it is estimated that by 2020, the amount of glycerol production will overpass the actual demand by at least six times [2]. Thus, researchers are more interested now-a-days to convert GL to some useful products so that the overall economics of the transesterification process becomes sustainable. Glycerol, because of its good stability, non-toxic nature, and hydrophilic properties can be utilized as a starting material for the production of different value-added chemicals through different catalytic processes [3]. Glycerol carbonate (GC) is such an important product from glycerol, which has many applications such as adhesives, paint, surfactants, lubricants, cement composite aggregates, plant bolster, monomer for the production of different biodegradable polymers and electrolyte for lithium-ion batteries [4,5]. Moreover, GC because of its certain properties such as non-toxic nature, water solubility, high boiling point, non-flammability and high biodegradability nature is considered as a green chemical for different industrial processes [6,7].

A variety of reaction routes for the production of GC from GL have been established till now such as; (i) reaction of GL with urea, (ii) carbonation of GL with phosgene, (iii) reaction of GL with CO_2 and (iv) transesterification of GL with organic carbonates. Among these different routes, transesterification of GL by using dimethyl carbonate (DMC) is considered as a prominent method for the synthesis of GC because of the involvement of non-toxic raw materials and requirement of mild operating conditions [8]. Other processes for GC synthesis have their own disadvantages such as, requirement of toxic phosgene for the route of carbonation of GL [9]. Low yield and the difficulty to activate CO_2 during the reaction of GL with CO_2 [10], and requirement of vacuum condition for the separation of ammonia produced as a by-product in the case of reaction with urea [11] hinders the efficiency of the process. The reaction of GL with ethylene carbonate produces ethylene glycol as a by-product. The high energy require to separate the high boiling point ethylene carbonate (BP 261 °C) and the by-product ethylene glycol (BP 197 °C) inhibits it's application for the GC synthesis [7].

Development of catalysts from waste materials has obtained significant attention in recent past in order to improve the energy

* Corresponding author.
E-mail address: kmohanty@iitg.ac.in (K. Mohanty).

https://doi.org/10.1016/j.jece.2019.102888
Received 29 September 2018; Received in revised form 17 December 2018; Accepted 3 January 2019
Available online 03 January 2019

I&EC research
Industrial & Engineering Chemistry Research

Article

Cite This: Ind. Eng. Chem. Res. 2019, 58, 15803−15817

pubs.acs.org/IECR

Exploring the Promotional Effects of K, Sr, and Mg on the Catalytic Stability of Red Mud for the Synthesis of Glycerol Carbonate from Renewable Glycerol

Bikashbindu Das and Kaustubha Mohanty*

Department of Chemical Engineering, Indian Institute of Technology Guwahati, Guwahati 781039, India

Supporting Information

ABSTRACT: The focus of this study was to utilize red mud (RM), an aluminum industry waste, for the preparation of various catalysts for the synthesis of glycerol carbonate (GC) from glycerol (GL). A series of catalysts were prepared by doping potassium, strontium, and magnesium on the surface of RM, and their effect on the stability of RM based catalysts was examined. From preliminary studies, K-doped RM catalysts were found to have better activity as well as stability than the Sr- and Mg-doped RM catalysts for the transesterification of GL. The RK-30%-800 catalyst prepared by 30% K loading and calcination at 800 °C produced the highest activity and stability compared to other K-doped catalysts. The better activity of the RK-30% catalyst was due to the presence of the maximum surface concentration of active K_2O, which was confirmed from the XRD analysis. The surface concentration of K_2O contributed significantly to the increased basic properties of the catalyst, which was quite evident from the acid−base titration, CO_2-temperature programmed desorption (CO_2-TPD), and Hammett indicator test. A probable mechanism of the GL transesterification process by using the RK-30%-800 catalyst was proposed. Moreover, effect of the presence of impurities on the catalytic activity, the reaction kinetics, reusability study, and deactivation mechanism were studied in detail here.

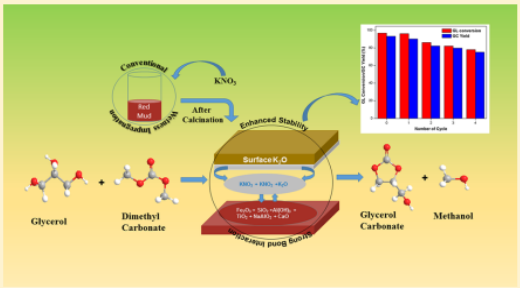

1. INTRODUCTION

Increasing global warming due to the release of greenhouse gases such as CO_2, NO, N_2O, and CH_4 from the combustion of fossil fuel has been a matter of concern for the entire scientific community. In the past few decades, significant contributions have been made to overcome the drawbacks and scarcity of conventional fossil fuels by finding various renewable energy sources. Renewable energy from various bioresources has excellent potential to reduce the adverse climatic effect and to provide energy security for the next generation. Biodiesel, a transesterification product of vegetable oil and methanol is considered as an alternative source of energy to conventional fossil fuel.[1] However, the process of biodiesel production involves the formation of glycerol (GL) as a byproduct.[2] The growing biodiesel production has generated a surplus amount of GL in the recent past, thereby demanding its effective utilization for the sustainability of biodiesel industries in the future. Tremendous efforts have been made to convert GL into value-added chemicals through processes such as selective oxidation, dehydration, hydrogenation, etherification, and transesterification.[2]

The bioroute synthesis with versatile reactivity has proven GL to be a green raw material for production of a variety of chemicals. Moreover, the presence of two primary and one secondary hydroxyl groups in GL creates the possibilities of producing several derivatives of the material through more than the usual number of reactions. The transesterification of GL with alkyl carbonates produces glycerol carbonate (GC), which is used for the production of lubricants, adhesives, and surfactants and as monomers for biodegradable polymer synthesis.[3,4] GC due to its water solubility, low flammability, low toxicity, and moisturizing nature is considered as a demanding chemical for cosmetics production and as a carrier solvent for medical preparation as well.[4] The process of GL transesterification with dimethyl carbonate (DMC) is considered as a green process for the production of GC due to the involvement of nontoxic chemicals and mild operating conditions.[5,6] Direct catalytic conversion of GL to GC through reaction with urea is also possible. However, it requires a vacuum condition for removing the ammonia produced during the reaction to accelerate the reaction toward the desired direction.[7] Alternatively, the reaction of GL with CO_2 for synthesizing GC is associated with disadvantages such as high reaction temperature, high pressure, and low yield. Similarly, the toxic nature of phosgene and CO limits its application for

Special Issue: Biorenewable Energy and Chemicals

Received: January 23, 2019
Revised: April 3, 2019
Accepted: April 4, 2019
Published: April 4, 2019

DOI: 10.1021/acs.iecr.9b00420
Ind. Eng. Chem. Res. 2019, 58, 15803−15817

Renewable Energy 143 (2019) 1791–1811

Contents lists available at ScienceDirect

Renewable Energy

journal homepage: www.elsevier.com/locate/renene

Review

A review on advances in sustainable energy production through various catalytic processes by using catalysts derived from waste red mud

Bikashbindu Das, Kaustubha Mohanty*

Department of Chemical Engineering, Indian Institute of Technology Guwahati, Guwahati 781039, India

ARTICLE INFO

Article history:
Received 16 February 2019
Received in revised form
11 May 2019
Accepted 28 May 2019
Available online 31 May 2019

Keywords:
Red mud
Waste utilization
Catalyst
Sustainable energy
Iron oxide

ABSTRACT

Conversion of wastes to energy and other value-added products is considered as a suitable method towards energy security. Wastes from various sources are becoming potential feedstocks for energy production through different techniques. The economy and sustainability of these processes demand the use of low-cost catalysts. Red mud (RM) is one of the most abundantly produced industrial wastes from aluminum industries. Such a huge production of RM, its alkaline nature and the presence of a small quantity of radioactive elements make it an environmental liability. Out of various utilization methods, RM as a catalyst for different chemical processes has been very successful. Presence of many valuable metals in RM, in particular, Fe makes it a suitable catalyst for energy production through processes such as pyrolysis, hydrotreating, transesterification and H_2 production from biomass and other sources. This article critically reviews the advances in sustainable energy production through different processes mentioned above by RM based catalysts. Different characterization, activation and stability study of RM along with outcomes and mechanism of these processes are discussed. Furthermore, drawbacks associated with the low catalytic activity of RM and works that need to be carried out in the future for the improvement of its catalytic activity are discussed in detail.

Contents

* Corresponding author.
E-mail address: kmohanty@iitg.ac.in (K. Mohanty).

https://doi.org/10.1016/j.renene.2019.05.114
0960-1481/

Sustainable Energy & Fuels

ROYAL SOCIETY OF CHEMISTRY

PAPER

View Article Online
View Journal

Cite this: DOI: 10.1039/d0se01476a

Microwave induced one-pot conversion of D-glucose to 5-hydroxymethylfurfural by a novel sulfate-functionalized Sn-red mud catalyst†

Bikashbindu Das and Kaustubha Mohanty *

The aqueous phase conversion of D-glucose to 5-hydroxymethylfurfural (5-HMF) under microwave irradiation using a red mud (RM) based catalyst modified with Sn and H_2SO_4 is reported. Acid (HCl)-treated RM (ARM) exhibited a surface area almost 8.4 times higher than that of RM. The AS-*x*-H catalyst obtained by doping of Sn followed by functionalization of sulfate groups on ARM showed improved Lewis and Bronsted acid characteristics. The catalyst was predominantly composed of SO_4^{2-}/Fe_2O_3–SnO_2 and $Fe_2(SO_4)_3$ as suggested by XRD analysis and well supported by XPS analysis. Other characterization techniques such as FESEM, FESEM-EDX, FTIR, ATR-FTIR, BET and NH_3-TPD were performed for a detailed understanding of the physicochemical properties of the prepared catalysts. AS-13-H produced a 5-HMF yield of 26.22% at 180 °C and 5 min from D-glucose with water as the solvent. In the presence of a solvent consisting of dimethyl sulfoxide (DMSO) and water in a weight ratio of 1 : 1, the 5-HMF yield improved to 53.8%. The synergistic interaction of Sn (13 wt%) with the components of ARM improved the catalytic stability due to which a satisfactory 5-HMF yield was found up to the fourth use. The characteristics of the spent catalyst were studied by FTIR and FESEM-EDX analysis and discussed in detail.

Received 2nd October 2020
Accepted 20th October 2020

DOI: 10.1039/d0se01476a

rsc.li/sustainable-energy

1. Introduction

In the past few decades, lignocellulosic biomass has emerged as a promising alternative to dwindling fossil fuels for fulfilling the rapid rise in worldwide energy demand.[1,2] One important platform chemical derived from cellulosic biomass is 5-hydroxymethylfurfural (5-HMF) which contains multiple functional groups such as hydroxyl, furan, and methyl groups.[3,4] These functional groups make 5-HMF an excellent raw material for the synthesis of chemicals that have wide application in pharmaceuticals, polymers, solvents, and biofuels.[5–7] Other derivatives of 5-HMF, such as 2,5-dimethylfuran, and 2,5-furandicarboxylic acid are also considered as high-value fuel additives.[8] For the synthesis of 5-HMF, various C6 sugar compounds such as glucose and fructose (FCT) have been reported so far.[8,9] It is found that fructose can produce a significant yield of 5-HMF in the presence of a suitable dehydration catalyst such as zeolite or other mineral acids.[9] However, the high cost of fructose, when considered for large-scale production, is regarded as a drawback that hinders its direct use for 5-HMF synthesis.[10] In contrast, glucose due to its low cost and abundancy could be considered as a suitable raw material for 5-HMF synthesis.[11] The production of 5-HMF from glucose involves the pathway of isomerization to fructose that undergoes further dehydration to 5-HMF (Scheme 1). For this, a catalytic system consisting of Lewis acid sites for isomerizing glucose to fructose and Bronsted acid sites for the dehydration of fructose to 5-HMF is desired.

Varieties of catalytic systems have been reported for 5-HMF synthesis in the recent past. The focus has always been on developing low-cost green catalysts that could efficiently produce 5-HMF from various resources with a considerable yield and selectivity. Few homogeneous catalysts such as H_2SO_4 and HCl with a solvent like ionic liquid have been reported.[12] However, homogeneous acidic catalytic systems have disadvantages of reactor corrosion and difficulty in catalyst separation. On the other hand, the use of heterogeneous catalysts could be considered as a suitable alternative for solving the issues of homogeneous catalytic systems. Solid acid catalysts such as zeolite, mesoporous silica, Sn-Mont, phosphates/sulfates of Zr, Cu, Nb, and Ti, and other carbon-based catalysts have been found to produce suitable results for 5-HMF synthesis.[13–19]

Achieving a suitable yield of 5-HMF directly from cellulose or glucose is a challenging task. The catalyst that is efficient for converting fructose to high yield 5-HMF is not that effective when cellulose or glucose is used as the raw material. For example, by using a sulfated zirconium oxide catalyst with ionic liquid as the solvent, 88.4% 5-HMF yield was obtained from

Department of Chemical Engineering, Indian Institute of Technology Guwahati, Guwahati-781039, India. E-mail: kmohanty@iitg.ac.in; Tel: +91-361-2582267

† Electronic supplementary information (ESI) available. See DOI: 10.1039/d0se01476a

Applied Catalysis A, General 622 (2021) 118237

Contents lists available at ScienceDirect

Applied Catalysis A, General

journal homepage: www.elsevier.com/locate/apcata

Sulfonic acid-functionalized carbon coated red mud as an efficient catalyst for the direct production of 5-HMF from D-glucose under microwave irradiation

Bikashbindu Das, Kaustubha Mohanty *

Department of Chemical Engineering, Indian Institute of Technology Guwahati, Guwahati, 781039, India

ARTICLE INFO

Keywords:
Red mud
Sulfonated catalyst
5 HMF
Microwave
D-glucose
Industry waste

ABSTRACT

Though suitable for the fructose conversion to 5-hydroxymethylfurfural (5-HMF), sulfonated carbon catalysts are inefficient for the direct glucose transformation to 5-HMF due to the lack of appropriate Lewis acids. Here, we have reported an efficient and inexpensive catalyst by suitably modifying red mud (RM), a by-product from the aluminum industry. The AD-1:1/SO_3H catalyst produced by the acid (HCl) treatment, carbon coating, and SO_3H grafting on RM exhibited enhanced surface area, mesoporous characteristics, and suitable Lewis and Bronsted acid sites. The XRD, FTIR, and XPS analysis suggested $Fe_2(SO_4)_3$, Fe_2O_3, and various carbon functionalities as the major active components in the AD-1:1/SO_3H catalyst. The NH_3-TPD analysis revealed an appreciable acid site density of 6.8 mmol g^{-1}. Under microwave heating at 180 °C, 30 min, and 90:10 DMSO/water weight percentage ratio, the catalyst produced a D-glucose conversion and 5-HMF yield of 93.05 % and 51.5 %, respectively.

1. Introduction

The growing demand for energy and chemicals with the depleting fossil resources has thrown a significant challenge for sustainable alternative development. Concerning this, lignocellulosic biomass has emerged as a potential substitute for delivering alternative fuels as well as other platform chemicals [1–3]. The US department of energy (DOE) has categorized 5-HMF under the top ten biomass-derived promising platform compounds for fuel and fine chemical applications [4]. The hydroxyl, furan, and methyl functional groups of 5-HMF make it suitable for the synthesis of multiple derivatives of it with applications in fuel, polymers, and other important chemicals. For instance, 2,5-dimethylfuran, the hydrogenation product, and 2,5-furandicarboxylic acid, the oxidation product of 5-HMF, are used as fuel and in the production of polymers, respectively [5,6]. Another important derivative is lactic acid, with substantial application in food, pharmaceutical, and polymer industries [7]. 5-HMF can be produced from different monomer sugars such as glucose and fructose with a higher yield from the latter one but less economically due to its higher cost. Contrarily, the low cost and easy availability of glucose make it a suitable starting material for the production of 5-HMF [8].

The high 5-HMF yield from fructose is facilitated by the thermodynamically favorable protonation of the C-2-OH group, resulting in a stabilized furan ring and accelerated dehydration reaction [8]. However, for glucose, the above pathway is thermodynamically less favorable. The 5-HMF synthesis from glucose is reported to occur by the isomerization to fructose first, preferably by a Lewis acid. The fructose is then dehydrated to 5-HMF by a Bronsted acid [8,9]. Various catalysts with suitable Lewis and Bronsted acidic characteristics both in homogeneous and heterogeneous forms have been tested for the 5-HMF synthesis from sugars [10–16]. Drawbacks such as separation difficulty, reactor corrosion, and in some cases, the high cost of homogeneous catalysts hinder their commercialization. Heterogeneous catalytic systems could avoid the above drawbacks, due to which they are the focus of current catalysis research. TiO_2 and ZrO_2 as bifunctional catalysts with acid-base properties have been used for promoting the 5-HMF synthesis from glucose [10]. Other bifunctional catalysts such as 2SZ@SBA-15-SO_3H-NH_2, UiO-66-NH_2-SO_3H-2/C_3N_4@PDA, and nitrogen-doped carbonaceous catalyst (NCC) were reported to have appreciable catalytic activity for the 5-HMF production from various carbohydrates [17–19]. For instance, the 2SZ@SBA-15-SO_3H-NH_2 catalyst prepared with zirconia grafted sulfated SBA-15 was further functionalized with SO_3H, and NH_2 groups could produce 42.2 % 5-HMF yield from cellulose under an ionic liquid ([BMIM]Cl) medium at 120 °C

* Corresponding author.
E-mail address: kmohanty@iitg.ac.in (K. Mohanty).

https://doi.org/10.1016/j.apcata.2021.118237
Received 17 April 2021; Received in revised form 6 May 2021; Accepted 28 May 2021
Available online 31 May 2021